SPACE SCIENCE AND TECHNOLOGY SERIES

Nanosatellites, CubeSats of the NewSpace Era for Space Observation 1

Evolution of the Space Era and Mechanics of Things for CubeSats

Pierre Richard Dahoo
Mustapha Meftah
Abdelkhalak El Hami

ISTE WILEY

Nanosatellites, CubeSats of the NewSpace Era for Space Observation 1

Nanosatellites, CubeSats of the NewSpace Era for Space Observation 1

Evolution of the Space Era and Mechanics of Things for CubeSats

Pierre Richard Dahoo
Mustapha Meftah
Abdelkhalak El Hami

ISTE
WILEY

First published 2025 in Great Britain and the United States by ISTE Ltd and John Wiley & Sons, Inc.

ISTE Ltd
27-37 St George's Road
London SW19 4EU
UK

www.iste.co.uk

John Wiley & Sons, Inc.
111 River Street
Hoboken, NJ 07030
USA

www.wiley.com

Library of Congress Control Number: 2025944642

British Library Cataloguing-in-Publication Data
A CIP record for this book is available from the British Library
ISBN 978-1-83669-021-4

The manufacturer's authorized representative according to the EU General Product Safety Regulation is Wiley-VCH GmbH, Boschstr. 12, 69469 Weinheim, Germany, e-mail: Product_Safety@wiley.com.

Contents

Foreword

Space exploration requires special technological achievements due, on the one hand, to the extreme conditions under which equipment aboard satellites or space probes operate (vacuum, temperature, vibrations, radiation, etc.); and, on the other hand, to the fact that space objects must evolve autonomously without direct operator intervention.

Considerable resources and expertise are required to operate devices in these conditions. This has limited the number of countries able to invest in this field via specific structures, such as space agencies.

Although space remains a field of attention and fascination for many, we often overlook the revolutionary applications that can only be carried out from space, and which concern our daily lives: numerous applications linked to a global vision of the Earth's surface, its environment and meteorological processes, communication and content dissemination, positioning, traceability and remote piloting from space, security and surveillance, the realization of certain biological processes and the impact on medical effects, improving our knowledge of the Universe and the evolution of other planets, etc. These ever-growing applications have made it a major economic sector with significant geopolitical and security implications.

Paradoxically, technological miniaturization and the privatization of the sector have opened up this industrial sector. Today, it is highly fragmented, in the same way as other state-owned sectors which have undergone this evolution following a strong opening-up and involvement of the private sphere. Many new players and ambitious initiatives are emerging. The fierce competition between stakeholders means that innovation is essential, as are changes to the way in which developments are managed, financed and marketed.

However, NewSpace cannot escape the experience accumulated over the years. The fundamentals have not changed, and the space environment calls for the development of ever more elaborate devices – automated, but just as robust, guaranteeing optimal operation in this hostile environment.

The agile method is the only way to learn about new challenges and identify critical points, without getting bogged down in systematic and costly approaches. With this in mind, in addition to a sound knowledge of all of the development and validation stages of the technology used, it is very instructive to analyze past successes and failures. This applies to even the most distant historical developments, right through to the successive stages in the development of a component. It is this analysis of failure that enables us to quickly focus on the most critical points, prioritize them and thus make the technical solutions considered much more reliable in a much shorter time.

Nanosatellites, CubeSats of the NewSpace Era for Space Observation 1, *2* and *3* are designed to provide readers with the basics through an analysis of space history and the various stages of instrument development. Based on feedback from developments and analyses carried out within the framework of research, these books will enable those who so wish to perfect their knowledge and vision of this fast-changing sector, and to better understand its evolution: from fundamentals to breakthroughs.

Philippe KECKHUT
September 2025

Introduction

The 21st century stands out in the history of human societies as a time of transition. We are witnessing a period in the history of humankind that allows for all kinds of lifestyle breakthroughs, thanks to the increase in entropy associated with the various degrees of freedom of action and activity possible. One of these fields of activity concerns the space age and the NewSpace era. The name could have been different, because the term “New” refers to something new, whereas the “Universe” has always been there. Technological prowess has enabled us to reach that which aroused the curiosity of the first astronomers.

The industrial revolution 4.0 of the 21st century prefigured the expected increase in the processes used in business activities. These are based on digital technologies using algorithms predefined by objectives, such as system integration, augmented reality, virtual reality, the digital twin, artificial intelligence (AI), short- and long-term logistics, data analysis for processing large databases, cybersecurity, the autonomous robot, additive manufacturing, the Internet of Things, cloud computing, bitcoin and the simulation of complex chemical and biological processes in biotechnologies (infotech, biotech, etc.).

Software development is driving digital transition processes and impacting decision-making support with the breakthroughs and democratization of AI. It should be noted that the contribution of IT tools and the development of technologies in the field of genetics and human genome sequencing since the 2000s have led to the emergence of a new discipline called paleogenomics. This was initiated by the recent Nobel Prize winner in Medicine and Physiology, Svante Pääbo, in 2022, as part of the study of ancient DNA through paleogenetics.

Alongside this reality, which is moving towards the 4.0+ revolution, we are observing through NewSpace a desire to increase our degrees of freedom. This is

leading us towards a new path, which may allow for the privatization of space and the realization of the dream of conquering space and the Universe.

The first two satellites, Sputnik 1 and Sputnik 2, were launched by the USSR in 1957, on October 4 and November 3, while Explorer 1 and Vanguard 1 were launched by the Americans shortly afterwards, in 1958, on February 1 and March 17. The first major discovery was the Van Allen belts by the Americans who, thanks to a magnetic recorder on board Explorer 3, were able to correctly interpret the signals transmitted by the first satellites, which had remained an enigma until then. These belts are named after Van Allen, who, with his team, developed many of the observation instruments carried as payloads on American satellites.

Technological advances and strategies for space exploration and observation have thus followed a trajectory. In its initial phase, in the 1960s, this trajectory began with a typology of satellites, either spherical or cylindrical in shape, with masses of no more than a hundred kilos, equipped with the latest technologies. From the mid-1970s to the present day, it has evolved towards more elaborate technological objects, exceeding a few thousand kilos and up to tens of tons.

The history of space exploration can be divided into several distinct periods. The foundations for this adventure were laid as early as 1957, with the acquisition of the knowledge and technologies needed to send man into space. The period from 1957 to the end of the Apollo program in 1972 was characterized by major advances, and is often referred to as the golden age of space exploration. During this period, the two world superpowers of the time, the United States and the Soviet Union, indirectly engaged in space competition.

The next period, from 1972 until the end of the Cold War in the early 1990s, was marked by geopolitical issues in an increasingly militarized environment. Satellites were mainly developed for military purposes, such as observation, listening, communication and navigation. At the same time, space research was booming, leading to major advances in scientific research and increased international cooperation.

Since the end of the Cold War in 1991, space exploration has evolved in a context of unipolar domination, with the United States in a predominant position. In the late 1990s, the NewSpace era emerged, marked by growing private initiative in the space industry. Enterprising personalities such as Elon Musk (SpaceX), Jeff Bezos (Blue Origin) and Richard Branson (Virgin Galactic) played a key role in this new era, with ambitious goals such as the exploration of Mars, the Moon and suborbital flights. NewSpace brings a new dynamic to the space industry, thanks to reusable launchers and the miniaturization of satellites.

Meanwhile, in 1999, California Polytechnic State University and Stanford University (USA) invented a new satellite format. It opened up new prospects for Earth observation. In 1999, as part of an educational project to imagine, design, implement, test and operate in space a complete spacecraft within a reasonable timeframe, as part of a three- to five-year program to train university students, CubeSats – cubes measuring $10 \times 10 \times 11.35$ cm (1U) – were created in California. They ushered in a new era in the conquest of space.

The immensity of the cosmos seemed essentially cold and barren until the middle of the 20th century, but the launch of Sputnik 1 marked the beginning of the space age. The dispatch of robotic scientific explorers across the Solar System, space observatories in Earth orbit, the development of advanced detection techniques and increasingly powerful telescopes have enabled us to acquire new knowledge through observation from space. All of this has completely revolutionized our vision of both planetary atmospheres and the interstellar medium, revealing an unsuspected molecular richness leading to the creation, alongside astrophysics, of new disciplines such as astrochemistry. In the wake of these developments, models of molecular physics and chemistry have made it possible to study chemical species using the theory of quantum mechanics, providing reliable, precise and high-quality analysis through spectroscopy. This tool provides the necessary information on parameters such as pressure, temperature, humidity, wind speed or solar flux, to understand the processes driving the dynamics of planetary atmospheres, particularly that of the Earth.

Thanks to ground-based microwave observatories in very dry, high-altitude regions (ALMA) or airborne observatories (stratospheric balloons, SOFIA), astrophysicists have access to a large battery of instruments dedicated to spectroscopy. These include spectrometers onboard space probes bound for Venus (Venus Express), Mars (Mars Express, TGO, etc.), Jupiter (Junon), Saturn (Cassini-Huygens), comets (Rosetta) or the terrestrial-based JWST (James Webb Space Telescope) observatory.

The future looks exciting in this field, with future observatories on Earth (E-ELT, etc.), in space (WFIRST) and on various planetary missions. The constellation of nanosatellites will enable us to refine the precision of our spatial and temporal measurements.

This book is the first of three and discusses the space age from its origins in the mid-20th century, through to the NewSpace era of the 21st century. Its content is drawn from lectures and seminars by Meftah, Dahoo and El Hami as part of their teaching and research activities. It also draws on feedback from research activities at the Laboratoire Atmosphères et Observations Spatiales (LATMOS) and at INSA

Rouen, resulting from research work in the fields of instrumentation and spectroscopy for astronomy and astrophysics as well as optimization in mechanics. Our research teams are also involved in space observation, both through the implementation of observation instruments and through the analysis of observation data in partnership with other national institutes and organizations (CNES, ONERA, etc.), international organizations (ESA, Institut royal d'aéronomie spatiale de Belgique (IASB), Institut Lafayette, Jet Propulsion Laboratory, etc.) or industrial partners (AMSAT-F, F6KRK, Electrolab, ACRI-ST, Adrelys, Hensoldt Space Consulting, Oledcomm, Nanovation, etc.), to name a few.

The aim of this book is to provide an overview of the knowledge required to build and use nanosatellites to observe the atmosphere of a planet, in particular the Earth, and to provide the spectroscopic tools needed to study them and the data required to understand global warming. It is presented from a systems engineering or systemic approach. Each chapter includes an appendix presenting the necessary mathematical, physical and mechanical knowledge, so that readers who wish to delve deeper into the concepts developed in the body of the chapter can do so. The bibliography, although not exhaustive, is substantial enough to allow for further reading.

Feedback from both CubeSat production and observation using the instruments on board UVSQ-SAT and INSPIRE-SAT 7 (International Satellite Program in Research and Education), launched in 2021 and 2023 respectively, are used to provide researchers, engineers, teachers and students in engineering schools, masters and bachelors programs, as well as business leaders, with the knowledge they need to engage in the socio-economic activities of NewSpace.

This first volume contains four chapters tracing the evolution of the space age and the context of a space observation mission using CubeSats as examples. CubeSats are within the reach of any group who wish to undertake them, thanks to their low cost and short implementation times. They can be used to collect data for the study of global warming, monitor the evolution of the Earth's atmosphere for research purposes, or invest in meteorology, communications or data collection (Big Data) through a network of satellites for industry. In the fourth and final chapter, an example of the implementation of a payload for observing the Sun and its effects is presented in the context of the third UVSQ-SAT NG CubeSat, scheduled for launch in 2025.

Chapter 1 traces the history of the space age from the orbiting of the first Sputniks, launched in 1957 by Russia and closely followed by the Explorer 1 and Vanguard 1 satellites, launched in 1958 by the United States, right up to the NewSpace of the 21st century. Following the initial phase of development exacerbated by the rivalry between the two countries in the context of the Cold War,

and leading to the first landmark events such as the first man and woman in space and the first man on the Moon, came the first applications of space activities of a scientific nature: on the one hand through the discovery of the Van Allen belts, and on the other hand through commercial applications for meteorology. This chapter focuses notably on methodological and technological innovations in complex systems engineering. It also looks at the societal impact of space technologies in the fields of research into observation of the Earth's atmosphere, in the context of global warming, exploration of the Solar System, and observation of the Universe through orbiting telescopes. Space-related socio-economic activities are mentioned in relation to data, whether for weather, telecommunications (telephone, radio, television, Internet), GPS (Global Positioning System) or the Internet of Things, as well as technological advances in reusable launchers, Earth–Moon and Earth–Mars space projects, nanosatellites and digital twins.

Chapter 2 discusses the orbital parameters of the CubeSat as it moves as an artificial satellite around the Earth. Following a reminder of the geometry of curves associated with conics and their analytical expressions in a Cartesian reference frame, the history of theoretical hypotheses resulting from ancient astronomers' observations of the sky is presented. The debate between the geocentric and heliocentric models of the Solar System for interpreting planetary motion is discussed, with mention of Copernicus, Kepler, Galileo, Newton and Einstein as the main contributors to heliocentrism and gravitation theories. In the same way, the different approaches (Newton, Lagrange, Hamilton, etc.) to dealing with system mechanics are presented for calculating the trajectory of systems subject to the force of gravitation, in particular the circular or elliptical orbit of a natural or artificial satellite around an attractor center at different altitudes. Six Kepler parameters are used to describe the orbit of a CubeSat around the Earth, with reference to the equatorial plane, in relation to which the perigee (periapsis or periastron, closest to a star) and apogee (apoapsis or apoastron, furthest from a star) are defined. For an elliptical orbit, these parameters enable a compromise to be found between two possibilities: high coverage and low resolution at apogee, and conversely low coverage and high resolution at perigee.

Chapter 3 presents satellite launchers from different countries or consortia. It shows the evolution of the public sector, with launchers from state institutions such as NASA at Cape Canaveral, ESA in French Guiana and the Russian space agency at Baikonur, and the private sector, with the development of the space industry and the number of sites and launchers (SpaceX, etc.). The new business model, which enables the launch of both large satellites and hundreds of small satellites (CubeSats, nanosatellites, etc.), is discussed, as it reduces launch and orbiting costs. The standards to be met and the constraints to which the launch and in-orbit procedures must conform are also presented.

Chapter 4 is devoted to small satellites, with masses ranging from 500 kg to four tons. The focus is on the manufacture of CubeSats, based on the methodology of university pioneers Jordi Puig-Suari of California Polytechnic State University and Bob Twiggs of Stanford University. The smallest CubeSat model, described as 1U, is a cube measuring $10 \times 10 \times 11.35$ cm, which can grow to 12U in volume depending on the payload it will carry for its data-gathering mission. The structure of a CubeSat, in particular its mechanical architecture in view of its payload, with reference to the UVSQ-SAT and UVSQ INSPIRE-SAT 7, as well as its main functions, are described, in particular those concerning the links between the satellite and the ground-based data collection stations. Mechanical optimizations, using finite element method simulations to ensure robustness against environmental constraints during launch and orbital motion, are also discussed.

1

The NewSpace Era

This chapter looks at the history of the space age from its very beginnings, marked in time by the International Geophysical Year (IGY) of 1957–1958 focusing on the event of peak solar activity, and against the backdrop of the Cold War between the USSR and the USA. This period of early discoveries, notably the Van Allen belts, was characterized by rivalry between the two world powers in the space race, with the first man (1961) and woman (1962) in space, and the first man on the Moon (1969). This was followed by a transition toward scientific objectives, such as the observation and collection of data on the Earth's atmosphere for meteorological purposes, and the exploration of the Solar System, in particular with Voyagers 1 and 2, which are still operational outside of the Solar System. This era has been driven by innovation, be it in project management (system approach, V-cycle, etc.) or technology (digital twins, solar panels, digital communications, etc.) to achieve the objectives of space projects driven by space agencies (NASA, ESA, etc.), with a focus on quality and reliability. Initially, satellites were spherical or cylindrical in shape, weighing no more than a hundred kilograms, but by the mid-1970s, they were weighing several thousand kilograms and could reach a weight of up to ten tons.

At the end of the 1990s, visionary entrepreneurs initiated daring projects, including the reuse of space launchers, suborbital flights and exploration of the Moon and Mars. In 1999, two American universities reduced the volume of satellites by inventing CubeSats and nanosatellites. This marked the dawn of the NewSpace era which redefined the space industry and its fields of activity, emphasizing innovation, cost reduction and increased private-sector participation in space exploration and exploitation, as embodied, for example, by SpaceX in the United States (2002) and Rocket Lab in New Zealand (2018).

For a color version of all of the figures in this chapter, see www.iste.co.uk/dahoo/nanosatellites1.zip.

1.1. The space age and its evolutions

The history of space exploration can be divided into four distinct periods. The initial period ran from 1957 with Sputnik 1 to 1970 with the end of the Apollo program. This was followed by the intermediate period from 1971 when military satellites were launched against a backdrop of geopolitical challenges, until the end of the Cold War in the early 1990s. It should be noted that, at the same time, space research experienced a significant boom, leading to major advances in scientific research and influential international cooperation.

At the end of the Cold War in 1991, space exploration evolved in a context of unipolar domination, with the United States in a predominant position. This was the beginning of the NewSpace era, marked by growing private initiative in the space industry (SpaceX, Elon Musk; Blue Origin, Jeff Bezos; Virgin Galactic, Richard Branson). NewSpace brought a new dynamic to the space industry, thanks to reusable launchers and the miniaturization of satellites. The democratization of access to space allows a greater number of operators, including start-ups and research laboratories, to participate in space exploration [NEW 80, LAU 97, POR 98, SID 00, DIC 06, BIG 14].

Meanwhile, a new satellite format, defined as part of an educational project in 1999 at California Polytechnic State University and Stanford University (USA), opened up new prospects for Earth observation. The idea was to imagine, design, implement, test and operate CubeSats (a 1U cube with dimensions of 10 x 10 x 11.35 cm) in space, as part of a three- to five-year university course. This approach represents a new era in the conquest of space [HEI 00, JAN 11, 21, 23], the developments of which are described in the appendix.

1.1.1. *The first artificial satellites*

Although Isaac Newton's work on gravity raised the theoretical possibility of orbiting an artificial satellite from Earth in 1687, it was not until the early 20th century that the theoretical work of Russia's Konstantine Tsiolkovsky and the experimental work of American Robert Goddard confirmed that a satellite could be launched by a rocket.

On October 4, 1957, the Earth's first artificial satellite was launched from the Baikonur cosmodrome by an R-7 Semiorka launcher (a large intercontinental ballistic missile). Sputnik 1 (meaning "satellite" or "companion" in Russian) is a sphere measuring 58 cm in diameter and weighing 83.6 kg. It was the first artificial

object launched into space. For 22 days, it transmitted data on solar winds, the Earth's magnetic field and cosmic rays. These were the first scientific data to be recorded directly from space. It was followed a month later by Sputnik 2, launched on November 3, 1957, with an animal on board, the dog Laïka. The onboard instruments detected radioactivity in the Van Allen radiation belts, but the origin of the signals transmitted was not identified, as they were picked up by nations other than the USSR.

As a reminder, the Van Allen radiation belts (see Figure 1.1)[1] are made up of a high density of energetic particles, originating from the solar wind in a toroidal zone of the Earth's magnetosphere around the magnetic equator. The encounter of these particles with the molecules of the Earth's upper atmosphere manifests itself in the form of polar aurorae.

It took the United States four months to respond and launch its own satellite, Explorer 1, from the famous Cape Canaveral base in Florida on February 1, 1958. This first American satellite was followed by Vanguard 1, launched from Cape Canaveral on March 17, 1958, which became the fourth artificial Earth satellite. Explorer 1's four-month mission also enabled Geiger counters to detect the Van Allen radiation belts. However, it was not until the data recorded by Explorer 3, launched on March 26, 1958, with the first onboard miniaturized magnetic tape recorder, that the riddle of the signals resulting from the presence of the Van Allen radiation belts was resolved.

Vanguard 1 was the first satellite to be equipped with solar cells (six), enabling its second transmitter to operate until May 1964, almost six years after its launch, whereas the mission of the first satellites did not exceed four months.

We should also mention the glorious achievements of the USSR, with the first man in space on April 12, 1961 (Yuri Gagarin) and the first woman in space on June 16, 1963 (Valentina Terechkova); and of the United States with the Apollo program, the first man on the Moon with the Apollo 11 mission and the moon landing on July 21, 1969 (Neil Armstrong, Buzz Aldrin and Michael Collins).

By 1957, space systems and associated missions had become indispensable tools for many disciplines involved in the study and observation of planet Earth and its near and distant environment, as well as the exploration of the near and far Universe [NEW 80, LAU 97, POR 98, SID 00, DIC 06, BIG 14, JAN 23].

1 See: https://en.wikipedia.org/wiki/Van_Allen_radiation_belt.

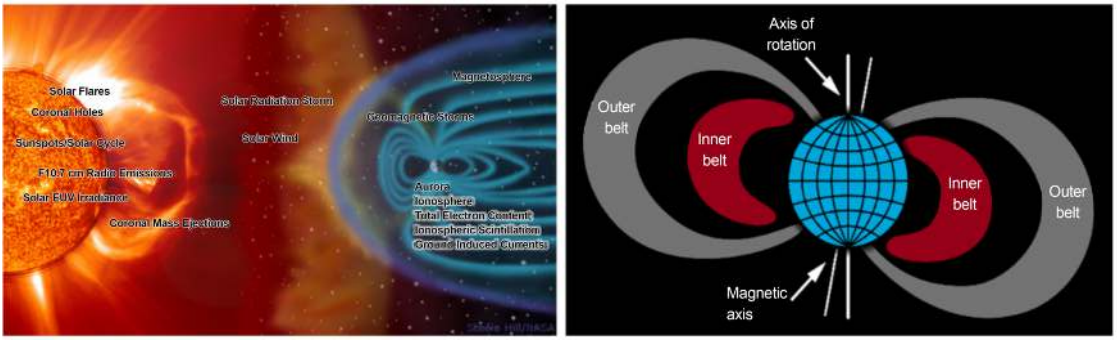

Figure 1.1. *Van Allen belts (NASA)*

1.1.2. *Planet Earth and its near and distant environment*

The formation of ozone holes in the stratosphere above the poles, which, as a result, could no longer sufficiently filter out ultraviolet radiation, or the increase in the greenhouse effect due to a rise in the amount of carbon dioxide in the atmosphere, are just two concrete examples of the benefits of observing the Earth and studying its near and distant environment in targeting the right causes to these harmful effects. Satellites have become indispensable in this field, not only for managing the Earth's natural resources, controlling the environment, protecting people and property in danger, providing meteorological services, studying the climate, space weather, etc., but also for telecommunications, telephony, communication for multimedia applications, navigation, defense, etc.

An illustrative example is the series of ten experimental meteorological satellites, Tiros-x (Television InfraRed Observation Satellite), launched between 1960 and 1965 by NASA (the US space agency) into polar orbit to supplement data obtained by traditional ground-based devices and used for weather forecasting. In an international cooperation between CNES (the French space agency) and NASA (the EOLE program), a first PEOLE satellite was also launched in 1970 by the Diamant rocket from the Kourou base in French Guiana, followed in 1971 by the EOLE satellite developed by CNES and launched by NASA from Wallops Island by the Scout rocket. These satellites retrieved meteorological data provided by 500 weather balloons launched from Argentina, drifting from west to east at an altitude of 12,000 m in the Southern Hemisphere on an eight-day cycle [MOR 66, 02, LET 13].

Since then, the analysis of the data collected by various observation instruments has shown that human activities are responsible for modifying the composition and the warming effect of the Earth's atmosphere. In light of the visible and measurable consequences on the ecosystem and climate, it is more than necessary to design instruments that can continuously monitor the state of the Earth's atmosphere by observing its near or distant environment, with quality data to benefit from subsequent analysis and correcting actions.

1.1.3. *Exploring the near and distant Universe*

Scientific missions enable us to study the nearby Universe in the solar system – for example, the Sun (see Figure 1.2(a))[2] and the terrestrial planets Mercury, Venus, Earth and Mars (see Figure 1.2(b)) – or the more distant Jovian planets, Jupiter, Saturn, Neptune and Uranus.

2 See: https://en.wikipedia.org/wiki/Sun.

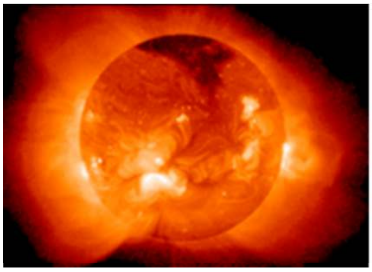

a) The sun

b) The telluric planets

Figure 1.2. *The Sun and the Solar System's telluric planets*

These observation and analysis activities can be carried out either by the study of the Earth from ground-based observatories or the ISS orbital station, or from space systems such as satellites, rovers, probes or orbiters launched to get as close as possible to the objects under study. Examples of the latter include Mars Express and Venus Express, orbiters dedicated to studying the atmospheres of Mars and Venus.

Mars Express (MEX) is the first European planetary mission to the Red Planet, developed in collaboration between LATMOS (formerly the French Aeronomy Service) in France, BIRA-IASB (Royal Belgian Institute for Space Aeronomy) in Belgium and IKI (Russian Space Research Institute) in Russia. Launched on June 2, 2003 by a Soyuz rocket, the 1270 kg orbiter was placed in an elliptical polar orbit around Mars on December 25, 2003, with a pericenter altitude of 259 km and an apocenter altitude of 11,559 km, for a period of 7.57 hours. A measurement and observation instrument, called SPICAM (Spectroscopy for the Investigation of the Characteristics of the Atmosphere of Mars), has enabled the spectroscopic study of the UV and IR signatures characteristic of the atmosphere of Mars. Dedicated primarily to the study of the atmosphere of Mars, the spectrometer operates in the ultraviolet and infrared ranges [BER 06].

The 1,042 kg ESA Venus Express orbiter was launched on November 9, 2005 by a Soyuz rocket, and was the first mission to apply solar and stellar occultation techniques to the atmosphere of Venus, with the SPICAV/SOIR (Solar Occultation in the InfraRed) instrument. Based on the SPICAM model, the SPICAV instrument (V for Venus) comprises a suite of three spectrometers with a variety of scientific objectives. As for SOIR, it is one of three high-resolution spectrometers on Venus Express, with a new optical design enabling it to achieve a resolution power $\lambda/\Delta\lambda$ = 15,000–20,000 for a volume and mass (6 kg) that are reasonable for space, working in the 2.2–4.3 μm range. This is the highest resolution for planetary space exploration [BER 07, 08].

1.1.4. *Space activities*

The space sector encompasses a wide range of activities and applications. The main ones are listed below:

1) Scientific research: space plays an essential role in scientific research, enabling us to observe the Universe, study cosmic phenomena, collect data on the Earth, explore the planets, etc.

2) Telecommunications: telecommunications satellites are used for long-distance communications, data transmission, television, broadcasting, cell phone networks, etc.

3) Navigation and positioning: satellite navigation systems such as GPS (Global Positioning System) enable the precise determination of position, speed and time

throughout the world, and are used in many sectors, including transport, logistics and cartography.

4) Earth observation: Earth observation satellites provide invaluable data and images for monitoring the environment, studying climate, meteorology, natural resource management, monitoring natural disasters, etc.

5) Space exploration: space exploration includes sending probes and robots to study planets, moons and asteroids, as well as sending astronauts to explore space and destinations such as the Moon, Mars and beyond.

6) Military and defense applications: space is used in military applications for surveillance, secure communication, intelligence, reconnaissance, etc.

7) Commercial applications: the space sector is increasingly exploited by private companies for activities such as space tourism, satellite launches, telecommunication services, Earth imaging, etc.

8) Education and awareness: the space field also plays an important role in educating and raising public awareness through education programs, exhibitions, events and activities designed to inspire future generations and promote interest in space exploration.

According to Janson, the space era can be divided into three periods since 1957: the first era from 1957 to 1970, the great era from 1971 to 1996 and the new space era from 1997 onward, which can be described as NewSpace [JAN 11, 21, 23].

1.2. NewSpace in the 21st century

Observation sciences and space technologies have followed a trajectory marked by technological transitions and strategic choices for exploration and observation, particularly by the American (NASA) and European (ESA) space agencies. In the initial phase of the 1960s, satellites equipped with the latest technologies were spherical or cylindrical in shape and weighed no more than 100 kg. Since the mid-1970s, however, the design of objects for observation and space technologies has given rise to a diversity of systems – be they satellites, probes, orbiters, rovers or drones – that are increasingly based on a systemic approach to design, sometimes relying on digital twins with weights in excess of a few thousand kilos and sometimes reaching tens of tons.

It was in 1999, outside the decision-making sphere of space agencies or military organizations, that a new era in the conquest of space began. Thanks to an educational project, the first CubeSats – cubes measuring 10 x 10 x 11.35 cm (1U) – saw the light of day in California, inspired by Professor Jordi Puig-Suari of

California Polytechnic State University and Professor Bob Twiggs of Stanford University [KIT 94, HEI 00]. The method implemented enabled a complete spacecraft to be designed, deployed, tested and operated in space within a reasonable timeframe, in a three- to five-year curriculum, to train academics with off-the-shelf technologies. The first six CubeSats were launched on June 30, 2003 by Eurockot's Rockot launcher from the Plesetsk site. This educational project democratized the use of small satellites that can be designed in a laboratory for space research programs, and paved the way for a sector of industrial activity in this field. Since 2013, space agencies have shown that the reliability of CubeSat missions can be greatly improved by optimizing design engineering.

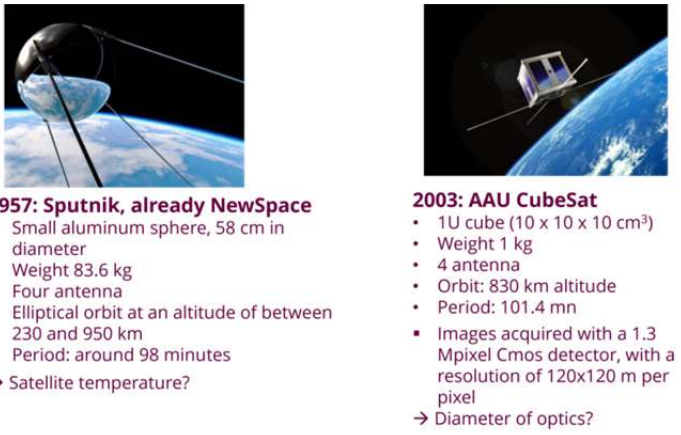

Figure 1.3. *Satellite evolution between 1957 and 2003*

Figure 1.3 summarizes the characteristics of the satellites designed in 1957, when the space age began, and those of the CubeSats developed in 2003. The diameter of the sphere has been reduced from 58 cm to a cube with sides of 10 cm, which means a reduction in volume by a factor of approximately 100. At the same time, the mass has been reduced by approximately 80, knowing that a cube is easier to build than a sphere. The orbit has moved from elliptical, with an altitude between 230 and 950 km, to circular at 850 km, but with an almost identical period (98 min vs. 104.1 min). The spectral range of observation is wider in range with the CubeSat which, in addition to four antennas in the microwave range, was equipped with Cmos detectors to record images. However, last but not least, the constraints of temperature and optical resolution have yet to be overcome.

NewSpace has been emerging since the 2000s, and a number of new challenges have arisen. The last decade has seen significant advances in space technologies and an intensification of public communication about space. Today, space exploration is

no longer the prerogative of government agencies, but is open to private enterprise, marking the beginning of the NewSpace era. This new space era has brought with it new participants and a deep transformation of the space ecosystem. NewSpace is attracting a great deal of interest, as its dynamic players are injecting new energy and speed into the space sector. This democratization of space has been made possible by the use of innovative reusable launchers and the increasing miniaturization of satellites. These advances, combined with the development of space tourism, the return to the Moon and the exploration of Mars, have rekindled the general public's enthusiasm for space. The conquest of space is inevitably accelerating, with projects for space travel, lunar and martian exploration. The American space agency, NASA, is preparing for an odyssey to Mars as part of its Artemis program. This new space age promises exciting discoveries and major technological achievements, paving the way for a future in which space exploration will play a central role.

Satellites play a major role in the new era of space conquest. A mass criterion is often used to classify satellites, as shown in Table 1.1, in the FAA (Federal Aviation Administration) classification in the United States. In this classification, the first Sputnik 1 satellite was of micro type, as was the first CubeSat of 2003, as shown in Figure 1.3. The Mars Express and Venus Express orbiters were in the category above, medium and mini respectively.

In economic terms, a low-orbit satellite costs between €8,000 and €12,000 per kg to build and launch. Compared with an average cost of €8 million for a medium-sized satellite with a mass of approximately 800 kg, a 10 kg CubeSat only costs €100,000, making it affordable for academic scientific research programs to observe the Earth [CAM 19].

Satellite class	Mass (Kg)
Very heavy	> 7100
Heavy	5401–7000
Large	4201–5400
Intermediate	2501–4200
Medium	1201–2500
Average	601–1200
Mini	201–600
Micro	11–200
Nano	1.1–10
Pico	0.09–1
Femto	0.01–0.1

Table 1.1. *Payloads and specifications*

1.2.1. *Development priorities for the NewSpace era*

A number of areas of development are emerging in this new NewSpace era:

1) *Satellite launches*: this is one of the largest sub-sectors of NewSpace. Satellite launch companies focus on the technology and infrastructure needed to send satellites into near-space and low-Earth orbit.

2) *Internet via satellite*: NewSpace companies focus on improving Internet connectivity through low-Earth orbit satellites, wireless broadband, optical communications and other technologies.

3) *Deep space exploration*: NewSpace companies are developing high-level missions to transport people and goods beyond the Earth's atmosphere to the Moon, the surface of Mars and beyond.

4) *Lunar landing*: NewSpace companies are mainly focused on missions to the Moon, or on construction products and infrastructure for lunar missions.

5) *Industrialization and manufacturing*: these include the development of spacecraft, hardware, propulsion systems, engines, etc.

6) *Earth observation*: imaging, tracking and analysis technologies are being developed to monitor weather, climate, marine data, GPS technology, etc.

7) *Asteroid mining*: these cutting-edge companies are developing technologies to extract water, rare minerals and metals from near-Earth asteroids.

8) *Space debris*: these analyze human-made objects orbiting the Earth. Debris has to be monitored to avoid collisions with satellites and spacecraft, etc.

9) *Space tourism*: access to space for individuals, explorers, etc.

How are research activities faring in the NewSpace era?

1.2.2. *Research development*

The following questions may be asked:

– Is NewSpace leading us toward the privatization of space?

– What kind of legislation and governance will be needed in the future?

– Are we facing a new paradigm (see Figure 1.4)?

This means that, alongside the major standard observation and analysis projects with space agencies (NASA, ESA, CNES, etc.), we need to be able to implement

new systems that are smaller, more efficient, less costly and faster, in an "agile" approach.

This implies greater flexibility, with public–private partnerships and the creation of international networks, to take a new approach to scientific research linked to planetary observation and data analysis.

By way of example, we can cite the spin-offs for scientific research of this new paradigm. LATMOS and OVSQ at the Université Versailles-Saint-Quentin-en-Yvelines have positioned themselves, within the framework of national and international collaborations, on atmospheric observation to provide data for climate studies, as shown in Figure 1.5. They used the CubeSats UVSQ-SAT [MEF 20] and INSPIRE-SAT 7 [MEF 22a] built by these two institutions thanks to Meftah and teams from LATMOS, OVSQ and UVSQ.

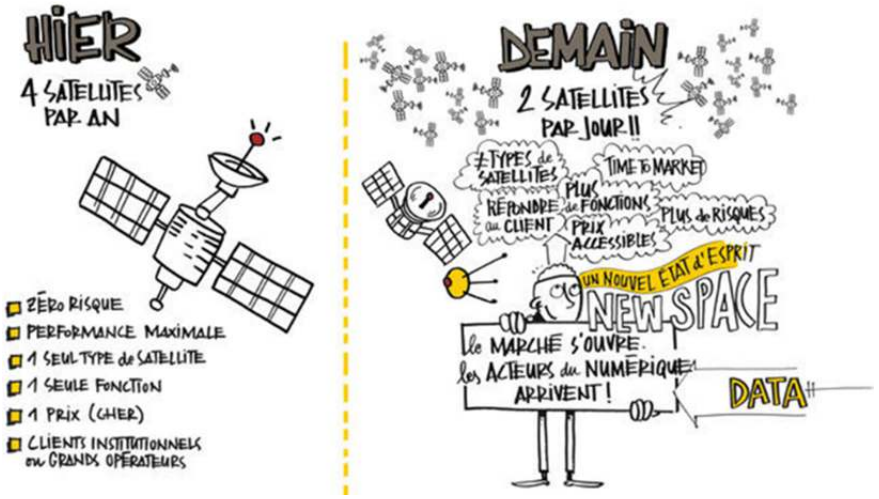

Figure 1.4. *A new paradigm for implementing space programs*

COMMENT ON FIGURE 1.4.– *The figure demonstrates the mass development of satellites by comparing the scale of production between the past and the future. In the past, only four satellites per year were put into orbit, compared to an expected two satellites per day in the future. The figure also compares the characteristics of the old versus new satellites. The satellites of the past have zero risks, maximal performance and there is only one type with one function. They are also expensive and used by institutional customers and major operators. The satellites of the future will be of different types, with multiple functions and carry multiple risks. They will be more affordable in price and open up the market to digital players.*

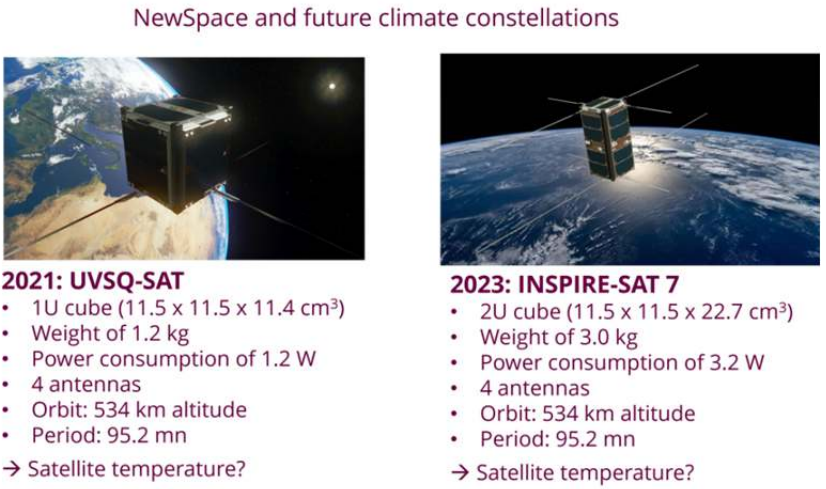

Figure 1.5. *Nanosats: UVSQ-SAT (2021); INSPIRE-SAT 7 (2023)*

1.3. The space system

Engineering is the application of science. Its aim is to convert scientific laws into applied reality, whether for medical concerns or space travel. In the process of designing intelligent objects, the engineer's job is to provide solutions to problems that ultimately have an impact on society. As a result, space programs have been the source of many innovations. They required the application of new project management methods for the manufacture of satellites intended to be propelled into space from launch sites, emphasizing a system approach to the design and manufacture of a satellite or probe [NAS 95, 19, GPG 07, CHI 17, MEF 22b].

Issues such as reliability, logistics, coordination of different teams (requirements management), evaluation measures and other disciplines become more difficult when large or complex projects are involved. This is why the so-called V-cycle method has been used as part of the system approach, as described in section 1.4.

Digital simulation methods based on a digital model of the physical system (the forerunner of the digital twin) were also used in the Apollo programs. The digital twin is a concept of virtual equivalent or dynamic digital representation of a real system.

The first definition was formulated by NASA in its Integrated Technology Roadmap (Technology Area 11: Modeling, Simulation, Information Technology & Processing Roadmap, 2010):

> A digital twin is a multiphysics, multiscale, probabilistic simulation of an as-built vehicle or system that uses the best available physical models, sensor updates, fleet history, etc., to mirror the life of its corresponding flying twin [SHA 10].

Let us also note Michael Grieves' definition of the digital twin [GRI 02] as "a set of information constructs that fully describe a potential or actual physical manufactured product, from the micro-atomic to the macro-geometric level".

Finally, we should also mention the implementation of a communication system to collect and transmit data in digital form, whether passive or active. The coupling of this system with the satellite's digital image has paved the way for Industry 4.0. This concerns the automation and exchange of data in manufacturing industries with the additional technology of cyber software, IoT, cloud, and including identification, problem-solving and decision-making (cognitive computing). IoST (Internet of Space Things) is emerging alongside IoT (Internet of Things).

It should also be noted that space activities are particularly focused on data, whether for observation or control, from satellites, telescopes or platforms. These include meteorology, telecommunications (telephone, radio, television, Internet), the GPS and the Internet of Things.

1.3.1. *The system concept*

The noun "system" is used in many different situations. It can be used to refer to air traffic control systems, the solar system or biological systems. The fact that the word is used in so many different ways is an indication of the complexity of the concept itself.

According to the Centre national de ressources textuelles et lexicales (National Center for Textual and Lexical Resources), a definition was proposed in 1552: "A whole whose parts are coordinated by a law"[3].

In Étienne Bonnot de Condillac's 1749 philosophical work *Traité des systèmes* [BON 49], the term is defined as:

> [The] arrangement of the different parts of an art or science in an order in which they all support each other and in which the latter are explained by the former. Those that give reason for the others are called principles.

3 [DET 87]: "I am ready to show you the composition of this System" (author's translation).

According to [DER 75], in general terms, a system is a set of dynamically interacting elements organized in function of a goal. A system can thus be considered as any entity, conceptual or physical, made up of interdependent parts. In other words, it is a set of elements in permanent interaction, organized and open to its environment, to which it must constantly adapt in order to survive (see Figure 1.6).

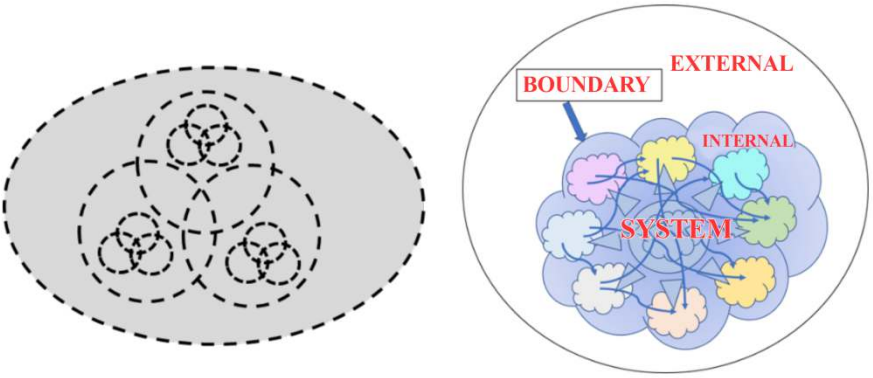

Figure 1.6. *System, subsystems and interrelationships*

A *system* is a set of elements interacting with each other according to certain principles or rules. It is determined by:

– its boundary, i.e. the criterion of belonging to the system (determining whether an entity belongs to the system or, on the contrary, is part of its environment);

– its interactions with its environment;

– its functions (which define the behavior of the entities making up the system, their organization and their interactions).

The system's approach stems from the 1940s encounter between biology and electronics:

– the birth of cybernetics (1948) [WIE 48], with the study of regulation in living beings and machines, and the introduction of the ideas of loop, feedback and regulation;

– a unitary vision of the world expressed by biologist Von Bertalanffy (1950) [VON 50, 68], with open systems everywhere.

The study of systems is carried out within the framework of the system's approach, which follows on from the methods advocated by the Palo Alto school

in the 1950s as well as the work of Gregory Bateson [PIC 13]. The system approach has been the subject of numerous publications and applications, whose non-exhaustive references are given in the appendix [CHU 68, ACK 74, MPH 74, WEI 75, LEM 77, FOR 84, FLO 93, 99, SEN 93, CHE 99, HIT 07, BOA 08, RAM 09, LAW 10, DEW 11, INC 12, 15].

1.3.2. *Designing a space system*

A space system must be considered within the framework of systems engineering, which is also one of the methodological products of space activities in project management. It is an interdisciplinary field of engineering, focusing on the design and management of complex engineering systems throughout their life cycle. Issues such as reliability, logistics, coordination of different teams (requirements management), evaluation measures and other disciplines become more difficult when dealing with major or complex projects. Systems engineering deals with work processes, optimization methods and tools for complex projects. It covers both technical and human disciplines, such as control engineering, industrial engineering, organizational studies, project management, etc. [DAH 21, 22, MEF 22b, 23].

1.3.3. *The two main sectors of a space system*

The space sector can be broken down into two sectors: that of the space vehicle design environment, the “space sector”, and that of the users who implement the vehicle’s functionalities, the “user sector”. In the system approach, these sectors are two subsystems that interact with each other.

The space sector

Space vehicles – satellites, probes, landers, rovers, orbiters – are characterized by their capacity and the type of mission to which they are dedicated. Applications can be scientific, commercial or military. Their definition must take into account all trajectories and orbits followed from launch to end-of-life. The mission-critical part of the spacecraft is called the payload.

The space sector includes the design of satellites from technical specifications. It can be divided into:

– the launch from a site, i.e. the launch center, the launcher and the operations to be carried out from launch into orbit to separation of the launcher from the satellite or probe;

– the operations, including a command and control center with radio links to steer the satellite, and a scientific mission center to process the data.

The user sector

The user sector includes the means for receiving, processing and distributing information associated with the space mission (mission center at one or more sites).

1.4. Implementing a space project

1.4.1. *The initial spatial project and management methods*

The two basic elements to consider when launching a space project are:

– a description of the idea;

– a technological presentation of the idea.

A project's conception and realization is shown in Figure 1.7. It starts with an idea and requires a budget and resources for its realization. The next step is to draw up a schedule and manage its implementation.

Figure 1.7. *Project management*

Project management involves setting up a program to achieve an objective, which is often the design of a product or service.

There are generally three essential stages:

– identifying and describing the project;

– organizing and planning the project;

– monitoring the project and managing discontinuities (or discrepancies) between forecast and actual status.

There are many methods available to help manage a project. The teamwork.com website indicates that there are some 8,462 project management methods.

To implement a space system, it is necessary to use a system approach for decision-making (DM) within the framework of collaborative engineering, in order to meet the requirement of integrating project management (PM) with systems engineering (SE).

The V-cycle is an example. This is shown in Figure 1.8 and is an example of project management. It is based on a cascade model theorized in the 1970s. It allows development processes to be represented linearly, which leads to sequencing in the processes in successive phases from design to realization and validation.

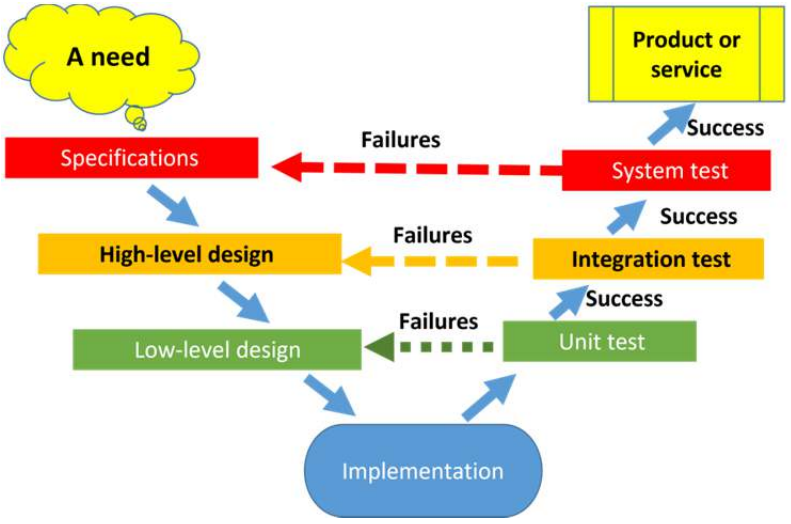

Figure 1.8. *The V-cycle for project management associates a validation phase with each implementation phase*

The V-cycle is a common graphic representation of the system's engineering life cycle, generally applied in the space industry. The left-hand side of the V-cycle represents concept development and the decomposition of requirements into functions and physical entities, which can be organized in the form of an architecture for design and development. The right-hand side of the V-cycle represents the integration of these entities (including appropriate testing to verify that they meet requirements) and their final transition to the field, where they are operated and maintained.

The implementation of a "small satellite" program can also rely on a simplified approach to guarantee the success of a mission, which has to be developed within a limited time (two years). LATMOS implements some of these programs using a simplified organizational structure. The aim is to promote an agile approach while avoiding the vertical management model, which often proves ineffective for rapidly driving a space program from its definition and analysis phase (phase 0/A) through to its exploitation phase (phase E). In this type of program, it is necessary to spur the active participation of the technical and scientific teams throughout the project, thus emphasizing flexibility in the face of possible changes and minimizing the importance of traditional procedures. Despite the simplified organization, a space project is still a complex process that requires meticulous planning, precise coordination and the consideration of numerous variables.

1.4.2. *Key issues from idea to realization*

When undertaking a space project, such as, for example, putting an atmospheric observation system into orbit from a CubeSat, it is necessary to formulate it in a few lines [MEF 23]:

– a description of the idea;

– a technological presentation of the idea.

Then, there are several questions to answer:

– What needs are being met?

– Who are the potential users?

– What is the type of project: experimental, application?

– What resources and budget are required for the program?

– What are the project contingencies?

– How do we obtain financing for the project?

– What do we bring that is new to the table?

– What sets this technology apart from competing technologies?

– What can we do that others cannot?

1.4.3. *Academia and industry*

1.4.3.1. *Academic state of the art*

– Which are the main academic laboratories (on an international scale) working in the project's technological field?

– What do they do exactly?

– What are the competing technologies?

– What are the strengths/weaknesses?

The answers to these questions can then be organized in an easy-to-read summary table.

1.4.3.2. *Industrial state of the art*

– Who are the main manufacturers (on an international scale) supplying the project's technological solutions?

– What do they do exactly?

– What are the competing technologies?

– What are the strengths/weaknesses?

1.4.4. *Questions and steps once the project is defined*

Once the project has been defined, the following questions are usually answered:

– What is it?

– Who is involved?

– How do we do what needs to be done?

We can then, for example, break down the space system into subsystems, such as:

– NewSpace launcher;

– satellite;

– transfer and landing vehicles;

– rover.

To carry out this project, we can then form four groups with a leader for the themes linked to each subsystem:

– a NewSpace launch group;

– a satellite group;

– a transfer vehicle and landing gear group;

– a rover group.

This is the approach adopted in the UVSQ-SAT (2021), INSPIRE-SAT 7 (2023) and UVSQ-SAT NG (2025) projects mentioned above [MEF 20, 22a, 23].

A system's complexity is motivating new approaches to their design, grouped together under the term "systems architecture". System architecture is a conceptual model of a system that describes its external and internal properties and how they are projected onto its elements, their relationships and the principles of system design and evolution.

Figure 1.9 shows an example of a satellite operation center linked to the space sector. The purpose of this device is to control the satellite and receive data from it. It is often associated with a scientific mission center, which enables the data to be processed. Figure 1.10 shows an example of a "project" breakdown. The space sector of this program is broken down into two segments: space and ground.

Every project is based on a stated objective, which requires programming of the tasks to be carried out, identification of the services to be called upon and the expected results. In the case of the design of an artificial satellite of the CubeSat type, the various phases can be summarized, as shown in Table 1.2.

As an example, we give a comparison of the procedures to be followed with regard to the different phases named by ESA and NASA, as well as the documents to be compiled in Table 1.3 [NAS 95, 19, ESA 09].

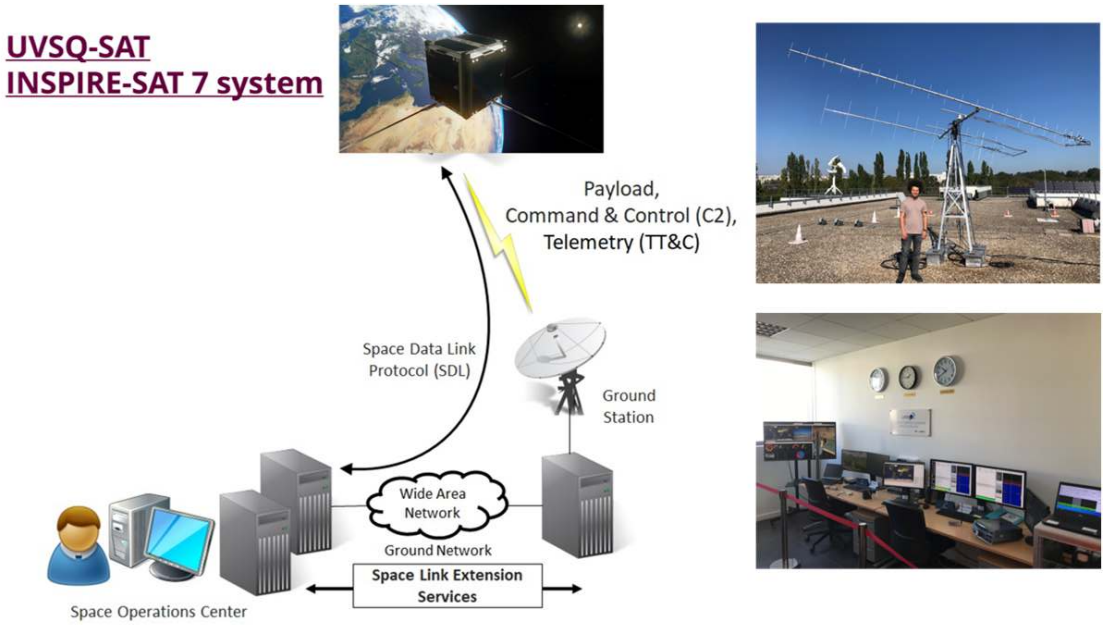

Figure 1.9. *Example of a satellite command and control center (applicable to UVSQ-SAT and INSPIRE-SAT 7 space missions)*

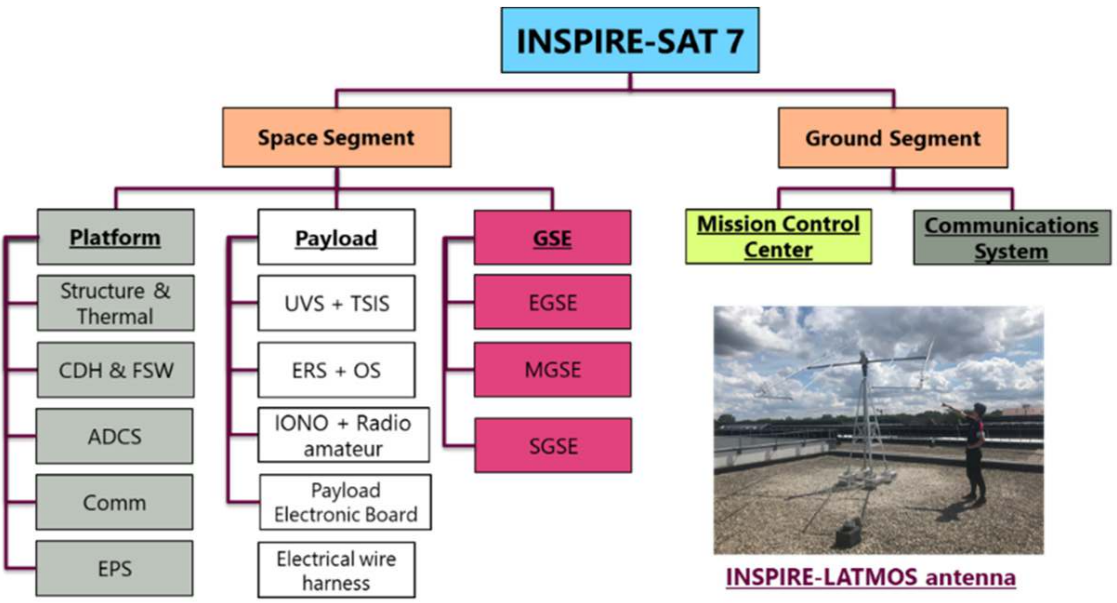

Figure 1.10. *INSPIRE-SAT 7 subsystems and interrelationships*

Phase	Process
0	**Analyze the mission**: define the objectives and list the various parties involved.
1	**Feasibility study**: carry out initial feasibility and sizing studies.
2	**Define preliminaries**: select technical solutions; study solutions and assess the feasibility of each one by identifying cost, operational, scheduling and organizational constraints.
3	**Define the project in detail**: express and finalize requirements and confirm the technical feasibility of the chosen solution based on the results of the studies.
4	**Carry out and qualify the project**: manufacture or acquire the space system and test its various components to qualify their performance.
5	**In-orbit phase**: satellite launch and constraints to be met with the launch organization and the first connection with the satellite in orbit.
6	**Operational phase**: data acquisition and satellite control.
7	**Service withdrawal phase**: close the project.

Table 1.2. *Design phases of a CubeSat nanosatellite*

Phase	ESA	NASA
0	Mission Analysis/Requirements Analysis (MDR)	Design studies (MCR)
1	Feasibility study (PRR)	Feasibility study (SRR-MDR)
2	Preliminary definitions (PDR)	Preliminary design (PDR)
3	Detailed definitions (CDR)	Final design and manufacturing (CDR-SIR)
4	Production/Qualification Test (AR)	System assembly, Integration/Testing (SAR-ORR)
5	Launch	Launch
6	Operation	Operations

Table 1.3. *ESA/NASA phases in satellite design*

COMMENT ON TABLE 1.3.– *MDR: mission definition review; PRR: preliminary requirements review; PDR: preliminary definition review; CDR: critical design review; AR: acceptance review; MCR: mission concept review; SRR: system requirements review; MDR: mission definition review; PDR: preliminary design review; CDR: critical design review; SIR: system integration review; SAR: system acceptance review; ORR: operational requirement review.*

1.5. Building a spacecraft

1.5.1. *Spacecraft subsystems*

A spacecraft such as a satellite or an orbiter is generally decomposed into two sub-assemblies [MEF 22b].

The *platform* (bus) is a device designed to support one or more payloads. It must provide the resources needed for proper operation under the required conditions.

The platform's main functions are:

– supporting structure and mechanisms;

– thermal control of equipment;

– propulsion and in-orbit attitude modification systems;

– energy storage and distribution;

– in-orbit attitude control to modify vehicle orientation and telemetry;

– remote control and vehicle location with a GPS device;

– onboard data processing, storage and management.

The *payload* is the set of elements designed to fulfill a scientific, commercial or military mission.

These are generally measuring or observation devices that collect data in line with the mission objectives, such as:

– the telescope;

– the spectrometer with the different UV, VIS, NIR, MIR, IR channels;

– the antennas;

– the LiDAR;

– the radiometer.

Examples of payloads are shown in Table 1.4. Their functions and the type of orbit associated with their observations are briefly described.

Payloads	Functions	Orbit type
Telescopes → Newton-type telescope → Two-mirror telescope (Cassegrain, Ritchey-Chrétien) …	Mirror telescope for small-field observation (a few degrees) and high spatial resolution (a few arcs) → Sun	Low orbit Heliosynchronous Geostationary
Radiometers → Measurement of emitted, diffused or reflected luminous flux	Imaging and radiation balances	Low orbit Heliosynchronous Geostationary
Lidars → Doppler (for speed measurements) → Pulsed (for distance or concentration measurements)	Measurements of concentrations, temperatures, species detection (water vapor, CO_2, etc.), velocity	Very low orbit Balloons Planes
Spectrometers → Vertical → Imager	Vertical atmospheric sounding or multi-spectral imaging	Low orbit Geostationary

Table 1.4. *Payloads and main functions*

1.5.2. *Example of an optical payload*

Optics is used in a wide range of instruments, such as altimeters, gyrometers, optical telecommunication and metrology systems, atomic clocks for service equipment, and equipment for observation and measurement in scientific experiments.

Onboard instruments are part of the satellite or orbiter payload. Figures 1.11 and 1.12 show examples of payloads for optical measurements using the Sun as a light source. The optical diagram of the space mission telescope is shown in Figure 1.11(a). It is a Ritchey–Chrétien telescope (specific Cassegrain) designed to eliminate the optical aberration known as “coma”. This space telescope acquired images of the Sun in the UV, visible and NIR wavelengths from June 2010 to mid-2014. Figure 1.11(b) shows the optical diagram of the SOLSPEC instrument. This is a Czerny–Turner spectrometer (double monochromator) that operated on board the International Space Station. This instrument measured the solar spectrum between 165 nm and 3,000 nm over approximately one solar cycle (from 2008 to 2017). Figure 1.12 shows a schematic diagram of a space radiometer. This design corresponds to that of the DIARAD instrument, which has been used on several space missions. In particular, it was used on board the SoHO solar and heliospheric observatory, which was launched into orbit in 1995 – and is still operational today. The aim of the DIARAD radiometer is to measure the total solar irradiance at the top of the atmosphere. This measurement is of major interest, as it enables us to track the evolution of solar flux over time.

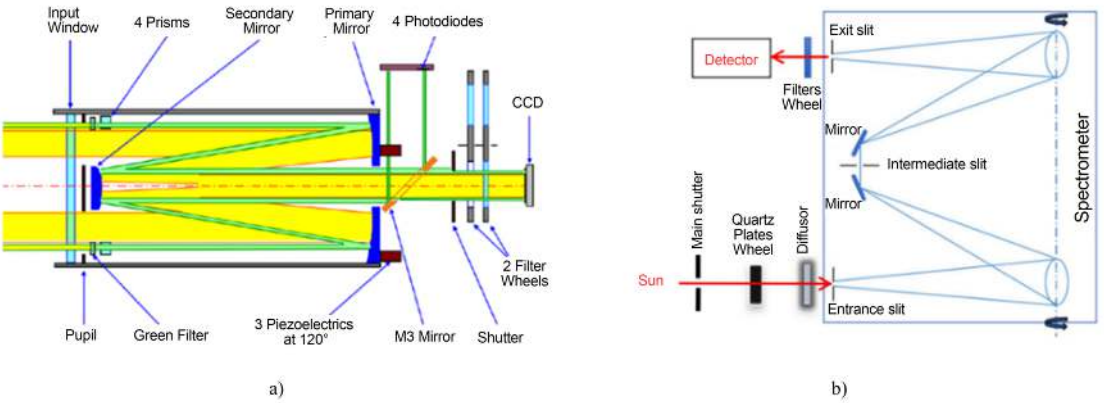

Figure 1.11. *Space instruments for observing the Sun.*
a) Ritchey–Chrétien telescope. b) Czerny–Turner spectrometer

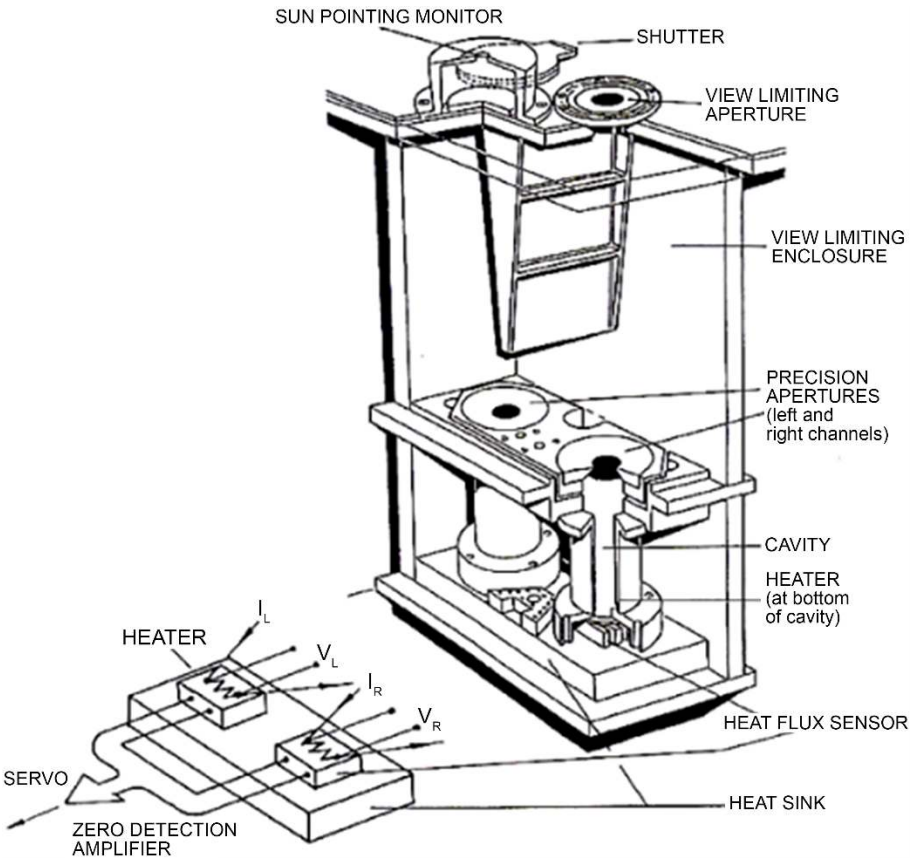

Figure 1.12. *Radiometer used to measure total solar irradiance*

Figure 1.13 shows an example of a LiDAR dedicated to the observation of atmospheric parameters. This is a ground-based laser remote sensing system based on a remote measurement technique that analyzes the properties of a beam of light reflected back to its transmitter. This device is installed at the Dumont-d'Urville base on Petrels Island, a few kilometers from Antarctica. This instrument can be used to measure aerosols, cirrus clouds and polar stratospheric clouds. Ground-based measurements are particularly interesting. They can be coupled with observations from space.

One of the challenges is to develop micro-LiDARs on board satellites to observe scientific variables of interest.

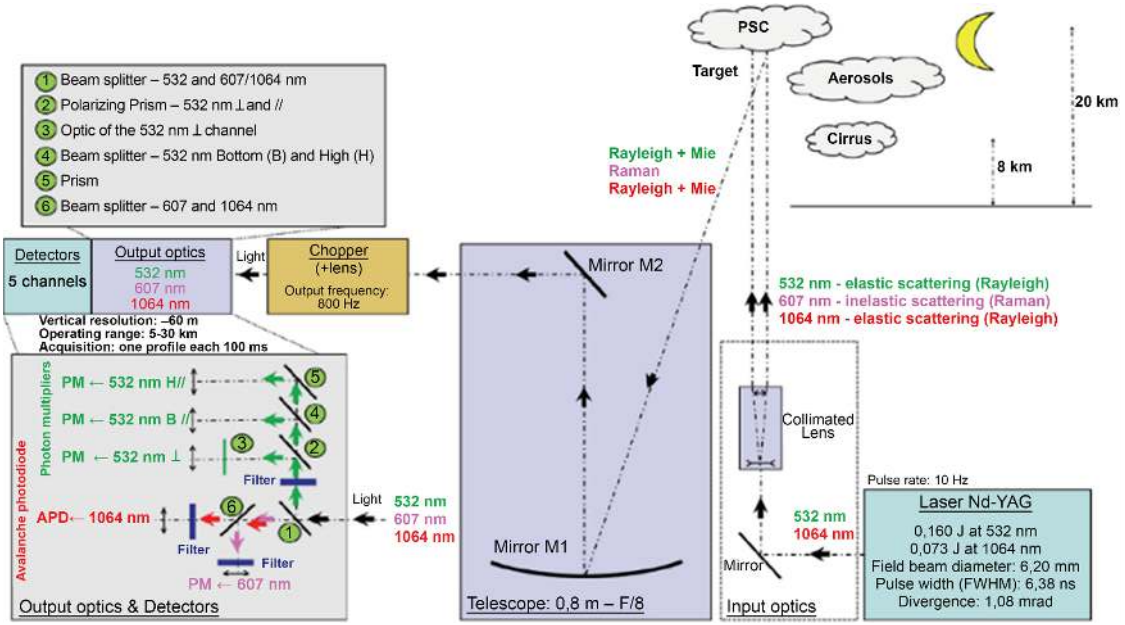

Figure 1.13. *Optical system for LiDAR measurements*

1.6. The digital twin of a space vehicle

The concept of the "digital twin", also known as the "mirror image" of the satellite system, was first proposed in the 1960s during the Apollo program.

NASA's system was used to drive back Apollo 13 (launched April 11, 1970) to Earth:

> Behind the scenes at NASA, there were 15 simulators used to train astronauts and mission controllers in all aspects of the mission, including several failure scenarios (some of which proved useful in averting disaster in Apollo 11 and 13, edla). The simulators represented one of the most complex technologies in the entire space program: the only real things in simulation training were the crew, cockpit and mission control consoles, everything else was an imaginary world created by a bunch of computers, lots of formulas and skilled technicians.

The idea was that if we created a digital representation of a physical object, we could then use it to better understand how it works and eventually control the physical object in its environment, particularly if the latter changes.

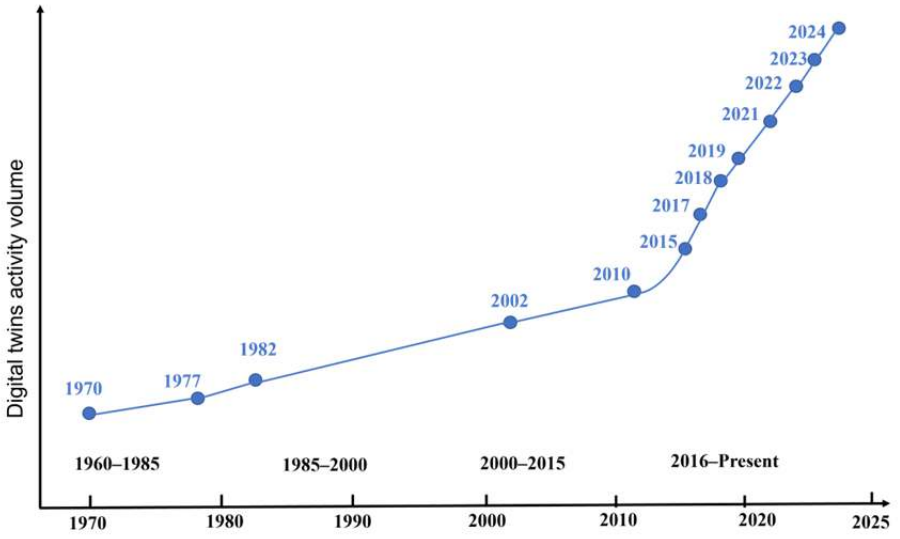

Figure 1.14. *Development of digital twin technology*

Figure 1.14 shows the development of this technology, which originated in the space industry. It has been made possible by the increasing digitization of processes in the manufacturing and service industries in the context of Factory 4.0 – a concept proposed in Germany in 2011 – and the democratization of the Internet of Things (IOT). The term "digital twin" (DT) was proposed by Michael Grieves of the University of Michigan in 2002 in connection with product lifecycle management [GRI 02, 05, 06, 16, GLA 12, DAH 22, 23, XIA 22].

A few dates represent key milestones in the development of digital twin technology:

– 1970: NASA uses matching technology for the Apollo 13 mission;

– 1977: flight simulators with numerical simulations were introduced;

– 1982: Autodesk launches AutoCAD, used to produce 2D and 3D models;

– from 1982 to 2002: AutoCAD became popular and was used in the design and engineering departments of almost all industries;

– 2002: Michael Grieves presents the concept of the digital twin at the University of Michigan;

– 2010: NASA and the USAF (US Air Force) publish articles on the digital twin;

– 2015: general electric "digital twin" wind farm initiative;

– 2017: the digital twin is ranked among the top 10 technology trends by Gartner;

– 2018: major software and industrial companies include the digital twin in their portfolio;

– 2019: the digital twin for rapid qualification of 3D-printed metal components;

– 2021: first international conference on digital twin technologies ICDTT 2021;

– 2022: proceedings of the first digital twin and edge AI workshop for industrial IoT, AIIOT '22;

– 2023: digital twins via data-driven strategies integrating a graphical neural network and IoT data;

– 2024: first international symposium on digital twins for healthcare.

A digital twin can be broken down into parts:

– the physical part, which has the ability to detect, monitor and actuate;

– the virtual or digital part, which has the capacity to link data and store information;

– the data part, which comes from the connection between the virtual and physical parts, and has the capacity to simulate, predict, optimize and delegate tasks to AI agents.

A spacecraft such as a satellite or orbiter is usually broken down into sub-assemblies. Its digital twin is a digital representation of these sub-assemblies. Sensors are implemented on the satellite to supply its digital twin with data in operational mode. This data constitutes in situ information, which engineers can use to analyze operational functions and optimize satellite operation.

Figure 1.15 shows the concept of the digital twin.

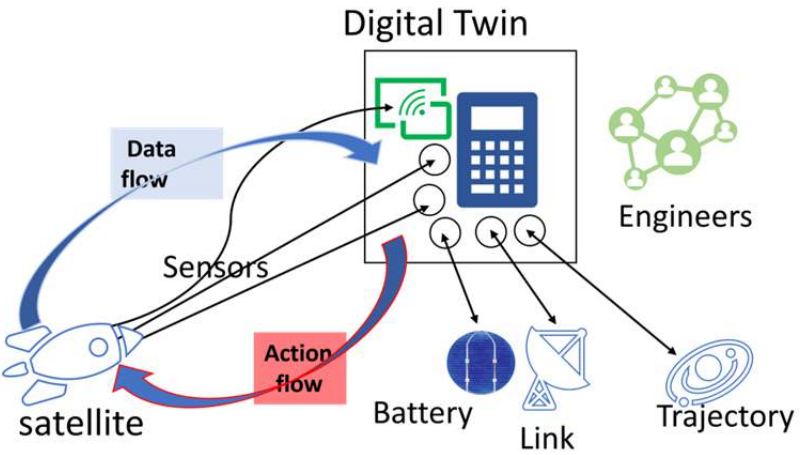

Figure 1.15. *Figure illustrating the concept of a satellite's digital twin*

It also provides useful feedback for future design and operation. For example, engineers can determine which parts wear out first and/or quickly. They can assess under which conditions the battery has to supply a lot of electrical energy and discharge faster. They can optimize the operation of sensors that retrieve information in operational mode for insurance companies and organizations verifying compliance with legal standards. Real-time satellite tracking, for example, can be used to acquire weather data, assess the state of atmospheric warming and track the flow of particles in the atmosphere.

Engineers can use the accumulated data from a large number of these digital twins to refine future satellite designs. They can optimize their performance in a system approach with a feedback effect, as shown in Figure 1.16.

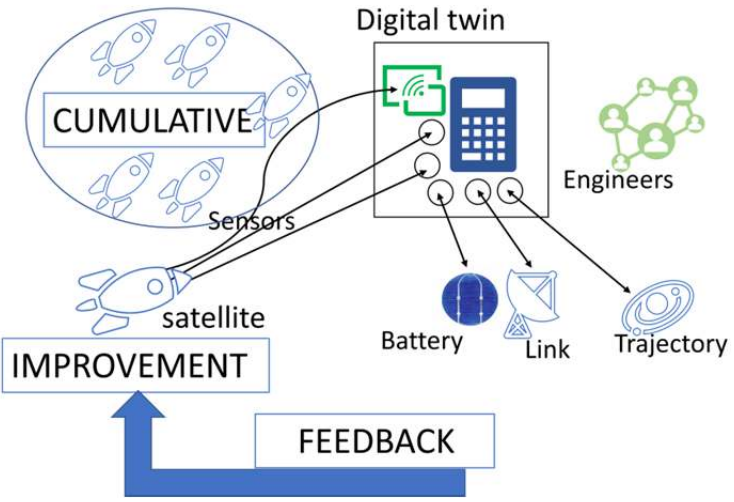

Figure 1.16. *Feedback from the digital twin of a satellite*

A *cognitive digital twin* is a virtual replica of a physical system or process that uses artificial intelligence (AI) and machine learning algorithms to simulate, predict and optimize its performance. Unlike a traditional digital twin, which focuses on monitoring and collecting data from physical assets, a cognitive digital twin is designed to learn and improve from the data collected. It uses advanced analytics and AI to identify patterns, predict outcomes and optimize its performance.

1.7. Conclusion

This chapter has covered the space age since its kick-off in 1957, describing its evolution, innovations and development prospects. It traces this evolution over a period of some three quarters of a century up to the NewSpace era, covering the diversity of both its context and its handling through numerous innovations in technologies and methods. The various sources of motivation that are worth noting: from rivalries between different political systems and underlying military activities, to research activities in the quest for knowledge, leading to the development of nanosatellites, or the realization of the dream of space travel and conquest, not to mention the socio-economic activities made possible, such as weather forecasting through more precise knowledge of atmospheric dynamics, data telecommunications for radio, television or the Internet, and the development of new digital-based technologies such as the Internet of Things or digital twins. In this respect, NewSpace and its expectations in terms of economic activities, production,

exchange and consumption should be conceived according to principles of systemic organization integrating humans and their environment. This is the approach developed by Passet in his book *L'économique et le vivant* [PAS 79], for whom the reproduction of the economic sphere cannot be thought of independently of the environment that encompasses and supports it.

1.8. Appendix

1.8.1. *Worldwide satellite development*

As described in section 1.1, Sputnik 1 and Explorer 1 were the first Soviet and American satellites launched in 1957 and 1958 respectively. They were technically classified as SmallSats. With the exception of Sputnik 2 and 3, all of the satellites launched in the 1950s were SmallSats, including Luna 1, 2 and 3 to the Moon's surface in the 1960s. SmallSats continued to be used in many countries for a variety of applications, as the launchers available could not lift heavier payloads until the 1960s.

The USSR's Strela constellation was developed for military communications, while in the USA, Ranger 7, 8 and 9, as well as Lunar Orbiter 1–5, were launched to study the Moon. SmallSats were also used in the Mariner (Mars probes) and Pioneer (interplanetary science) programs.

Countries other than the USA and USSR began launching SmallSats in the 1960s, the first being Canada's Alouette 1 and 2 and ISIS-1, the UK's Ariel 1 and 3, Italy's San Marco 1, France's Asterix and FR-1, etc. Most of these satellites carried instruments for measuring radiation, electric and/or magnetic fields, as well as for telecommunications experiments.

China, Japan, Czechoslovakia and India joined the movement in the 1970s with Dong Fang Hong 1 (173 kg), Ohsumi and Shinsei (24 kg and 64 kg), Magion 1 (15 kg) and Aryabhata (360 kg), respectively. Spacefaring nations considered as small ones continued to launch a few SmallSats, but thanks to increased launch capacities, the USA and the Soviet Union expanded their mission portfolios with larger satellites, such as those for the Viking or Mariner programs in the USA, or the Luna, Mars and Venera programs in the Soviet Union.

SmallSats continued to be used by the major space nations, but in smaller numbers and for more specific missions, such as Pioneer 10 (260 kg) in interplanetary space or Uhuru (141 kg) for X-ray spectroscopy astronomy. In a first case of "piggybacking", a 35 kg PFS-1 "subsatellite" was even superimposed on Apollo 15 and 16 in the 1970s to study the lunar environment [LIN 75].

In the 1980s, other nations began to gain direct access to space with large satellites, such as Bulgaria 1300, a 1,500 kg satellite from Bulgaria, or Morelos 1, a 650 kg satellite from Mexico. The first satellite launched by Israel in 1988, the 155 kg Ofeq-1, was a SmallSat. Most of the nations that had already gained access to space launched large satellites, with a few exceptions such as Japan's 216 kg Tenma, for X-ray spectroscopy astronomy, and Czechoslovakia's Magion program, with a 52 kg satellite.

Large satellites were generally conceived in the 1990s, with a few exceptions such as Japan's launch of Hiten and its Hagoromo sub-satellite, with a total mass of 197 kg, which were the first non-American, non-Soviet satellites to reach the Moon. After that, a growing number of countries took an interest in space. All of them launched SmallSats, including North Korea and Argentina, with the exception of Turkey.

The golden age of satellite design, no longer limited by the launch capabilities of SmallSats, began in the 2000s. Today, most small spacecraft developed are CubeSats (1U CubeSat is a 10 x 10 x 11.35 cm cube), which are standardized nanosatellites (cubesat.org) that were created in 1999 at Stanford and Cal Poly San Luis Obispo universities. The introduction of this standard democratized the transport of such spacecraft in spring-loaded deployers (also known as P-PODs), considerably facilitating access to space for this class of satellites. Similarly, standardized subsystems have emerged that enable a CubeSat project to be built from scratch and launched typically after a maximum of three years of development, with an associated cost of approximately 500,000 USD per unit. Today, CubeSats are used in a variety of programs for scientific, military and/or commercial applications, mainly in LEO, and more recently in interplanetary space too. Scientific spin-offs with SmallSats have been discussed in various groups such as COSPAR [MIL 19], NASA [TAN 21] and the Keck Institute [NOR 14].

SmallSats are currently used for scientific missions in the fields of heliophysics, astrophysics, earth sciences, planetary sciences, astrochemistry and astrobiology.

Examples include heliophysics missions such as MinXSS [MOO 18] and MinXSS-2 [MAS 20] to measure solar soft X-ray spectra, CeREs [KAN 18] to measure radiation belt electron excitation and loss, spectra and microbursts, CuPID [WAL 21] to measure soft X-rays emitted by the solar wind, and Picard to measure total solar irradiance and absolute spectral irradiance [COR 13, MEF 16].

INSPIRE, International Satellite Program in Research and Education, includes several CubeSats in orbit for exploring the ionosphere [EVO 18], studying the Earth's radiation budget (BRT or ERB: Earth Radiative Budget) [MEF 21] and probing the ionosphere [CHI 22]. The CubeSats (UVSQ-SAT and INSPIRE SAT-7) operated by

LATMOS are part of this program. A third French CubeSat, UVSQ SAT NG, has been developed for launch in 2025.

Although military applications are not well documented, in recent years, defense agencies have been acquiring commercial data from SmallSats constellations, showing an interest in such missions. Military SmallSats missions include the ELISA constellation, based on the Myriade platform, which is a constellation of the French military [DAN 19]. The US Naval Research Laboratory Graduate School is also interested in the satellite class, as evidenced by the launch of NPSAT-134 in 2019 for education and technology [SAK 02, 06, NPS 19].

Many publications now rely on imagery data from commercially available constellations such as PLANET (DOVE constellation), such as tropical forest carbon stock [CSI 19] or coral reef assessment [ASN 17]. Spire also provides Earth observations and GNSS-R data to NOAA and NASA [JAL 20].

The number of missions under development is now booming. Capabilities and technologies are becoming ever more advanced, not only in the military field, but also in scientific and commercial applications [KOS 19, JAN 23, SON 24].

1.8.2. *Electromagnetic theory*

This appendix gives a summary of the equations and other theorems essential for understanding electromagnetic phenomena, and in particular for interpreting the existence of the Van Allen belts (see Figure 1.1) and the aurora borealis. Further details on their application can be found in specialized books [MAX 54, BRU 65, FEY 65, LAN 66b, 69, DEB 68, MIZ 72, JAC 98, HEC 05]. For readers unfamiliar with the notions of scalar (one value), vector (three values or three components) and operations on these quantities, please refer to the appendix in Chapter 2 of this book.

The work of Dufay (1698–1739) and Benjamin Franklin (1706–1790) led to the postulation of the existence of two types of charge, positive and negative. In 1799, Volta invented the battery as a source of electrical energy. In an electrically conductive wire, an electric current can be made to flow, which is the movement of a set of particles carrying an electric charge. These particles are called “electrons”, a term rooted in the Greek word amber. This term comes from Thales of Miletus, who identified the electrification of objects by friction in the 6th century BCE, 600 years before the modern era, or 27 centuries ago. In 1802, André-Marie Ampère (1775–1836) proposed the concept of electric current to explain the discharge of the Volta battery. The study of circuits and currents is one of the phenomena studied in electrokinetics.

Electrostatics is the part of physics that studies phenomena related to static-electrified bodies (positive and negative charges), and magnetostatics is the part of physics that studies phenomena related to moving electrified bodies.

In electrostatics, the space around a point charge Q (unit of charge: coulomb, symbol: C) or a charge distribution (see Figure 1.17) can be assimilated to a polar vector field (see the appendix in Chapter 2) that can act on charged objects. This vector field is called the "electric field" or "electrostatic field" of the charge Q placed in P, whose expression $\vec{E}(M)$ (unit of $\vec{E}(M)$: volt per meter, V/m) at point M is given by Coulomb's law, such that:

$$\vec{E}(M) = \frac{1}{4\pi\varepsilon_0}\frac{Q\overrightarrow{PM}}{\|\overrightarrow{PM}\|^3} = \frac{1}{4\pi\varepsilon_0}\frac{Q\,\overrightarrow{u_r}}{r^2} \qquad [1.1a]$$

where P is the point where this charge is located, ε_0 is the electrical permittivity of vacuum ($\varepsilon_0 = 8.854\ 10^{-12}\ \frac{F}{m}$ or $\frac{1}{4\pi\varepsilon_0} = 9\ 10^9\ \frac{Nm^2}{C^2}$) and r is the distance between P and M. The electric field of a charge Q is the force per unit charge around the charge Q. It is a polar vector, so the electric field is parallel to planes of symmetry and perpendicular to planes of antisymmetry.

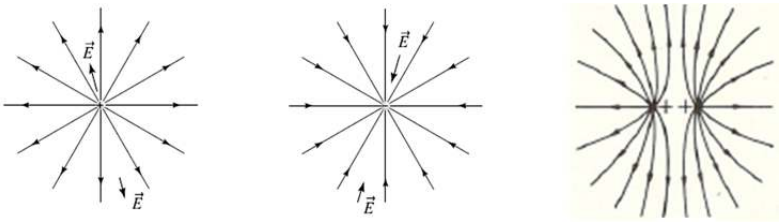

a) A charge > 0 b) A charge < 0 c) Two charges > 0

Figure 1.17. *Electric field around point charges*

It should be noted that the notion of field was first formulated in magnetism, following the work of Faraday, by determining the properties of a magnet (see Figure 1.18) consisting of a north pole and a south pole. The field lines follow a trajectory from the north pole to the south pole. Unlike electrical phenomena, which are due to the existence of two types of charge, it is not possible to isolate magnetic charges, so every magnetic system has a north and a south pole. Quantum theory, by postulating the existence of spin variables in the quantum domain, has made it possible to explain the physical phenomenon whereby transition elements such as iron, cobalt and nickel lead to magnets, which is not possible with other transition elements. Explanations of these phenomena can be found in works dealing with quantum theory [KEM 37, MES 64, COH 73, LAN 75, SAK 11]. In Chapter 4 of [DAH 16], we have given some background on this phenomenon.

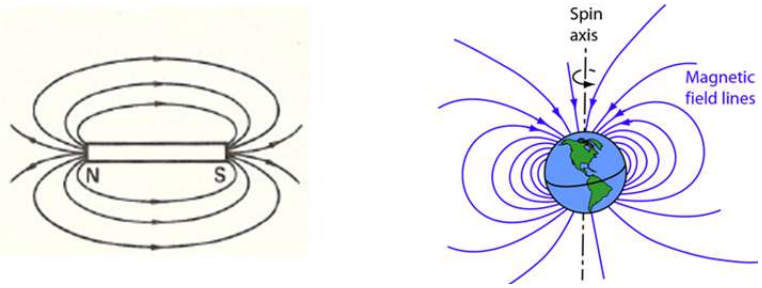

a) A magnet b) The Earth

Figure 1.18. *Magnetic field around a magnet or the Earth*

Any point charge q in space is subjected to a force given by $\vec{F}(M) = q\vec{E}(M)$. Coulomb's law can then be expressed as the force exerted by Q on q, between two point charges, in the following form:

$$\vec{F}(M) = \frac{1}{4\pi\varepsilon_0}\frac{Qq\overrightarrow{PM}}{\left\|\overrightarrow{PM}\right\|^3} = \frac{1}{4\pi\varepsilon_0}\frac{Qq\,\overrightarrow{u_r}}{r^2} \qquad [1.1b]$$

In magnetostatics, the space around a charge or a distribution of charges in permanent motion (see Figure 1.19) can be assimilated to a field of axial vectors $\vec{B}(M)$ (unit of $\vec{B}(M)$: tesla, T) (see the appendix in Chapter 2), which can act on charged objects. This field of vectors is called a "magnetic field" or "magnetic induction field", whose expression $\vec{B}(M)$ at point M for a point charge q moving with velocity $\vec{v}$ at point P (see Figure 1.19(a)) is given by Biot and Savart's law, such that:

$$\vec{B}(M) = \frac{\mu_0}{4\pi}\frac{q\vec{v}\wedge\overrightarrow{PM}}{\left\|\overrightarrow{PM}\right\|^3} = \frac{\mu_0}{4\pi}\frac{q\vec{v}\wedge\overrightarrow{u_r}}{r^2} \qquad [1.2a]$$

where P is the point where this charge is located, μ_0 is the magnetic permeability of vacuum ($\mu_0 = 1.256\ 10^{-6}\ \frac{H}{m}$ or $\frac{\mu_0}{4\pi} = 10^{-7}\ \frac{Tm}{A}$), and r is the distance between P and M. The fact that the $\vec{B}(M)$ field is the vector product between $q\vec{v}$ and $\overrightarrow{PM}$ gives it symmetry properties different from those of the electric field, particularly in a reflection in a plane of symmetry. The magnetic induction field is perpendicular to the symmetry planes and parallel to the antisymmetry planes.

If we consider the magnetic field of a set of charges in permanent motion, such as a current I flowing through a wire (see Figure 1.19(b)), equation [1.2a] shows that the expression of this field is given by the following equation:

$$d\vec{B}(M) = \frac{\mu_0}{4\pi}\frac{Id\vec{l}\wedge\overrightarrow{PM}}{\left\|\overrightarrow{PM}\right\|^3} = \frac{\mu_0}{4\pi}\frac{Id\vec{l}\wedge\overrightarrow{u_r}}{r^2} \qquad [1.2b]$$

where P is the point where the oriented $d\vec{l}$ wire element carrying current I is located, μ_0 is the magnetic permeability of vacuum and r is the distance between P and M.

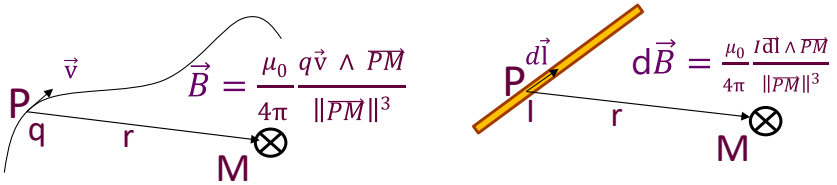

a) A point charge: q b) A set of charges: I

Figure 1.19. *Magnetic field around permanently moving charges*

In the static regime (independent of time), the work of the electric force from point A to point B does not depend on the path followed, because it is a conservative force. This property can be translated for the electric field by saying that the circulation of the field between two points A and B does not depend on the path followed, meaning that on a closed contour, this circulation is zero (Kirchhoff's second law or loop rule for voltages):

$$\oint \vec{E}(M) d\vec{l} = 0 \qquad [1.3a]$$

It is then possible to postulate the existence of an electric potential V from which the electric field is derived via the following relation:

$$\vec{E}(M) = -\overrightarrow{\text{grad}V} \qquad [1.3b]$$

Just as the electric force of a point charge q in the electric field of a source charge is given by $\vec{F}(M) = q\vec{E}(M)$, we can determine the electrical potential energy acquired by the charge q by the product W = qV.

Electrical phenomena can therefore be interpreted by means of an electric field if electric force is of interest, or an electric potential if electric energy is of interest.

Using the Stokes–Ampère theorem:

$$\oint \vec{E}(M) d\vec{l} = \iint curl\vec{E}(M) d\vec{S} \qquad [1.3c]$$

under static conditions, the property of null circulation of the electric field can be expressed by the following Maxwell equation:

$$\overrightarrow{curl}\vec{E} = \vec{0} \qquad [1.3d]$$

Note that equation [1.3d] is compatible with relation [1.3b], since we have:

$$\overrightarrow{curl}\vec{E} = -\overrightarrow{curl}\overrightarrow{\text{grad}}V = \vec{0} \qquad [1.3e]$$

In the case of the magnetic induction field $\vec{B}$, the magnetic force $\vec{F}$ is expressed differently depending on whether we are considering a point charge moving at speed $\vec{v}$, in which case, the force has the expression:

$$\vec{F} = q\vec{v} \wedge \vec{B} \qquad [1.4a]$$

or depending on whether we consider a set of charges moving in steady state in a wire in the form of a current I, in which case, the elementary force $d\vec{F}$ over an elementary length of wire $d\vec{l}$ has the expression:

$$d\vec{F} = Id\vec{l} \wedge \vec{B} \qquad [1.4b]$$

Expressions [1.4a] and [1.4b] are called Lorentz and Laplace forces, respectively.

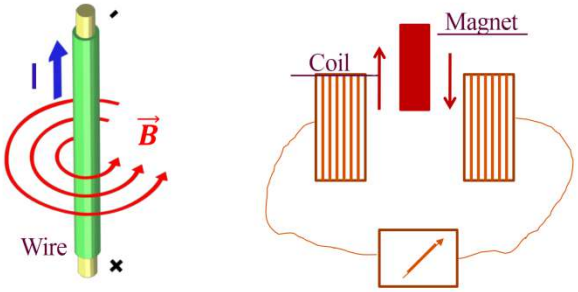

a) Static $\vec{B}$ field around a wire

b) Variable $\vec{B}$ field inside a coil

Figure 1.20. *Static and dynamic magnetic fields*

In the case of a wire carrying a current I, the magnetic field lines are circular. By integrating the expression in [1.2] for a wire of length l tending toward infinity, we can show that the expression for this field at point M, at a distance of r from the center of the wire in a perpendicular plane, is given by:

$$\vec{B}(M) = \frac{\mu_0 I}{2\pi r}\vec{u}_\varphi \qquad [1.5a]$$

$\vec{u}_\varphi$ is the unit vector tangent to the circle of radius r (see the appendix in Chapter 2).

If the wire is placed in a magnetic field, the total force on the wire of length l is given by:

$$\vec{F} = BIl\vec{u}_{\perp} \quad [1.5b]$$

$\vec{u}_{\perp}$, the unit vector that gives the orientation of the force $\vec{F}$, is perpendicular to the wire and the field $\vec{B}$.

When the physical situation presents symmetries such as the wire of length l assimilated to a wire of infinite length through which a current I flows (see Figure 1.20(a)), we can use the Stokes–Ampère theorem to show that the circulation of $\vec{B}(M)$ on a closed contour is as follows:

$$\oint \vec{B}(M)d\vec{l} = \mu_0 I = \mu_0 \iint \vec{j}d\vec{S} = \iint \overrightarrow{curl}\vec{B}(M)d\vec{S} \quad [1.6a]$$

where $\vec{j}$ is the current density vector passing through the oriented surface that lies on the closed contour. Note that the current I, which is the amount of charge passing through the surface S per unit time $I = \frac{dq}{dt}$, is also given by the flux of $\vec{j}$ through this surface $I = \iint \vec{j}d\vec{S}$.

Applying this theorem, we can easily show, given the symmetry properties of the magnetic field $\vec{B}(M)$, that its expression is indeed given by equation [1.5a], hence $\frac{\mu_0 I}{2\pi r}\vec{u}_{\varphi}$.

Furthermore, it allows us to show, in the static regime, another Maxwell equation, which is given by:

$$\overrightarrow{curl}\vec{B} = \mu_0\vec{j} \quad [1.6b]$$

In the static regime, it can be shown that this relationship leads to the conservation law of the current density vector $\vec{j}$ (Kirchhoff's first law or junction rule for current) by applying the div operator to both terms of the equation, so that:

$$div\overrightarrow{curl}\vec{B} = 0 = \mu_0 div\vec{j} \Rightarrow div\vec{j} = 0 \quad [1.6c]$$

In the variable regime (time dependent), experiments on the effects of magnetic fields led to the laws of Lenz (1834) and Faraday (1831), which show that when the flux of the magnetic field $\vec{B}$ through a circuit varies (see Figure 1.20(b)), an electromotive force on the mobile charges (the electrons) gives rise to a current that flows through the circuit. The direction of this current is such that it produces a field $\vec{B}'$ which tends to cancel out the variation in the variable magnetic field $\vec{B}$.

The Lenz–Faraday law is expressed as:

$$e = -\frac{d\Phi}{dt} \qquad [1.7a]$$

where e is the potential difference that gives rise to the current and $\Phi = \iint \vec{B} d\vec{S}$ is the flux of $\vec{B}$ across the surface crossed by the circuit.

Given the relationship between an electric field and the potential difference [1.3a], it is possible to express e as the circulation of an electromotive electric field, such that:

$$\oint \vec{E}(M) d\vec{l} = e = -\frac{d\Phi}{dt} = -\frac{\partial}{\partial t} \iint \vec{B} d\vec{S} \qquad [1.7b]$$

This electromagnetic induction phenomenon is used in many applications (motors, generators, transformers, induction plates, eddy currents) and is studied in electrical engineering for its industrial applications. Applying the Stokes–Ampère theorem [1.3c], equation [1.7b] leads, in the dynamic (time-varying) regime, to the following Maxwell equation:

$$\overrightarrow{curl}\vec{E} = -\frac{\partial \vec{B}}{\partial t} \qquad [1.7c]$$

which differs from equation [1.3d], valid in the static regime, and is to be compared with equation [1.6b]. To symmetrize the effect of $\vec{B}$ and $\vec{E}$ in a time-varying regime, Maxwell proposed the following equation:

$$\overrightarrow{curl}\vec{B} = \mu_0 \vec{j} + \mu_0 \varepsilon_0 \frac{\partial \vec{E}}{\partial t} \qquad [1.7d]$$

from which it can be shown that visible light is only a small part of a much broader spectrum of electromagnetic waves, all propagating at the same speed as light.

Note that from Maxwell's postulate, we can associate a displacement current with the variation of the electric field as a function of time, such that:

$$\vec{j}_D = \varepsilon_0 \frac{\partial \vec{E}}{\partial t} \qquad [1.7e]$$

In a dynamic regime or time varying operation, this current is used to interpret the coupling that can occur between the two plates of a capacitor.

Finally, application of Gauss's theorem allows us to connect the electric field flux $\vec{E}$ across a closed surface to its sources expressed as a charge density, such that:

$$\oiint \vec{E} \cdot d\vec{S} = \iiint \text{div}\vec{E} d\tau = \frac{1}{\varepsilon_0} \iiint \rho d\tau \quad [1.8a]$$

where $\Phi = \oiint \vec{E} \cdot d\vec{S}$ is the flux of $\vec{E}$ through a closed surface, $\iiint \rho d\tau$ is the amount of charge contained within the surface and ε_0 is the electrical permittivity of vacuum.

The volume integral $\iiint \text{div}\vec{E} d\tau$ is the transformed form of the flux Φ by Green–Ostrogradski's theorem. This gives us the first Maxwell equation (Maxwell–Gauss) between the divergence of the electric field and its sources, such that:

$$\text{div}\vec{E} = \frac{\rho}{\varepsilon_0} \quad [1.8b]$$

Given the absence of magnetic charges in volume, we obtain the following expression in the case of field $\vec{B}$:

$$\text{div}\vec{B} = 0 \quad [1.8c]$$

The last expression leads us to postulate the existence of a vector potential $\vec{A}$ (the analogue of the scalar potential V associated with the electric field), such that:

$$\vec{B} = \overrightarrow{curl}\vec{A} \quad [1.8d]$$

Equation [1.8b] shows that Maxwell's postulate [1.7d] leads, by application of the div operator, equation [1.7d] to the following expression for the conservation of electric charge in the form:

$$\frac{\partial \rho}{\partial t} + div\vec{j} = 0 \quad [1.8e]$$

In steady state, equation [1.6c] holds true.

1.8.3. *Light–matter interaction*

In the context of light–matter interaction, electromagnetic waves are used to study a physico-chemical system: molecules, materials, aerosols, atmosphere and environment. The properties and characteristics of matter can be analyzed by making it interact with electromagnetic waves (see Figure 1.21).

Generally speaking, the electromagnetic wave incident on the object under study is generated in a known state using a suitable source and filter system. In space, the Sun is often used as a light source. A detection system consisting of detectors and

suitable filters is used to measure changes in the electromagnetic wave relative to its initial state at incidence. By studying changes in the characteristics of the reflected, transmitted or scattered electromagnetic wave, we can determine the properties of the system under study, or identify it when it is absorbed.

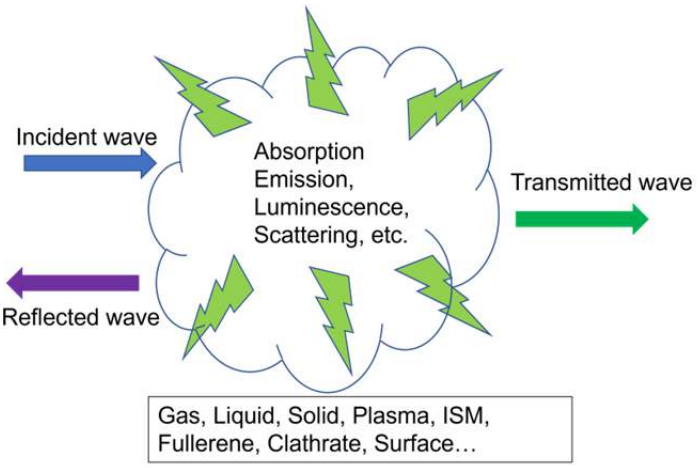

Figure 1.21. *Light–matter interaction*

Maxwell showed that electrical and magnetic phenomena can be described in a vacuum, in the presence of charges and currents, by means of four equations, whose expressions are:

$$\vec{\nabla}E = div\vec{E} = \frac{\rho}{\varepsilon_0} \quad [1.9a]$$

$$\vec{\nabla} \wedge \vec{E} = \vec{curl}\vec{E} = -\frac{\partial \vec{B}}{\partial t} \quad [1.9b]$$

$$\vec{\nabla}\vec{B} = div\vec{B} = 0 \quad [1.9c]$$

$$\vec{\nabla} \wedge \vec{B} = curl\ \vec{B} = \mu_0\ \vec{j} + \varepsilon_0 \frac{\partial \vec{E}}{\partial t} \quad [1.9d]$$

These equations, which achieve the unification of electric and magnetic phenomena, summarize the local properties of the electric field $\vec{E}$ and magnetic field $\vec{B}$ in terms of the sources ρ, the charge density vector, and j, the current density vector, and where μ_0 is the magnetic permeability of vacuum and ε_0 is the electric permittivity of vacuum.

In the MKS system of units, these fields and sources are defined by vector $\vec{E}$ in Vm^{-1}, vector $\vec{B}$ in Tm^{-1}, ρ in Cm^{-3} and j in Am^{-3}.

It can be shown that Maxwell's equations lead to a propagation equation for the $\vec{E}$ and $\vec{B}$ fields in the form:

$$\Delta \vec{F} - \mu_0 \varepsilon_0 \frac{\partial^2 \vec{F}}{\partial t^2} = \Delta \vec{F} - \frac{1}{c^2} \frac{\partial^2 \vec{F}}{\partial t^2} = 0 \qquad [1.10]$$

where $\vec{F}$ represents the $\vec{E}$ or $\vec{B}$ fields.

In electromagnetic theory, Maxwell's equations lead to the same expression for wave velocity c in vacuum in terms of the electrical permittivity ε_0 and magnetic permeability μ_0 of vacuum for all radiations (see Table 1.5). With $\varepsilon_0 = 8.86\ 10^{-12}$ Fm^{-1} and $\mu_0 = 4\pi 10^{-7}$ Hm^{-1}, c is equal to 310^8 ms^{-1} (2.9979245810^8 ms^{-1}).

The wave front carrying an electric field and a magnetic induction field moves transversely to these fields, unlike mechanical longitudinal waves whose movement is in the direction of the mechanical phenomena (compression–expansion). The energy carried by the wave travels perpendicular to the electrical and magnetic phenomena. The direction of wave propagation is parallel to the direction of $\vec{E} \times \vec{B}$, which is perpendicular to the wavefront. Thus, we define the Poynting vector $\vec{S}$ to represent the energy flux per unit time by:

$$\vec{S} = \frac{1}{\mu_0} \vec{E} \times \vec{B} \qquad [1.11a]$$

expressed in joules per second per unit area: $[J/(s.m^2)]$.

From the electromagnetic energy density, *u* is given by the formula:

$$u = \frac{\varepsilon_0}{2} \vec{E}^2 + \frac{1}{2\mu_0} \vec{B}^2 \qquad [1.11b]$$

and by using the balance equation translating the conservation of electromagnetic energy in a vacuum – for in the absence of matter there is no loss of energy, and therefore no dissipation – we can show that:

$$\frac{\partial}{\partial t} u + \mathrm{div} \vec{S} = 0 \qquad [1.11c]$$

The norm of the Poynting vector therefore represents the instantaneous power carried by the electromagnetic wave across a unit surface, perpendicular to its direction of propagation.

Maxwell's equations show that light is a transverse electromagnetic wave, which can be decomposed into two linearly independent electrical components, corresponding to the polarization of light. It propagates as two mutually coupled vector fields, $\vec{E}$ and $\vec{B}$. Table 1.5 summarizes the different domains of electromagnetic waves. Optics corresponds to the frequency range between 10^{12} Hz (far IR) and 10^{16} Hz (far UV), while the visible spectrum extends from 4 10^{14} to 8 10^{14} Hz.

Field	Associated frequencies
Cosmic rays	10^{14} GHz and above
Gamma rays	10^{10}–10^{13} GHz
X-rays	10^{8}–10^{9} GHz
Ultraviolet radiation	10^{6}–10^{8} GHz
Visible Light	10^{5}–10^{6} GHz
Infrared radiation	10^{3}–10^{4} GHz
Microwaves	3–300 GHz
Radio waves	470–806 MHz
Short waves	54–216 MHz

Table 1.5. *Electromagnetic waves and associated frequencies*

Classically, light–matter interaction can be established using Poynting's theorem, which establishes a relationship between electromagnetic energy, the Joule effect and the flux of the Poynting vector, such that:

$$\frac{\partial}{\partial t}u + \mathrm{div}\vec{S} = -\vec{j}.\vec{E} \qquad [1.11d]$$

where the term $\vec{j}.\vec{E}$ represents the Joule-effect dissipation term in the presence of matter, $\vec{j}$ being the current density vector and $\vec{E}$ being the electric field of the wave.

At the atomic or molecular scale, the process of light–matter interaction is of a quantum nature. In this case, to interpret the photoelectric effect, we must consider that light is made up of energy grains, according to Einstein's corpuscular formulation of light. Each energy grain corresponds to a quantum of energy carried by a photon.

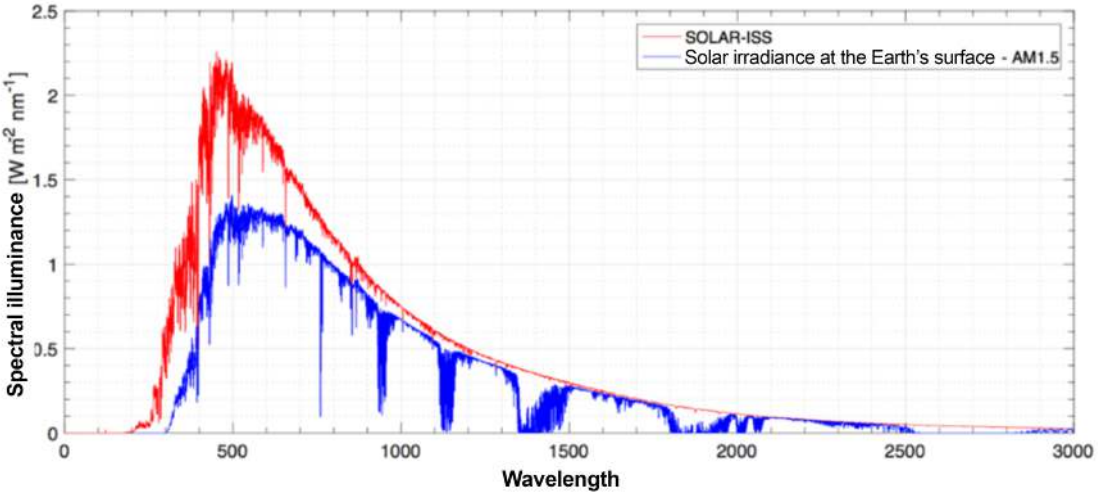

Figure 1.22. *The Sun's emission spectrum and spectral solar irradiance at the Earth's surface ([MEF 18], Solar-ISS, A & A, 2018)*

The energy E of a photon is expressed as a function of its frequency ν, such that:

$$E = h\nu \quad [1.12a]$$

and its momentum p is given by De Broglie's relation (which De Broglie applied to the electron, regarded as a particle, thus giving it wave properties) as a function of its wavelength λ:

$$p = h/\lambda \quad [1.12b]$$

Note that this interpretation a posteriori justifies the method proposed by Planck, who had hypothesized the quantization of matter in terms of oscillators capable of emitting and absorbing light in the form of energy quanta given by the relation $E = h\nu$. Although, after Maxwell's work it had been established that light is a transverse wave made up of an electric field and a magnetic induction field in a plane perpendicular (the wavefront) to its propagation, the quantization of oscillator energy had enabled Planck to interpret the emission spectrum of a black body at temperature T, such as, for example, the Sun (see Figure 1.22), by the following formula:

$$U(\nu, T) = \frac{8\pi h\nu^3}{c^3} \frac{1}{\exp\left(\frac{h\nu}{kT}\right) - 1} \quad [1.13]$$

where $U(\nu, T)$ is the spectral energy density at temperature T, h is Planck's constant and k is Boltzmann's constant.

Figure 1.22 shows different solar spectra (at the top of the atmosphere (red) and on the ground (blue)). The top-of-atmosphere spectrum was obtained with the SOLAR/SOLSPEC instrument (see Figure 1.11).

An absorption or emission corresponds to a transition between two energy levels (see Figure 1.23) by the absorption of a photon (induced absorption) or by the emission of a photon (induced or stimulated emission) as proposed by Einstein.

For each frequency range, it is customary to identify a wave by a parameter specific to the field of application, according to the scientific or user communities (see Tables 1.5 and 1.6).

In the energy scale, we use the relationship E = hν, and the electromagnetic wave is characterized by its frequency expressed in hertz (Hz). The wave can also be characterized in terms of its wave number (σ) or in electron volt (eV). A wave can also be characterized by its wavelength, expressed in nanometers (nm), microns (μm) or angströms (Å) on the momentum scale. Figure 1.24 summarizes these different notations.

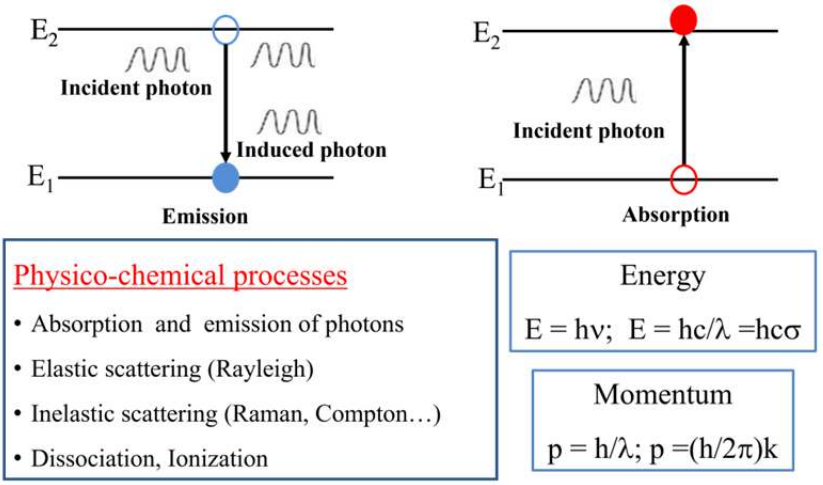

Figure 1.23. *Light–matter interaction, a quantum phenomenon*

Field of application	Associated frequencies
Sterilization	10^{14} GHz and above
Vision	10^{10}–10^{13}GHz
Photography	10^{8}–10^{9} GHz
Radar, microwaves	10^{6}–10^{8} GHz
Satellite communication	10^{5}-10^{6} GHz
UHF television	10^{3}–10^{4} GHz
VHF television VHF, FM waves	3–300 GHz
Radio waves, small waves	470–806 MHz
AM Radio	54–216 MHz
Cancerotherapy	3–25 MHz
RX-ray examination	535–1605 KHz

Table 1.6. *Frequency-dependent use*

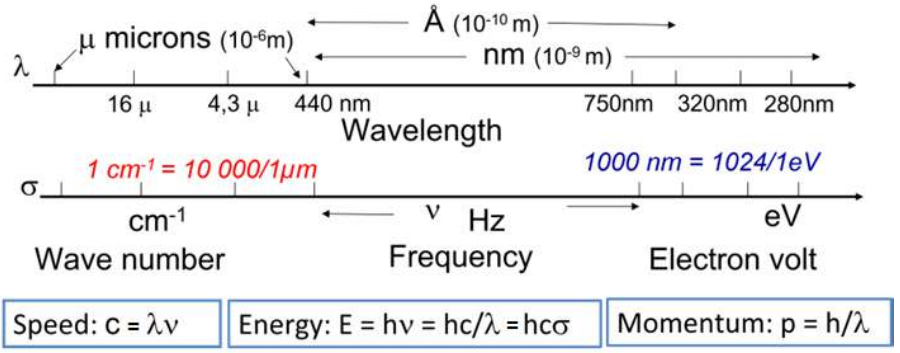

Figure 1.24. *Characterization of light in the electromagnetic spectrum*

The relationship between frequency and wavelength is $\lambda = c/\nu$, where c is the speed of light. In space, we distinguish between the optical and microwave domains, such that:

Optical domain:

– gamma rays → wavelengths < 0.3 Å;

– x-rays → wavelengths from 0.3 Å to 100 Å;

– ultraviolet (UV) → wavelengths from 10 nm to 400 nm;

– visible (VIS) → wavelengths from 400 nm to 700 nm;

– violet (400–446 nm); blue (446–500 nm); green (500–578 nm);

– yellow (578–592 nm); orange (592–620 nm); red (620–700 nm);

– infrared → wavelengths from 0.76 μm to 500 μm.

Radio-electric domain:

– microwaves and radar → wavelengths from 1 mm to 10 cm;

– radios → wavelengths greater than 10 cm.

Electronvolt (eV)	Frequency (ν)	Wavelength (λ)	Wave number (σ)	Temperature
1	2.418 10^{14} Hz	12,339 Å	8065.5 cm^{-1}	11,605 K

Table 1.7. *Scale conversions*

2

Orbital Parameters of a CubeSat

The laws of mechanics made it possible to calculate the orbit of a natural or artificial satellite around an attracting center. It took almost 4,000 years for the laws or principles of Copernicus, Kepler, Galileo, Newton and Einstein to be gradually established. These allowed us to describe the motion of a massive object in the gravitational field of the Earth or a planet, as well as the development of mechanics and its mathematical tools. For instance, given the Earth's heliocentric motion around the Sun, a satellite's orbit is calculated by applying Newton's universal law of attraction and laws of motion, which also allow us to trace Kepler's empirical laws. It should be noted that when the system of interacting particles is greater than two, it is more convenient to use the Lagrange method to calculate the particle trajectories. The orbit of a natural or artificial satellite around the center of an attractor can be circular or elliptical and positioned at different altitudes. Six so-called "Keplerian" parameters are used to describe the orbit of a satellite around the Earth in the equatorial plane, taken as the reference plane. The design of a spacecraft requires a good knowledge of its orbit. However, as each spacecraft is designed for a specific space mission, this orbit is itself a function of the type of observations that a satellite, probe or orbiter is likely to make while moving in the particular orbit. Lower altitudes are preferred for high-resolution observations, and higher altitudes cover a large area in a single observation, implying lower spatial resolution. A compromise between these two spatial coverage possibilities is generally achieved by choosing an elliptical orbit. This provides high spatial resolution but low coverage around the periastron (*periapsis*), the closest point to the planet under observation in the plane of the orbit, and high coverage but low spatial resolution around the apocenter (*apoapsis*), the furthest point from the planet in the same plane.

For a color version of all of the figures in this chapter, see www.iste.co.uk/dahoo/nanosatellites1.zip.

2.1. Using conics to describe a satellite orbit

2.1.1. *Conics*

The Earth moves in an ellipse around the Sun. An ellipse is a section of a cone, called a conic. In Euclidean geometry, a conic can be obtained by the intersection of a plane with a cone of revolution, as shown in Figure 2.1, for different conics: the parabola, the circle, the ellipse or a hyperbola.

The locus of the points of a conic is defined by a straight line called the "directrix" and a point called the "focus". The directrix is the straight line which, together with the point called the focus, defines a conic as the locus of points whose distance from the focus is proportional to the horizontal distance from the directrix, e being the constant of proportionality (see Figure 2.2(a)).

If e = 1, the conic is a parabola, if e < 1, it is an ellipse, and if e > 1, it is a hyperbola.

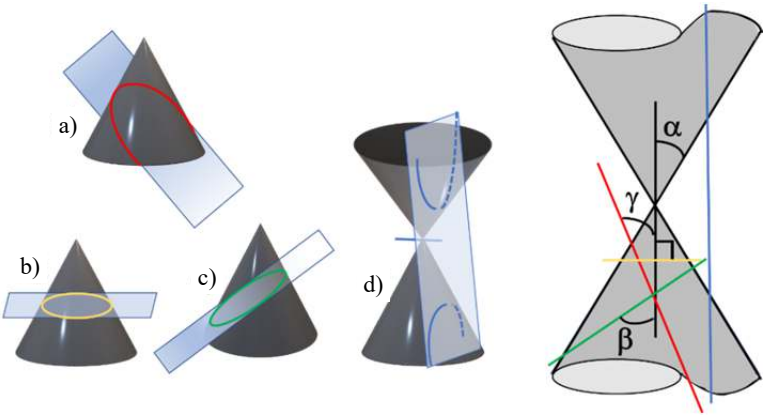

Figure 2.1. *a) Parabola, b) circle, c) ellipse and d) hyperbola*

In the appendix to his *Discourse on the Method* [DES 37], "Geometry", René Descartes transforms the way mathematicians approach geometric problems by laying the foundations for analytical geometry. This approach enabled curves and geometric shapes to be represented by mathematical equations, thus establishing a relationship between algebra and geometry. Conics can now be expressed as algebraic equations, and the curve of a conic can be represented by equations in polar or Cartesian coordinates. The algebraic equations are given in Figure 2.2, with a directrix as the reference point for a current point P on the conic (see Figure 2.2(a)) or in a Cartesian axis system (see Figure 2.2(b)).

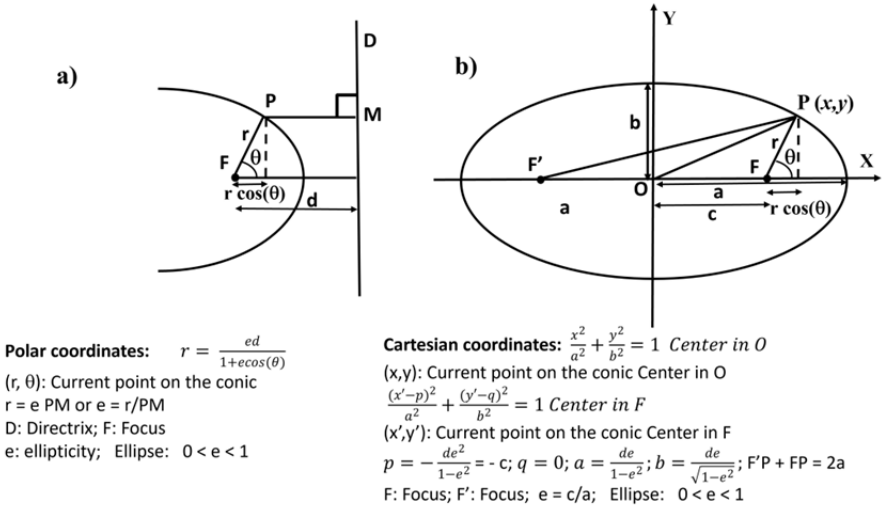

Figure 2.2. *Polar and Cartesian algebraic equations of an ellipse*

Conics are curves that describe the trajectory in a plane of a planet around the Sun in the Solar System, or of a satellite around a planet. Depending on the point of view adopted, they are perceived as sections of cones materialized by the intersection of a plane in 2D dimension with a cone in 3D dimension, or as trajectories described by algebraic equations in a given reference frame.

2.1.2. *Observations, analyses and laws of physics*

The Latin root of the term "physics" is *physica*, which comes from the Greek *physiké*, meaning "knowledge of nature". In physics, as in other fields of research, scientists attempt to identify the characteristics of the phenomena they study, based on observations and data analysis, and to deduce laws from them. The process of understanding observational data is carried out within the limits of the technological means available, and consequently the construction of this knowledge is in perpetual evolution.

2.1.3. *From Babylon's Goseck to Aristotle's Ancient Greece*

Archaeoastronomy suggests that knowledge of the solar cycle was important in determining the time of sowing, harvesting and the various stages of agricultural work. The first sites (Goseck, Stonehenge, etc.) identified as astronomical

observatories, in particular for tracking the movement of the Sun, Moon and stars, served, on the one hand, as instruments for tracking time by dating the equinoxes, and, on the other, as places of worship and centers of social life [NOR 96, AVE 97, RUG 99, RUG 05, PAS 06, PAR 08, SCH 18, ENG 24, GOS 24, SCH 24].

The oldest known astronomical tables on the observation of celestial bodies come from Babylon and date back approximately 2,000 years (Egypt, Mesopotamia) [PAR 50, NEU 55, NEU 60, NEU 67, NEU 75, CLA 95, PIN 97, SWE 98, SWE 00, HUN 01, SHA 03, RAD 11, DEJ 21]. The measurement methods of the time show that the movements of these bodies in the sky appear to be approximately circular.

Eudoxius of Cnidus (390 to 347 BCE), one of Plato's astronomers who had studied astronomy at the Heliopolis observatory in Egypt, was responsible for the theory of planetary motion known at the time (five nonfixed stars: Aphrodite-Venus, Hermes-Mercury, Cronos-Saturn, Ares-Mars and Zeus-Jupiter), in a cosmological system based on homocentric spheres. The spherical planets, including the Sun, described circular trajectories around the immobile Earth, the center of the world [LAS 66, DIC 85, ROB 09]. The Greeks, influenced by Plato, adopted this explanation of the Universe, with the planets in circular motion centered on the Earth [MAC 37, TOO 87, JUS 24].

This cosmological system was later perpetuated by Aristotle (*On Physics*), with the division of the Universe into two parts, the Cosmos, synonymous with perfection, subject to laws different from the terrestrial laws of the sublunary world, which govern the dynamics and imperfect evolution of the Earth, Moon and Sun system [DIC 70, MUG 71].

At the time of Hipparchus (130, 2nd century BCE), who invented trigonometry, the astrolabe, explained eclipses, determined longitudes, etc., and Ptolemy (150, 2nd century CE), who published the *Almagest*, etc., planetary motion was therefore considered to be combinations of circular motions (epicycles of ancient theories), because perfect motion could only be uniform and circular. Moreover, the movement of the stars could only be geocentric, with the Earth immobile at the center of the Universe, until Copernicus challenged this hypothesis [TOO 87, JUS 24, JON 10].

2.1.4. *Copernicus' heliocentric approach and Kepler's laws*

Copernicus' work [COP 43], published in 1543 in *De Revolutionubus orbium coelestium*, favors a heliocentric approach, with the heart of the Universe centered on the Sun, and the Earth revolving around it like any other planet (*planètos* in Greek means "wandering star") in a circular motion with epicycles, and a constant

speed to explain the planets' movements. Note that Archimedes reports in his writings (*L'Arénaire*, from the Latin *arena*, meaning sand or *sand reckoner*) [MUG 71] that Aristarchus of Samos (310–230 BCE) [HEA 13, DIC 70, LLO 70] had already proposed a heliocentric approach, placing the center of the Universe at the center of the Sun, with a radius of the Universe extending well beyond the Sun–Earth radius, to take account of distant stars, which were, like the Sun, fixed in the Universe. In his model, the Earth describes a circular motion around the star on a spherical surface with a radius smaller than that of the sphere of the Universe, which includes the distant stars [EVA 98, LIN 04, JON 10].

Later, based on the astronomical observations of Tycho Brahe [BRA 02], Johannes Kepler [KEP 09, KEP 19] adopted Copernicus' heliocentric system [COP 43, GIN 73, CAS 93], but corrected the latter's two other hypotheses (epicycles and constant velocity), enabling him to easily explain planetary motion (Astronomia nova [KEP 09]; Harmonices Mundi [KEP 19]) by integrating them into three laws (Kepler's laws), which are stated as follows:

– The planets orbit elliptically, with the Sun at one of their foci (see Figure 2.3(a)) (1609).

– The area (A_1) swept by the Sun–planet vector ray, when the planet passes from a point P_1 to a point P_2, is equal to that (A_2) swept in the same time Δt when the planet passes from a point P_3 to a point P_4: "the line segment connecting the Sun to a planet sweeps equal areas for equal durations" (see Figure 2.3(b)) (1609).

– If T is the planet's period of revolution (time for a complete revolution), and a is the semi-major axis of its orbit around the Sun, the ratio T^2/a^3 is constant and takes the same value for all planets. Another way of formulating this law is as follows: "the squares of the periods are proportional to the cubes of the axes of the orbits" (see Figure 2.4) (1618).

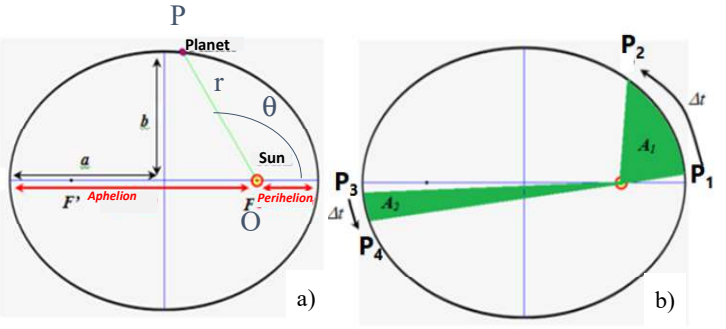

Figure 2.3. *Kepler's first and second laws*

Third law: the law of periods

For every planet in the solar system, the ratio between the square of the period "T" of revolution and the cube of the semi-major axis "a" is the same:

$$\frac{T^2}{a^3} = \frac{4\pi^2}{GM_s}$$

The value "$\frac{4\pi^2}{GM_s}$" is a constant. It is called the constant of the law of areas. It does not depend on the planet in question. It depends only on the gravitational constant (G = 6.67. 10^{11} SI) and the mass of the sun (M_S)

Figure 2.4. *Kepler's third law*

The heliocentric hypothesis considerably improves our understanding of planetary motion. Kepler's laws based on observation are descriptive and improve our understanding of the movement of stars in the sky. However, they are not based on any physical principles.

2.1.5. *The Galilean frame of reference and Galileo's principle of relativity*

In those days, planets were considered to be massless bodies moving in fixed orbits. Galileo Galilei came to the same conclusions as Copernicus about the position of the Earth and other planets in relation to the Sun: in 1610, using his astronomical telescopes, he first observed three small stars next to Jupiter, then a fourth, and published his findings in *Sidereus nuncius* [GAL 10]. This discovery was the starting point for the noun "satellite", since to describe Jupiter's "little companion stars", Kepler, in his *Narratio* [KEP 10] coined the neologism *satellite* ("bodyguard" in Latin). Today, systems orbiting planets, whether natural or artificial, are called "satellites".

Galileo first put forward the concept of relativity in *Riposta* ("Answer"), which, circulated privately to defend Copernicus's heliocentric hypothesis [GAL 32b, DRA 53]. Indeed, on the basis of several experiments conducted aboard moving ships, he concluded: "[…] Nor will you be able to determine whether the ship is moving or standing still by events concerning your person". This observation, repeated in his *Dialogue Concerning Two Chief World Systems*, published in 1632 [GAL 32a], thus poses the problem of the principle of relativity. Seen from the Earth, it is the Sun and the other planets that appear to be moving, and if it were possible to place ourselves at the level of the Sun, it would be the Earth and the other planets that would be in motion. Galileo's experiments thus posed the problem of the principle of relativity [SHE 70].

Albert Einstein, in *The Theory of Special and General Relativity*, asks the same question based on a thought experiment [EIN 05, EIN 15, EIN 16, EIN 38, ROS 93]:

> Suppose I am standing in front of the window of a uniformly moving train carriage, and I drop a stone onto the embankment without giving it any impulse. I can then see the stone falling in a straight line (disregarding the influence exerted by air resistance). But a pedestrian observing the mischief on the path will notice that the falling stone describes a parabola. I now ask: are the points reached by that the stone as it travels really located on a straight line or on a parabola?

The answer reads:

> The stone describes a straight line with respect to a coordinate system rigidly linked to the carriage, but describes a parabola with respect to a coordinate system linked to the ground. This example shows that there is no motion per se, but a trajectory relative to a given reference body.

To describe a physical process taking place in nature, we need to define a reference frame. All motion is then related to this frame of reference, in other words, a system of coordinate axes that allows us to locate the position of particles in space, and to a clock that indicates time. There are frames of reference where the free motion of bodies occurs at a constant speed, i.e. the motion of bodies not subject to the action of external forces. These reference frames are called "inertial" or "Galilean". For example, a frame of reference attached to the Earth in its rotational motion is not a Galilean frame of reference.

If two reference frames are in uniform rectilinear motion relative to each other, and if one of them is inertial, the other will also be inertial (all free motion is also uniformly rectilinear). There are therefore as many inertial reference frames, in uniform translation with respect to each other, as we can imagine.

However, although his observations contradicted the cosmological system adopted since Aristotle, for political and religious reasons, Galileo had to reject the heliocentric hypothesis (*Dialogue concerning the two chief world systems*, 1632) which he had initially defended:

> On June 22, 1633, before the court [...], he repudiated under oath the heliocentric doctrine as contrary to the Christian faith [BER 17].

Heliocentrism would be rehabilitated a century after Galileo's trial and eventually adopted [DRA 57, FIN 89, BLA 91, SHE 03]:

> A century after the trial, […] the optical proofs of heliocentrism were recognized and a mausoleum was erected to Galileo in a Florentine church. In 1741, the official *imprimatur* was given to Galileo's writings.

Galileo had also demonstrated through experiments that all massive objects move in the same way in the gravitational field, irrespective of their mass. At the time, he lacked the mathematical tools, notably the differential calculus that would be independently invented by Newton and Leibniz to calculate the duration of trajectories. He is also credited with the study of the free fall of several masses in the Earth's gravitational field from the top of the Leaning Tower of Pisa. The masses reach the ground at the same time, whatever their value, assuming that the effects of friction with the air are negligible.

2.1.6. *Newton's law of universal gravitation*

It was in 1686 that these empirical laws were justified by Newton's discovery [NEW 12] of the law of universal gravitation between two masses m and M separated by a distance r:

$$\vec{F} = -G\frac{mM}{r^2}\vec{u}_r \qquad [2.1]$$

where $\vec{F}$ is the attractive force between masses m and M, a central force that varies with $1/r^2$, oriented along the unit vector $\vec{u}_r$ (see Figure 2.3(a): $\vec{u}_r = \frac{\overrightarrow{OP}}{|\overrightarrow{OP}|}$) and acting along the straight line connecting the center of the masses (the "–" sign reflects the attractive nature of the force exerted by the Sun on the Earth), and G being the gravitational constant ($6.6743\ 10^{-11}$ nm^2/kg^2).

Kepler's empirical laws can be traced back to the law of universal gravitation, and are thus based on physical principles derived from the laws of conservation (*Philosophiæ naturalis principia mathematica*, Newton) [NEW 87]. Considering, for example, the motion of the Earth around the Sun, it is shown that since the attractive force between the planets is radial, this leads to making the angular momentum $\vec{L} = \vec{r} \wedge m\frac{d\vec{r}}{dt} = m\frac{d\vec{A}}{dt}$ ($\frac{d\vec{L}}{dt} = \vec{r} \wedge \vec{F} = \vec{0}$) constant, so that the trajectory takes place in a plane perpendicular to $\vec{L}$, which corresponds to part of the first law for trajectory in a plane and to the second law for equality of swept areas over the same duration, since $\vec{L}$ is proportional to the swept area $|\vec{A}|$ per unit time.

To show that this trajectory is an ellipse, we need to use polar coordinates and Binet's formulas for calculating acceleration in a frame of reference centered on the

Sun (see Figure 2.3(a)): OP = r and θ being the angle between OP and Ox. Solving the differential equation in variables u = 1/r and θ leads to the polar equation of an ellipse.

Newton's laws of motion (*Philosophiæ naturalis principia mathematica*) [COH 71, WES 80, NEW 87, NEW 99] determine the trajectory of any system subjected to a force. They are expressed as follows:

– Principle of inertia (first law): a body persists in its state of rest or uniform rectilinear motion, unless it is forced to change this state by the action of a force:

> A free particle, isolated in space, remains at rest or moves at constant speed.

– Fundamental principle of dynamics (second law): the rate of change of a body's motion is proportional to the force applied and takes place in the direction of the force:

> The total force $\vec{F}$ acting on a particle is equal to the product of its mass m by the acceleration $\vec{a}$ such that $\vec{F} = m\vec{a} = \frac{d(m\vec{v})}{dt}$.

– Principle of equal action and reaction (third law): for every action, there is an equal and opposite reaction (see Figure 2.3(a)):

> When two particles interact, the force $\vec{F}_{OP}$ exerted by one noted O on the other noted P is equal and opposite to the force $\vec{F}_{PO}$ exerted by P on O ($\vec{F}_{OP} = -\vec{F}_{PO}$).

Applying Newton's second law, we calculate an acceleration $\vec{a}$ equal for all masses, such that:

$$\vec{a} = \frac{\mathrm{d}\vec{v}}{\mathrm{dt}} = -\mathrm{G}\frac{\mathrm{M}}{(\mathrm{R}+\mathrm{h})^2}\vec{u}_r \qquad [2.2]$$

where R is the radius of the Earth, h is the distance of the object above the Earth's surface, G is the gravitational constant, M is the mass of the Earth and $\vec{u}_r$ is the unit vector radius on the line of action of the gravitational force between the center of the Earth and the barycenter of the object.

They show that the motion of a body of mass m in the gravitational field does not depend on mass, since inertial mass is equal to gravitational mass.

From the differential equation for velocity, we can calculate the time taken by an object launched, for example, with zero velocity from height h (leaning tower of Pisa) and show that it is the same for all objects, whatever their respective masses, in line with Galileo's observations in his experiments on falling bodies. In this context, it is worth noting that Newton's first law is equivalent to Galileo's formulation of the motion of free objects: "A body subjected to zero force must have a constant velocity".

Unlike Kepler's laws, which are based on observations, Newton's laws are postulates. They lead, notably through the second law of the fundamental principle of dynamics, to differential equations that allow us to calculate the trajectory of particles subjected to a force, in this case the force of gravitation, such that:

$$\vec{F} = m\frac{d\vec{v}}{dt} = -G\frac{mM}{r^2}\vec{u}_r \qquad [2.3a]$$

Newton's law of gravitation can be expressed as a gravitational field $\vec{g}$ which is the force exerted per unit mass and which derives from a potential $U(r) = -G\frac{M}{r}$, such that:

$$\vec{g}(r) = -G\frac{M}{r^2}\vec{u}_r = -grad\ U(r) \qquad [2.3b]$$

where r is the distance from the center of mass M to the point where the field is evaluated.

Newton's equations are simply expressed in a Cartesian coordinate system, but have a more complicated form in a cylindrical or spherical coordinate system, even if the same reference frame is used, as shown in Figure 2.5.

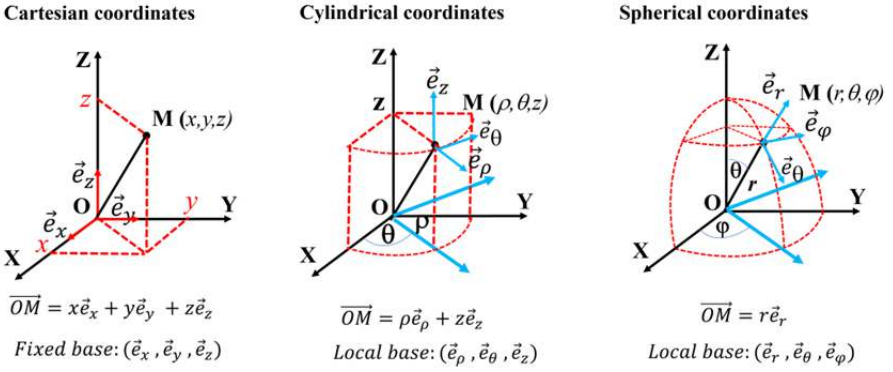

Figure 2.5. *Coordinate systems*

2.1.7. *Lagrange's and Hamilton's analytical mechanics*

When the system of interacting particles is greater than two, it is more convenient to use the method of Joseph-Louis Lagrange (1788) [LAG 88] to calculate particle trajectories. This method uses generalized coordinates, which have the advantage of not changing form when moving from one coordinate system to another.

If we consider a mechanical system made up of a particle of mass m in a Cartesian coordinate system, its kinetic energy T has the following expression:

$$T = \frac{1}{2}mv^2 = \frac{1}{2}m(\dot{x}^2 + \dot{y}^2 + \dot{z}^2) \quad [2.4]$$

In the generalized Lagrange coordinate system, T has the following expression:

$$T = \frac{1}{2}mv^2 = \frac{1}{2}m(\dot{q}_1^2 + \dot{q}_2^2 + \dot{q}_3^2) \quad [2.5]$$

where q_i are three generalized coordinates, corresponding to the number of degrees of freedom.

If we know that this particle is constrained to move on a sphere, the expression of kinetic energy is the same in Cartesian coordinates. However, with the Lagrange system, its expression is as follows:

$$T = \frac{1}{2}mv^2 = \frac{1}{2}m(\dot{q}_1^2 + \dot{q}_2^2) \quad [2.6]$$

Because of the constraint, there are only two degrees of freedom left. They could be, for example, the angles θ and φ of the spherical coordinate system (see Figure 2.5).

If, while constrained to move on a sphere, the particle is held by a wire fixed to one pole of the sphere, the expression of T will be the same in the Cartesian system. However, in the Lagrange system, the system has only one degree of freedom. The expression of this kinetic energy is therefore:

$$T = \frac{1}{2}mv^2 = \frac{1}{2}m\dot{q}_1^2 \quad [2.7]$$

The constraints reduce the system's degrees of freedom.

Lagrange constructed a mechanics to exploit the dynamics of a multi-particle system or sub-system under stress, which is widely used to study systems with n material points, which have 3n degrees of freedom, since each point has three

degrees of freedom. These are not necessarily the Cartesian coordinates of a point, and can be spherical or cylindrical coordinates, depending on the symmetry of the problem under consideration. These coordinates, which identify the n points, are called "generalized coordinates" and symbolically noted q (($q = (q_1, q_2, \ldots., q_{3n})$).

To determine the mechanical state of the system, it is also necessary to give the generalized velocities, which are the derivatives of the generalized coordinates with respect to time, and symbolically noted $\dot{q}$ ($\dot{q} = (\dot{q}_1, \dot{q}_2, \ldots., \dot{q}_{3n})$). Knowing the coordinates q and velocities $\dot{q}$ at an instant t allows us to determine the state of the system and the accelerations $\ddot{q}$ at that instant. As a result, the subsequent motion of the system can be calculated over an infinitesimally small-time interval Δt ($dt = \lim_{\Delta t \to 0} \Delta t$). The equations of motion are obtained from the relations that relate accelerations to velocities and coordinates, knowing that $\ddot{q} = \frac{d\dot{q}}{dt} = \frac{d}{dt}(\frac{dq}{dt}) = \frac{d^2q}{dt^2}$.

The law of motion of mechanical systems is not determined from Newton's laws, but from the principle of least action [LAG 56], Hamilton's principle [HAM 34] and Maupertuis' principle [MAU 44]. In this framework, we define the Lagrange function of the mechanical system, which formally depends on generalized coordinates, generalized velocities and time: $L(q, \dot{q}, t) = L(q_1, q_2, \ldots., q_{3n}, \dot{q}_1, \dot{q}_2, \ldots., \dot{q}_{3n}, t)$.

$$L(q, \dot{q}, t) =$$

The action, symbolically denoted by S, is defined by an integral of the system's Lagrange function between two instants noted t_1 and t_2 as:

$$S = \int_{t_1}^{t_2} L(q, \dot{q}, t)\, dt \qquad [2.8]$$

where the time dependence of the Lagrange function is not always explicit and is achieved through $q(t)$ and $\dot{q}(t)$. In this case, S is said to be a functional, or a function of functions.

The principle of least action consists of varying the functional S (variational calculation) by increasing $q(t)$ and $\dot{q}(t)$ $(q(t) + \delta q(t), \dot{q}(t) + \delta \dot{q}(t))$ and calculating the corresponding variation in S. By canceling this variation, we obtain the Lagrange equation, or the Euler–Lagrange equation [WHI 37, PAR 43, LAP 43–46, LAG 56, FEY 63, SOM 64b, LAN 66a, GOL 76, ARN 78, LAN 86, GOL 01, MAR 03, TAY 05], or Lagrange equations (if we take into account n particles and 3n degrees of freedom), which are written as follows:

$$\frac{d}{dt}\frac{\partial}{\partial \dot{q}}\big(L(q, \dot{q}, t)\big) - \frac{\partial}{\partial q}\big(L(q, \dot{q}, t)\big) = 0 \qquad [2.9a]$$

$$\frac{d}{dt}\frac{\partial}{\partial \dot{q}_i}\left(L(q,\dot{q}\,t\,)\right) - \frac{\partial}{\partial q_i}\left(L(q,\dot{q}\,t\,)\right) = 0 \qquad [2.9b]$$

where *i* varies from 1 to 3n.

Generally speaking, the Lagrangian of a system is expressed as the difference between its kinetic energy $T(\dot{q})$ and its potential energy $V(q)$, such that:

$$L(q,\dot{q}\,t\,) = T\left(q(\dot{t})\right) - V(q(t)) \qquad [2.10]$$

where the time dependence can be expressed in terms of generalized coordinates and generalized velocities. In this case, Lagrange's equations result in:

$$\frac{d}{dt}\frac{\partial}{\partial \dot{q}}T\left(q(\dot{t})\right) = -\frac{\partial}{\partial q}V(q(t)) \qquad [2.11]$$

Given the expression for kinetic energy and the fact that the gravitational force is a conservative force derived from a potential ($F(q) = -\frac{\partial}{\partial q}V(q(t))$), Lagrange's equation reverts to Newton's equation as follows:

$$\frac{dmq(\dot{t})}{dt} = F(q) \qquad [2.12]$$

In this way, the principle of least action is equivalent to Newton's second law, but leads to a system of differential equations that do not depend on time. The principle of least action makes it possible to formulate the laws of dynamics in a generalized coordinate system, without any reference to particular coordinates. The principle of least action states that if we seek to determine the trajectory of a material point between instants t_1 and t_2, then calculating the action integral between t_1 and t_2 leads to a stationary value on the trajectory actually followed by the particle.

Hamilton's equations can also be used to determine the motion of a system of particles. The Hamilton function is defined using:

$$H = \sum_i^{3n} p_i q_i - L(q_1, q_2, \ldots., q_{3n}, \dot{q}_1, \dot{q}_2, \ldots., \dot{q}_{3n}, t) \qquad [2.13]$$

where $p_i = \frac{\partial L}{\partial \dot{q}_i}$ is the canonical momentum.

Hamilton's equations of motion are written as follows:

$$\frac{\partial H}{\partial q_i} = -p_i \qquad [2.14a]$$

$$\frac{\partial H}{\partial p_i} = \dot{q}_i \quad [2.14b]$$

$$\frac{\partial H}{\partial t} = -\frac{\partial L}{\partial t} \quad [2.14c]$$

Usually, the Hamilton function of a system is expressed as a sum of its kinetic energy $T(\dot{q})$ and its potential energy $V(q)$, such that:

$$H(q,p,t) = T(p(t)) + V(q(t)) \quad [2.15]$$

2.1.8. *The principles of relativity and equivalence*

Newton's law of gravitation paved the way for celestial mechanics. However, it also raised the question of the stability of the Solar System and its planets, which are not only attracted to the Sun, but also to each other. This contradicts Kepler's model in the sense that the small perturbations caused by the attraction of the planets to each other prevent elliptical orbits from being fixed. For example, Jupiter is affected in its trajectory by Saturn, and Neptune is affected by Uranus. However, these deviations are calculable, and it is thanks to the work of Joseph-Louis Lagrange and Pierre-Simon de Laplace [LAP 43–46, 94] that it was shown that the semi-major axes have periodic variations that remain small for the Jupiter–Saturn pair. When the calculation is performed for the planet Mercury, Newton's law of gravitation does not give a satisfactory result for the calculating of the secular variation (long-term changes) corresponding to the rotation of the planet's semi-major axis.

Newton assumed that there is a fixed absolute space among all stars and galaxies in which his equation is true without the need to apply corrections to fictitious forces. Such an absolute space would have to contain physical entities in addition to the object being measured. Otherwise, it would not be possible to establish a reference frame for measuring acceleration. The existence of stars (or the Universe) is therefore essential to absolute space and Newton's equation. Describing the processes taking place in nature requires a reference frame, meaning a system of coordinates (x, y, z) to locate the position of particles in space, and a clock to indicate time t.

Experience reveals the existence of the principle of relativity. This principle states that all of the laws of nature are identical in all reference frames of inertia. This means that the equations translating the laws of nature are invariant to the transformations of coordinates and time corresponding to a change of inertial reference frame. Expressed in terms of coordinates (x, y, z) and time t, the equation describing a law of nature has the same form whatever the chosen frame of reference.

The interaction between the particles of a mechanical system is described by means of the interaction potential energy, which is a function of the coordinates of these particles. This implies the instantaneity of interactions, meaning an infinite propagation speed of this interaction. In this case, the forces exerted by the other particles in the system on a given particle depend at all times solely on the position of the particles.

Michelson and Morley [MIC 87] have shown that the measurement of the speed of light cannot be used to determine absolute space. The speed of light is identical in all reference frames. In the theory developed by Albert Einstein, the speed of propagation of interactions is considered finite, being equal to the speed of propagation of light (c = 2, 99 792 458 10^8 ms^{-1}) according to the *principle of relativity* enunciated in 1905 as part of the *theory of special relativity*. This principle implies that time is not absolute, and that its measurement leads to different values in different inertial reference frames moving in uniform translation with respect to one another.

Bear in mind that reference frames in which the free motion of bodies, or the motion of bodies not subject to the action of external forces, takes place with a constant velocity (generally parallel to the Ox axis) are said to be inertial or Galilean; in accordance with experimental evidence, which reveals the existence of the principle of relativity. From the relationship between the coordinates along the Ox and Ox' axes, given $x = x' + vt'$, it is easy to see that acceleration in the two axis systems coincides.

Einstein has shown that, under the assumption that c has the same value in all inertial reference frames, when moving from one inertial reference frame R to another R' in motion relative to R, with a constant velocity v taken parallel to the Ox axis, the following equations apply in terms of space–time coordinates:

$$x = \gamma(x' + \beta ct') \qquad x' = \gamma(x - \beta ct) \qquad [2.16a]$$

$$y = y' \qquad y' = y \qquad [2.16b]$$

$$z = z' \qquad z' = z \qquad [2.16c]$$

$$ct = \gamma(ct' + \beta x') \qquad ct' = \gamma(ct' - \beta x') \qquad [2.16d]$$

where c is the speed of light, $\beta = \frac{v}{c}$ and $\gamma = \frac{1}{\sqrt{1-\frac{v^2}{c^2}}}$.

When v is very small, Galileo's equations can be used to switch from the (x, y, z) coordinate system to the (x', y', z') coordinate system. Within the framework of the

theory of special relativity, with c having the same value in all inertial reference frames, the wavefront of light emitted from the origin of the coordinate system (x, y, z, t) at time t = 0 is given by:

$$c^2t^2 - x^2 - y^2 - z^2 = 0 \quad [2.17a]$$

If the coordinate system (x', y', z', t') coincides with the coordinate system (x, y, z, t) at time t = 0, then the following also applies:

$$c^2t'^2 - x'^2 - y'^2 - z'^2 = 0 \quad [2.17b]$$

which implies that, since the relative velocity between the two systems is constant, time t' must flow differently from t. In four-dimensional space–time (Minkowski space), each point s is an event, so that the wavefront describes a cone around the time axis t, called the "light cone", which as a function of s has the following expression:

$$s^2 = c^2t^2 - x^2 - y^2 - z^2 \quad [2.17c]$$

An event is on the cone if $s^2 = 0$, is considered time-like if $s^2 > 0$ and is considered space-like if $s^2 < 0$.

The simultaneity of the falls of material bodies already described with Galileo's experiment from the top of the Leaning Tower of Pisa is easily interpreted by the equivalence between inertial mass and gravitational mass in Newton's second law. Mach proposed that the mass of an object should somehow reflect the entire Universe. This is known as *Mach's principle* [MAC 19]. The consideration of noninertial reference frames led Einstein to formulate the equivalence principle.

The transition from the theory of special relativity to the theory of general relativity is based on Einstein's *equivalence principle* (1907), which states that the effects of the gravitational field are identical to the effects of acceleration in a non-Galilean frame of reference, as experienced by an observer in an elevator in nonuniform motion. Einstein also predicts that if light can enter through a hole in an elevator in free fall in the gravitational field, the observer inside will see that the light follows a parabolic trajectory, whereas an observer on the ground will see rectilinear light propagation. Einstein deduced that the gravitational field can deflect light, even though a photon has no mass. These considerations were translated into the theory of general relativity in 1915 in the form of a field equation [EIN 15, EIN 16, BOR 62, WEI 72, MIS 73, WHE 92]:

$$R_{ik} - \frac{1}{2}g_{ik}R + g_{ik}\Lambda = \frac{8\pi G}{c^4}T_{ik} \quad [2.18]$$

where the indices i and k represent the dimensions of space–time, with i and k = 0, 1, 2 or 3, 0 being referred to the time coordinate t, 1 to the spatial coordinate x, 2 to the spatial coordinate y and 3 to the spatial coordinate z. The expressions on the left-hand side of the equation represent the curvature of space–time, the first term R_{ik} being the Ricci curvature tensor, the second one being the metric tensor g_{ik} multiplied by R, the scalar curvature, and the third one, the product of the metric tensor g_{ik} multiplied by Λ, the cosmological constant. On the right-hand side, we have a term representing the effect of mass and energy in the form of a product of the energy-impulse tensor multiplied by a term comprising the ratio of the product of 8 pi and the gravitational constant, and the speed of light to the 4th power. Given that there are four values of i and k, equation [2.18] represents a priori 16 equations that reduce to 10 in total. These equations indicate that mass is responsible for the curvature of space–time and that the curvature of space–time is responsible for the displacement of mass. The equations were published by Albert Einstein in 1915 [EIN 15] in the form of the tensor equation [2.18], which relates the curvature of local space–time (expressed by the Einstein tensor on the left) to the local energy, momentum and stress in that space–time (expressed by the stress-energy tensor on the right).

It was not until 1915, for example, that Einstein's theory of general relativity improved on Newton's law of universal gravitation, making it possible to calculate the advance of Mercury's perihelion in its elliptical trajectory around the Sun, in line with observations. This phenomenon refers to the slight rotation of Mercury's elliptical orbit around the Sun, which could not be fully explained by Newtonian mechanics alone (Mercury anomaly).

Indeed, by applying Einstein's equation [3.18] to Mercury's motion, we can calculate Mercury's perihelion advance. The contribution of general relativity theory leads to the following expression:

$$\Delta\omega = \frac{6\pi GM}{c^2 a(1-e^2)} \qquad [2.19]$$

where $\Delta\omega$ is the advance of Mercury's perihelion at each orbit, a is the semi-major axis of the ellipse and e is its eccentricity. This calculation gave an additional precession of approximately 43 arc-seconds per century, corresponding exactly to the unexplained part of the observed advance of Mercury's perihelion.

Expressed as a function of coordinates and time, the equation describing a law of nature has the same form, whatever the chosen reference frame of inertia. In 1905 [EIN 05], Albert Einstein completely abandoned the concept of absolute space and extended the concept of relativity of physical measurements to include the

measurement of the speed of light. Einstein demonstrated that this new point of view provides a deeper understanding of physical quantities such as momentum, energy and fields. A noninertial frame of reference is equivalent to a gravitational field. In a uniformly accelerated noninertial frame of reference, freely moving bodies will undergo a constant acceleration opposite to that of the frame of reference.

This history of the establishment of the laws of gravitation shows that it took almost 4,000 years for the laws of Copernicus, Kepler, Newton, Einstein and probably others to be gradually put in place to describe a reality based on different principles that are better specified in their applications, such as the principle of relativity, Mach's principle or the principle of equivalence.

In this respect, let us quote Karl Popper in the conduct of the search for knowledge by scientific methods and the criterion of demarcation between science and nonscience [POP 45, POP 59, POP 63, POP 72]:

> The criterion of scientificity of a theory resides in the possibility of invalidating, refuting or testing it.

It should be noted, however, that this method is suited to the natural sciences concerning inert matter, for which deduction is appropriate. For the life sciences, however, the test phase is not always possible, and it is the inductive method that is appropriate, eventually based on a statistical approach.

We can also recall the methodology Descartes left us in his *Discourse on the method* [DES 37], in the form of rules to follow in the pursuit of knowledge:

– First rule: "never to accept anything for true which I did not clearly know to be such". This is the rule of evidence. Accept as true only the obvious, the certain, not the probable.

– Second rule: "to divide each of the difficulties under examination into as many parts as possible, and as might be necessary for its adequate solution". This is the rule of dividing the complex into simple elements (analysis). We must examine the objects of knowledge, see what is simple and what is compound, analyze what is compound and explain it by its simple constituents.

– Third rule: "to conduct my thoughts in such order that, by commencing with objects the simplest and easiest to know, I might ascend by little and little, and, as it were, step by step, to the knowledge of the more complex". This is the rule of order. This order is the order of reasons. We must start from the obvious and deduce. It is the order of reasons, not of subjects: we do not necessarily start with the most important or the most fundamental.

– Fourth rule: “to make enumerations so complete, and reviews so general that I might be assured that nothing was omitted”. This is the rule of enumeration. To carry out a complete, general review of objects, which calls for prudence and circumspection.

From Ptolemy and Aristotle’s geocentric model, we arrive at Copernicus’ heliocentric model, despite politico-religious opposition. Newton’s system of axes pointing to the stars defined an absolute frame of reference to describe mechanical motion, based on his three laws of motion, and Galileo’s principle of relativity led to inertial frames of reference in which motion are relative. Following Newton’s law of gravitational attraction, Newton’s three laws of motion make it possible to interpret Kepler’s three empirical laws within the framework of Copernicus’ heliocentric model, and to interpret Galileo’s observations on the free fall of bodies. Lagrange’s formalism enabled him and Laplace to demonstrate the stability of planetary motion around the Sun, and to interpret the perihelion advance observed for all planets except Mercury. As a first step, Einstein improved Galileo’s principle of relativity by including time as a parameter that can vary as space coordinates do in the motion of a material body. Einstein also set a limit to the propagation of electromagnetic interaction at a distance, via the speed of light, within the framework of special relativity. Following the principle of equivalence, which enabled Einstein to consider the motion of bodies in noninertial reference frames while maintaining the principle of relativity, he demonstrated that even light, which has no inert mass, can follow a curved trajectory in the vicinity of a massive body. Within the framework of the theory of general relativity, Einstein [EIN 38] showed, with a different approach to Newton’s, that it is the curvature of space–time that is responsible for the effects of gravitation.

2.2. Selecting orbital parameters

2.2.1. *Keplerian parameters of a satellite’s orbit around the Earth*

The orbit of an object such as a natural or artificial satellite around a central body, which can be a planet or a star, is defined by means of six parameters called “Keplerian elements”, as shown in Figure 2.6 for a satellite orbiting the Earth:

– the semi-major axis a and the eccentricity e define the shape of the orbit;

– the inclination i indicates the angle between the orbital plane and a reference plane (e.g. the equatorial plane of the central body or that of the Earth);

– the longitude Ω of the ascending node indicates the angle between a reference direction in the reference plane and the direction of the ascending node;

– the argument ω of the periastron, or perigee, represents the angle (in the plane of the orbit) between the direction of the ascending node and that of the periastron, which completes the characterization of the object's orbit;

– the true anomaly ν, on the other hand, gives the object's position on the orbit at a given date (which is indicated at the same time as the value of the previous six elements).

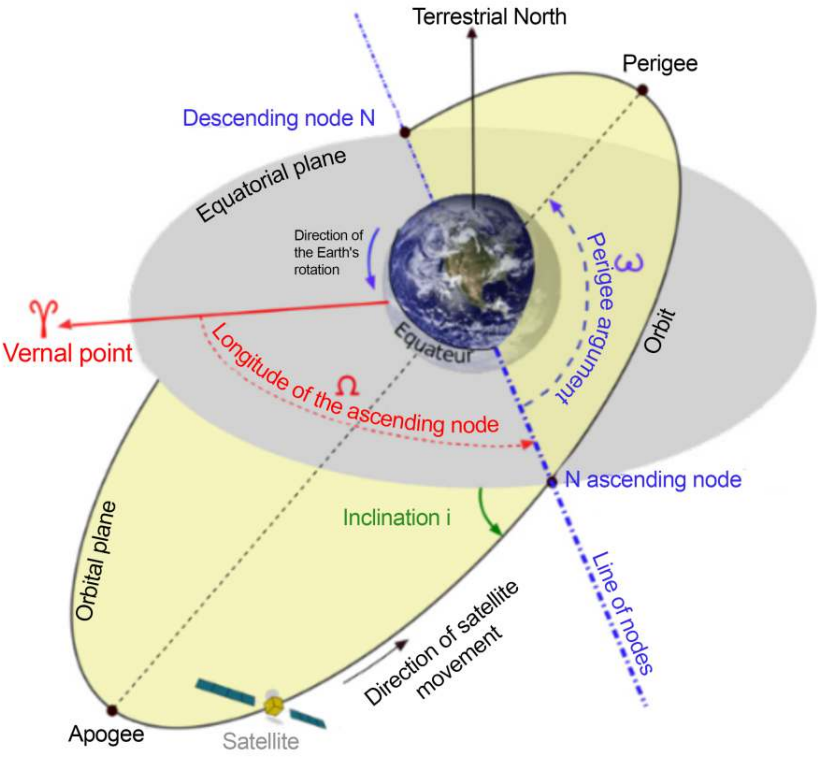

Figure 2.6. *Keplerian parameters of a satellite's orbit around the Earth with the equatorial plane as a reference plane*

An orbit has two nodes: an ascending node and a descending node, which are the points of intersection between the orbit and the reference plane. The ascending node is the point in the orbit where the satellite crosses the reference plane in the direction of celestial north. In contrast, the descending node is the point in the orbit where the satellite crosses the reference plane in the direction of celestial south.

When describing the orbit of an object around the Earth or the orbit of a planet around the Sun, we use the direction of the mean vernal point γ calculated at 01/01/2000 12:00:00 (Julian date J2000). The vernal point is the position of the Sun as seen from Earth at the vernal equinox. The corresponding vector is therefore defined by the intersection of the Earth's equatorial plane and the ecliptic (the plane of the Earth's orbit around the Sun (see Figure 2.7)).

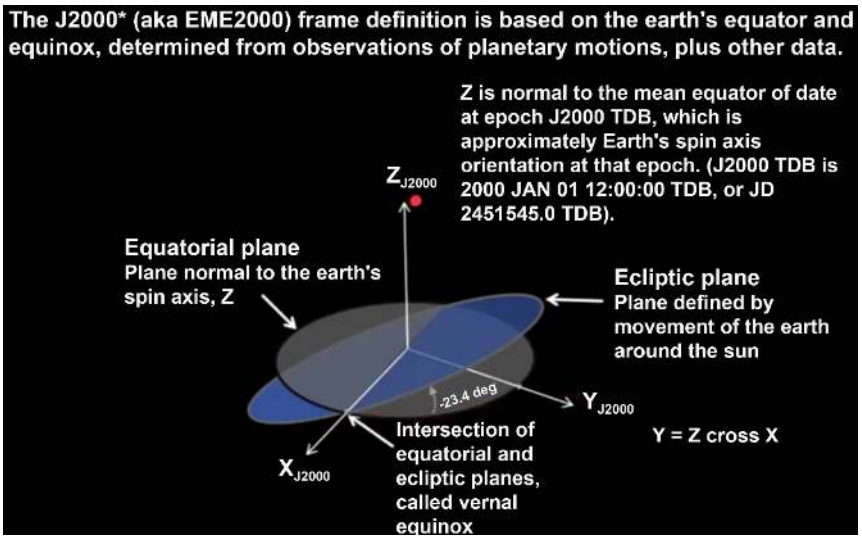

Figure 2.7. *The vernal point defined by the intersection of the Earth's equatorial plane and the ecliptic*

Based on Newton's laws of motion and the law of universal gravitation, calculating the velocity v (in ms^{-1}) of a satellite in its orbit around the Earth leads to the following expression:

$$v = \sqrt{\frac{G}{MR}} \qquad [2.20]$$

where M (in kg) is the mass of the Earth, R (in m) is the distance between the center of the Earth and the satellite, and G is the universal gravitational constant.

To calculate the Earth's orbit around the Sun, we replace the mass M by that of the Sun, and the corresponding value of R between the center of the Earth and that of the Sun.

2.2.2. *The different types of orbit*

The orbit of a natural or artificial satellite around an attracting center can therefore be of two types, circular or elliptical, and positioned at different altitudes:

– The *circular orbit*, as its name suggests, its trajectory is circular. It has neither apogee (the point of orbit closest to the Earth) nor perigee (the point of orbit furthest from the Earth).

– The *elliptical orbit* is not circular. It has an apogee and a perigee.

The inclination of the orbit relative to the equatorial plane is also important as it determines the overall coverage of a planet throughout a mission. Equatorial orbits do not allow for observation of the polar regions, unlike polar orbits, whose inclination is close to 90°. A polar orbit is ideal for global coverage of a planet.

Three different orbits can then be distinguished according to their altitude (see Figure 2.8):

– *Low orbit*: this is, as its name suggests, the lowest orbit, and therefore the closest to the Earth. It is located between 200 and 2,000 km in altitude.

– *Medium orbit*: this is located above low orbit. It is therefore further from the Earth than low orbit, and lies between 2,000 and 35,786 km in altitude.

– *High orbit*: this is the furthest orbit from the Earth. It is above the medium orbit, at an altitude of over 35,786 km. High orbit can be confused with geostationary orbit.

There are two quite different types of orbit:

– *Geostationary orbit*: this is a circular orbit with an inclination of zero. This means it follows the trajectory of the equator. A satellite placed in a geostationary orbit is always above the same point on the Earth, which is an advantage for telecommunications.

– *Sun-synchronous orbit*: for an artificial satellite, this is an orbit in which the angle between the orbit plane and the direction of the Sun remains more or less constant. The satellite will therefore pass over a given point on Earth at the same local solar time.

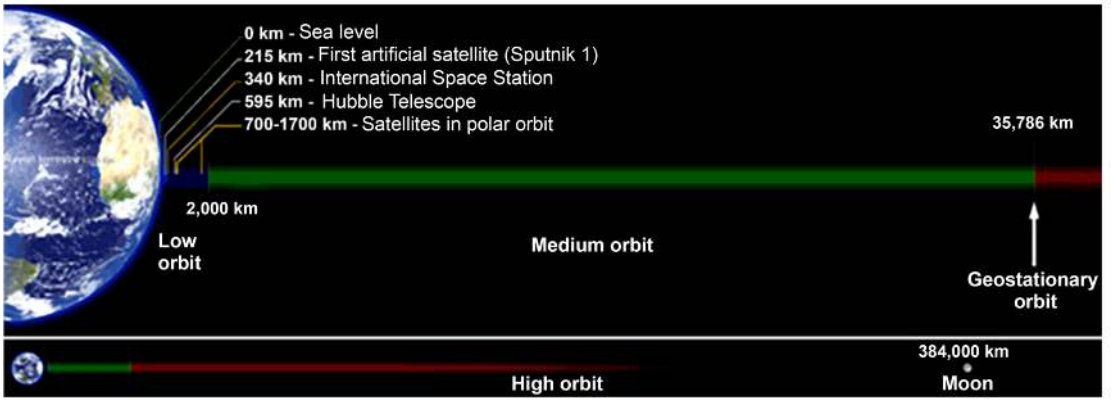

Figure 2.8. *Low, medium and high orbits according to altitude*

The geostationary or geosynchronous orbit (GEO) is very popular with telecommunications satellites. It is ideal for applications requiring a fixed satellite position relative to the Earth:

– semi-major axis: 42,164 km;

– inclination: < 0.1 degree;

– orbital period: 86,164 seconds.

The geostationary transfer orbit, GTO, is a provisional orbit. All geostationary satellite launches pass through this transfer orbit (with the exception of some Russian satellites launched with Proton rockets). The launch vehicle injects the satellite into this orbit. The satellite is consequently fitted with an engine so as to propel and place it into its orbit. Its characteristics are as follows:

– perigee altitude: 180 km;

– apogee altitude: 35,780 km;

– inclination ≅ 7 degrees;

– orbital period: 37,800 seconds.

Low-Earth orbit (LEO) is a circular orbit at an altitude of 200–2,000 km, at a steep angle to the equator (from 50° to over 90°). Applications include observation, meteorology and telecommunications (satellite constellation).

The sun-synchronous orbit (SSO), at an altitude of between 600 km and 800 km, is such that the direction of the Sun is always at an angle to the orbital plane. The area covered by the satellite is thus always observed at the same time. This is the preferred orbit for high-resolution terrestrial observation (SPOT, HELIOS, ERS, TOPEX, etc.).

Other orbits include the high eccentric orbit (HEO).

2.2.3. *Orbit parameters, beta angle and orbit eclipse duration*

The parameters of a satellite's orbit around an attracting mass center can be determined from Newton's laws of motion and the universal law of gravitation. With reference to Figure 2.6, we can calculate the following.

– The orbit's period:

$$T = 2\pi\sqrt{\frac{a^3}{\mu}} = 2\pi\sqrt{\frac{(R_E + \frac{h_a + h_p}{2})^3}{Gm_E}} \qquad [2.21]$$

where a is the orbit's semi-major axis, μ is the Earth's standard gravitational parameter (3.986004418 10^{14} m^3s^{-2}) according to the WGS84 standard, R_E is the Earth's mean radius (6.371009 10^6 m), G is the gravitational constant, m_E is the Earth's mass and *ha* and *hp* are the satellite's altitude at apogee and perigee respectively.

– The inclination i:

$$\mathrm{i} \simeq \arccos\left(-\frac{2}{3}\frac{\Omega_h}{J_2}\left(\frac{a}{R_E}\right)^2\sqrt{\frac{a^3}{\mu}}\right) \quad [2.22]$$

where Ω_h is the rate of precession. For Sun-synchronous motion, the rate of precession Ω_h is equal to the average motion of the Earth around the Sun, which is 360° per sidereal year (1.9910 10^{-7} radians per second). J_2 is the coefficient of the second zonal term (1.082626174 10^{-3}), corresponding to the flattening of the Earth according to the EGM2008 standard.

– The eccentricity e:

$$\mathrm{e} \simeq -\frac{1}{2}\frac{J_3}{J_2}\frac{R_E}{a}\sin i \quad [2.23]$$

where J_3 is the third-order coefficient of the zonal harmonics of the gravity field model according to the EGM2008 standard.

– The shape of the orbit:

$$\mathrm{h} = \frac{a(1-e^2)}{1+e\cos\theta} - R_E \quad [2.24]$$

– The apogee and the perigee are given by:

$$\mathrm{h_a} = \mathrm{a}(1+\mathrm{e}) - \mathrm{R_E} \quad [2.25a]$$

$$\mathrm{h_p} = \mathrm{a}(1-\mathrm{e}) - \mathrm{R_E} \quad [2.25b]$$

– The satellite's speed:

$$\mathrm{v} = \sqrt{\frac{\mu}{\mathrm{R_E}+\mathrm{h}}} \quad [2.26]$$

The beta angle (see Figure 2.9):

$$\beta = \arcsin(\cos\Gamma\sin\Omega\sin i - \sin\Gamma\cos\varepsilon\cos\Omega\sin i + \sin\Gamma\sin\varepsilon\cos i) \quad [2.27]$$

where Γ is the true solar ecliptic longitude, Ω is the right ascension of the ascending node (RAAN) and ε is the obliquity of the ecliptic (~ 23,44 degrees).

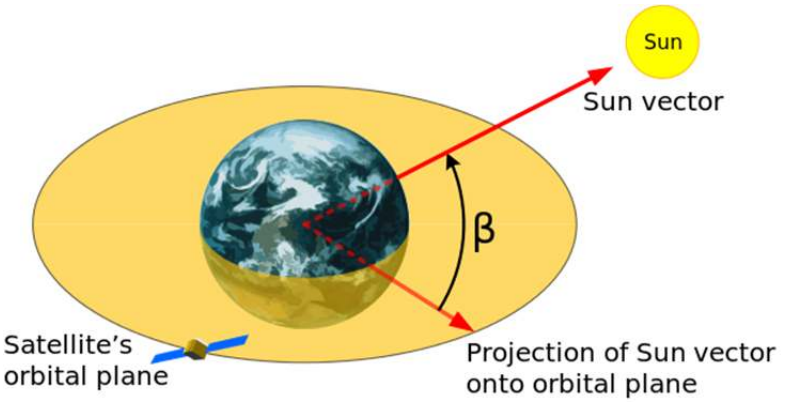

Figure 2.9. *Beta angle on the orbit*

The true solar ecliptic longitude Γ is obtained from the following equations:

$$L = 280.46 + 0.9856474\ (JDN - 2451545) \quad [2.28a]$$

$$g = 357.528\ + 0.9856003\ (JDN - 2451545) \quad [2.28b]$$

$$\Gamma = L + 1.915\sin(g) + 0.02\sin(2g) \quad [2.28c]$$

where L is the Sun's mean longitude in degrees, g is the Sun's mean anomaly in degrees and JDN is the Julian day number. Γ is equal to 0 degrees when the Sun is at the vernal equinox of spring (March 20) and varies from 0° to 360°. Assuming that the Earth's orbit around the Sun is almost circular, variations due to seasonal changes ($\dot{\Gamma}$) are close to 0.986 degrees per year.

The Sun's declination is calculated as follows:

$$\delta = \arcsin(\sin(\varepsilon)\sin(\Gamma)) \quad [2.29]$$

The oblateness of the Earth is the cause of the variation for right ascension (Ω) and the argument of the periapsis (ω).

The variation in the angular rate of the ascending node due to precession of the orbit function of orbit altitude and inclination is defined as follows:

$$\dot{\Omega} \simeq -\frac{3}{2}J_2\left(\frac{R_E}{a}\right)^2\sqrt{\frac{\mu}{a^3}}\cos i \quad [2.30]$$

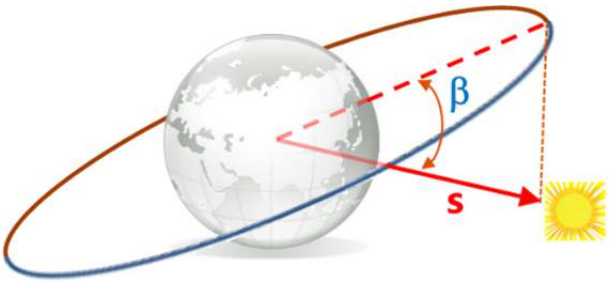

Figure 2.10. *Eclipse of the Sun in orbit*

The choice of orbit and the duration of eclipses are fundamental parameters for:

– scientific observations;

– power balances, etc.

The duration (T_e) of the solar eclipse over one revolution is determined as follows:

$$T_e = f_e T \qquad [2.31]$$

where f_e is the eclipse fraction.

The eclipse fraction is determined using:

$$f_e = \frac{1}{\pi} arcos\left(\frac{\sqrt{h^2+2R_E h}}{(R_E+h)cos\beta}\right) \quad if\ |\beta| < |\beta *| \qquad [2.32]$$

where $\beta * = arcsin\left(\frac{R_E}{R_E+h}\right)$. Otherwise, $f_e = 0$.

2.3. Conclusion

The orbital parameters of a CubeSat or any other artificial satellite are indicators or characteristic elements of information that can be used to describe its trajectory around a body of greater mass. This trajectory can be calculated using the laws of classical mechanics, the theory of universal gravitation and Newton's differential calculus. This chapter traces the history of advances in astronomy: from the first astronomical sites to the first theoretical proposals, through Kepler's work and Newton's law of gravitation, right up to the birth of classical mechanics with

Newton's laws and his method of differential calculation, Leibniz's method as well as Lagrange's work. This chapter shows how interest in celestial objects since Antiquity, based on the traces left by our ancestors, has led to the mechanics of systems and the laws enabling the construction of models in line with physical reality. These include the heliocentrism of the Solar System, the elliptical motion of Mercury and the constant evolution of gravitational theories (Newton and Einstein). This evolution of science, thanks to the continuous improvement in our understanding of natural phenomena, is achieved by comparing theories with observations (Descartes, Comte, Bacon, Popper, etc.). This is made possible by the use of instruments to probe the Solar System as well as the Universe, thanks to satellites whose trajectories are defined by parameters adapted to all.

2.4. Appendix

2.4.1. *Coordinate systems and point mechanics*

Determining the trajectory of a point mass using Newton's laws of motion means determining the positions of the mass at different times. To do this, we need to find a reference frame that allows us to locate the point object at different times.

In classical mechanics, reference frames are chosen according to the symmetry of the problem addressed. If the symmetry is that of a cube or a parallelepiped, the motion is more easily determined in a Cartesian frame of reference. The cylindrical reference frame is used if the symmetry is suitable, as for axisymmetric motion. The spherical reference frame is used if the symmetry is suitable for motion on the surface of a sphere, for example.

Before presenting these references in three-dimensional (3D) space, let us take a look at the situation in two-dimensional (2D) space. Descartes invented the method to represent a point in a system of perpendicular axes by means of a pair of points marked (x, y), which represent the distance to be covered on each axis to reach the point marked M, as shown in Figure 2.11.

Space is represented as a grid of squares materialized by parallel straight lines perpendicular to axes OX, the x-axis, and OY, the y-axis. In accordance with Euclid's axioms, two parallel lines never meet. By giving ourselves a metric, the length between two points, we can give values to x and y relative to an origin represented by the axes OX for the y-value and OY for the x-value, and which pass through the origin O. By applying the Pythagorean theorem, we can calculate the distance between two points, as shown in Figure 2.11, in the expression for the distance OM, which is $\sqrt{x^2 + y^2}$.

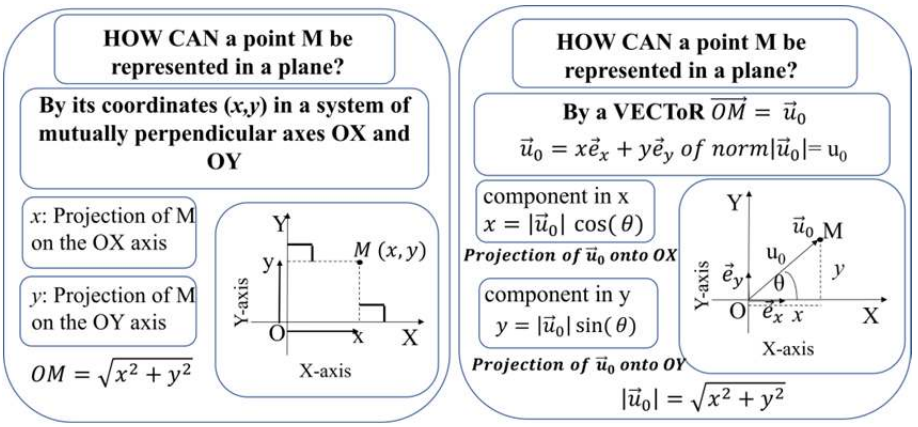

Figure 2.11. *Cartesian representation of a point in 2D space*

This point can also be represented by a vector starting from the origin and whose components are x and y, as shown in Figure 2.11. Vector notation is useful for representing velocity, acceleration, force, moment; in other words, any quantity characterized by a scalar value representing its amplitude or modulus, and a direction and sense in that direction.

The vector notation of a vector $\vec{v}$ can be in the form of a linear combination of independent basis vectors or in the form of column vectors, such that:

$$\vec{v} = x\vec{\imath} + y\vec{\jmath} = x\vec{e}_x + y\vec{e}_y \qquad [2.33a]$$

$$\vec{v} = \begin{pmatrix} x \\ y \end{pmatrix} \qquad [2.33b]$$

The base vectors $\vec{\imath}$ and $\vec{\jmath}$ have length equal to 1 and are represented as:

$$\vec{\imath} = \vec{e}_x = \begin{pmatrix} 1 \\ 0 \end{pmatrix} \qquad [2.34a]$$

$$\vec{\jmath} = \vec{e}_y = \begin{pmatrix} 0 \\ 1 \end{pmatrix} \qquad [2.34b]$$

In the Cartesian system, these base vectors are fixed and do not change over time.

In this case, the two-dimensional space is associated with a vector space, with rules for addition, subtraction and multiplication between vectors internally, and rules for external multiplication by real variables or real constants.

Consider two vectors $\vec{v}_1 = \begin{pmatrix} x_1 \\ y_1 \end{pmatrix}$ and $\vec{v}_2 = \begin{pmatrix} x_2 \\ y_2 \end{pmatrix}$.

The addition or subtraction of two vectors can be written as follows:

$$\vec{v}_1 \pm \vec{v}_2 = \begin{pmatrix} x_1 \\ y_1 \end{pmatrix} \pm \begin{pmatrix} x_2 \\ y_2 \end{pmatrix} = \begin{pmatrix} x_1 \pm x_2 \\ y_1 \pm y_2 \end{pmatrix} \quad [2.35a]$$

i.e. each component is added or subtracted:

$$\vec{v}_1 \pm \vec{v}_2 = (x_1 \pm x_2)\vec{\imath} \pm (y_1 \pm y_2)\vec{\jmath} \equiv \begin{pmatrix} x_1 \pm x_2 \\ y_1 \pm y_2 \end{pmatrix} \quad [2.35b]$$

Multiplication by a constant λ is written as follows:

$$\lambda\vec{v}_1 = \lambda \begin{pmatrix} x_1 \\ y_1 \end{pmatrix} = \begin{pmatrix} \lambda x_1 \\ \lambda y_1 \end{pmatrix} \equiv \lambda x_1 \vec{e}_x + \lambda y_1 \vec{e}_y \quad [2.35c]$$

Scalar product:

$$\vec{v}_1 \cdot \vec{v}_2 = \begin{pmatrix} x_1 \\ y_1 \end{pmatrix} \cdot \begin{pmatrix} x_2 \\ y_2 \end{pmatrix} = x_1 x_2 + y_1 y_2 = \vec{v}_2 \cdot \vec{v}_1 \quad [2.36a]$$

The result of the scalar product is a scalar. The scalar product is commutative and symmetrical. We verify the following:

$$\vec{\imath} \cdot \vec{\jmath} = \begin{pmatrix} 1 \\ 0 \end{pmatrix} \cdot \begin{pmatrix} 0 \\ 1 \end{pmatrix} = 0 \quad [2.36b]$$

The scalar product is used to calculate the norm (intensity or length) of a vector:

$$|\vec{v}_1| = \sqrt{\vec{v}_1 \cdot \vec{v}_1} = \sqrt{\begin{pmatrix} x_1 \\ y_1 \end{pmatrix} \cdot \begin{pmatrix} x_1 \\ y_1 \end{pmatrix}} = \sqrt{x_1^2 + y_1^2} \quad [2.37a]$$

The geometrical point of view of the scalar product:

$$\vec{v}_1 \cdot \vec{v}_2 = |\vec{v}_1||\vec{v}_2| \cos(\vec{v}_1, \vec{v}_2) = |\vec{v}_1||\vec{v}_2| cos\theta \quad [2.37b]$$

It represents the projection of $\vec{v}_2$ onto $\vec{v}_1$ multiplied by the norm of $\vec{v}_1$.

Vector product:

$$\vec{v}_1 \wedge \vec{v}_2 = \begin{pmatrix} x_1 \\ y_1 \end{pmatrix} \wedge \begin{pmatrix} x_2 \\ y_2 \end{pmatrix} = (x_1 y_2 - x_2 y_1)\vec{k} = (x_1 y_2 - x_2 y_1)\vec{e}_z \quad [2.38a]$$

where $\vec{k}$ or $\vec{e}_z$ is a vector perpendicular to the OXY plane, such that $\vec{k} = \vec{\imath} \wedge \vec{\jmath}$ or $\vec{e}_z = \vec{e}_x \wedge \vec{e}_y$.

The vector product gives a vector that is in the direction perpendicular to the plane in which $\vec{v}_1$ and $\vec{v}_2$ lie. It is not commutative like the scalar product. It is an antisymmetric product.

We check that $\vec{\imath} \wedge \vec{\jmath}$:

$$\vec{\imath} \wedge \vec{\jmath} = \begin{pmatrix}1\\0\end{pmatrix} \wedge \begin{pmatrix}0\\1\end{pmatrix} = 1\vec{k} \qquad [2.38b]$$

It is more convenient to add a component of column-vector form to calculate the vector product. This is known as a "pseudo-vector".

In this case, the calculation is as follows:

$$\vec{v}_1 \wedge \vec{v}_2 = \begin{pmatrix}x_1\\y_1\\0\end{pmatrix} \wedge \begin{pmatrix}x_2\\y_2\\0\end{pmatrix} = \begin{pmatrix}0\\0\\x_1y_2 - x_2y_1\end{pmatrix} = (x_1y_2 - x_2y_1)\vec{k} \qquad [2.38c]$$

The geometrical point of view of the vector product:

$$\vec{v}_1 \wedge \vec{v}_2 = |\vec{v}_1||\vec{v}_2| \sin(\vec{v}_1, \vec{v}_2)\, \vec{k} = |\vec{v}_1||\vec{v}_2| sin\theta\, \vec{k} \qquad [2.38d]$$

It represents the oriented surface of the parallelogram built on $\vec{v}_1$ and $\vec{v}_2$. The vector product is useful for calculating the flux of a vector field across a surface. Changing the position of the vectors in the vector product leads to the same surface, but oriented in the opposite direction.

When the 2D system under consideration is of circular symmetry, as in the case of an object constrained to move on a circle, it is more convenient to use the polar coordinate system. A point M is then represented by its polar coordinates (r, θ). The vector $\overrightarrow{OM}$ is then expressed in the base adapted to the polar coordinates.

Figure 2.12 shows a comparison between the representation of a point in the Cartesian coordinate system, with the grid based on straight lines used to determine the (x, y) pairs, and the polar coordinate system, with concentric circles of increasing radii starting from the origin O to locate the radius r and an array of intersecting straight lines starting from O to locate the angle θ that the direction OM makes with the x-axis.

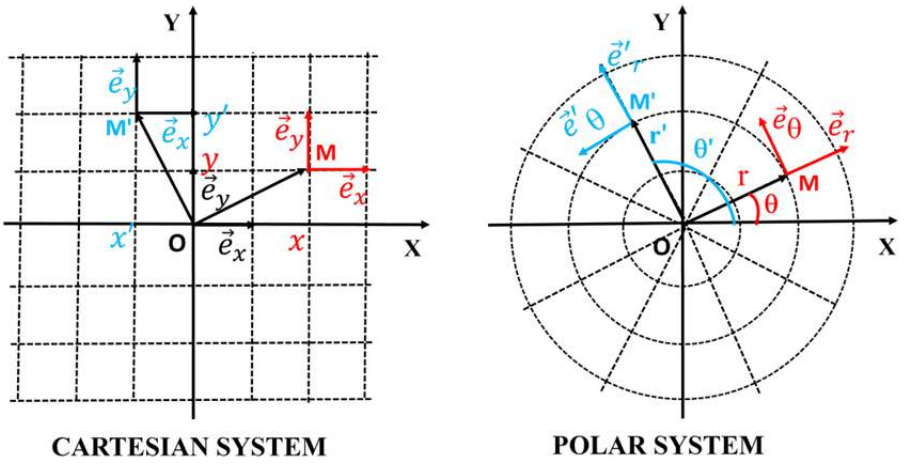

Figure 2.12. *Representation of a point in 2D space: Cartesian and polar systems*

Figure 2.12 shows two points, M and M′, with coordinates (x, y) and (x', y') in the Cartesian system and coordinates (r, θ) and (r', θ') in the polar system. When we consider the base vectors that allow us to represent these points vectorially, we can determine the following for the Cartesian system:

$$\overrightarrow{OM} = x\vec{e}_x + y\vec{e}_y \equiv \begin{pmatrix} x \\ y \end{pmatrix} \quad [2.39a]$$

$$\overrightarrow{OM'} = x'\vec{e}_x + y'\vec{e}_y \equiv \begin{pmatrix} x' \\ y' \end{pmatrix} \quad [2.39b]$$

and for the polar system in the base $(\vec{e}_r, \vec{e}_\theta)$:

$$\overrightarrow{OM} = r\vec{e}_r \equiv \begin{pmatrix} r \\ 0 \end{pmatrix} \quad [2.39c]$$

$$\overrightarrow{OM'} = r'\vec{e}'_r \equiv \begin{pmatrix} r' \\ 0 \end{pmatrix} \quad [2.39d]$$

Even if $r' = r$, the unit base vectors are oriented differently in the polar system, whereas in the Cartesian system, the base vectors are identical. In the polar system, the unit base vectors are defined locally, at the location of point M or M′, whereas in the Cartesian system, the base vectors are fixed. This means that when an object moves, the local base vectors are modified and therefore depend on time, which is not the case for the base vectors of the Cartesian system. This peculiarity of local bases must be taken into account when calculating their rates of change.

It can be shown by expressing the polar base vectors in the Cartesian system that we have the following relationships between $\vec{e}_r$ and $\vec{e}_\theta$:

$$\vec{e}_\theta = \frac{\partial \vec{e}_r}{\partial \theta} \text{ and } -\vec{e}_r = \frac{\partial \vec{e}_\theta}{\partial \theta} \qquad [2.39e]$$

Figure 2.13 summarizes the representation of a point in both Cartesian and polar systems for a two-dimensional space.

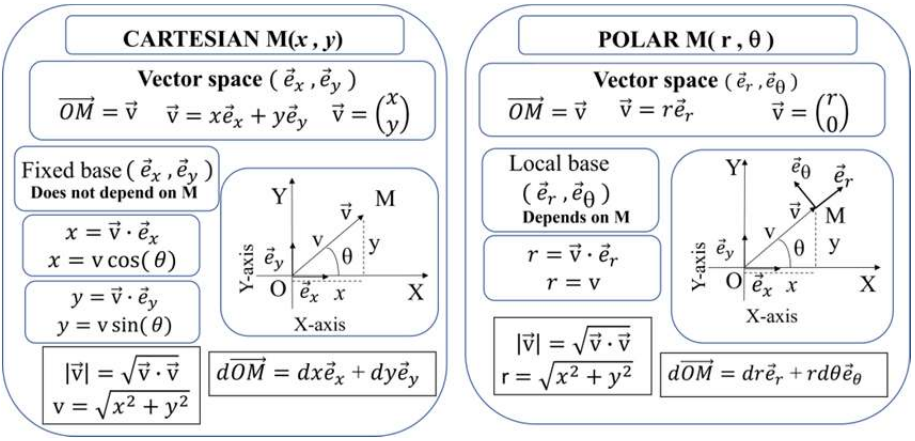

Figure 2.13. *Representation of a point in 2D space: Cartesian and polar systems*

In three-dimensional space, we add an axis (OZ axis) perpendicular to the XOY plane for the Cartesian system, and likewise we add an axis (OZ axis) perpendicular to the XOY plane in which polar coordinates are defined for the cylindrical system. In this case, $\vec{e}_z$, the third base vector, is the same in both systems and does not vary over time. Therefore, in the Cartesian system, a point M with coordinates (x, y, z) will be represented by the vector $\overrightarrow{OM}$ in the fixed base ($\vec{e}_x$, $\vec{e}_y$, $\vec{e}_z$), such that:

$$\overrightarrow{OM} = x\vec{e}_x + y\vec{e}_y + z\vec{e}_z \equiv \begin{pmatrix} x \\ y \\ z \end{pmatrix} \qquad [2.40a]$$

and a point M with coordinates (ρ, θ, z) for the cylindrical system will be represented by the vector $\overrightarrow{OM}$ in the local basis ($\vec{e}_\rho$, $\vec{e}_\theta$, $\vec{e}_z$), such that:

$$\overrightarrow{OM} = \rho\vec{e}_\rho + z\vec{e}_z \equiv \begin{pmatrix} \rho \\ 0 \\ z \end{pmatrix} \qquad [2.40b]$$

Figure 2.13 shows the representation of a point M in both Cartesian and polar coordinate systems, specifying the fixed or local base and the expressions for an elementary displacement.

A third system is also available for 3D, using spherical coordinates (see Figure 2.14) to locate a point on a sphere, such as the Earth.

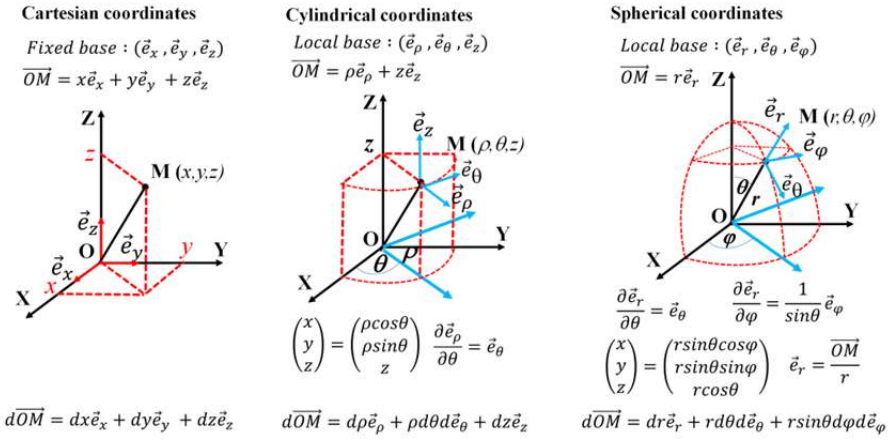

Figure 2.14. *Coordinate systems in a 3D space*

The spherical coordinate system is adapted to spherical symmetry. The three parameters used to locate a point M on a sphere are:

– the distance from point O at the center of the sphere (origin of the coordinate system) to point M, which is its radius *r*;

– the angle θ between the axis passing through O and M and the OZ axis taken as a reference, which can vary from 0 to π, with point M describing a semicircle in the ZOM plane;

– the angle φ that the ZOM half-plane makes with a reference plane defined by the ZOX plane, which can vary from 0 to 2π.

In this system, the vector $\overrightarrow{OM}$ in the local basis $(\vec{e}_r, \vec{e}_\theta, \vec{e}_\varphi)$ is written as follows:

$$\overrightarrow{OM} = r\vec{e}_r \equiv \begin{pmatrix} r \\ 0 \\ 0 \end{pmatrix} \qquad [2.40c]$$

Using the relationship that gives the components $\vec{e}_r$ in the fixed base $(\vec{e}_x, \vec{e}_y, \vec{e}_z)$, it can be shown that the vectors $\vec{e}_\theta$ and $\vec{e}_\varphi$ can be obtained from the base vector $\vec{e}_r$ by the following operations:

$$\vec{e}_\theta = \frac{\partial \vec{e}_r}{\partial \theta} \quad [2.40d]$$

$$\vec{e}_\varphi = \frac{1}{sin\theta}\frac{\partial \vec{e}_r}{\partial \varphi} \quad [2.40e]$$

It is sometimes useful to determine the surface and volume elements in these coordinate systems. The volume elements are determined from the expressions for the elementary displacement $d\overrightarrow{OM}$, recalled in Figure 2.14, by multiplying the terms that give the elementary displacements according to each base vector. For the three coordinate systems, Cartesian, cylindrical and spherical respectively, we calculate the following:

$$dV = dxdydz \quad [2.41a]$$

$$dV = \rho d\rho d\theta dz \quad [2.41b]$$

$$dV = r^2 dr sin\theta d\theta d\varphi \quad [2.41c]$$

For surface elements, it is necessary to choose the surface to be considered. In the Cartesian system, the volume element is a cube with sides of elementary lengths dx, dy and dz, with six different faces. A surface is obtained by the vector product of the two vectors on each of the six faces. When z is held constant, the two vectors to be considered are given by the components of the elementary displacement $d\overrightarrow{OM}$ on the surface in question, i.e. (see Figure 2.14) $d\overrightarrow{OM}(\mathrm{z = constant}) = \mathrm{d}x\vec{e}_x + dy\vec{e}_y$. Evaluating the vector product:

$$d\vec{S}_z = \mathrm{d}x\vec{e}_x \wedge dy\vec{e}_y = \mathrm{d}x\mathrm{d}y(\vec{e}_x \wedge \vec{e}_y) = \mathrm{d}x\mathrm{d}y\vec{e}_z \quad [2.42a]$$

The elementary surface vector is determined for the surface at Z = constant. In expression [2.42a], the surface normal $\vec{e}_z$ is a pseudo-vector or vector oriented with the rule that the surface normal vector always points outside the elementary volume.

Likewise, we evaluate the various vector products for the elementary surfaces at x = constant and y = constant to obtain:

$$d\vec{S}_x = \mathrm{d}y\vec{e}_y \wedge dz\vec{e}_z = \mathrm{d}y\mathrm{d}z\,(\vec{e}_y \wedge \vec{e}_z) = \mathrm{d}x\mathrm{d}y\vec{e}_x \quad [2.42b]$$

$$d\vec{S}_y = \mathrm{d}z\vec{e}_z \wedge dx\vec{e}_x = \mathrm{d}x\mathrm{d}z(\vec{e}_z \wedge \vec{e}_x) = \mathrm{d}x\mathrm{d}z\vec{e}_y \quad [2.42c]$$

For the cylindrical system, we evaluate the surface element at ρ = constant and z = constant to determine:

$$d\vec{S}_\rho = \rho \mathrm{d}\theta \vec{\mathrm{e}}_\theta \wedge dz\vec{\mathrm{e}}_z = \rho \mathrm{d}\theta \mathrm{d}z\,(\vec{\mathrm{e}}_\theta \wedge \vec{\mathrm{e}}_z) = \rho \mathrm{d}\theta \mathrm{d}z\vec{\mathrm{e}}_\rho \quad [2.43a]$$

$$d\vec{S}_z = \mathrm{d}\rho\vec{\mathrm{e}}_\rho \wedge \rho \mathrm{d}\theta\vec{\mathrm{e}}_\theta = \rho \mathrm{d}\rho \mathrm{d}\theta(\vec{\mathrm{e}}_\rho \wedge \vec{\mathrm{e}}_\theta) = \rho \mathrm{d}\rho \mathrm{d}\theta\vec{\mathrm{e}}_z \quad [2.43b]$$

For the spherical system, we evaluate the surface element at r = constant to determine:

$$d\vec{S}_r = r\mathrm{d}\theta\vec{\mathrm{e}}_\theta \wedge r\sin\theta d\varphi\vec{\mathrm{e}}_\varphi = r^2 \sin\theta \mathrm{d}\theta d\varphi(\vec{\mathrm{e}}_\theta \wedge \vec{\mathrm{e}}_\varphi) = r^2 \sin\theta \mathrm{d}\theta d\varphi\vec{\mathrm{e}}_r \quad [2.44]$$

This last expression is used, for example, to calculate the solid angle at which a luminous flux reaches the surface of a detector. Each point on the surface is considered to be the origin of a sphere whose elementary surface, at a distance of r from the aperture diaphragm of the detector, makes an angle with the normal on the surface of the diaphragm.

2.4.2. *Classical point mechanics*

Kinematics is the study of the geometry of motion through the trajectory followed by a point. It was developed by adding the variable time to the geometric variables of position. The term "reference frame" is used to locate a point or object. The set of all coordinate axis systems linked to a single reference solid S constitutes a point of reference. The set of a coordinate system linked to a reference solid S and a chronology constitutes a reference frame.

In the context of planetary motion around the Sun, Newton's laws of motion can, to a first approximation, be applied to point masses (Gauss's theorem assimilates a planet or star to a point mass at its center). The introduction of the mass variable into the study of motion led to the construction of dynamics, which assimilates every geometric point to a point mass.

The transformation of velocities by the law of compositions leads to the equations of kinematics, when we pass from one Galilean or inertial frame of reference to another Galilean or non-Galilean frame of reference. The position of a material point in space is determined by its radius vector $\overrightarrow{\mathrm{OM}} = \vec{r}$, whose components coincide with its Cartesian coordinates x, y, z in the Cartesian system. The derivative of $\vec{r}$ with respect to time t, $\vec{\mathrm{v}} = \frac{d\vec{r}}{dt}$, is called the velocity and the

second derivative $\vec{a} = \frac{d^2\vec{r}}{dt^2}$, the acceleration of the point. Note that we use the following notations for the first and second derivatives, such that $\vec{v} = \dot{\vec{r}}$ and $\vec{a} = \ddot{\vec{r}}$.

Whether in 2D or 3D, expressions for velocity and acceleration are straightforward in the Cartesian system, as it is sufficient to differentiate the components of the vector, such that:

$$\vec{v} = \frac{d\overrightarrow{OM}}{dt} = \frac{dx}{dt}\vec{e}_x + \frac{dy}{dt}\vec{e}_y + \frac{dz}{dt}\vec{e}_z \quad [2.45a]$$

$$\vec{a} = \frac{d^2\overrightarrow{OM}}{dt^2} = \frac{d^2x}{dt^2}\vec{e}_x + \frac{d^2y}{dt^2}\vec{e}_y + \frac{d^2z}{dt^2}\vec{e}_z \quad [2.45b]$$

When the coordinate system is such that the bases are local, the change in base orientation during movement must be taken into account.

In 2D in the polar system, velocity $\vec{v}$ corresponds to:

$$\vec{v} = \frac{d\overrightarrow{OM}}{dt} = \frac{dr}{dt}\vec{e}_r + r\frac{d\vec{e}_r}{dt} = \frac{dr}{dt}\vec{e}_r + r\frac{d\vec{e}_r}{d\theta}\frac{d\theta}{dt} = \frac{dr}{dt}\vec{e}_r + r\omega\vec{e}_\theta \quad [2.46a]$$

where $\frac{dr}{dt}\vec{e}_r$ is the relative speed along the radius, $r\omega\vec{e}_\theta$ is the driving speed perpendicular to the radius and ω is the angular speed of rotation. To derive $\vec{e}_r$ with respect to time, we used the relationship $\frac{d\vec{e}_r}{d\theta} = \vec{e}_\theta$.

Similarly, for the acceleration $\vec{a}$, we can calculate:

$$\vec{a} = \frac{d^2\vec{v}}{dt^2} = \frac{d^2r}{dt^2}\vec{e}_r + \frac{dr}{dt}\frac{d\vec{e}_r}{d\theta}\frac{d\theta}{dt} + \frac{dr}{dt}\omega\vec{e}_\theta + r\frac{d\omega}{dt}\vec{e}_\theta + r\omega\frac{d\vec{e}_\theta}{d\theta}\frac{d\theta}{dt} \quad [2.46b]$$

$$\vec{a} = \frac{d^2\vec{v}}{dt^2} = \frac{d^2r}{dt^2}\vec{e}_r + 2\frac{dr}{dt}\omega\vec{e}_\theta + r\frac{d\omega}{dt}\vec{e}_\theta - r\omega^2\vec{e}_r \quad [2.46c]$$

where $\frac{d^2r}{dt^2}\vec{e}_r$ is the relative acceleration along the radius, $-r\omega^2\vec{e}_r$ is the driving acceleration along the radius, or normal acceleration, $2\frac{dr}{dt}\omega\vec{e}_\theta$ is the driving acceleration perpendicular to the radius, or tangential acceleration, $r\frac{d\omega}{dt}\vec{e}_\theta$ is the driving acceleration perpendicular to the radius and $\frac{d\omega}{dt}$ is the angular acceleration of rotation.

In circular motion, the relative velocity is zero and the angular velocity of rotation is constant, so the expressions for velocity and acceleration are reduced to:

$$\vec{v} = \frac{d\overrightarrow{OM}}{dt} = r\omega\vec{e}_\theta \quad [2.47a]$$

$$\vec{a} = \frac{d^2\vec{v}}{dt^2} = -r\omega^2\vec{e}_r = -\frac{v^2}{r}\vec{e}_r \quad [2.47b]$$

If we consider any trajectory, we can approximate it by a set of circular trajectories of different radii at each point along the trajectory. At each point M on the trajectory, the velocity of the particle is tangent to the trajectory at that point, as in circular motion, and has the following expression:

$$\vec{v} = \frac{d\overrightarrow{OM}}{dt} = v\vec{e}_t \quad [2.48a]$$

The tangent vector is equivalent to the $\vec{e}_\theta$ vector of circular motion.

The derivative of the velocity $\vec{v}$ leads to the acceleration $\vec{a}$, which involves the derivative of the modulus of the velocity v and the tangent vector $\vec{e}_t$ such that:

$$\vec{a} = \frac{d\vec{v}}{dt} = \frac{dv}{dt}\vec{e}_t + v\frac{d\vec{e}_t}{dt} = \frac{dv}{dt}\vec{e}_t + \frac{v^2}{R}\vec{e}_n \quad [2.48b]$$

where R is the radius of curvature at the point considered on the trajectory and $\vec{e}_n$ is the vector normal to the trajectory obtained from $\vec{e}_t$ by rotation of $\frac{\pi}{2}$ (trigonometric direction).

2.4.3. *The metric tensor in general relativity*

To determine the distance between two points in two-dimensional space in the Cartesian coordinate system, we apply the Pythagorean theorem. This states that the square of the length of the hypotenuse of a right-angled triangle is equal to the sum of the squares of the distances of the other sides (see Figure 2.15). When the triangle is not right-angled, the Al-Kachi or cosine–sine formula is used.

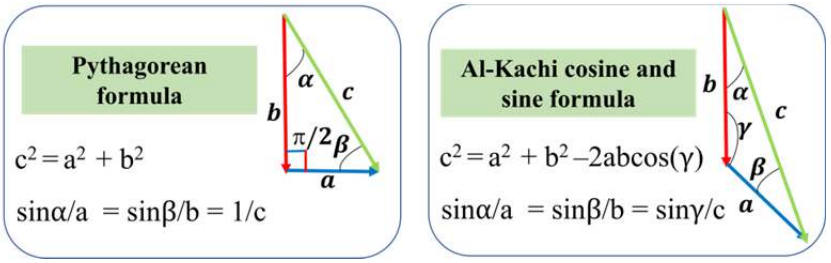

Figure 2.15. *Length of a side of a triangle: Pythagoras and Al-Kachi*

The reason for using the Pythagorean theorem in the Cartesian coordinate system is that we use the Euclidean space to grid 2D space with lines parallel to the x-axis and y-axis (see Figure 2.12). These two sets of lines being perpendicular to each other. The distance between two points marked by the pairs (x_1, y_1) and (x_2, y_2) is given by the metric defined from the Pythagorean theorem, such that:

$$\text{a} = x_2 - x_1,\ b = y_2 - y_1, \text{ and } c^2 = a^2 + b^2 \qquad [2.49a]$$

This metric is used to convert coordinate intervals into distances using a scale of graduations.

Similarly, in a three-dimensional space, let s^2 be the squared distance between two points marked by the coordinates (x_1, y_1, z_1) and (x_2, y_2, z_2) in the following form:

$$s^2 = (x_2 - x_1)^2 + (y_2 - y_1)^2 + (z_2 - z_1)^2 \qquad [2.49b]$$

If the "grid" used to locate a point is not built on parallels that form a 90° angle with each other, then Al-Kachi's formula (see Figure 2.15) must be used in 2D space. Two lengths and an angle are needed to determine the length between two points. In a three-dimensional space, we need three lengths and three angles, requiring us six parameters to determine the length between two points.

In classical mechanics, a point in space is identified by three parameters that depend on the coordinate system used to describe the geometry of that space: Cartesian, cylindrical or spherical (see Figure 2.14). To describe motion in these spaces, we determine the trajectory followed by a material point under the effect of the gravitational force between two masses, using a fourth variable given by a clock to measure the elapsed time. Time is the same in all inertial spaces, because the interaction between two masses is assumed to be instantaneous, meaning that its propagation speed is infinite.

Einstein has shown that it is necessary to consider the time it takes for this interaction to propagate. Einstein postulated that the limiting speed of propagation could not exceed the speed of light or of an electromagnetic wave, all of which, irrespective of their frequency or wavelength, propagate at the same speed c. In this case, it is necessary to include time as a parameter that can change when calculating the trajectory of a particle, especially when its speed is close to that of light. In this case, the motion of any object must be determined in a four-dimensional space that includes the time t associated with the three space variables (x, y, z). The transformation formulas, which allow us to move from one inertial reference frame to another in a uniform translational motion parallel to the OX axis (formulas [2.16a], [2.16b], [2.16c], [2.16d]), have made it possible to establish an equivalence

between the variables *ct* and *x* in special relativity. In this theory, space is described locally by a Euclidean space at each point, so that the interval between two points in special relativity is given by the generalized Pythagorean formula, if we allow the time axis to be imaginary by using the quantity i such that a point or event in a four-dimensional space is given by (i*ct*, *x*, *y*, *z*). In this case, we can write that:

$$ds^2 = (icdt)^2 + (dx)^2 + (dy)^2 + (dz)^2 \qquad [2.49c]$$

The metric is thus defined locally at each point in a Euclidean space. Conventionally, these four coordinates are identified by the parameters (x_0, x_1, x_2, x_3).

In general relativity, a four-dimensional space is constructed in a Riemann space where, unlike Euclidean space, two parallels can meet (the reference points are not necessarily inertial reference points). Determining the length between two events is no longer performed with the generalized Pythagorean formula, but rather by including other parameters in the calculation, as is the case with Al-Kachi's 2D formula. In the 3D formula, six parameters are needed to calculate the length, and the 4D formula, four more. The matrix representation of the metric tensor used to evaluate length therefore comprises ten elements represented in a 4 x 4 matrix, such that:

$$g_{ik} = \begin{pmatrix} g_{00} & g_{01} & g_{02} & g_{03} \\ g_{01} & g_{11} & g_{12} & g_{13} \\ g_{02} & g_{12} & g_{22} & g_{23} \\ g_{03} & g_{13} & g_{23} & g_{33} \end{pmatrix} \qquad [2.50]$$

Note that the matrix is symmetrical with respect to the main diagonal.

Figure 2.11 shows the need for a metric tensor to evaluate distances in two-dimensional space. Measuring a distance requires a ruler to evaluate the distance between two points. Coinciding the two grid systems, Cartesian, on the one hand, and polar, on the other, is only possible if we measure distances gradually, using intervals between two closely spaced points (events), which is over an infinitesimal distance.

When comparing the polar and Cartesian coordinate systems, we observe that the Cartesian grid is built on perpendicular lines, just as for the polar grid (see Figure 2.12). However, the distance measurement is on a curve in the direction defined by the base vector $\vec{u}_\theta$. As an example, let us calculate the metric tensor to go from coordinates (*x*, *y*) to coordinates (*r*, *θ*) by means of infinitesimal differences, such that:

$$dx = cos\theta dr - rsin\theta d\theta \qquad [2.51a]$$

$$dy = sin\theta dr + rcos\theta d\theta \qquad [2.51b]$$

The length of the interval is calculated using the Pythagorean theorem:

$$ds^2 = dx^2 + dy^2 \quad [2.51c]$$

We have:

$$dx^2 = cos^2(\theta)\, dr^2 + r^2 sin^2(\theta) d\theta^2 - 2rcos\theta sin\theta dr d\theta$$

$$dy^2 = sin^2(\theta)\, dr^2 + r^2 cos^2(\theta) d\theta^2 + 2rcos\theta sin\theta dr d\theta$$

$$ds^2 = dr^2 + r^2 d\theta^2$$

In this case, the metric tensor that allows us to switch from Cartesian coordinates to polar coordinates (old components as a function of new ones) is given by:

$$\begin{pmatrix} g_{00} & g_{01} \\ g_{01} & g_{11} \end{pmatrix} = \begin{pmatrix} 1 & 0 \\ 0 & r^2 \end{pmatrix} \quad [2.52]$$

In general, if we switch from one coordinate system (x, y) to another (x', y'), such that:

$$dx' = \alpha dx + \beta dy \quad [2.53a]$$

$$dy' = \gamma dx + \delta dy \quad [2.53b]$$

we calculate ds^2 such that:

$$dx'^2 = \alpha^2\, dx^2 + \beta^2 dy^2 + 2\alpha\beta dx dy$$

$$dy'^2 = \gamma^2\, dx^2 + \delta^2 dy^2 + 2\gamma\delta dx dy$$

$$ds^2 = (\alpha^2 + \gamma^2)\, dx^2 + (\beta^2 + \delta^2)\, dy^2 + 2(\alpha\beta + \gamma\delta) dx dy$$

so that the metric tensor is given by:

$$\begin{pmatrix} g_{00} & g_{01} \\ g_{01} & g_{11} \end{pmatrix} = \begin{pmatrix} (\alpha^2 + \gamma^2) & (\alpha\beta + \gamma\delta) \\ (\alpha\beta + \gamma\delta) & (\beta^2 + \delta^2) \end{pmatrix} \quad [2.53c]$$

Similarly, Einstein's metric tensor allows us to move from a non-inertial reference frame, characterized by a curvature of space–time, to another in four-dimensional space.

3

Space Launchers for CubeSat Satellites

Launching a satellite into orbit requires a launcher to lift it above the Earth's atmosphere. Initially, launchers were provided by state institutions, such as NASA at Cape Canaveral, ESA in French Guiana and the Russian Space Agency at Baikonur.

As the space industry has developed, the number of sites and launchers has increased. Today, in addition to institutional launchers, private companies such as SpaceX are also active in the launcher market. This has helped to reduce the cost of launch and orbiting, which in turn has benefited CubeSats.

3.1. Propulsion systems and launch sites

A satellite is put into orbit by a launcher, which is the external subsystem to be considered when designing a satellite. Launchers are equipped with a propulsion system that enables them to overcome the Earth's gravitational pull in order to bring the satellite above the Earth's atmosphere and position it in its final orbit around the Earth or another planet.

A satellite's propulsion system has two functions:

– transferring the spacecraft from the launch vehicle orbit to its final orbit, or to an interplanetary trajectory for scientific missions;

– station keeping (in-orbit control) and attitude control in certain satellite operating modes.

For a color version of all of the figures in this chapter, see www.iste.co.uk/dahoo/nanosatellites1.zip.

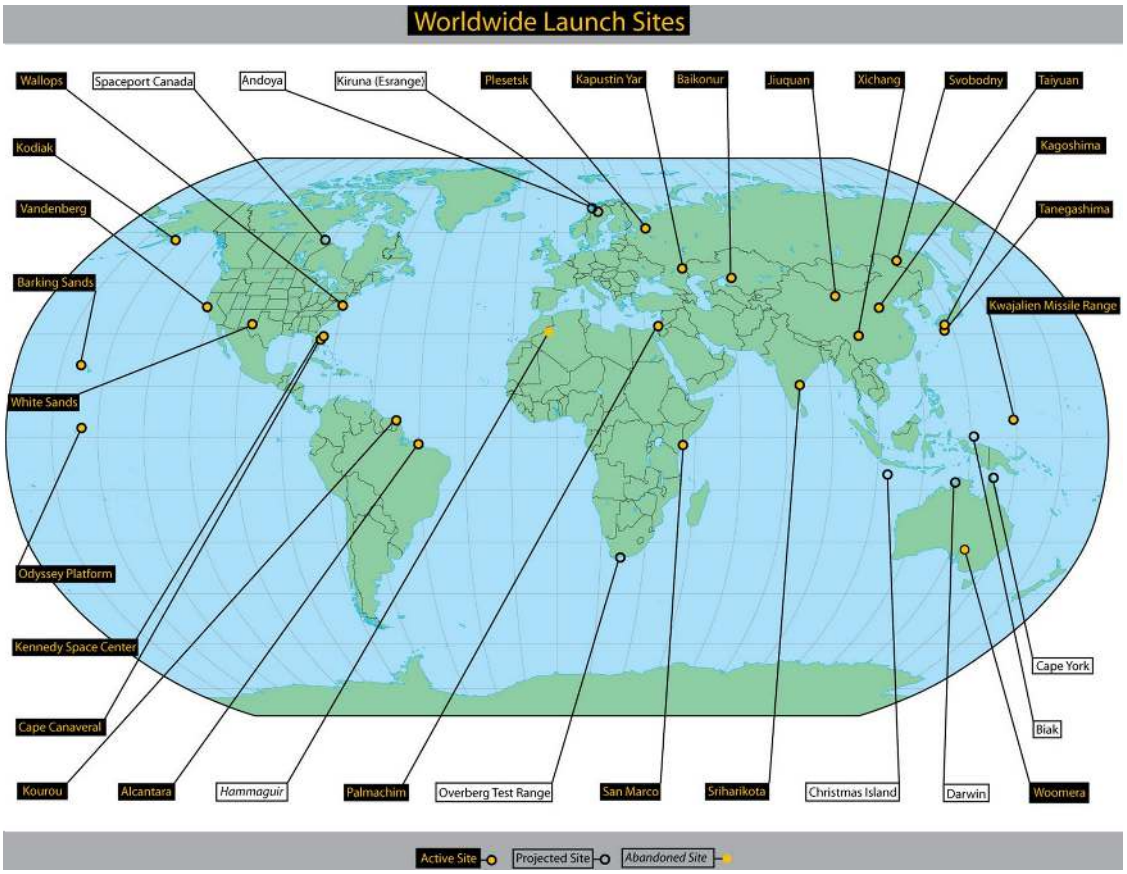

Figure 3.1. *Active and decommissioned launch sites worldwide*

The propulsion system must provide forces and torques with thrust forces ranging from a few mN to a few hundred N. These thrusts are obtained by ejecting pressurized, high-temperature gases that are expanded through a convergent–divergent supersonic nozzle.

The propulsion system is made up of the thrusters, the components needed to store and supply propellant to the thrusters, and sometimes a sub-assembly for pressurizing the propellant tanks. The mass of such a system can represent up to 20% of a satellite's total mass. A distinction must be made between dry mass and the mass of onboard propellants.

Initially, when the space age began, launchers were provided by state institutions such as NASA at Cape Canaveral and the Russian Space Agency at Baikonur, followed a little later by ESA through France in French Guiana. As the space industry has grown, so has the number of sites and launchers.

Today, in addition to other state institutions such as China, India and Canada, private companies such as SpaceX are taking over to exploit the launcher market and participate in the space industry. Figure 3.1 maps the various active or soon-to-be-active launch sites and those that have been decommissioned.

3.2. Launcher selection and satellite orbiting

This section looks at the criteria for selecting a space launcher to put satellites into orbit, as well as the main geographical areas where these launches take place.

Selecting a launcher depends on a number of parameters, such as:

– desired orbital parameters: the characteristics of the desired orbit (altitude, inclination, type of orbit) strongly influence the choice of a launcher. Some launchers are optimized for low, medium or geostationary orbits;

– launcher reliability: reliability is crucial, as it affects the probability of mission success. Launchers with a track record of success are often preferred;

– number of launches in a year: a high launch rate may indicate a launcher's maturity and operational capability;

– launcher vibration levels (quasi-static, sine, random, acoustic, shock, etc.): vibrations (quasi-static, sine, random, acoustic, shock) can affect satellite integrity and must be minimized;

– launch cost: cost is a major factor influencing the economic viability of the mission;

– geographic launch zone: the geographic position of the launch site can influence possible trajectories and logistics costs;

– geopolitical situation: geopolitical tensions may affect access to certain launchers or launch sites;

– ITAR-licensed equipment: the US International Traffic in Arms Regulations (ITAR) regulate the export of sensitive technologies. Satellites containing components subject to ITAR may be restricted to use on US launch vehicles.

In terms of launch density, the major satellite launch zones are the United States, the European Union, Russia and China (see Figures 3.2 and 3.3).

The Kennedy Space Center in the United States, Baikonur in Kazakhstan (Russia), the Guiana Space Center (Europe) and the Xichang launch base in China are the main key centers.

As shown in Figure 3.3, there are very few centers operated by countries in the Southern Hemisphere.

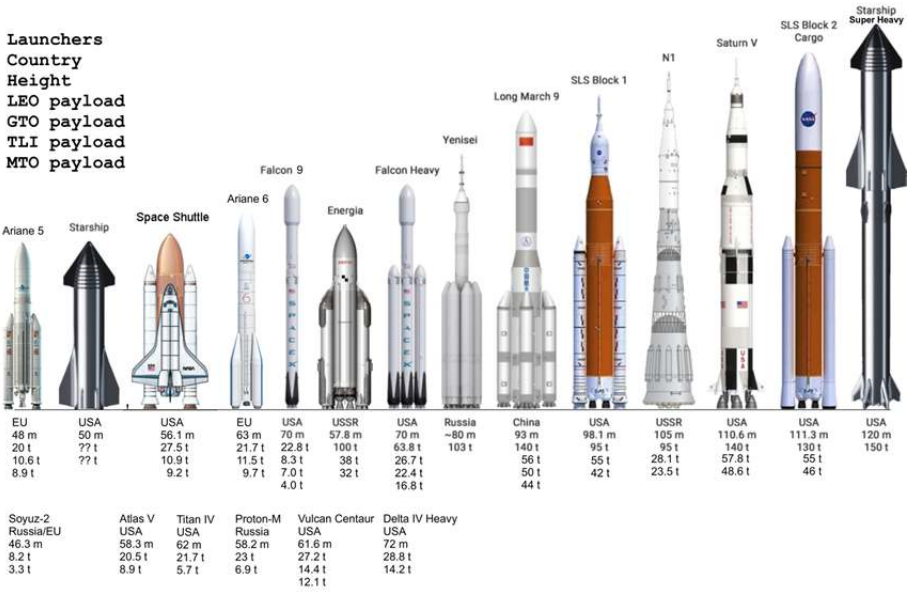

Figure 3.2. *The different launchers in the world's four main zones*

Figure 3.3. *Launch sites around the world*

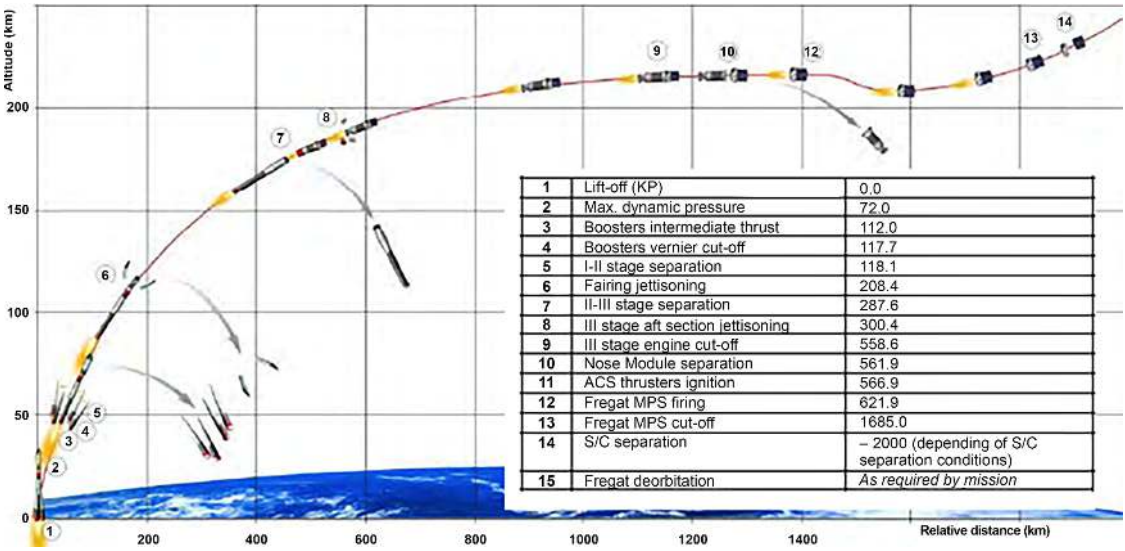

1	Lift-off (KP)	0.0
2	Max. dynamic pressure	72.0
3	Boosters intermediate thrust	112.0
4	Boosters vernier cut-off	117.7
5	I-II stage separation	118.1
6	Fairing jettisoning	208.4
7	II-III stage separation	287.6
8	III stage aft section jettisoning	300.4
9	III stage engine cut-off	558.6
10	Nose Module separation	561.9
11	ACS thrusters ignition	566.9
12	Fregat MPS firing	621.9
13	Fregat MPS cut-off	1685.0
14	S/C separation	– 2000 (depending of S/C separation conditions)
15	Fregat deorbitation	*As required by mission*

Figure 3.4. *The different phases in putting a satellite into orbit*

In the case of CubeSats, the relevant values for a 3U CubeSat (see Figure 3.2) are payload and thrust.

In summary, the choice of a space launcher is a complex process that depends on many technical, economic and geopolitical factors.

The main launch centers are located in the Northern Hemisphere (see Figure 3.3), reflecting the historical and current concentration of space capabilities in these regions. This analysis highlights the crucial considerations that influence decisions in the field of space launches.

Figures 3.4 and 3.5 show the various phases of the launch process. In the case of Figure 3.4, which concerns a Soyuz-type launcher, no parts of the launcher are recovered. The various phases are shown in Table 3.1.

Stages	Phases	Parameters
1	Take-off (KP)	0.0
2	Maximum dynamic Pressure	72.0
3	Intermediate thrust boosters	112.0
4	Vernier cut-off boosters	117.7
5	Separation of stages I-II	118.1
6	Jettisoning the faring	208.4
7	Separation of stages II-III	287.6
8	III Rear stage clearance	300.4
9	III Motor stage shutdown	558.6
10	Separation of nose module	561.9
11	ACS thruster ignition	566.9
12	Firing the MPS Frigate	621.9
13	MPS Frigate cut-off	1685.0
14	S/C Separation	- 2000 (Depends on S/C separation conditions)
15	De-orbiting the Frigate	Depending on mission requirements

Table 3.1. *The different phases in putting a satellite into orbit*

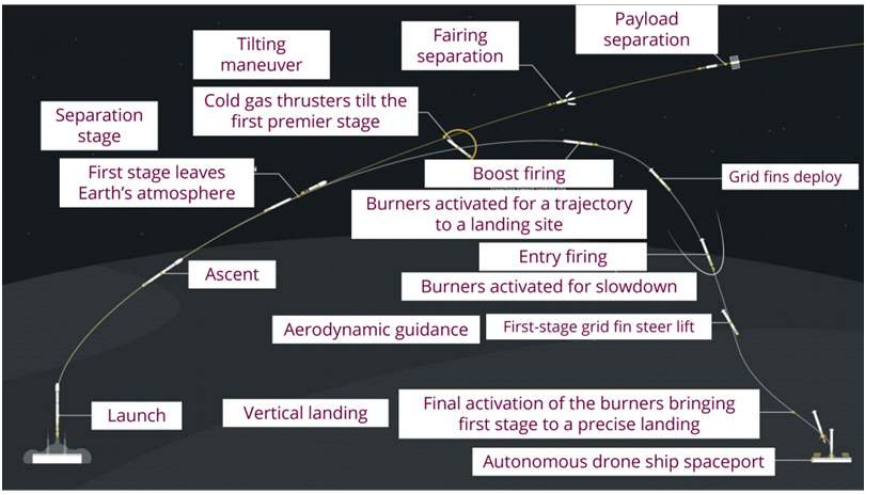

Figure 3.5. *The launch phase and recovery of launcher components*

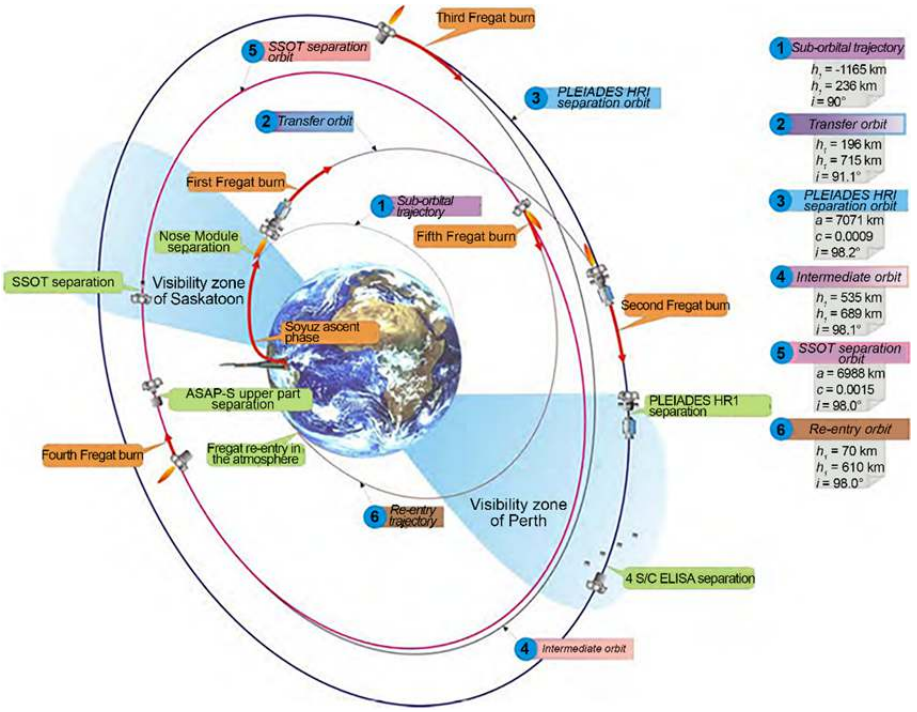

Figure 3.6. *Trajectories during launch and orbit with Soyuz*

Unlike the type of launch illustrated in Figure 3.4, the example shown in Figure 3.5 concerns launchers that can be recovered for reuse.

Here, we distinguish between two phases in the trajectory: the orbiting phase and the recovery phase.

The different phases in the orbiting of a satellite are carried out on different trajectories.

In the case shown in Figure 3.6, a Soyuz rocket has six different stages in the launch and orbiting phase of its trajectories around the Earth. The trajectory parameters are given in Table 3.2.

Stages	1	2	3	4	5	6
h_p (Km)	-1165	196		535		70
h_a (Km)	236	715		689		610
i (degrees)	90	91.1	98.2	98.1	98.0	98.0
a (Km)			7071		6988	
e (Km)			0.0009		0.0015	

Table 3.2. *The different trajectory parameters in orbiting*

– Stage 1 corresponds to the launch from the launch pad on a suborbital trajectory in the ascent phase.

– Stage 2 corresponds to the first firing of the frigate or rocket for orbit transfer to the second trajectory.

– Stage 3 corresponds to the separation orbit after the second rocket firing, for an orbit on which there are different load separations from the parent rocket: 1) Pleiades-HR1; 2) 4 S/C ELISA.

– Stage 4 corresponds to the third firing of the frigate or rocket for the intermediate orbit.

– Stage 5 corresponds to the SSOT separation orbit after the fourth rocket firing, for an orbit in which there are different load separations from the parent rocket: 1) the upper part (ASAP-S); 2) SSOT.

– Stage 6 corresponds to the re-entrance orbit after the fifth rocket firing, for an orbit on which the rocket re-enters the Earth's atmosphere.

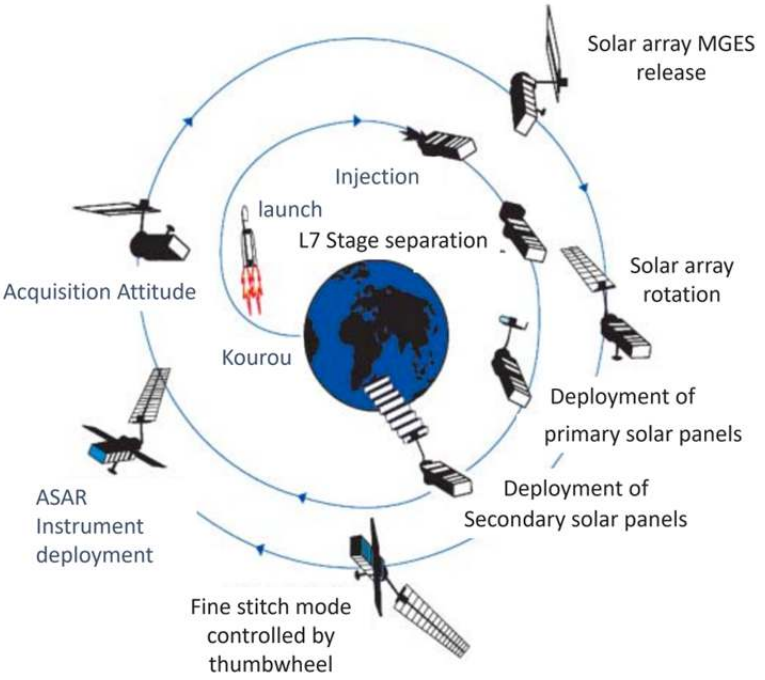

Figure 3.7. *The different phases and trajectories of Ariane*

In the case shown in Figure 3.7, the different phases from launch to orbit can be distinguished in the trajectories followed around the Earth by an Ariane rocket.

3.3. Important parameters for launcher selection

When designing a space system, it is necessary to anticipate the vibration and acoustic parameters of launchers in order to constrain their effects. Tables 3.3 and 3.4 show the frequency characteristics of the Soyuz launcher.

Direction	Frequency range (Hz)						
	1–5	5–10	10–20	20–30	30–40	40–60	60–100
	Sine amplitude (g)						
Longitudinal	0.4	0.5	0.8	0.8	0.5	0.5	0.3
Lateral	0.4	0.6	0.6	0.4	0.4	0.3	0.3

Table 3.3. *The characteristic frequencies of a Soyuz launcher (sine)*

Octave Center Frequency (Hz)	ST-type fairing
	Flight limit level (dB) (reference: 0 dB = 210^{-5} Pa)
31.5	86
63	92
125	93
250	99
500	103
1000	107
2000	113
OASPL (1) (20-2828 Hz)	118.3

(1) OASPL: Overall Sound Pressure Level

Table 3.4. *The characteristic frequencies of a Soyuz launcher (acoustic)*

Figure 3.8 shows the expected PSD (power spectral density) as a function of vibration frequency in random mode for a Falcon 9.

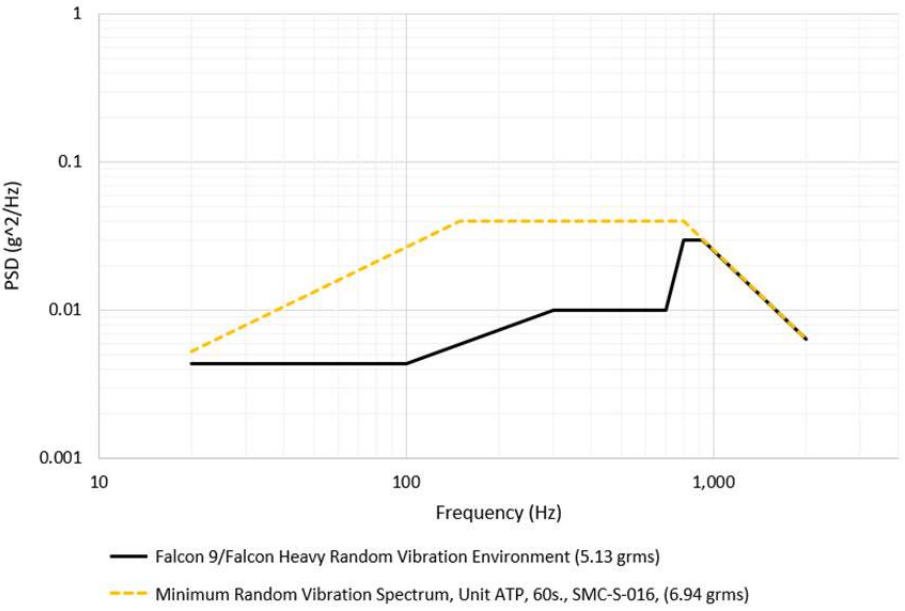

Figure 3.8. *Falcon 9 vibration parameters in log–log scale*

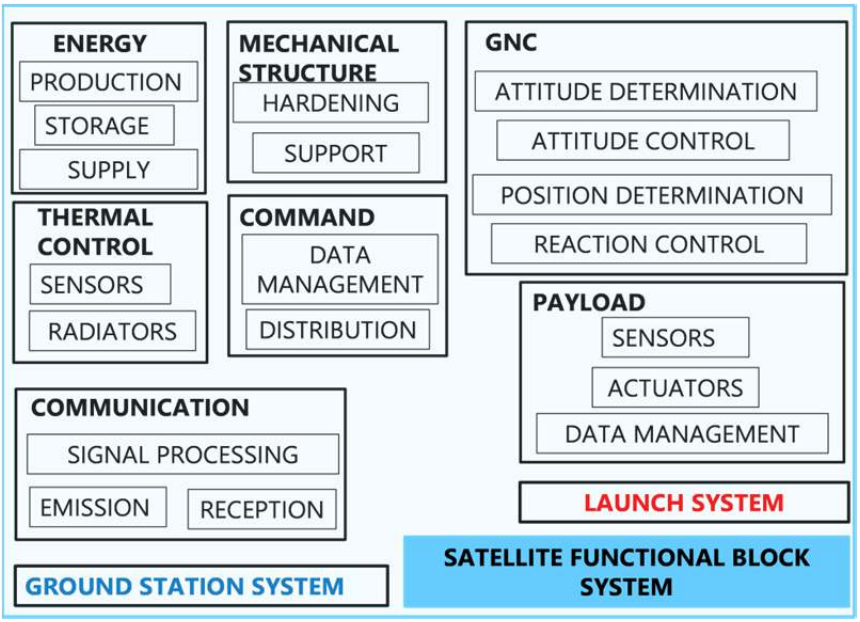

a)

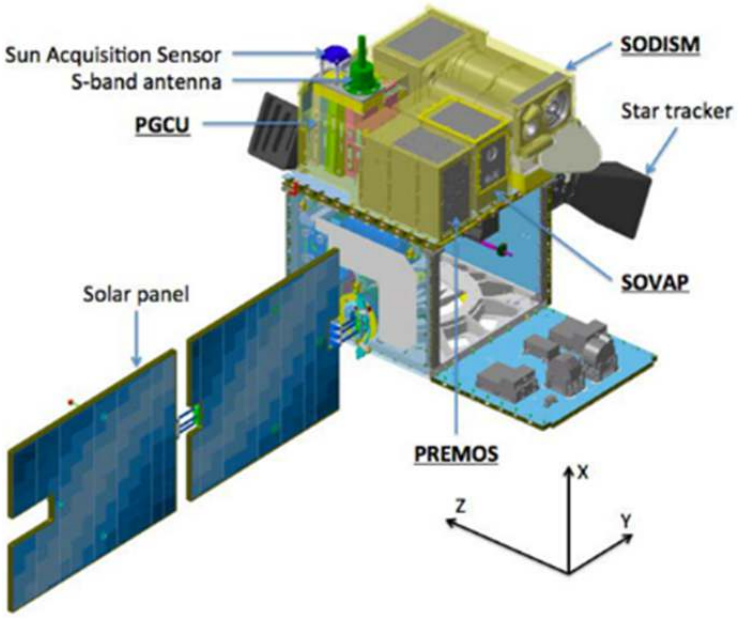

b)

Figure 3.9. *a) Block diagram; b) example of a satellite*

There is a quasi-static regime of 15 g around an average of 33 Hz, and a percussion regime corresponding to a shock of 1,000 g at 1,000 Hz.

It is therefore necessary to anticipate the various impacts and consequences on the satellite system.

A block diagram and an example are given in Figure 3.9 for a reminder of the various subsystems and the physical parameters to be considered such as volume, mass balance, power balances, linkage balances, *scientific need,* etc.

UVSQ-SAT is made up of several subsystems, including the mechanical structure, the power subsystem, the thermal control subsystem, the attitude determination and control subsystem (ADCS), the command and data handling subsystem (CDHS), the communication subsystem and the payload subsystem (Earth Radiation Sensor (ERS), UVS, TSIS and a three-axis accelerometer/ gyroscope/compass (TW sensor)).

To illustrate the key elements involved in putting a satellite into orbit, Figure 3.10 shows those of INSPIRE-SAT 7: launch, ejection, deployment, reception of the beacon identification signal and flight operations.

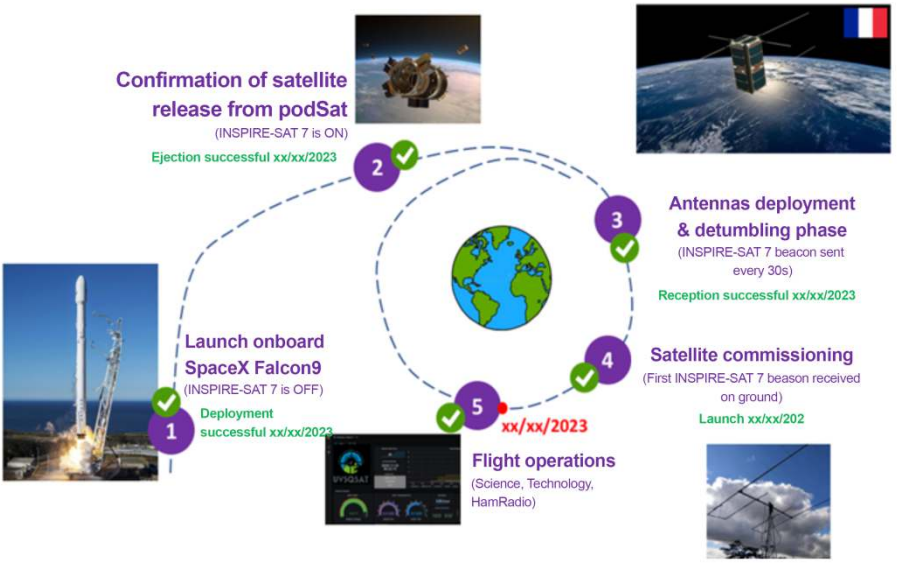

Figure 3.10. *Key milestones in the launch of INSPIRE-SAT 7*

3.4. Setting up and maintaining a satellite

As described in section 3.1, the main functions of a propulsion system are to transfer the satellite from the launch vehicle injection orbit to its final orbit (or to an interplanetary trajectory for scientific missions), and to provide station keeping (in-orbit control), as well as attitude control in certain satellite operating modes.

The parameters given for each phase can be identified as examples of the requirements of a propulsion system with a specific impulse (50–2,500 s) in the two main phases of orbit and attitude transfer and control.

– the transfer phase:

- spin 3–15 rpm,
- apogee 1,500 m/s,
- despin 15–0 rpm;

– the orbit and attitude control phase:

- fine positioning 8.5 m/s,
- N/S positioning 45 m/s per year,
- E/O positioning 3.5 m/s per year,
- deorbiting 6 m/s,
- attitude acquisition 8,500 Ns,
- three-axis control 10^5 Ns;

– a launcher can rely on different types of propulsion:

- solid propellant,
- cold gas (0.05–20 N),
- liquid, electric, plasma (0.1 N),
- electrostatic (0.02 N),
- electrothermal (0.2 N), etc.;

– ergol consumption, specific impulse and thrust: when launching a rocket, the parameters to consider are mass consumption of ergol, specific impulse and thrust.

The mass of ergol consumed in kg is given by the following equation:

$$\Delta M = M_0 \left(1 - e^{\frac{\Delta V}{g_0 I_{sp}}} \right) \qquad [3.1]$$

where M_0 (kg) is the launch mass, ΔV (ms^{-1}) is the velocity increment and $g_0 = 9.81\ ms^{-2}$ is the standard acceleration of gravity.

I_{sp} (s) is the specific impulse of the thruster, which can be expressed as:

$$I_{sp} = \frac{F}{g_0 \dot{m}} \quad [3.2]$$

where F (N) is the thrust and $\dot{m}$ (kgs^{-1}) is the mass flow rate.

The thrust F (N) of the thruster is written as:

$$F = \dot{m} V_S + A_S (P_S - P_{cc}) \quad [3.3]$$

where V_S (ms^{-1}) is the ejection velocity, A_S (m^2) is the nozzle outlet cross-section, P_S (Pa) is the pressure in the outlet plane and P_{cc} (Pa) is the external pressure.

To launch a rocket into orbit, it is necessary to know the weight of the rocket, the thrust of the engine and the resistance of the air. These are the three forces to which the rocket is subjected, as shown in Figure 3.11.

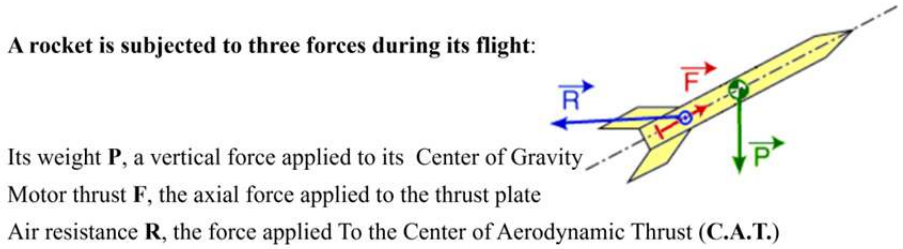

Figure 3.11. *The three forces (weight, thrust and resistance) in rocket take-off*

The variation Δv (m/s) in rocket velocity between the beginning and end of the propulsion phase is given by the following formula:

$$\Delta v = v_e ln \frac{m_0}{m_1} \quad [3.4]$$

where v_e (m/s) is the gas ejection velocity, m_0 is the total mass of the spacecraft at the start of the propulsion phase and m_1 is the total mass of the spacecraft at the end of the propulsion phase. m_0 and m_1 are expressed in the same units.

It is necessary to determine the forces and torques at work as the satellite moves along its trajectory in order to keep it on station.

The UVSQ-SAT CubeSat satellite is equipped with various subsystems and sensors, some of which are used to determine its attitude (ADCS and CDHS). These instruments are attached to the chassis of the spacecraft body. The CubeSat will orbit the Earth on an elliptical or circular trajectory, depending on the type of mission. A priori, at least two reference points are needed to locate the instruments and determine the satellite's attitude, i.e. one that is fixed in relation to the chassis system and one to the Earth system. This involves aligning the satellite's trihedron as closely as possible with the orbital reference frame in relation to which the satellite's orbit is defined, while ensuring stability and limiting angular velocities around the satellite's position.

Since the Earth rotates around its axis of revolution, it is also possible to have a third reference frame linked to the center of the Earth. Furthermore, the gyroscope measures angular velocity in the frame of reference linked to the satellite body, relative to an inertial frame of reference. Consequently, a reference frame is required. We can thus define an Earth-centered inertial reference frame and an Earth-centered orbit reference frame:

– *Earth-centered inertial reference frame* (ECI): the reference frame is defined with an origin at the Earth's center of mass. The X axis is defined as the axis of the vernal equinox at J2000, representing the intersection between the equatorial and ecliptic planes. The Z axis is defined as the Earth's rotation axis at J2000. Finally, the Y axis is defined along the above directions to create an orthogonal base. This reference frame is mainly used to describe the latitude and longitude of the satellite's center of mass in its orbit.

– *Earth-centered Earth-fixed reference frame* (ECEF): the reference frame is defined with an origin at the Earth's center of mass. Its X axis is defined at the intersection of the prime meridian of Greenwich and the equator. Its Y axis is the intersection of the equatorial plane and longitude 90°. The Z axis extends across the true North and South Poles, and coincides with the Earth's axis of rotation.

– *Earth-centered orbit reference frame* (OC): the reference frame is defined with an origin at the Earth's center of mass, with the X axis toward perigee, the Y axis along the semi-small axis and the Z axis perpendicular to the orbital plane to complete the straight-line system.

The different faces of the CubeSat are named in relation to the reference frame of the chassis, as shown in Figure 3.12. Two opposite faces correspond to an axis. The frame of reference of each instrument is fixed relative to the frame of reference

of the CubeSat chassis. The instrument undergoes a single constant rotation relative to the satellite frame of reference. This rotation must be applied for measurements to be referenced to the satellite frame of reference.

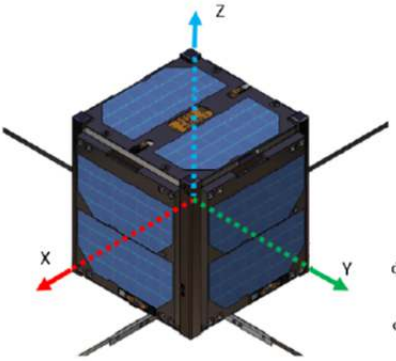

$$3-axis\ gyrometer: \quad \omega = \{\omega_X, \omega_Y, \omega_Z\}$$

$$3-axis\ magnetometer: \quad \mathrm{B} = \{\mathrm{B}_X, \mathrm{B}_Y, B_Z\}$$

$$6-panels\ photodiodes: \quad \Phi\mathrm{p} = \{\Phi\mathrm{p}_{+X}, \Phi\mathrm{p}_{-X}, \Phi p_{+Y}, \Phi p_{-Y}, \Phi\mathrm{p}_{+Z}, \Phi\mathrm{p}_{-Z}\}$$

$$6-ERS\ CNT: \quad \Phi cnt = \{\Phi\mathrm{cnt}_{+X}, \Phi\mathrm{cnt}_{-X}, \Phi cnt_{+Y}, \Phi cnt_{-Y}, \Phi\mathrm{cnt}_{+Z}, \Phi\mathrm{cnt}_{-Z}\}$$

$$6-ERS\ OSR: \quad \Phi osr = \{\Phi\mathrm{osr}_{+X}, \Phi\mathrm{osr}_{-X}, \Phi osr_{+Y}, \Phi osr_{-Y}, \Phi\mathrm{osr}_{+Z}, \Phi\mathrm{osr}_{-Z}\}$$

Figure 3.12. *The instrumental frame of reference is fixed relative to that of the satellite*

In this case, the Orbit Reference Frame (O) is used. It is defined so that its origin is located at the center of the CubeSat or satellite. The origin rotates relative to the ECI with an angular velocity of w_0. Its Z axis points toward the center of the Earth (the nadir). The X axis is perpendicular to the preceding axis in the direction of spacecraft motion. The Y axis completes the system in a right-axis frame of reference. The orbital frame of reference is used for attitude control.

Note that the axes involved in attitude control are such that: the x-axis is that of roll (left-to-right motion), unit of orbital velocity, tangent to the orbit; the y-axis is that of pitch (forward-to-reverse motion), unit of angular momentum, normal to the trajectory; the z-axis is that of yaw (motion around a vertical axis), geocentric.

If we denote w_b^i the angular velocity vector of the CubeSat body in the ECI, and I its moment of inertia matrix ($I_{xx} = I_{yy} = I_{zz} \cong 0.00205$ kg m^2), we can demonstrate that:

$$I\dot{w}_b^i = \mathrm{T}_{GG} + \mathrm{T}_{Aero} + \mathrm{T}_r + \mathrm{T}_M - w_b^i\left(Iw_b^i + h\right) - \dot{h} \qquad [3.5]$$

where $\dot{w}_b^i$ is the time derivative of w_b^i, T_{GG} is the gravity gradient (disturbance torque), T_{Aero} is the aerodynamic drag (disturbance torque), T_r is the residual torque, T_M is the control magnetic torque (with a control magnetic moment), h is the angular momentum vector of the reaction wheels and $\dot{h}$ is the time derivative.

Unit quaternions provide a convenient mathematical notation for representing the orientation and rotation of three-dimensional objects. In comparison with Euler angles, they are simpler to compose and avoid the problem of gimbal blocking. In comparison with rotation matrices, they are numerically more stable and can be more efficient.

In this case, the matrix equation in terms of quaternions has the following expression:

$$\begin{bmatrix} \dot{q}_1 \\ \dot{q}_2 \\ \dot{q}_3 \\ \dot{q}_4 \end{bmatrix} = \frac{1}{2} \begin{bmatrix} 0 & w_{oz} & -w_{oy} & w_{ox} \\ -w_{oz} & 0 & w_{ox} & w_{oy} \\ w_{oy} & -w_{ox} & 0 & w_{oz} \\ -w_{ox} & -w_{oy} & -w_{oz} & 0 \end{bmatrix} \begin{bmatrix} q_1 \\ q_2 \\ q_3 \\ q_4 \end{bmatrix} \quad [3.6]$$

where w_{ox}, w_{oy} and w_{oz} are the components of the angular velocity of the CubeSat body (w_b^O) (see Figure 3.13).

This angular velocity vector is linked to the body of the CubeSat (moving vector). It is expressed as a function of the angular velocity vector linked to the body of the CubeSat, w_b^i, in the ECI by the following relationship:

$$w_b^o = w_b^i - \mathrm{A}_{o/b}[0 - w_o\ 0]^T \quad [3.7]$$

where $\mathrm{A}_{o/b}$ is the transition matrix from reference system i (coordinate system linked to the Earth-centered orbit frame of reference) to reference system o (coordinate system linked to the orbit frame of reference centered on the CubeSat, the moving frame of reference). $[0 - w_o\ 0]^T$ is the transpose of the vector oriented along the Oy axis of the o frame of reference.

The coordinate transformation matrix $\mathrm{A}_{o/b}$ has the following expression:

$$A_{o/b} = \begin{bmatrix} q_1^2 - q_2^2 - q_3^2 + q_4^2 & 2(q_1q_2 + q_3q_4) & 2(q_1q_3 - q_2q_4) \\ 2(q_1q_2 - q_3q_4) & -q_1^2 + q_2^2 - q_3^2 + q_4^2 & 2(q_2q_3 + q_1q_4) \\ 2(q_1q_3 + q_2q_4) & 2(q_2q_3 - q_1q_4) & -q_1^2 - q_2^2 + q_3^2 + q_4^2 \end{bmatrix} \quad [3.8]$$

Figure 3.13 shows an example of an open-loop simulation with actuation of a magnetic coupler. In the absence of actuation, the UVSQ-SAT rotates with natural spin. After ten hours of natural spin, a 0.2 Am^2 actuation simulation is run along the CubeSat's X axis.

An actuation lasting 600 seconds alters the motion of the CubeSat, as shown in Figure 3.13. An actuation lasting 120 seconds generates a change in attitude rate greater than 0.05 radians per second (along the Y axis).

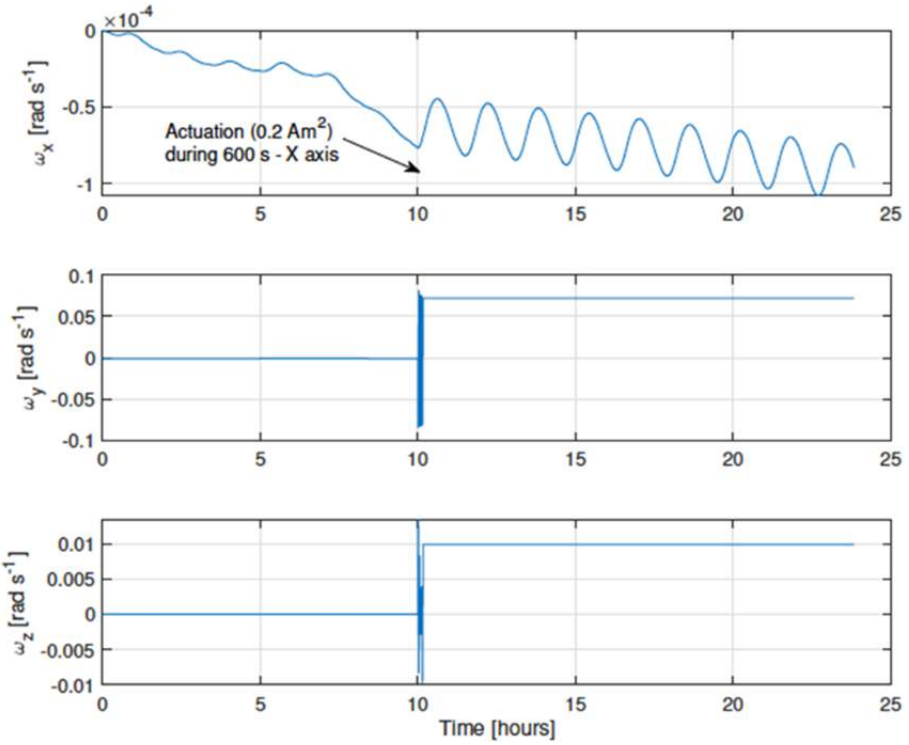

Figure 3.13. *Components of the angular velocity of the CubeSat body (w_b^O)*

Figure 3.14 shows the UVSQ-SAT example of CubeSat attitude measurement. Remember that a satellite's attitude is the orientation of a three-dimensional frame of reference linked to the satellite in relation to another frame of reference. The frame of reference outside the satellite is chosen from an inertial frame of reference (ECI) or a local orbital frame of reference (O): X in the direction of the satellite velocity vector (determined solely by the orbit), Z directed toward the center of the Earth and Y, so that (X, Y, Z) forms a direct trihedron. The X and Z axes are both contained in the orbital plane. Attitude control corresponds to the control of orientation in space and movements back and forth (pitch), left and right (roll) and around a vertical axis (yaw). The satellite's attitude is determined by measurements along the three axes of the magnetic field, as well as other measurements with onboard instruments such as the three-axis accelerometer, three-axis gyroscope and solar photodiodes. The gyroscope makes it possible to eliminate outliers in the initial determination of the satellite's attitude by magnetic and solar measurements (ground data processing). A method based on Kalman's extended multiplicative filter is used to determine the attitude, as shown in Figure 3.14.

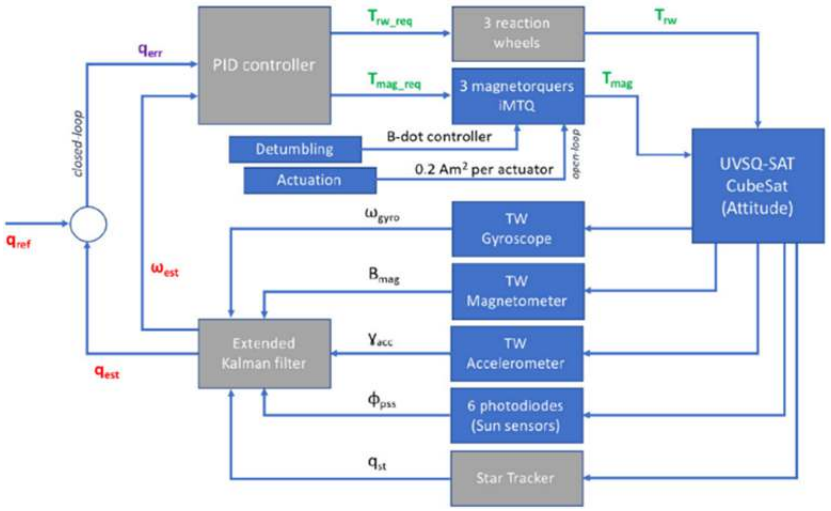

Figure 3.14. *ADCS general control loop on a CubeSat. In blue, the ADCS subsystems used in the UVSQ-SAT mission*

The gyroscope measures the CubeSat's rotation speed. The magnetometer measures the Earth's magnetic field. This provides a vector that is used to estimate the spacecraft's attitude. In addition, a magnetic field model is used to predict the direction of the field and its intensity at the spacecraft's position. The accelerometer measures the acceleration of the CubeSat, but these measurements are not used in determining the CubeSat's attitude. The six low-resolution photodiodes provide an estimate of the vector pointing toward the Sun in the CubeSat body axis reference frame.

The UVSQ-SAT CubeSat has three magnetic couplers. The UVSQ-SAT iMTQ board features a set of three perpendicular electromagnetic coils or actuators (two torsion bars for the X and Y axes with an actuator power per rod of 0.2 W, and an air coupler for the Z axis with an actuator power of 0.7 W). This is used with other vectors to provide CubeSat attitude information.

The three magnetic couplers create a magnetic field that interacts with the Earth's magnetic field. They are used to tilt the satellite after P-POD deployment. A tumbling mode is also available to reduce the movement of the CubeSat. UVSQ-SAT, with its iMTQ card, uses a simple algorithm to decelerate satellite rotation. The couplers are also used to rotate the CubeSat (actuation). In the case of UVSQ-SAT, it is only possible to operate the couplers using a CubeSat remote control (open loop).

The servo-control system used to maintain the CubeSat's attitude is made up of the sensor subsystems gyroscope, magnetometer, accelerometer, six photodiodes

and Star Tracker, which supply dynamic position and orientation data. After filtering, the data is sent to a PID, which receives the value of the error on the estimated position quaternion with respect to the reference value, and the estimated value of the angular orientation. The latter outputs two signals corresponding to the required values of T_M and T_r, the required control magnetic torque (with a control magnetic moment) and the required residual torque, to activate the three reaction wheels and three magnetic couplers (iMTQ) for CubeSat station keeping.

The satellite's spin movement is made possible by the use of "magnetic couplers". It is possible to vary the magnetic moment by up to 0.2 Am^2 (0.2 per Tesla) for each axis of the UVSQ-SAT, with maximum power consumption of the iMTQ on the electronic board close to 1.2 W.

The magnetic torque T_M is given by:

$$T_M = M_m B \qquad [3.9]$$

where M_m is the magnetic moment and B is the geomagnetic field.

A magnetic coupler with a dipole moment of 0.2 Am^2 is a good compromise for flexibility (see Figure 3.13, valid up to a 3U CubeSat). In less than 120 seconds of activation, the CubeSat can be moved to reach the desired target point (see Figure 3.14).

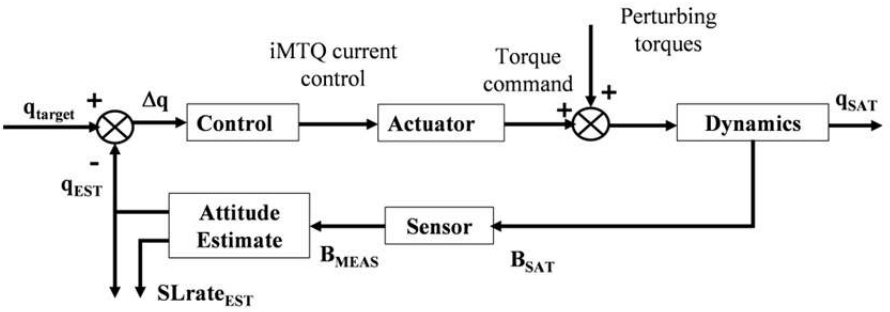

Figure 3.15. *UVSQ-SAT control system diagram*

The Earth's magnetic field, which can be measured by UVSQ-SAT, varies in intensity mainly as a function of latitude (ϕ) and altitude (h). A simplified model leads to the following expression for the field B:

$$B(x,y,z) = B_0 \left(\frac{R_E}{R_E+h}\right)^3 + \sqrt{1+3sin^2(\phi)} \qquad [3.10]$$

where B_0 is equal to 30 μT and ϕ is the latitude measured from the equator (0 degrees) to the poles (90 degrees).

3.4.1. *CubeSat trajectory*

The equations of motion are linearized to determine the CubeSat's trajectory. The dynamic equation expresses the orientation motion as a function of the torques experienced by the satellite.

In its local reference frame, the application of the moment of inertia theorem leads to the following equation:

$$I\frac{d}{dt}\left(\vec{\omega}_{b/I}\right) + \vec{\omega}_{b/I} \wedge I\vec{\omega}_{b/I} = \sum \vec{C}^b \quad [3.11]$$

where I is the inertia matrix, $\vec{\omega}_{b/I}$ is the angular velocity of the satellite in its frame b relative to the inertia frame I, and $\sum \vec{C}^b$ is the sum of the torques acting on the satellite.

The kinematic equation in terms of the quaternion $\boldsymbol{q}(t)$ is used to determine velocity variations and is written as follows:

$$\frac{d}{dt}\boldsymbol{q}(t) = \frac{1}{2}\left(\boldsymbol{\omega_{b/o}} \otimes \boldsymbol{q}\right) \quad [3.12]$$

where the quaternion $\boldsymbol{\omega_{b/o}} = (0, \vec{\omega}_{b/o})$.

The linearization assumption is justified in the case of small perturbations between each estimate, leading to $\vec{\omega}_{est,k+1} = \vec{\omega}_{est,k} + \overrightarrow{\delta\omega}$.

The expression for the state vector is given by $\vec{X}(t) = \begin{pmatrix} \overrightarrow{\delta\omega}(t) \\ \delta\boldsymbol{q}(t) \end{pmatrix}$, so that the dynamic equation is written in the following form:

$$\frac{d}{dt}\begin{pmatrix} \overrightarrow{\delta\omega}(t) \\ \delta\boldsymbol{q}(t) \end{pmatrix} = F(\tilde{x}(t), t)\begin{pmatrix} \overrightarrow{\delta\omega}(t) \\ \delta\boldsymbol{q}(t) \end{pmatrix} \quad [3.13]$$

The observation model leads to the following equations:

$$\vec{e}_k = \vec{y}^b_{mes,k} \wedge \vec{y}^b_{est,k} = \vec{y}^b_{mes,k} \wedge P^b_0\left(\boldsymbol{q}_{est,k}\right)\vec{y}^0_k \quad [3.14]$$

with $\vec{y}^0_k$ determined using the magnetic field model.

From the expressions $\frac{d\vec{r}(t)}{dt} = \vec{V}(t)$ and $\frac{d\vec{V}(t)}{dt} = \vec{\Gamma}_g + \vec{\Gamma}_{aero}$, the new state vector takes the following form:

$$\vec{X}(t) = \begin{pmatrix} \overrightarrow{\delta\omega}(t) \\ \delta\boldsymbol{q}(t) \\ \vec{r}(t) \\ \vec{V}(t) \end{pmatrix} \quad [3.15]$$

In-orbit maneuvers to maintain the satellite in orbit are mainly of two types: major, requiring high-speed increments, or impulse, for in-orbit satellite maintenance.

– major, requiring high-speed incrementation:

- apogee maneuver from GTO orbit to geostationary orbit,

- orbital inclination correction,

- change of program for a space probe, e.g. diversion to a new comet,

- deorbiting maneuver for a return to Earth from an orbital station,

- injection into a hyperbolic escape orbit in preparation for interplanetary travel;

– impulse, to maintain a satellite in orbit:

- minor corrections to orbital parameters,;

- corrections to avoid collisions,

- orbital time recalibration,

- adjustment of arrival time on a planet.

3.5. Conclusion

Putting a satellite into orbit requires the use of a launcher. In the 21st century, launchers are being proposed by public state bodies or private companies following the evolution of the space age presented in the first chapter. Legislation imposes standards that satellite manufacturers must meet. Satellite specifications are fairly restrictive in terms of safety, avoidance of collision with other elements in orbit, and controlled degradation and end-of-life cycle. The selection of a launcher depends on standard parameters, such as cost and deadlines, and also on the geopolitical situation and the availability of the launcher. Given the laws of physics, these launchers are able to put satellites into orbit, generally at altitudes which are

between 500 and 600 km above the Earth's surface for CubeSats and higher for larger satellites. The altitude of the orbit entails different standards to be met, which are more stringent above 600 km.

3.6. Appendix

3.6.1. *The mechanics of a solid body*

When studying the orbit of a solid object such as a natural or artificial satellite around a central body, which may be a planet or a star, it is necessary to have at least two axis systems: one coincident with the moving solid and the other coincident with the attracting center. The difference between a material point and a solid body regarded as rigid to a first approximation, i.e. not subject to vibrations, is that the solid can be in translational motion as well as in rotational motion.

Two coordinate systems are therefore used to describe the motion of the solid (see Figure 3.16): an "immobile system", i.e. a Galilean system XYZ with center O, and a moving coordinate system X′ = x, Y′ = y, Z′ = z (when O and G coincide), which is assumed to be rigidly connected to the solid body and to participate in all its translational and rotational motions. As usual, the origin of the moving system is placed at the body's center of inertia G. In this case, the position of the solid relative to the stationary system is completely determined if the position of the moving system is given.

Let $\vec{R}$ be the radius vector indicating the position of the origin G of the moving system (see Figure 3.16). The orientation of the axes of the latter with respect to the immobile system is defined by three independent angles. With the three components of the vector $\vec{R}$, the system linked to the solid is described by means of six coordinates, making the solid body a mechanical system with six degrees of freedom.

To study the motion of a point M(x, y, z) linked to the moving solid, marked by the radius vector $\vec{R}'$(X′, Y′, Z′) in the fixed reference frame, we decompose the motion into a translation-only motion from the origin to the center of inertia G($d\overrightarrow{OG}(X,Y,Z)$) and a rotation-only motion of the reference frame of center G($x = 0, y = 0, z = 0$) defined by a given axis of rotation marked by a vector $\vec{n}$ and an angle of rotation $d\psi$.

Thus, the elementary displacement $d\overrightarrow{OM}(X',Y',Z')$ of any point M(x, y, z) is given by the expression:

$$d\overrightarrow{\mathrm{OM}} = d\overrightarrow{\mathrm{OG}} + d\psi\vec{n} \wedge \overrightarrow{\mathrm{GM}} \qquad [3.16]$$

where $d\overrightarrow{OG}$ is the displacement of the center of inertia G in its translational motion and that of the point M which changes position during rotation by an angle $d\psi$ around the axis passing through G and tracked down by the vector $\vec{n}$.

Calculating the velocity of point M(x, y, z) leads to the following expression:

$$\vec{v} = \frac{d\overrightarrow{OM}}{dt} = \frac{d\overrightarrow{OG}}{dt} + \frac{d\psi}{dt}\vec{n} \wedge \overrightarrow{GM} = \frac{d\vec{R}}{dt} + \frac{d\psi}{dt}\vec{n} \wedge \vec{r} = \vec{V} + \vec{\Omega} \wedge \vec{r} \qquad [3.17a]$$

where $\vec{V}$ is the speed of the center of inertia G in its translational motion and $\vec{\Omega}$ is the angular speed of rotation of the satellite or solid body of direction defined by the axis of rotation $\vec{n}$.

Note that if point M has a velocity $\left(\frac{d\overrightarrow{GM}}{dt}\right)_G = \left(\frac{d\vec{r}}{dt}\right)_G = \vec{v}'$ relative to the moving frame of reference, which moves while rotating, the velocity of point M(x, y, z) is written as follows:

$$\vec{v} = \frac{d\overrightarrow{OM}}{dt} = \vec{V} + \left(\frac{d\overrightarrow{GM}}{dt}\right)_G + \vec{\Omega} \wedge \vec{r} = \vec{V} + \vec{v'} + \vec{\Omega} \wedge \vec{r} \qquad [3.17b]$$

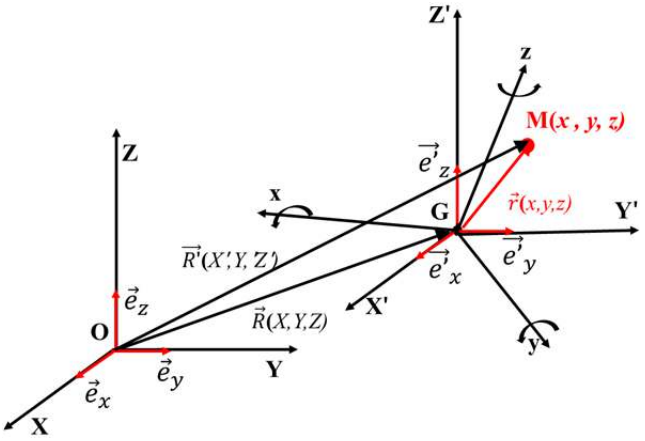

Figure 3.16. *Systems of direct orthonormal axes: fixed (O, X, Y, Z), associated with the reference frame of the center of forces (the Earth or the Sun) and assumed to be Galilean, (G, x, y, z) linked to the equilibrium configuration of the satellite (artificial or natural) and (G, X', Y', Z') linked to the satellite in its translational motion*

When $\vec{v}'$ is equal to zero, the acceleration of point M(x, y, z) is written as follows:

$$\vec{a} = \left(\frac{d(\vec{V}+\vec{\Omega}\wedge\vec{r})}{dt}\right)_O = \left(\frac{d\vec{V}}{dt}\right)_O + \left(\frac{d\vec{\Omega}\wedge\vec{r}}{dt}\right)_O = \left(\frac{d\vec{V}}{dt}\right)_O + \left(\frac{d\vec{\Omega}}{dt}\wedge\vec{r}\right)_O + \left(\vec{\Omega}\wedge\frac{d\vec{r}}{dt}\right)_O$$

[3.18]

where $\frac{d\vec{V}}{dt}$ is the acceleration of the center of inertia G in its translational motion. This gives rise to a driving force (force field of the equivalence principle) when multiplied by the point mass located at M.

By expanding expression [3.18], we get:

$$\vec{a} = \left(\frac{d\vec{V}}{dt}\right)_O + \left(\frac{d\vec{\Omega}}{dt}\right)_O \wedge \vec{r} + \vec{\Omega}\wedge\left(\vec{\Omega}\wedge\vec{r}\right) \qquad [3.19]$$

where $\vec{\Omega}$, the angular speed of rotation of the satellite or solid, is assumed to be non-uniform, leading to the term $\frac{d\vec{\Omega}}{dt}\wedge\vec{r}$, and where the term $\vec{\Omega}\wedge\left(\vec{\Omega}\wedge\vec{r}\right)$ due to the rotation of the reference system linked to the satellite gives rise to an inertial acceleration that results in a so-called "centrifugal" inertial force when multiplied by the point mass located at M.

If point M has a velocity $\vec{v}'$ relative to the moving frame of reference, which moves while rotating, the acceleration of point M(x, y, z) is written as follows:

$$\vec{a} = \frac{d\vec{OM}}{dt} = \left(\frac{d\vec{V}}{dt}\right)_O + \left(\frac{d\vec{v}'}{dt}\right)_O + \left(\frac{d\vec{\Omega}}{dt}\right)_O \wedge \vec{r} + \left(\vec{\Omega}\wedge\frac{d\vec{r}}{dt}\right)_O \qquad [3.20]$$

In this case, we have:

$$\left(\frac{d\vec{v}'}{dt}\right)_O = \left(\frac{d\vec{v}'}{dt}\right)_G + \vec{\Omega}\wedge\vec{v}' \qquad [3.21a]$$

and:

$$\left(\vec{\Omega}\wedge\frac{d\vec{r}}{dt}\right)_O = \vec{\Omega}\wedge\left(\left(\frac{d\vec{r}}{dt}\right)_G \wedge \left(\vec{\Omega}\wedge\vec{r}\right)_O\right)_O = \vec{\Omega}\wedge\vec{v}' + \vec{\Omega}\wedge\left(\vec{\Omega}\wedge\vec{r}\right) \qquad [3.21b]$$

By expanding expression [3.20], we determine the following expression:

$$\vec{a} = \left(\frac{d\vec{V}}{dt}\right)_O + \left(\frac{d\vec{v}'}{dt}\right)_G + 2\vec{\Omega}\wedge\vec{v}' + \frac{d\vec{\Omega}}{dt}\wedge\vec{r} + \vec{\Omega}\wedge\left(\vec{\Omega}\wedge\vec{r}\right) \qquad [3.22]$$

where, in addition to the relative acceleration of point M in the translating and rotating frame of reference, an inertial or Coriolis acceleration term appears. This gives rise to a Coriolis inertial force when multiplied by the mass of point M.

Note that this Coriolis inertia term can become significant in a CubeSat's in-flight reliability issue if the subsystems attached to the satellite frame are not rigidly fixed to the frame.

3.6.2. *Euler angles and rotation matrix*

In order to study block rotations of a rigid system, we rely on the identification of the axis of rotation defined by a unit vector $\hat{n}$ and the angle of rotation ϕ. The two angles (polar, θ, and azimuthal, φ), which in the spherical coordinate system identify the unit vector and the angle of rotation, ϕ, show that three parameters are needed to define a rotation in three-dimensional space. The same rotation can also be defined using three Cartesian components of the vector $\hat{n}\phi$. This method is not easy to apply when studying the properties of rotations. For example, the addition of vectors of type $\hat{n}\phi$ is not possible if successive rotations are to be characterized [HAM 62, LIP 65, EDM 74, GIL 74, LAN 75, SAK 94, TIN 03].

It is easier to use 3 X 3 orthogonal matrices, which form the SO(3) group under the matrix multiplication operation (S for special, O for orthogonal and 3 for dimension 3). It is therefore customary to define the rotation of the molecule's frame of reference in terms of the three Euler angles, which position the moving frame of reference in relation to the fixed one, by means of three rotations around three axes. These rotations and axes are defined as a rotation by an angle $\theta\,(0 \leq \theta \leq 2\pi)$ around the Z axis of the fixed frame of reference [HAM 62, LAN 66a, ROS 67, EDM 74], a rotation by an angle $\varphi\,(0 \leq \varphi \leq \pi)$ around the line of nodes (new position of the OY axis of the starting fixed frame of reference after the first rotation) and a rotation by an angle $\chi\,(0 \leq \chi \leq 2\pi)$ around the z = z' axis of the moving frame of reference (final position of the OZ axis of the starting fixed frame of reference).

If we refer to R(θ, φ, χ) as the operator corresponding to the three rotations and defined by $R(\theta,\varphi,\chi) = \exp\left(\frac{-i\chi}{\hbar}J_z\right)\exp\left(\frac{-i\varphi}{\hbar}J_{y'}\right)\exp\left(\frac{-i\theta}{\hbar}J_Z\right)$, it can be seen that we can define the rotation operation with respect to the fixed axes such that $R(\theta,\varphi,\chi) = \exp\left(\frac{i\chi}{\hbar}J_Z\right)\exp\left(\frac{i\varphi}{\hbar}J_Y\right)\exp\left(\frac{i\theta}{\hbar}J_Z\right)$ using the transformations $R_{y'}(\varphi) = R_Z(\theta)\,R_Y(\varphi)\,R_Z^{-1}(\theta)$ and $R_{z'}(\chi) = R_{y'}(\varphi)\,R_Z(\chi)\,R_{y'}^{-1}(\varphi)$, where the three matrices refer to rotations around fixed axes.

Let $(O,\vec{X},\vec{Y},\vec{Z})$ and $(O,\vec{x},\vec{y},\vec{z})$ be two direct orthonormal coordinate systems. The orientation of the reference frame $(O,\vec{x},\vec{y},\vec{z})$ with respect to the reference frame $(O,\vec{X},\vec{Y},\vec{Z})$ can be broken down into three successive elementary rotations, namely $\boldsymbol{\varphi}$ "precession", $\boldsymbol{\theta}$ "nutation" and $\boldsymbol{\chi}$ "proper rotation" (Euler angles), according to the following layout:

$(O, \vec{X}, \vec{Y}, \vec{Z}) \quad \rightarrow \quad (O, \vec{x}, \vec{y}, \vec{z})$

– *rotation* $\boldsymbol{\varphi}$ *around axis* OZ $(O, \vec{X}, \vec{Y}, \vec{Z}) \rightarrow (O, \vec{x}_1, \vec{y}_1, \vec{z}_1)$ with $Oz_1 = OZ$

– *rotation* $\boldsymbol{\theta}$ *around axis* Oy_1 $(O, \vec{x}_1, \vec{y}_1, \vec{z}_1) \rightarrow (O, \vec{x}_2, \vec{y}_2, \vec{z}_2)$ with $Oy_2 = Oy_1$

– *rotation* $\boldsymbol{\chi}$ *around axis* Oz_2 $(O, \vec{x}_2, \vec{y}_2, \vec{z}_2) \rightarrow (O, \vec{x}, \vec{y}, \vec{z})$ with $Oz = Oz_2$

with reference to Figure 3.17.

1) *Rotation of angle* $\boldsymbol{\varphi}$ $(0 \; to \; 2\,\pi)$ *around axis OZ.*

The basis vectors of $(O, \vec{x}_1, \vec{y}_1, \vec{z}_1)$ are expressed in terms of the basis vectors of $(O, \vec{X}, \vec{Y}, \vec{Z})$:

$$\vec{x}_1 = cos\,\varphi\ \vec{X} + \sin\varphi\ \vec{Y} + 0 \times \vec{Z} \qquad [3.23a]$$

$$\vec{y}_1 = -\,sin\,\varphi\ \vec{X} + \cos\varphi\ \vec{Y} + 0 \times \vec{Z} \qquad [3.23b]$$

$$\vec{z}_1 = 0 \times \vec{X} + 0 \times \vec{Y} + 1 \times \vec{Z} \qquad [3.23c]$$

which can be written in matrix form as:

$$\begin{pmatrix} \vec{x}_1 \\ \vec{y}_1 \\ \vec{z}_1 \end{pmatrix} = \begin{pmatrix} \cos\varphi & \sin\varphi & 0 \\ -\sin\varphi & \cos\varphi & 0 \\ 0 & 0 & 1 \end{pmatrix} \begin{pmatrix} \vec{X} \\ \vec{Y} \\ \vec{Z} \end{pmatrix} \qquad [3.23d]$$

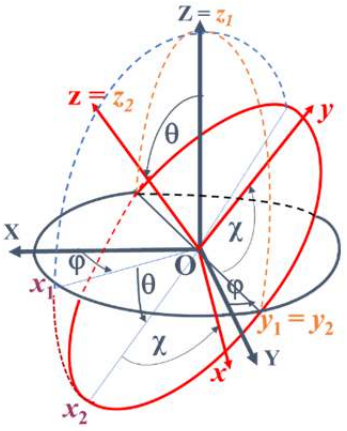

Figure 3.17. *Euler angles for moving from one reference frame (O, X, Y, Z) to another (O, x, y, z)*

2) *Rotation of angle* $\boldsymbol{\theta}$ $(0\ to\ \pi)$ *around axis* Oy_1.

The basis vectors of $(O, \vec{x}_2, \vec{y}_2, \vec{z}_2)$ are expressed in terms of the basis vectors of $(O, \vec{x}_1, \vec{y}_1, \vec{z}_1)$:

$$\vec{x}_2 = cos\,\theta\ \vec{x}_1 + 0 \times \vec{y}_1 - \sin\theta\ \vec{z}_1 \quad [3.24a]$$

$$\vec{y}_2 = 0 \times \vec{x}_1 + 1 \times \vec{y}_1 + 0 \times \vec{z}_1 \quad [3.24b]$$

$$\vec{z}_2 = sin\,\theta\ \vec{x}_1 + 0 \times \vec{y}_1 + \cos\theta\ \vec{z}_1 \quad [3.24c]$$

which can be written in matrix form as:

$$\begin{pmatrix} \vec{x}_2 \\ \vec{y}_2 \\ \vec{z}_2 \end{pmatrix} = \begin{pmatrix} \cos\theta & 0 & -\sin\theta \\ 0 & 1 & 0 \\ \sin\theta & 0 & \cos\theta \end{pmatrix} \begin{pmatrix} \vec{x}_1 \\ \vec{y}_1 \\ \vec{z}_1 \end{pmatrix} \quad [3.24d]$$

3) *Rotation of angle* $\boldsymbol{\chi}$ $(0\ to\ 2\,\pi)$ *around axis* Oz_2.

The basis vectors of $(O, \vec{x}, \vec{y}, \vec{z})$ are expressed in terms of the basis vectors of $(O, \vec{x}_2, \vec{y}_2, \vec{z}_2)$:

$$\vec{x} = cos\,\chi\ \vec{x}_2 + \sin\chi\,\vec{y}_2 + 0 \times \vec{z}_2 \quad [3.25a]$$

$$\vec{y} = -\,sin\,\chi\ \vec{x}_2 + \cos\chi\,\vec{y}_2 + 0 \times \vec{z}_2 \quad [3.25b]$$

$$\vec{z} = 0 \times \vec{x}_2 + 0 \times \vec{y}_2 + 1 \times \vec{z}_2 \quad [3.25c]$$

which can be written in matrix form as:

$$\begin{pmatrix} \vec{x} \\ \vec{y} \\ \vec{z} \end{pmatrix} = \begin{pmatrix} \cos\chi & sin\,\chi & 0 \\ -\,sin\,\chi & \cos\chi & 0 \\ 0 & 0 & 1 \end{pmatrix} \begin{pmatrix} \vec{x}_2 \\ \vec{y}_2 \\ \vec{z}_2 \end{pmatrix} \quad [3.25d]$$

The base vectors of the $(\mathrm{O}, \vec{x}, \vec{y}, \vec{z})$ frame are written in terms of the base vectors of the $(\mathrm{O}, \vec{\mathrm{X}}, \vec{\mathrm{Y}}, \vec{\mathrm{Z}})$ frame by multiplying the matrices and respecting the order of rotation operations:

$$\begin{pmatrix} \vec{x} \\ \vec{y} \\ \vec{z} \end{pmatrix} = \begin{pmatrix} \cos\chi & sin\,\chi & 0 \\ -\,sin\,\chi & \cos\chi & 0 \\ 0 & 0 & 1 \end{pmatrix} \begin{pmatrix} \cos\theta & 0 & -\sin\theta \\ 0 & 1 & 0 \\ \sin\theta & 0 & \cos\theta \end{pmatrix} \begin{pmatrix} \cos\varphi & \sin\varphi & 0 \\ -\sin\varphi & \cos\varphi & 0 \\ 0 & 0 & 1 \end{pmatrix} \begin{pmatrix} \vec{X} \\ \vec{Y} \\ \vec{Z} \end{pmatrix}$$

[3.26a]

Finally, the unitary rotation transformation matrix $R(\varphi,\theta,\chi)$, which is the product of the three matrices, is ultimately expressed as:

$$R(\varphi,\theta,\chi) = \begin{pmatrix} cos\,\varphi\ \cos\theta\cos\chi - \sin\varphi\sin\chi & \sin\varphi\cos\theta\cos\chi + \cos\varphi\sin\chi & -sin\,\theta\ \cos\chi \\ -\cos\varphi\cos\theta\sin\chi - \sin\varphi\cos\chi & -sin\,\varphi\ \cos\theta\sin\chi + \cos\varphi\cos\chi & \sin\theta\sin\chi \\ \cos\varphi\sin\theta & \sin\varphi\sin\theta & \cos\theta \end{pmatrix} \quad [3.26b]$$

3.6.3. *Quaternions*

A quaternion is a hypercomplex number that is an extension of complex numbers in four dimensions, invented by Sir William Rowan Hamilton in 1843 [HAM 44–50]. A quaternion is a quadruplet of real numbers where the first element is a "scalar" (q_0) and the three elements are grouped in the form of a "vector" or "pure imaginary" number $\vec{q} = (q_1, q_2, q_3)$.

A quaternion **q** is written in the following form:

$$\boldsymbol{q} = (q_0, \vec{q}) \quad [3.27]$$

or as an extension of a complex number $\boldsymbol{z} = a + ib = |z|e^{i\theta} = |z|(\cos\theta + isin\theta)$, operating in two-dimensional space, to a hypercomplex number operating in four-dimensional space, in the form:

$$\boldsymbol{q} = q_0 + iq_1 + jq_2 + kq_3 = q_0 + \vec{q} \quad [3.28]$$

with $i^2 = -1, j^2 = -1, k^2 = -1, ijk = -1$ and $ij = k = -ji, jk = i = -kj, ki = j = -ik$. Quaternions are used or operate in four-dimensional space. A quaternion can be represented by q_0, a scalar, and $\vec{q}$, a vector.

In the same way that operations with complex numbers can be interpreted as a computational method for representing rotations in 2D, quaternions can be used to extend the notion of rotation in three dimensions to that in four. Calculating with quaternions avoids the gimbal effect when using three rotations with Euler angles to move from one frame of reference to another in 3D.

3.6.3.1. *Quaternion operations*

Let there be two quaternions, p and q:

$$p = p_0 + p_1 i + p_2 j + p_3 k \quad [3.29a]$$

$$q = q_0 + q_1 i + q_2 j + q_3 k \quad [3.29b]$$

3.6.3.1.1. Addition

Adding p and q leads to:

$$p + q \equiv (p_0 + q_0) + (p_1 + q_1)i + (p_2 + q_2)j + (p_3 + q_3)k \quad [3.30a]$$

$$p + q \equiv (p_0 + \vec{p}) + (q_0 + \vec{q}) = (p_0 + q_0, \vec{p} + \vec{q}) \quad [3.30b]$$

3.6.3.1.2. Multiplication

Multiplying p and q leads to:

$$\begin{aligned} pq \equiv\ & p_0q_0 + p_0\vec{q} + q_0\vec{p} + \vec{p} \times \vec{q} - \vec{p} \cdot \vec{q} \\ =\ & (p_0q_0 - \vec{p} \cdot \vec{q},\ p_0\vec{q} + q_0\vec{p} + \vec{p} \times \vec{q}) \end{aligned} \quad [3.31a]$$

where the operations between vectors correspond to the outer product (vector product) and the inner product (scalar product).

Note that multiplication is associative and distributive, but not commutative, because:

$$\begin{aligned} qp \equiv\ & p_0q_0 + p_0\vec{q} + q_0\vec{p} - \vec{p} \times \vec{q} - \vec{p} \cdot \vec{q} \\ =\ & (p_0q_0 - \vec{p} \cdot \vec{q},\ p_0\vec{q} + q_0\vec{p} - \vec{p} \times \vec{q}) \end{aligned} \quad [3.31b]$$

3.6.3.1.3. Conjugation

Conjugating p and q leads to:

$$q^* = q_0 - q_1i - q_2j - q_3k \quad [3.32a]$$

$$p^* = p_0 - p_1i - p_2j - p_3k \quad [3.32b]$$

so:

$$q^* \equiv q_0 - \vec{q} \quad [3.32c]$$

$$p^* \equiv p_0 - \vec{p} \quad [3.32d]$$

and we get:

$$(pq)^* \equiv q^*p^* \quad [3.32e]$$

3.6.3.1.4. Length (metric)

The length of the quaternion q is obtained from:

$$|q| = \sqrt{q^* q} = \sqrt{q_0^2 + q_1^2 + q_2^2 + q_3^2} \quad [3.33]$$

3.6.3.1.5. Normalization

Normalizing the quaternion q amounts to constructing a quaternion $\hat{q}$ of norm equal to 1. This is obtained as follows:

$$\hat{q} = \frac{q}{|q|} \quad [3.34]$$

3.6.3.1.6. The inverse of a quaternion

The inverse of the quaternion q can be used for the division operation and can be defined from:

$$q q^{-1} = q^{-1} q = 1 \quad [3.35a]$$

so that:

$$q^{-1} = \frac{q^*}{|q|^2} \quad [3.35b]$$

Unit quaternions can be used to represent a rotation in three-dimensional space.

3.6.4. *Lagrange points*

In 1772, Joseph-Louis Lagrange [LAG 67, 72] was interested in solving the three-body problem in a situation where the mass of one of the bodies could be neglected. He was thus able to demonstrate the existence of equilibrium points known as "Lagrange points". He developed mathematical methods for analyzing the motions of celestial bodies. His work laid the foundations for many later breakthroughs in celestial mechanics.

Lagrange discovered five positions in the plane where a small mass can remain in equilibrium under the influence of the gravitational forces of two large masses. These points are now known as Lagrange points, or libration points, and are denoted as L_1, L_2, L_3, L_4 and L_5. These are positions where an object of negligible mass can remain in equilibrium. This is because the gravitational attraction of the two large masses is balanced by orbital forces (centrifugal force and Coriolis force in a rotating frame of reference).

The key steps of the calculation and the results of the work in his dissertation *Essai sur le problème des trois corps* (Essay on the three-body problem) can be summarized as follows.

The problem addressed was the determination of the motion of three bodies subject to their mutual attraction according to Newton's laws, in the special case where two of the bodies are of large mass (M_1 and M_2) and the third body is of negligible mass ($m << M_1$ and M_2). The case of an artificial satellite of the CubeSat type (m_c) orbiting the Earth, in the gravitational field of the Sun (M_S) and the Earth (M_T), is an example of such a situation. By formulating the problem in terms of potential energy, Lagrange used the mathematical methods he developed using the calculus of variations to obtain his results. He determined these equilibrium points by solving the associated differential equations. Figure 3.18 shows the location of these points in a plan depicting the potential energy map for the Sun–Earth system.

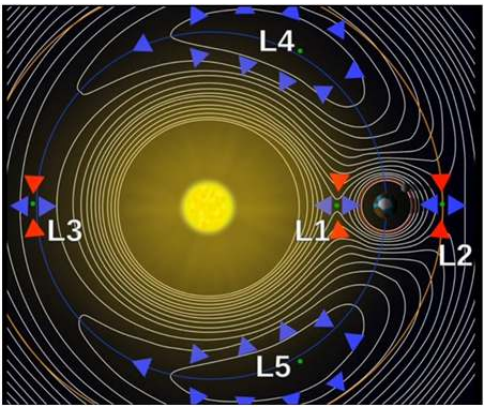

Figure 3.18. *Potential energy map of the Sun–Earth system illustrating the location of Lagrange points*

Three of these points are unstable (crest point for L_1, L_2 and L_3) and two are stable (saddle point for L_4 and L_5). The unstable points are located on the straight line connecting the two large masses. The stable points are at the vertices of a rhombohedron inscribed with two equilateral triangles symmetrical with the large masses located at the other two vertices (see Figure 3.19). L_4 is upstream of the Earth's orbit, and L_5 is downstream. Points L_4 and L_5 are stable orbit locations, provided that the mass ratio between the two large masses exceeds 24.96. This condition is satisfied for both the Earth–Sun and Earth–Moon systems, as well as for many other pairs of Solar System bodies. Objects found orbiting at points L_4 and L_5 are often called Trojans, in reference to the names of the three large asteroids,

Agamemnon, Achilles and Hector, which orbit at points L_4 and L_5 in the Jupiter–Sun system.

Lagrange also developed part of the theory of perturbations, used to study the effects of perturbing forces on the orbits of celestial bodies. This theory makes it possible to understand deviations in the orbits of planets and satellites due to the influence of other bodies. Lagrange points have become the preferred locations for placing orbital devices to observe and study the Universe (the birth of stars, the formation and evolution of primitive galaxies, as well as the chemistry of the space environment) or the Sun. At point L_2, we find the JWST (James Webb Space Telescope – 2021–2040: to observe and study the Universe, mainly in the IR, to study the density of matter and dark matter and the age of the Universe), Herschel (2009–2013: astronomical observations in the far IR and submillimeter domains), Planck (2009–2013: to map the minute variations in temperature and intensity of the Cosmic Microwave Background), WMAP (Wilkinson Microwave Anisotropy Probe – 2001–2010: to map the anisotropy of the Cosmic Microwave Background) and PLATO (PLAnetary Transits and Oscillations – 2026: to discover and characterize Earth-like exoplanets around nearby stars).

3.6.5. *Calculating the L1 and L2 Lagrange points of the Sun–Earth system*

The three-body problem can be solved within the framework of the universal law of gravitation and Newton's laws by neglecting the mass of one of the bodies in relation to the other two. This is equivalent to neglecting the effect of this mass (third body) on the other two (Newton's third law of action and reaction, as recalled in Chapter 3). In the case of the Sun–Earth system, with masses $M_S = 1.9891 \times 10^{30}$ kg and $M_T = 5.972 \times 10^{24}$ kg, and a CubeSat-type satellite with mass m_c of less than 100 kg, this situation is reached.

Before determining the position of the Lagrange points (see Figure 3.19), it is interesting to consider Kepler's formula, recalled in Chapter 2 (see Figure 2.4), expressed as follows:

$$T = 2\pi\sqrt{\frac{r^3}{GM_c}} \qquad [3.36]$$

where T is the orbital period of a satellite around a body of greater mass M_C, r is the radius of the satellite's orbit, assumed to be circular around the mass M_C, and G is the gravitational constant. The product GM_c, which is called the gravitational parameter, is a constant. This formula shows that if the orbit radius increases (respectively decreases), the period increases (respectively decreases), corresponding to a lower

(respectively higher) velocity $v = \omega r = \frac{2\pi r}{T} = \sqrt{\frac{GM_c}{r}}$ on the orbit. This result is consistent with what is observed for a planet's velocity at *periapsis* (greater velocity, because of a smaller radius) and *apoapsis* (lower velocity, because of a greater radius).

The Sun–Earth system is a configuration of two masses in circular rotation (approximating the Earth's trajectory around the Sun) around their center of gravity. The Lagrange points are the points in rotation with the same period at which the infinitesimal mass undergoing no force is located. Noting $\vec{R}_S$ and $\vec{R}_T$ as the position vectors of the Sun and Earth respectively in the reference frame of the center of mass, we have:

$$M_S\vec{R}_S + M_T\vec{R}_T = \vec{0} \qquad [3.37a]$$

Approximating the real elliptical motion by a circular motion for the bodies, we can use Kepler's law to determine the angular velocity of rotation of the fictitious particle of reduced mass at position $\vec{r} = \vec{R}_S - \vec{R}_T$, which is given by:

$$\omega = \frac{v}{r} = \sqrt{\frac{G(M_S+M_T)}{|\vec{R}_S-\vec{R}_T|^3}} \qquad [3.37b]$$

If we look at points L_1 and L_2, the position of the center of mass implies that the term $|\vec{R}_S - \vec{R}_T|$ represents the distance between the center of the Sun and the center of the Earth, which will be denoted as R.

For a satellite positioned at L_1, denoting l_1 as the distance between the center of the Earth and the point L_1, the application of Newton's second law and the law of universal gravitation (Chapter 2) leads to the following projected expression of the force on the straight line connecting the center of the Earth and the Sun:

$$m_c a_c = \frac{GM_S m_c}{(R-l_1)^2} + \frac{GM_T m_c}{{l_1}^2} \qquad [3.38a]$$

In the rotating reference frame (see the appendix in Chapter 2), we have:

$$a_c = \omega^2(R - l_1) = (\frac{2\pi}{T})^2(R - l_1) \qquad [3.38b]$$

so that after simplifying equation [3.38a] by dividing by the mass m_c, we get:

$$(\frac{2\pi}{T})^2(R - l_1) = \frac{GM_S}{(R-l_1)^2} + \frac{GM_T}{{l_1}^2} \qquad [3.38c]$$

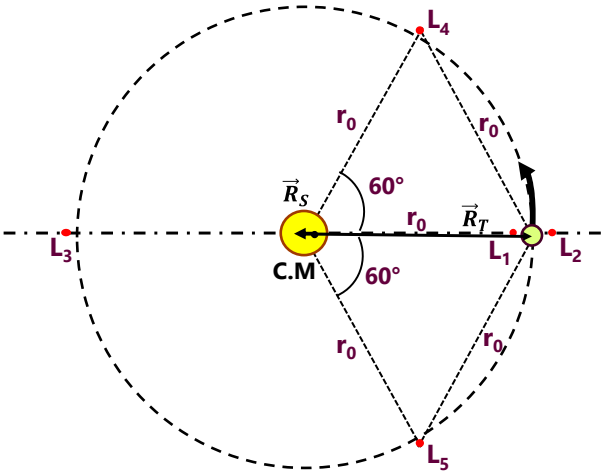

Figure 3.19. *Lagrange points L_i (i = 1 to 5) and center of mass (C.M)*

```
G=6.67e-11;
MT=5.972e24;
MS=1.989e30;
r=1.496e11;
h0=5e8;
hmax=3e9;
h=200;
l=0 : h-1;
x=h0 + l*((hmax-h0)/h);
y1= (G.*MS./((r-x).^2))-(G*MT./x.^2);
figure
plot(x,y1)
title('L1 Point')
xlabel('x')
ylabel('y1')
hold on
y2= G.*MS.*(r-x)./r.^3;
plot(x,y2)
xlabel('x')
ylabel('y2')
hold off
```

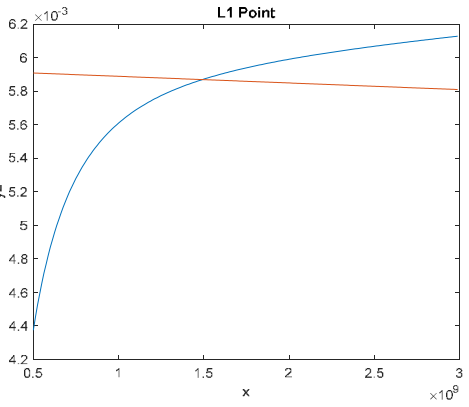

Figure 3.20A. *L1 Lagrange points by the graphical method with Matlab*

```
G=6.67e-11;
MT=5.972e24;
MS=1.989e30;
r=1.496e11;
h0=5e8;
hmax=3e9;
h=200;
l=0 : h-1;
x=h0 + l*((hmax-h0)/h);
y1= (G.*MS./((r+x).^2))+(G*MT./x.^2);
figure
plot(x,y1)
title('L2 Point')
xlabel('x')
ylabel('y1')
hold on
y2= G.*MS.*(r+x)./r.^3;
plot(x,y2)
xlabel('x')
ylabel('y2')
hold off
```

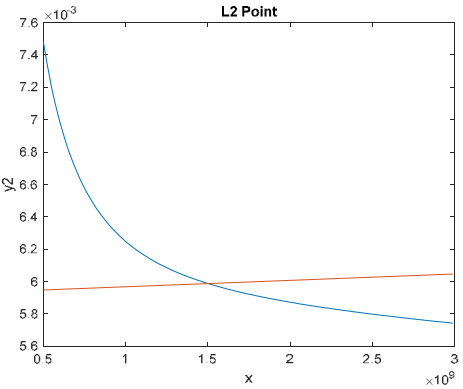

Figure 3.20B. *L2 Lagrange points by the graphical method in Matlab*

Proceeding in the same way for point L_2, we obtain the corresponding equation:

$$\left(\frac{2\pi}{T}\right)^2 (R + l_2) = \frac{GM_S}{(R+l_2)^2} + \frac{GM_T}{{l_2}^2} \qquad [3.38d]$$

Then, it suffices to solve equations [3.38c] and [3.38d] graphically or analytically to find l_1 and l_2.

With the following values for G = 6.67×10^{-11} Nm^2/kg^2, R = 1.496×10^{11} m, $M_S = 1.9891 \times 10^{30}$ kg, $M_T = 5.972 \times 10^{24}$ kg and T = 86,400 × 365.25 s, we can calculate l_1 and l_2.

The result can be improved by adding the mass M_L of the Moon to that of the Earth, such that $M_L = 0.0123M_T$. This gives the values $l_1 = 1.493\ 10^9 m$ and $l_2 = 1.511\ 10^9 m$.

Figures 3.20A and 3.20B show an example of a Matlab program used to determine l_1 and l_2 respectively.

3.6.6. *Center of inertia for a two-body system*

The three-body problem can be solved within the framework of the universal law of gravitation and Newton's laws. This is possible if the mass of one of the bodies is neglected, which is equivalent to considering the motion of a mass in the gravitational field of a two-body system.

The problem of a system composed of two bodies interacting gravitationally can be simplified by decomposing the motion of the two bodies into two motions: that of the system's center of inertia and that of a fictitious mass, called the "reduced mass". The system's Lagrange function can be used to determine the motion [LAN 66a].

Denoting M_S and M_T as the mass of the Sun and the Earth respectively, and $\vec{R}_S$ and $\vec{R}_T$ as the position vectors of the Sun and the Earth respectively, the center-of-mass reference frame of this system is defined by equation [3.37a], i.e. $M_S\vec{R}_S + M_T\vec{R}_T = \vec{0}$. If we refer to the relative position of the Earth with respect to the Sun as $\vec{R} = \vec{R}_S - \vec{R}_T$, we can calculate the expression for the Lagrangian of the Sun–Earth system as follows:

$$L = \frac{1}{2}M_S\dot{\vec{R}_S}^2 + \frac{1}{2}M_T\dot{\vec{R}_T}^2 - U(|\vec{R}|) \qquad [3.39a]$$

where $U(|\vec{R}|)$ is the potential energy of the Sun–Earth system, which depends only on the distance between the two bodies.

In the center of inertia reference frame, we can express $\vec{R}_S$ and $\vec{R}_T$ as a function of $\vec{R}$ as follows:

$$\vec{R}_S = \frac{M_T}{M_S + M_T}\vec{R} \qquad [3.39b]$$

$$\vec{R}_T = -\frac{M_S}{M_S + M_T}\vec{R} \qquad [3.39c]$$

so that the Lagrangian (equation [2.10]) can be written as follows:

$$L = \frac{1}{2}m\dot{\vec{R}}^2 - U(|\vec{R}|) \qquad [3.39d]$$

where $m = \frac{M_S M_T}{M_S + M_T}$ is the reduced mass of the system. The problem of the Earth's rotation around the Sun can be reduced to that of a particle of mass m moving in the gravitational field that derives from the potential $U(|\vec{R}|)$ symmetrical with respect to the stationary coordinate origin. The problem of the motion of two interacting material points by a gravitational force reduces to that of the motion of a point in a

given external field, which derives from the potential $U(|\vec{R}|)$, which amounts to determining the motion of mass m in a central field.

For the solution $\vec{R}(t)$ of the two-body problem, the motions of the Sun and the Earth are given by the trajectories $\vec{R}_S(t)$ and $\vec{R}_T(t)$ of the masses M_S and M_T taken separately in the inertial reference frame calculated by formulas [3.39b] and [3.39c]. The rotation period of mass m is the same as that of the Earth around the Sun. This means that in the frame of reference of the center of inertia of the Sun and the Earth, masses M_S and M_T also have the same rotation periods.

In the central field, the momentum of mass m relative to the center of the field (center of inertia of the Sun–Earth system) is conserved.

In fact, we can write that the time derivative of the angular momentum of the motion of mass m with respect to the center of inertia $\vec{L}_O$ is given by the expression:

$$\frac{d\vec{L}_O}{dt} = \overrightarrow{OP} \wedge \vec{F} = R\vec{u}_r \wedge -G\frac{mM}{R^2}\vec{u}_r = \vec{0} \qquad [3.39e]$$

since $\vec{u}_r \wedge \vec{u}_r = \vec{0}$, and where O is the center of inertia, P is the center of mass m, R is the distance between the center of inertia and the center of mass m, M is the total mass at the center of inertia ($M = M_S + M_T$) and G is the gravitational constant. As a result, $\vec{L}_O$ maintains the same orientation and amplitude over time.

Since $\vec{L}_O = \overrightarrow{OP} \wedge m\vec{v} = r\vec{u}_r \wedge mv\vec{u}_t$, $\vec{u}_r$ and $\vec{u}_t$, which are the unit vectors along the radius and tangent to the trajectory respectively, are perpendicular to $\vec{L}_O$.

Since $\vec{L}_O$ keeps the same orientation and amplitude over time, this means that the plane formed by $r\vec{u}_r$ and $v\vec{u}_t$ does not vary over time and that the trajectory of mass m around the center of inertia remains in the same plane.

It is more convenient in this case to express the Lagrangian [3.39d] in polar coordinates (R, φ) as follows:

$$L = \frac{1}{2}m\dot{R}^2 + \frac{1}{2}mR^2\dot{\varphi}^2 - U(|\vec{R}|) \qquad [3.39f]$$

Using equation [2.11] from Chapter 2, it is easy to show that conservation of angular momentum leads to the following expression for L_O:

$$L_O = \frac{1}{2}mR^2\dot{\varphi} \qquad [3.39g]$$

From the expression [3.39f], we can calculate the generalized coordinates, in this case, the canonical generalized momenta by $p_i = \frac{\partial L}{\partial \dot{q}_i}$, to determine the Hamiltonian of the system or calculate the energy function of the system, such that:

$$E = \frac{1}{2}m\dot{R}^2 + \frac{1}{2}mR^2\dot{\varphi}^2 + U\left(\left|\vec{R}\right|\right) = \frac{1}{2}m\dot{R}^2 + \frac{{L_O}^2}{2mR^2} + U\left(\left|\vec{R}\right|\right) \quad [3.40a]$$

from which we can determine R and φ, and the period of motion around the center of inertia.

For $\dot{R}$, we obtain from:

$$\dot{R}^2 = \frac{2}{m}\left(E - U\left(\left|\vec{R}\right|\right)\right) - \frac{{L_O}^2}{m^2R^2} \quad [3.40b]$$

which allows us to calculate *t* in the following form:

$$t = \int \frac{1}{\sqrt{\frac{2}{m}\left(E - U\left(\left|\vec{R}\right|\right)\right) - \frac{{L_O}^2}{m^2R^2}}} dR + Const \quad [3.40c]$$

and, from equation [3.39g], to express φ as a function of R in the following form:

$$\varphi = \int \frac{\frac{{L_O}^2}{R^2}}{\sqrt{2m\left(E - U\left(\left|\vec{R}\right|\right)\right) - \frac{{L_O}^2}{R^2}}} dR + Const \quad [3.40d]$$

Formulas [3.40c] and [3.40d] give the general solutions for the motion of mass m in the gravitational field of total mass M, located at the center of inertia. These formulas are valid for a satellite of negligible mass compared to the masses M_S and M_T, insofar as the satellite does not influence the motion of the Sun and the Earth. Equation [3.40c] gives the distance R as a function of time, and the trajectory equation, meaning R as a function of φ or vice versa, is given by [3.40d].

Note that in the energy expression, [3.40d] shows that the radial part of the motion can be considered to be determined by an effective potential given by $\frac{{L_O}^2}{2mR^2} + U\left(\left|\vec{R}\right|\right)$. The term $\frac{{L_O}^2}{2mR^2}$ corresponds to the centrifugal energy of mass m in the inertial frame of reference.

The values of R for which we have equality:

$$E = \frac{{L_O}^2}{2mR^2} + U\left(\left|\vec{R}\right|\right) \qquad [3.40e]$$

lead to the limits in terms of the radius of motion, since these are the points for which we have $\dot{R} = 0$. These are points of trajectory reversal, where the function R(t) changes from an increasing to a decreasing value and vice versa, while $\dot{\varphi}$ is not necessarily zero. For trajectories between bounded values R_{min} and R_{max}, the trajectory is inside a ring bounded by circles of radii R_{min} and R_{max}, the trajectory not necessarily being a closed curve as φ varies. These formulas can be used to calculate satellite trajectories at Lagrange points.

Therefore, in the reference frame rotating around the center of mass, the centrifugal force and the Coriolis force according to equations [3.18] and [3.22] must be taken into account in the application of Newton's second law, so that the expression of the force on the mass is given by:

$$\vec{F}_{m_C} = -G\frac{M_S m_C}{\left|\vec{r}_c - \vec{R}_S\right|^3}\left(\vec{r}_c - \vec{R}_S\right) \pm G\frac{M_T m_C}{\left|\vec{r}_c - \vec{R}_T\right|^3}\left(\vec{r}_c - \vec{R}_T\right) + m_C\vec{\Omega}^2\vec{r}_c - 2m_C\vec{\Omega}\wedge\dot{\vec{r}}_c \qquad [3.41]$$

Satellites at Lagrange points are subject to both of these forces, giving them a trajectory around the Lagrange point when the thrusters maintain the satellites around L1 and L2, which are unstable points.

3.6.7. *SU(2) and SO(3) groups*

A correspondence exists between the SO(3) group of rotations defined in the physical space of rotations and the SU(2) group defined in the quantum space of spins. The elements presented can be found in references [HAM 62] (Chapter 8), [GIL 74] (Chapter 5) or [LIP 65] (Chapters 1 and 2).

SU(2) is the set of 2 × 2 complex matrices, M, with determinants equal to +1, and which satisfy the property $M^{\dagger}M = I$:

$$M = \begin{pmatrix} a & b \\ -b^* & a^* \end{pmatrix} \text{ with } |a|^2 + |b|^2 = 1 \qquad [3.42a]$$

Only three independent parameters are needed to determine the elements of the SU(2) matrix M. A commonly used form is written as follows:

$$M = \begin{pmatrix} cos\frac{\theta}{2}e^{\frac{i}{2}(\psi+\phi)} & sin\frac{\theta}{2}e^{\frac{i}{2}(\psi-\phi)} \\ -sin\frac{\theta}{2}e^{\frac{-i}{2}(\psi-\phi)} & cos\frac{\theta}{2}e^{-\frac{i}{2}(\psi+\phi)} \end{pmatrix} \quad [3.42b]$$

with $0 \leq \theta \leq \pi$, $0 \leq \psi \leq 4\pi$ and $0 \leq \phi \leq 2\pi$.

The 2×2 matrix, which is a representation of the O(3) rotation group, is called the $D_{1/2}$ irreducible representation.

The vectors that transform in SU(2) are spinors that can form a basis for the spin operator $\hat{S}$. Spinors are used to represent the ½-spin fermions [LAN 75] used in Dirac's theory (Dirac used Pauli matrices to construct the definite 4×4 matrices of the Dirac equation and called this four-dimensional space the space of bi-spinors, which includes particles and antiparticles; we therefore restrict ourselves to the space of particles), which can be written as Φ_α, where $\alpha = 1, 2$. This can be considered analogous to 3D vectors in the case of the SO(3) rotation group. We can write that $\Phi'_\alpha = M_{\alpha\beta}\Phi_\beta$.

There is a homomorphism between the SU(2) group and the SO(3) group (each element of SO(3) corresponds to two elements of SU(2)). If $M \in SU(2)$ has as its image $R(M) \in SO(3)$, then we have $R(M) = R(-M)$.

The application between SU(2) and SO(3) can be chosen in the following form:

$$R_{ik}(M) = \frac{1}{2}Tr(\sigma_i M \sigma_k M^{-1}) \quad \text{where} \quad i,k = 1,2,3 \quad [3.43a]$$

where σ_i are the Pauli matrices defined by:

$$\sigma_1 = \begin{pmatrix} 0 & 1 \\ 1 & 0 \end{pmatrix},\ \sigma_2 = \begin{pmatrix} 0 & -i \\ i & 0 \end{pmatrix} \text{ and } \sigma_3 = \begin{pmatrix} 1 & 0 \\ 0 & -1 \end{pmatrix} \quad [3.43b]$$

We deduce that SO(3) representations are SU(2) representations. On the contrary, the spinorial representations of SU(2) have no analogues in SO(3). The 2×2 matrix representation of SU(2) corresponds to the lowest dimension of the spinorial representations of SU(2).

3.6.7.1. *SU(2) and SO(3) representations*

The SU(2) representation is the one used in angular momentum theory in quantum mechanics.

Indeed, kets are defined from the common eigenfunctions of the operators l^2 and l_z, denoted as $|lm\rangle$ with $l = 0, \frac{1}{2}, 1, \frac{3}{2}, 2, \ldots$ and $m = -l, -l+1, \ldots, l-1, l$. To each l corresponds a distinct irreducible representation of SU(2), and the number of possible values of m, namely 2l + 1, gives the dimension of the representation.

Representations for which l is an integer are equivalent to SO(3) representations and correspond to boson representations. Those for which l is a half-integer are equivalent to SU(2) representations and correspond to fermion representations.

4

Designing a CubeSat

Over the past six decades, hundreds of microsatellites, nanosatellites and even picosatellites have been launched for educational, experimental and operational purposes. These small satellites vary in mass from a few grams to approximately 500 kg, covering nearly eight orders of magnitude. Ultra-small passive yoctosatellites have also been launched: approximately 480 million passive copper dipoles with a mass of 41 μg, as part of the West Ford project, to create an in-orbit distributed X-band reflector. The university training program in California, led by Jordi Puig-Suari of California Polytechnic State University and Bob Twiggs of Stanford University, has begun to democratize the processes involved in building a small satellite. For example, a CubeSat with minimum dimensions of 10 x 10 x 11.35 cm (1U) or maximum dimensions of 24U can be assembled from its various subsystems in a very short time, compared with the time required to build a space mission. Implementation methods must follow procedures that guarantee the safe operation of the CubeSat space system in compliance with the constraints of the specifications for its launch and functionalities, as well as those imposed by legislation, such as for the trajectory followed or its end-of-life disintegration. With NewSpace, start-ups and small teams of researchers and students can launch projects that only two decades ago were the preserve of governments.

4.1. CubeSats, microsats, nanosats and picosats engineering systems

4.1.1. *Systems approach and engineering*

A space program brings together three entities: a space agency, a group of scientists for research activities and a dedicated industrial sector. Implementing a

For a color version of all of the figures in this chapter, see www.iste.co.uk/dahoo/nanosatellites1.zip.

space program is a complex process on a timescale that can be measured in decades. The evolution of spacecraft design technologies and methods has enabled us to design highly sophisticated systems in terms of volume, mass, shape, cost and payloads, to suit the purpose of the mission, whether for scientific research, military or commercial activities. Before satellite mass reduction and launch costs became affordable for academics, space missions were only conceivable for governments thanks to their financial and logistical resources.

As described in Chapter 1, the aim of the 1999 CubeSats project by Professors Jordi Puig-Suari, California Polytechnic State University (Cal Poly), and Bob Twiggs, Space Systems Development Laboratory (SSDL), Stanford University, was to provide affordable access to space for the scientific community through university training programs. The "CubeSat 1999" project features not only the use of commercially available technologies with enough robustness to enable the satellite to be operational for at least two years, but also completion times that are much shorter than those of a standard space mission, thanks to the ease with which the modules making up the satellite can be integrated. These two breakthroughs lead to development costs that are affordable for university programs. This approach has democratized access to space and made it possible to manufacture entire satellite systems. However, it must be approached within the framework of systems engineering by any team of scientists or engineers wishing to devote themselves to such a task. As a result, many institutions, including major universities, smaller universities, high schools, colleges and even elementary schools, have been able to build their own space programs using their CubeSats [KIT 94, HEI 00, CHI 17].

Twiggs and Puig-Suari developed the CubeSat as a 10-centimeter (4-inch) cube with a volume of exactly 1 liter and a mass of less than 1.33 kg (2.93 lbs). They also designed a mechanism called P-POD (Poly-Picosatellite Orbital Deployer) to house the CubeSats during launch. Once the launcher's main mission has been secured, the P-POD attached to the launcher can eject the CubeSats into space. A CubeSat can also be launched from the International Space Station (ISS). CubeSat projects are small-scale, low-cost, multidisciplinary projects where student teams can learn and apply systems engineering. The CubeSat program, design specifications and test requirements are described at cubesat.org [LEE 08, LEE 14, CUB 24].

Implementation methods must follow procedures that guarantee the CubeSat space system's operational safety. This applies equally to its end-of-life cycle in terms of its disintegration on entry into the atmosphere, its orbital trajectory to avoid collisions, particularly with the ISS, and the procedures followed for its manufacture. This approach can be dated from 2013 onwards, when space agencies began to take an interest and the space market opened up to the commercial sector. In this context, the recommendations of the 2016 GAO Report (Government Accountability Office November report to congressional committees) [GAO 16] are worth mentioning:

> Systems engineering (SE) is the primary means of determining whether and how the challenge posed by a program's requirements can be met with the resources available. It is a disciplined learning process that translates capability requirements into terms of specific design features, and thus identifies the key risks to be resolved. Our previous work on best practice has indicated that if programs apply detailed SE before product development begins, the program can resolve these risks through additional trade-offs and investments, ensuring that risks have been sufficiently reduced or eliminated. If a program is pursued, it means that the risks are clearly identified and understood, and that it is in this case adequately resourced.

A number of CubeSat features can be found on nanosat.eu/cubesat. The elements for building a CubeSat can be found in CubeSat 101: Basic Concepts and Processes for First-Time CubeSat Developers NASA CubeSat Launch Initiative, 2017 [CHI 17].

4.1.2. *Key satellite design parameters*

In any satellite, we can identify the key elements that make it operational. These include devices for:

– data management and control by an Open Source onboard computer;

– data backup using SD-type storage cards;

– command, control and data processing;

– energy distribution by batteries;

– communication (uplink and downlink);

– recognition of the satellite by a coded signal (beacon);

– navigation and routing;

– transformation of solar energy by solar panels;

– antenna communication;

– detection of the Earth's magnetic field (magnetometer);

– radiation detection;

– detection of electrons and charged particles.

The first major subsystem is that which enables the satellite to transmit a Morse-coded beacon signal for identification. The system must be designed with

components of sufficient quality for adequate longevity, with an RF domain emission and an electronic system for:

– power amplification of the signal to be transmitted;

– antenna matching for the beacon frequency;

– interfacing with other boards and components as required by the system:

> The 145.830 MHz signal is generated using a quartz crystal. The signal frequency is assigned by the International Amateur Radio Union (IARU). OOK modulation for the beacon's Morse code is achieved by switching the power amplifier on and off. The data transmitted by the beacon contains the satellite's identification information.

A second element is the communications subsystem, which plays a key role in the satellite system. It determines whether the satellite is operable in orbit. In the event of failure, the satellite becomes unusable.

A third important subsystem is the interface between the CubeSat and the launch vehicle. It provides an attachment to a launcher (or rocket), protects the CubeSat during launch and releases it into space at the appropriate moment. The standard deployment system to which all CubeSat developers conform obeys the common physical requirements of an ejection device, which is called a P-POD (Poly-Picosatellite Orbital Deployer). The P-POD is designed as a parallelepiped-shaped tube that can hold up to 34.05 cm x 10 cm x 10 cm of deployable material. When ejected, the CubeSat will rotate, and onboard magnets will stabilize it in the Earth's magnetic field.

Finally, as indicated in the first chapter, the satellite's mission, based on its scientific objectives, will determine the payload that will make up the satellite's other subsystems.

4.1.3. *CubeSat design requirements and constraints*

When designing a CubeSat, at least the following requirements and constraints must be taken into account:

– requirements and specifications;

– mission requirements and acceptable degraded modes;

– national and international regulations;

– system cost objectives (development, station keeping, etc.);

– launch vehicle;

– space environment;

– existing or emerging technologies;

– experience feedback;

– satellite compatibility with existing ground-based resources;

– organization and human resources;

– emerging NewSpace strategies and agile development methods.

4.2. CubeSat structure

A CubeSat must meet certain *criteria in terms of shape, size and weight*. We will present the essential elements in the implementation of a CubeSat, taking as examples UVSQ-SAT, launched in 2021 [MEF 20] and INSPIRE-SAT 7, launched in 2023 [MEF 22a].

A CubeSat can be used alone (1 unit, 1U) or in a group (up to 24 units, 24U). Table 4.1 gives a list of the different units possible by assembly of units, as well as maximum masses by type. The value of n in n U refers to volume, and in this scale represents approximately n times 1,000 cm^3.

Figure 4.1 shows UVSQ-SAT, launched in 2021. It is a satellite in the nanosat category (between 1.1 and 10 kg) (Table 1.1, Chapter 1), as its mass is 1.2 kg. It is in cubic form, with dimensions of 11.5 x 11.5 x 11.4 cm^3, in the so-called 1U category.

Type	Dimensions	Mass
1U	10 x 10 x 11.35	1–1.33 Kg
1.5 U	10 x 10 x 17.03	< 1.5 Kg
2 U (Double)	10 x 10 x 22.70	< 2 Kg
3 U (Triple)	10 x 10 x 34.05	< 3 Kg
6 U (x 6)	20 x 10 x 34.05	< 6 Kg
12 U	20 x 20 x 34.05	< 12 Kg
16 U	20 x 20 x 45.4	< 16 Kg
24 U	20 x 30 x 45.4	< 24 Kg

Table 4.1. *Different CubeSats stacks*

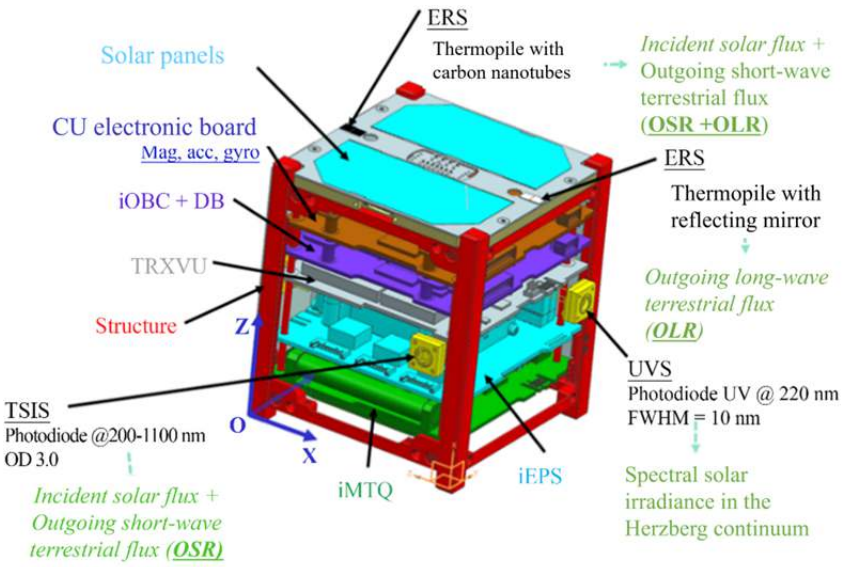

Figure 4.1. *UVSQ-SAT [MEF 20]*

INSPIRE-SAT 7, shown in Figure 4.2, also falls into the nanosat category (Table 1.1, Chapter 1), as its mass is 3 kg. It is a cube with dimensions of 11.5 x 11.5 x 22.7 cm^3, in the so-called 2U category.

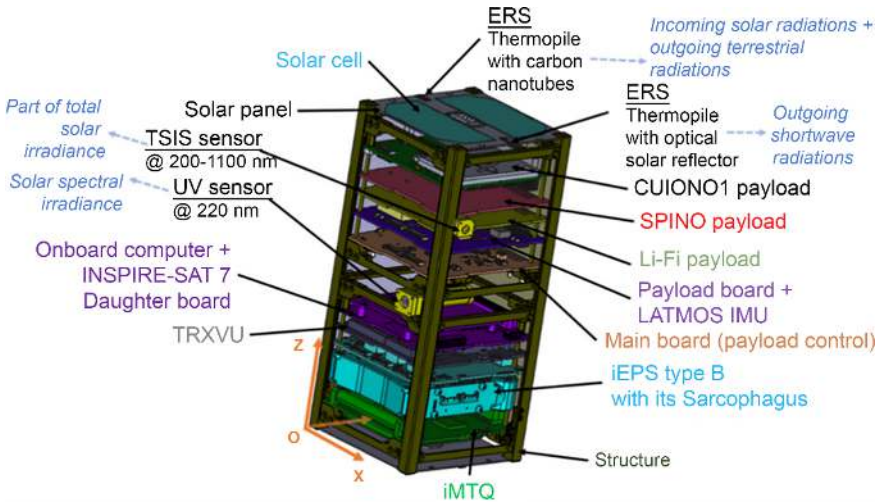

Figure 4.2. *INSPIRE-SAT 7 [MEF 22a]*

CubeSats comprise a series of identically contoured modular housings that are stacked one on top of the other to form the body of each 1U and 2U nanosatellite. The modules are held together by tie rods running through the entire stack to allow a certain dissipation of vibratory energy. They are made up of various subsystems and modules: batteries, uplink, downlink, power system, thermal control, propulsion system, telemetry, tracking and control system, onboard data processing, attitude determination and control system (ADCS) and payload module (Earth observation compartment with sensors and detectors).

Both CubeSats are fitted with standardized equipment (the space platform), including magnets to stabilize the CubeSat in the Earth's magnetic field, communications with a ground station, and a Morse beacon for identification on an amateur radio frequency. Differences lie in the payload – depending on their mission – and concerns the onboard instruments, as well as the volume or improvements in the equipment needed to operate the satellite.

The UVSQ-SAT is a CubeSat dedicated to Earth and Sun observation as part of an educational, technological and scientific mission. It comprises a space segment and a ground segment using at least one UHF/VHF antenna at Observatoire de Versailles-Saint-Quentin-en-Yvelines (France). The ground segment covers all activities from monitoring/controlling the CubeSat to generating and distributing the data produced.

Figure 4.1 shows a UVSQ-SAT representation obtained from computer-aided design software, on which the layout of all of the printed circuit boards (PCBs) can be seen:

– iEPS, for electric power supply, is the power supply subsystem;

– iMTQ, for MagneTorQuer board, provides stabilization in the Earth's magnetic field after launcher ejection;

– iOBC and DB, for onboard computer and daughter board, manage steering and control data;

– TRXVU, for VHF/UHF transceiver (V-uplink, U-downlink), provides communication and solar panels for battery power:

- VHF: 145.830 MHz (uplink),

- UHF: 437.020 MHz (downlink).

The primary scientific objective of the orbiting UVSQ-SAT demonstrator is to measure incoming solar radiation (total solar irradiance) and outgoing terrestrial radiation (longwave radiation and shortwave radiation leaving the upper atmosphere). These measurements are made using twelve miniaturized terrestrial radiative sensors

(based on thermopiles, the advantages of carbon nanotubes and Qioptiq optical solar reflectors). The expected measurements could thus make it possible to better constrain the Earth's radiation balance and, more importantly, the Earth's energy imbalance (EEI), which is defined as the difference between incoming solar radiation and outgoing terrestrial radiation (longwave and shortwave radiations). Direct determination of the EEI is very difficult, as the EEI is two orders of magnitude less than the incoming and outgoing radiation fluxes of the Earth system.

The second scientific objective is to monitor solar spectral irradiance in the Herzberg continuum (200–242 nm) using four photodiodes, which benefit from the intrinsic advantages of Ga_2O_3 alloy-based sensors. Solar UV variability over time has important implications for atmospheric chemistry and its modeling.

The UVSQ-SAT is also equipped with an accelerometer, a gyroscope and a three-axis compass to estimate the satellite's attitude.

The instruments corresponding to these objectives, and which make up the *UVSQ-SAT payload*, are shown in Figure 4.1 by their acronyms and functions during the mission:

– Measuring incoming shortwave radiation (ISR) and outgoing shortwavelength Radiation (OSR), and, when fitted with reflectors, for measuring outgoing long wavelength radiation (OLR).

– UVS (UV photodiode at 220 nm with a FWHM resolution of 10 nm) and TSIS (UV photodiode in the 200–1,100 nm band with an optical aperture of 3.0): UV sensors that make up DEVINS (DEep uV INnovative detector technologies for Space observations).

– The three-axis accelerometer/gyroscope/compass, located above the payload electronics board.

In summary, the mechanical structure of the CubeSat, which is in itself a subsystem of the UVSQ-SAT satellite system, is made up of various subsystems:

– power supply;

– thermal control;

– attitude determination and control (ADCS);

– data processing (CDHS);

– communication;

– payload (ERS, DEVINS);

– three-axis accelerometer/gyroscope/compass (TW sensor).

The UVSQ-SAT CubeSat structure complies with the CubeSat standard and is compatible with the ISIPOD or QuadPack CubeSat deployer. The satellite structure includes two separation switches. These ensure that the UVSQ-SAT CubeSat is inactive during launch and pre-launch activities.

UVSQ-SAT materials and the selection of coatings must comply with specific requirements. These include total mass loss (TML) of less than 1% and volatile condensable collected matter (VCM) of less than 0.1%, in accordance with the European Space Agency's guidelines for spacecraft cleanliness control (ESA-PSS-51).

The INSPIRE-SAT 7 shown in Figure 4.2 is a representation provided by computer-aided design software. It is presented as an arrangement of all of the printed circuit boards (PCBs), in its 2U dimensions, such as the UVSQ-SAT shown in Figure 4.1 in its 1U dimensions, with power consumption limited to 3W. INSPIRE-SAT 7 is composed of several subsystems, such as the mechanical structure, the power supply subsystem, the attitude determination and control subsystem (ADCS), the telemetry/monitoring and command and data processing subsystem (CDHS), the communication subsystem and the thermal control subsystem.

While designed as a continuation of the UVSQ-SAT, with high-quantum-efficiency ultraviolet and infrared sensors to measure the Earth's energy (or radiation) balance (ERB) at the top of the atmosphere (TOA), it has also been developed to probe the ionosphere. As such, it also carries the payloads (Earth Radiative Sensors (ERS); Total Solar Irradiance Sensors (TSIS); UltraViolet Sensors (UVS) present on the UVSQ-SAT.

As part of its mission, it is also equipped with the Ionospheric payload (CUIONO1) and antenna for probing the ionosphere to study the climate, a Light Fidelity (Li-Fi) demonstrator, a wireless communication system using waves in the near IR-visible range instead of metal wires for mission testing, the SPINO device (an amateur radio audio transponder), the LATMOS three-axis accelerometer/ gyroscope/compass and the Inertial Measurement Unit (IMU) to meet mission requirements.

The INSPIRE-SAT 7 power subsystem is different from that used in the UVSQ-SAT. It is based on an electrical power supply (iEPS) that includes a four-cell battery with a capacity of 45 Wh. INSPIRE-SAT 7 consists of six solar panels with 20 high-efficiency Azur Space solar cells (30% for early life). The solar cells are capable of generating between 3.5 W and 3.8 W (orbital average power (OAP) in LEO).

The INSPIRE-SAT 7 ADCS subsystem is identical to that used in UVSQ-SAT. It is mainly based on a Magnetorquer (iMTQ) card and six coarse photodiodes to estimate the direction of the Sun. INSPIRE-SAT 7 does not have an active pointing

system such as UVSQ-SAT. It is equipped with a TRIAD (Tri-Axial Attitude Determination) device and a MEKF (Multiplicative Extended Kalman Filter) to determine the satellite's attitude. It should be noted that these methods have been validated with UVSQ-SAT data in orbit, and thus represent an important challenge for the INSPIRE-SAT 7 scientific analysis.

Category	Sub-system	Maximal Mass (g)
Mechanical	Structure (STS-2U)	231.0
Communication	Communication board (TRXVU)	84.7
	Antenna (AntS) - top + Antennas (AntS) - bottom	190.3
CDHS	On-Board Computer (iOBC + DB)	112.2
Power	Electrical Power System (iEPS – type B – 45 WH)	347.6
	Solar panels (SPA 3G30A)	561.0
ADCS	Magnetorquers board (iMTQ)	220.0
Payload	Photodiodes (TSIS + DEVINS + OS) - 14	120.0
	IR detectors (ERS) - 12	96.0
	IMU (TW)	30.0
	Payload board (PB)	80.0
	Front End Electronic (FEE)	120.0
	Harness & other	110.0
	Radio-Amateur Payload	80.0
	Oledcomm payload	70.0
	Totem electronic board (IONO sensor)	137.0
	Additional mass (structure, antenna, ...)	160.0
TOTAL	INSPIRE-SAT 7	2749.8

Table 4.2. *INSPIRE-SAT 7 CubeSat mass balance*

Category	Sub-system	Power – Safe mode	Power - Nominal mode (TBC)
Mechanical	Structure (STS-2U)	-	-
Communication	Communication board (TRXVU)	480	617.5
	Antenna (AntS) - top + Antennas (AntS) - bottom	46	51.6
CDHS	On-Board Computer (iOBC + DB)	437	490.3
Power	Electrical Power System (iEPS – type B – 45 WH)	104	116.7
	Solar panels (SPA 3G30A)	-	-
ADCS	Magnetorquers board (iMTQ)	0	0
Payload	Photodiodes (TSIS + DEVINS + OS) - 14	0	20
	IR detectors (ERS) - 12	0	20
	IMU (TW)	0	60
	Payload board (PB)	0	140
	Front End Electronic (FEE)		
	Harness & other	-	-
	Radio-Amateur Payload	0	200
	Oledcomm payload	0	50
	Totem electronic board (IONO sensor)	0	1 400
	Additional power (structure, antenna, ...)	-	-
TOTAL	INSPIRE-SAT 7	1067 mW	3166.1

Table 4.3. *INSPIRE-SAT 7 CubeSat power balance*

The communication subsystem is based on a VHF/UHF transceiver (TRXVU) and a deployable antenna system (two 60 cm-long antennas for VHF, two 20 cm-long antennas for UHF). The satellite communicates in the amateur band (UHF selection of 437.410 MHz and VHF of 145.970 MHz), which requires validation by the International Amateur Radio Union (IARU).

Category	Sub-system	TM (Bytes)
Mechanical	Structure (STS-2U)	0
Communication	Communication board (TRXVU)	37
	Antenna (AntS) - top + Antennas (AntS) - bottom	40 + 40 = 80
CDHS	On-Board Computer (iOBC + DB)	116
Power	Electrical Power System (iEPS – type B – 45 WH)	121
	Solar panels (SPA 3G30A)	36
ADCS	Magnetorquers board (iMTQ)	29
Payload	Photodiodes (TSIS + DEVINS + OS) - 14	56
	IR detectors (ERS) - 12	96
	IMU (TW)	28
	Payload board (PB)	4
	Front End Electronic (FEE)	32
	Harness & other	0
	Radio-Amateur Payload	100
	Oledcomm payload	100
	Totem electronic board (IONO sensor)	600 k
	Additional mass (structure, antenna, ...)	0
TOTAL	INSPIRE-SAT 7	600 835

Table 4.4. *INSPIRE-SAT 7 CubeSat telemetry report*

Category	Sub-system	TC (Bytes)
Mechanical	Structure (STS-2U)	0
Communication	Communication board (TRXVU)	18
	Antenna (AntS) - top + Antennas (AntS) - bottom	36
CDHS	On-Board Computer (iOBC + DB)	18
Power	Electrical Power System (iEPS – type B – 45 WH)	18
	Solar panels (SPA 3G30A)	18
ADCS	Magnetorquers board (iMTQ)	18
Payload	Photodiodes (TSIS + DEVINS + OS) - 14	22
	IR detectors (ERS) - 12	22
	IMU (TW)	22
	Payload board (PB)	22
	Front End Electronic (FEE)	22
	Harness & other	0
	Radio-Amateur Payload	20
	Oledcomm payload	100
	Totem electronic board (IONO sensor)	100
	Additional mass (structure, antenna, ...)	0
TOTAL	INSPIRE-SAT 7	456

Table 4.5. *INSPIRE-SAT 7 CubeSat remote control summary*

Tables 4.2–4.5 summarize the main characteristics of the INSPIRE-SAT 7 CubeSat in terms of mass balance, power balance, CT and TM:

> TM/TC communication is provided in VHF (GFSK, adjustable baud rate), UHF (GFSK, adjustable baud rate).

4.3. CubeSat mission implementation

In the case of the UVSQ-SAT, launched in 2021 [MEF 20], there are four distinct mission concepts that can be separated into operational phases (CONOPs):

– Pre-launch and launch operations.

– Launch of operations in the preparation phase and in-orbit verification of the satellite platform: deployment of the UVSQ-SAT from the CubeSat deployer, automatic activation of the satellite by the separation switches, automatic initialization of the onboard software a few seconds after satellite separation, deployment of the deployable structures (antenna), automatic activation of the satellite ADCS to perform autonomous stabilization of the spacecraft, verification of the link between the ground and the satellite, restitution of the satellite's orbit thanks to initial visibilities, verification that all of the platform's satellite services are working, activation of the payload and verification of the functionality of all payload instruments.

– Verification and operation of in-orbit instruments: preliminary configuration, operational configuration of the satellite, calibration/validation (CalVal) of payload instruments and comparison with payload ground calibration (ERS, reactivity, solar absorption (200–2,500 nm), emittance (approximately 10 m), bidirectional reflectance distribution function for different incidence angles, etc.), DEVINS (reactivity, sensor slit function, calibrations against national SI standards, etc.) and performance validation. On a routine basis, the CubeSat observes the Earth and Sun full-time. A monthly calibration is carried out to characterize the angular sensitivity of the sensors (ERS and DEVINS).

– Managing the end-of-life of the UVSQ-SAT CubeSat.

4.4. Communications and ground connections

A space link is a communication link between the CubeSat and its associated ground system. When designing the space system, it is necessary to anticipate not only all of the modes of operation in orbit (see Figure 4.3), but also the different impacts and consequences on volumes, mass balances, power balances, link balances, scientific requirements, etc.

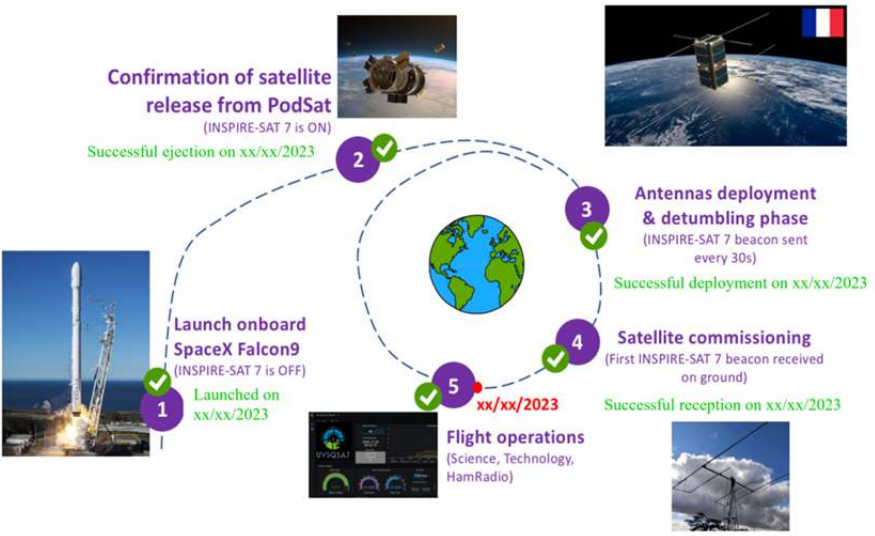

Figure 4.3. *UVSQ-SAT in-orbit operations*

One of the subsystems concerns communication and links with ground operators via a command and data processing system (CDHS-TRXVU). Most currently active CubeSats communicate with ground stations on frequency bands that correspond to amateur satellite frequencies (HAM radio) or are specifically allocated to space communications.

The HAM radio frequencies generally used are in the 145.8–146 MHz range in the VHF band, and 435–438 MHz in the UHF band. The VHF and UHF bands are often duplexed to increase the overall bandwidth.

The CubeSat CDHS-TRXVU system manages all data sent and received by the CubeSat, including scientific data and CubeSat or payload operations. The system is connected to RF transmitter and receiver units that provide the only gateway for data entering or leaving the spacecraft.

A space link protocol is a communication protocol designed for use on a space link or in a network containing one or more space links. The basic data stream on a space link consists of telemetry (TM) and remote control (TC) data. Thus, the TM downlink and TC uplink provide a communication channel between the CubeSat and operators on the ground.

On the uplink, the CDHS-TRXVU system receives and decodes all commands and data for platform and payload operations from the communication system. These commands (TC) are then directed to the appropriate subsystem, or executed directly at the platform level. Payload command management is not necessarily performed by the CDHS system, but rather is transmitted in a fully encapsulated form directly to the payload. TCs are divided into the following categories:

– direct commands to the CubeSat for reconfiguration;

– application-specific commands.

On the downlink, the CDHS system collects various types of data from either the platform's subsystems or scientific payloads, and multiplexes them into transfer frames for transmission to the ground. TM data can be divided into the following categories:

– CubeSat HK data;

– orbit data (position);

– payload data (scientific data);

– remote control reception status (CLCW);

– memory dump data.

As far as communication is concerned, various INSPIRE network antennas are available for communication with the UVSQ-SAT satellite.

LATMOS (Laboratoire Atmosphères et Observations Spatiales, France), latitude 48.777969 N, longitude 2.048264 E:

– VHF: 145.830 MHz (uplink);

– UHF: 437.020 MHz (downlink).

LASP (Laboratory for Atmospheric and Space Physics, USA), latitude 40.00844 N, longitude 105.24836 W (TBC):

– VHF: TBD (uplink);

– UHF: TBD (downlink).

NCU (National Central University, Taïwan), latitude 24.96800 N, longitude 121.19220 E (TBC):

– VHF: TBD (uplink);

– UHF: TBD (downlink).

Figure 4.4 shows the electrical and telecommunications characteristics of CubeSat UVSQ-SAT (INSPIRE-5).

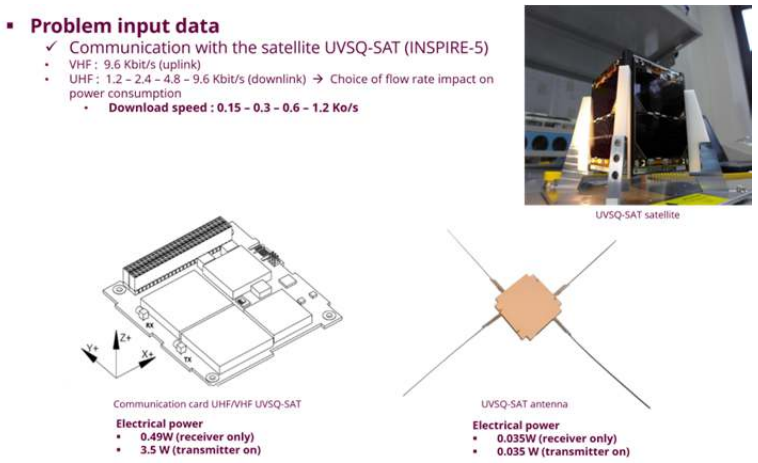

Figure 4.4. *UVSQ-SAT communication subsystem*

For the UVSQ-SAT project, three launch options (Table 4.6) were available for putting the CubeSat into orbit.

Launch	Option 1	Option 2	Option 3
Country	India	Europe	Russia
Launcher	PSLV	VEGA	Soyuz
Period	Q4 2020	End 2020	Q4 2020/Q1 2021
Orbit parameter range for auxiliary load	475-575 Km SSO, LTDN 09:30 to 10:30 h	450-600 Km SSO, LTDN 06:00 or 10:30 h	475-500 Km SSO, LTAN 10:30 h
Launch adapter options	QuadPack/DuoPack	QuadPack/DuoPack	QuadPack/DuoPack

Table 4.6. *In-orbit proposals received following the PUMA call for tenders*

Given the orbit in which the CubeSat would be moving, it was necessary to take into account the impact of the UVSQ-SAT satellite's altitude on the size of the circle of visibility of the antenna (see Figure 4.5) corresponding to the different options.

In Figure 4.5, the minimum elevation corresponds to:

– the angle between the local horizon and the limit of the cone of visibility;

– the minimum elevation of 0° in theory;

– in real-life situations, buildings, vegetation and landforms impose a minimum angle for communications to be established with a satellite;

– 5° minimum to send a command in amateur radio bands, P = 100 W maximum.

Figure 4.5. *UVSQ-SAT communication subsystem*

As part of the CubeSat manufacturing project, it was therefore necessary to formalize the situation related to the three launch options. The objectives of the working group involved in this communication subsystem for the CubeSat ground link were defined as follows:

– to study the various cases associated with the different antennas available;

– to determine the daily visibility time of the UVSQ-SAT satellite;

– to determine the data download capacity;

– to determine the power consumed (instantaneously and during an orbit) when downloading data.

Simulation of the satellite trajectory helps to anticipate the consequences of the launch context by performing the following operations:

– calculating the satellite's ground track on the rotating Earth, i.e. the imaginary line that determines the areas overflown by the satellite (see Figure 4.6);

– calculating the visibility cone trace (circle of visibility) as a function of altitude and ground station (see Figure 4.7).

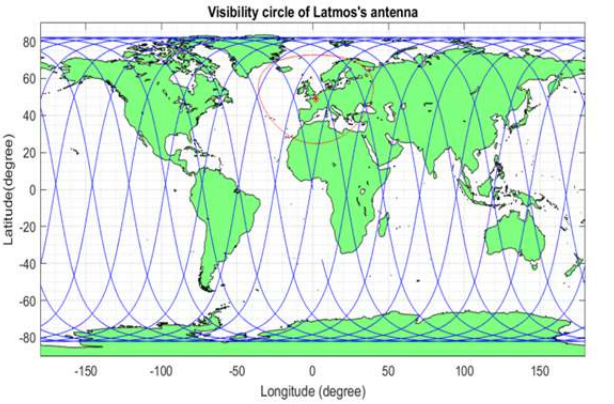

Figure 4.6. *Simulation of the UVSQ-SAT ground track on a rotating Earth*

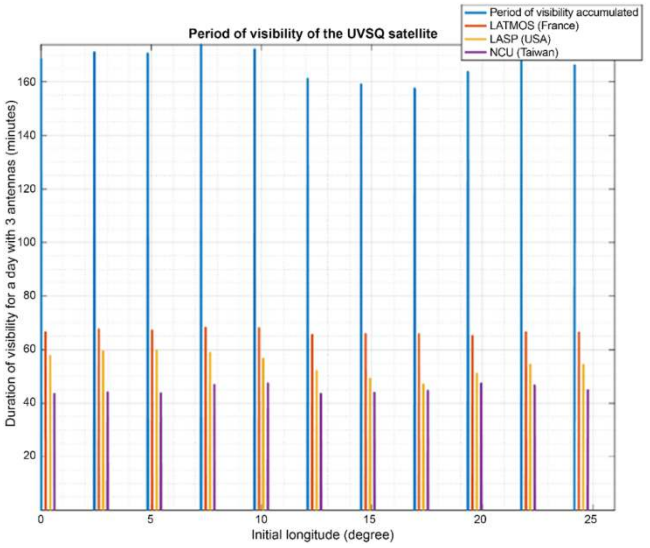

Figure 4.7. *Simulation of the UVSQ-SAT visibility period*

4.5. CubeSat architecture

The general architecture of a CubeSat or satellite is divided into two parts: the platform and the payload. Figure 4.8 shows an example with the PICARD microsatellite (Jean Picard, French astronomer, 1620–1682), designed to

simultaneously measure the total and spectral solar irradiance, the diameter and shape of the Sun, and probe its interior using helioseismology [COR 13]. These measurements provide information on the variability of these parameters as a function of solar activity.

The payload corresponds to the onboard instruments used to carry out the main mission. It is made up of secondary structures supported by the satellite's primary structure. PICARD's payload consisted of SOVAP (Solar VAriability PICARD), PREMOS (PREcision Monitor Sensor) and SODISM (Solar Diameter Imager and Surface Mapper).

The platform consists of a primary structure. This is the support structure through which all forces are transmitted to the launcher interface. This is the system's skeleton.

In a satellite, it performs various functions:

– interface with the launcher;

– energy generation and storage;

– control of the satellite's attitude (orientation in space) and orbit (position in space);

– management of information gathered on the status of all sub-assemblies by means of onboard intelligence (flight software);

– links with the ground for tracking (telemetry), control (remote control) and localization by the ground;

– embeds the payload (instruments) on a baseplate that ensures high positioning stability.

4.5.1. *Mechanical architecture of a CubeSat*

The structural function of a satellite or sub-assembly must guarantee:

– the preservation of the system's integrity;

– the system's stability;

– the system's rigidity, which guarantees its dynamic behavior.

We also need to consider constraints relating to manufacturing processes, choice of materials and selection of industrial sub-assemblies (motors, electronic units, etc.).

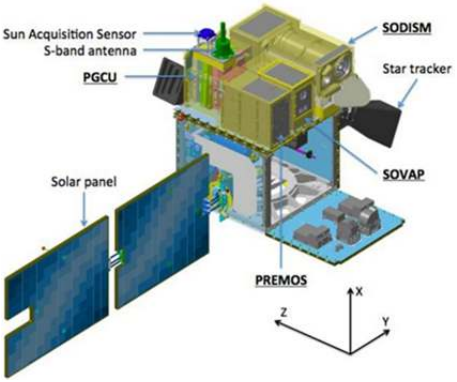

Figure 4.8. *General architecture of the PICARD microsatellite*

The mechanical architecture activity must take into account the following:

– the "launcher" mechanical interfaces;

– the requirements imposed by the environment (clean room, launcher, in-orbit, etc.);

– the requirements imposed by development and ground integration (modularity, ease of integration, handling, transport, etc.);

– the needs to ensure the satellite's main functions (thermal control, attitude and orbit control system, change of configuration, relative positioning of the various components, overall dimensions and fixing of the various components, etc.).

The main outputs expected from a satellite architecture are as follows:

– the geometric database (CAD → CATIA, Siemens NX, etc.);

– the list of materials and processes;

– the mechanical interface file;

– the mass, center of gravity and inertia (MCI) balance;

– the layout justification file;

– the breakdown into sub-assemblies to control balances and industrial responsibilities according to the breakdown made;

– the mechanical calculations and demonstration of resistance to "launcher" environments;

– the scale model to be delivered to the "launcher" authorities.

Materials	Vf	d	E_1	E_2	G_{12}	ν_{12}	σ_{1t}^R	ε_{1t}^R	σ_{1c}^R	σ_{12}^R	σ_{2t}^R	α_1	α_2	K_1	K_2
	%		(GPa)	(GPa)	(GPa)		(MPa)	%	(MPa)	(MPa)	(MPa)	($10^{-6}.K^{-1}$)		($Wm^{-1}K^{-1}$)	
First generation carbon fibers															
T300/epoxy	60	1.55	130	10	5	0.35	1600	1.1	1500	100	60	0	35	4.2	0.7
M40/epoxy	60	1.65	251	7	4.5	0.3	1200	0.6	900	80	45	-0.5	35	55	1.3
GY 70/V108	60	1.7	290	6.8	5	0.3	800	0.3	600	40	25	-1	35	80	5
Second generation carbon fibers															
M155J/M18	60	1.62	310	6	4.1	0.29	1800	0.58	640	58	25	-1	34	51	1
K135 2U/954.3	60	1.8	370	5.3	4.2	0.29	1600	0.43	390	59	24	-1	30	100	1
FT700/magnesium matrix	50	1.95	320	20	*	0.3	900	0.3	*	*	#20	0	25	#290	90
K135/M22	60	1.8	365	5.6	4.2	0.29	1760	0.38	380	93	10	-0.9	27	100	1
K139/Aluminum	60	2.2	370	24	10	0.2	1200	-	300	64	35	0.47	8.2	130	150
Glass R/Epoxy	60	2	52	14	4.7	0.3	1900	3.6	970	#100	#20	5.5	30	0.5	-
Kevlar 49/Epoxy	60	1.4	84	6	2.1	0.35	1400	1.9	280	#100	#20	-0.4	60	0.5	-
Aluminum AU4G	-	2.8	72	-	28.5	0.33	390	-	-	-	-	23	-	150	-
Titanium TA6V	-	4.5	110	-	40	0.33	900	-	-	-	-	8	-	7.2	-
Invar	-	2.8	145	-	58	0.25	380	-	-	-	-	1	-	-	-
zerodur	-	2.5	190	-	40	0.15	100	-	-	-	-	0.05	-	-	-
SiC	-	3.2	420	-	180	0.16	480	-	-	-	-	2	-	180	-

Table 4.7. *Mechanical characteristics of materials used*

Materials	E Pa	G Pa	ν	ρ Kg/m3	λ W/m.K	Cp J/kg.K	CTE m/m/°C	Re MPa	Rp MPa
Titanium Ta6V	1.05 + 11	3.92 + 10	.34	4420.	7.2	540	7.9–6	847	924
Aluminum A7075	7.3 + 10	2.72 + 10	.34	2800.	134.	940	2.2–5	340	400
Aluminum A2618 T851	7.3 + 10	2.72 + 10	.34	2760.	159.	940	2.2–5	372	441
Invar	1.45 + 11	5.8 + 10	.25	8100.	10.5	510.	1.5–6	310	500
SIC	4.2 + 11	1.8 + 11	.16	3200.	180	680.	2.–6	–	300
Steel AISI 304L (X2CrNi1810E)	2.03 + 11	7.87 + 10	.29	7850.	16.2	502	1.7–5	210	564
Carbon/carbon parallel layup	6.9 + 10	2.78 + 10	.24	1750.	34	760	-6.–7	–	97
Piezo ceramic	3.8 + 10	1.46 + 10	.3	7700.			3.5–6		
Zerodur class 0	9.1 + 10	3.91 + 10	.15	2530.	1.6	810.	2.–8	–	50

Table 4.8. *Mechanical and thermal properties of the materials*

4.5.2. *Materials for mechanical architecture*

The materials used in space vehicles can be similar to those used in the automotive and aeronautics industries. They can be aluminum-based, for example, or in the form of composite materials that reduces weight.

It should be noted that most of the materials used are isotropic. Their mechanical properties are identical in all directions. The mechanical characteristics of the materials generally used to manufacture a CubeSat are given in Tables 4.7 and 4.8. Table 4.8 also gives the thermal characteristics of the materials listed [MEF 22b].

The Von Mises stress value is used to determine whether a given material will yield or fracture. It is mainly used for ductile materials, such as metals. The Von Mises yield criterion states that if the Von Mises stress of a material under load is equal to or greater than the yield limit of the same material under simple tension, the material will fracture. In the case of plane loading (normal stress σ and shear stress τ), we have:

– Tresca stress: $\sigma_e = (\sigma^2+4\tau^2)^{0.5}$;

– Von Mises stress: $\sigma_e = (\sigma^2+3\tau^2)^{0.5}$.

In terms of material strength, σ_e is used to determine the material's elasticity range, such that:

– $\sigma e < Re \rightarrow$ elastic domain;

– $\sigma e > Re \rightarrow$ plastic domain;

– $\sigma e \geq Rp \rightarrow$ material failure.

In the case of (isotropic) metallic materials, the classic criteria for initial damage are yield strength (Von Mises) or first material failure.

In the case of a composite material, it consists of a matrix (resin) and reinforcements (fibers), as shown in Figure 4.9.

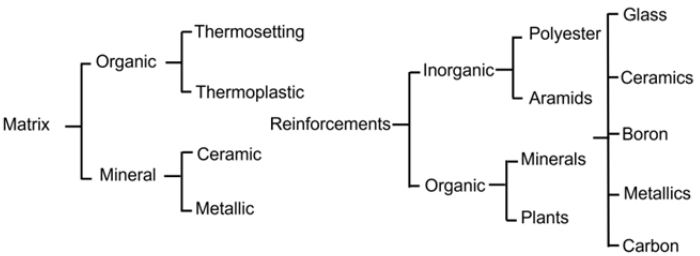

Figure 4.9. *Architecture of a composite material*

Resins	T_f(°C)	ρ(Kg/m³)	ε_t^R(%)	σ_t^R(MPa)	σ_c^R(MPa)	E(Gpa)
Polyesters	60 to 100	1,140	2 to 5	50 to 85	90 to 200	2.8 to 3.6
Phenolics	120	1,200	2.5	40	250	3 to 5
Epoxides	290	1,100 to 1,500	2 to 5	60 to 80	250	3 to 5

Table 4.9. *Thermomechanical properties of thermosetting resins*

Resins	T_f(°C)	ρ(Kg/m³)	ε_t^R(%)	σ_t^R(MPa)	σ_c^R(MPa)	E(Gpa)
Polyamid	65 to 100	1,140		60 to 85		1.2 to 2.5
Propylene	900	1,200		20 to 35		1.1 to 1.4

Table 4.10. *Thermomechanical properties of thermoplastic resins*

Reinforcements	ρ(Kg/m³)	σ_t^R(MPa)	σ_c^R(MPa)	E(Gpa)
AS_4	1,800		3,599	235
T300	1,700	1.2	3,654	231
IM6		0.88	1,460	
IM8	1,800		5,171	310
Kevlar 49	1,440	2.5	3,620	124
Glass E	2,580	3.5	3,450	69

Table 4.11. *Mechanical properties of fibers*

The thermomechanical characteristics of resins are given in Tables 4.9 (thermoset) and 4.10 (thermoplastic), while Table 4.11 provides fiber characteristics.

Mechanical strength is assessed using criteria derived from isotropic materials. The Tsai–Hill criterion focuses on the very poorly defined notion of stress at fracture, without taking nonlinear effects into account. For very critical stresses, composites are generally subject to diffuse and progressive damage. The exponent ^{e} is used to identify the characteristic values of the material.

The criterion classically used is in the following form:

$$\left(\sigma_{11}/\sigma_{11}^e\right)^2 + \left(\sigma_{22}/\sigma_{22}^e\right)^2 - \left(\sqrt{\sigma_{11}\sigma_{22}}/\sigma_{11}^e\right)^2 + \left(\sigma_{12}/\sigma_{12}^e\right)^2 = 1 \qquad [4.1]$$

If the calculation gives a value of less than 1, there is no break in the fold in question.

In the case of glass materials found in spacecraft payloads, Weibull's law [WEI 51] is used to predict the probability ($P_f = 1 - \exp\left(-\left(\sigma/\sigma_0\right)^m\right)$, where σ represents the tensile stress at the material surface) of failure, as listed in Table 4.12.

Material	Fracture toughness (MPa–$\sqrt{m}$)	m	σ_0 (MPa)	P_f	Surface finish
N-BK7	0.85	30.4	70.6	0	SiC 600
N-BK7	0.85	13.3	50.3	3.36×10^{-12}	D4
N-BaK1	—	8.2	58.9	2.31×10^{-3}	SiC 600
F2	0.55	25	57.1	0	SiC 600
SF6	0.7	5.4	49.2	2.47×10^{-5}	SiC 600
Zerodur®	0.9	5.3	293.8	2.5×10^{-9}	Optical polish
Zerodur®	0.9	16	108	0	SiC 600

Table 4.12. *Mechanical properties of glass*

Table 4.13 summarizes the physical properties of space glass.

Glass Properties

Material	n_d	Transmission range (μm)	E (GPa)	α ($\times10^{-6}$/°C)
N-BK7	1.5168	0.2–2.5	82	7.1
Borofloat 33 borosilicate	1.4714	0.35–2.7	64	3.25
Calcium fluoride	1.4338	0.35–7.0	75.8	21.28
Clearceram®-Z (CCZ) HS	1.546	0.5–1.5	92	0.02
Fused silica	1.4584	0.18–2.5	72	0.5
Germanium	4.004 (@ 10 μm)	2.0–14.0	102.7	6.1
Magnesium fluoride	1.3777 (n_o) 1.3895 (n_e)	0.12–7.0	138	13.7 (∥) 8.9 (⊥)
P-SK57	1.5843 (after molding)	0.35–2.0	93	7.2
Sapphire	1.7659 (n_o) 1.7579 (n_e)	0.17–5.5	400	5.6 (∥) 5.0 (⊥)
SF57	1.8467	0.4–2.3	54	8.3
N-SF57	1.8467	0.4–2.3	96	8.5
Silicon	3.148 (@ 10.6 μm)	1.2–15.0	131	2.6
ULE® (Corning 7972)	1.4828	0.3–2.3	67.6	0.03
Zerodur®	1.5424	0.5–2.5	90.3	0.05 (Class 1)
Zinc selenide (CVD)	2.403 (@ 10.6 μm)	0.6–16	67.2	7.1
Zinc selenide (Cleartran)	2.2008 (@ 10 μm)	0.4–14.0	74.5	6.5

Glass Properties (cont.)

Material	ρ (g/cm^3)	dn/dT (absolute) ($\times10^{-6}$/°C)	ν	λ (W/mK)	K (10^{-12}/Pa)
N-BK7	2.51	1.1	0.206	1.11	2.77
Borofloat 33 borosilicate	2.2	–	0.2	1.2	4
Calcium fluoride	3.18	–11.6	0.26	9.71	–1.53 @ 546 nm ($q_1 - q_2$)
Clearceram®-Z (CCZ) HS	2.55	–	0.25	1.54	–
Fused silica	2.2	11	0.17	1.35	3.5
Germanium	5.33	396	0.28	58.61	–
Magnesium fluoride	3.18	1.1 (n_o)	0.271	11.6	–
P-SK57	3.01	1.5	0.249	1.01	2.17
Sapphire	3.97	13.1	0.27	46	–
SF57	5.51	6	0.248	0.62	0.02
N-SF57	3.53	–2.1	0.26	0.99	2.78
Silicon	2.33	130	0.279	137	–
ULE® (Corning 7972)	2.21	10.68	0.17	1.31	4.15
Zerodur®	2.53	15.7	0.243	1.6	3
Zinc selenide (CVD)	5.27	61 @ 10.6	0.28	18	–1.6
Zinc selenide (Cleartran)	4.09	40 @ 10.6 54.3 @ 0.632	0.28	27.2	–

Table 4.13. *Glass properties*

4.5.3. *The environment of mechanical architecture*

Satellite architecture must be rigorously analyzed and designed to withstand the mechanical launch environment.

The various “dimensioning” events are lift-off (acoustic), asymmetrical extinction of liquid propellant boosters (lateral dynamics), stage extinctions (longitudinal dynamics), separations (fairing, stages and launcher/satellite generating shocks):

– continuous static acceleration of up to 10 g longitudinally (to be verified according to the launcher);

– low-frequency longitudinal vibrations (for example, 1 g sine in the 5–100 Hz band);

– low-frequency lateral vibrations (for example, sine wave of 0.8 g in the 2–100 Hz band);

– random vibrations of 8 g in the 20–2,000 Hz band;

– acoustic environment (broadband spectrum from 20 to 10,000 Hz in a reverberant field of approximately 150 dB);

– shocks respecting the 1,000 g/1,000 Hz rule.

A satellite architecture must be rigorously analyzed and studied to cope with the orbital environment, in terms of the following behaviors:

– thermoelastic and the effect of temperature cycling in orbit;

– hygroelastic;

– vibrations in orbit.

Hygroelastic behavior is particularly relevant to organic matrix composites. Composite systems undergo deformation as a function of the moisture retained by the materials.

Vibrations are caused by the forces (a few mN to a few N) of mechanisms (inertia wheels, gyroscopes, moving parts). Optical observation payloads (typically 150 μrad precision for a CubeSat) impose constraints on the satellite’s dynamic responses in all ranges of vibration frequencies.

This is a complex problem because the levels remain low and the satellite’s fine dynamics are not necessarily mastered. The NewSpace approach allows us to take risks and test these systems in orbit very quickly.

A satellite architecture must be rigorously analyzed and designed to cope with the general space environment.

The materials most sensitive to the space environment are:

– optical materials (glass substrate);

– polymeric materials;

– metallic materials are not very sensitive, except for special functions (magnetism, etc.).

As shown in Figure 4.10(a), an environment is characterized in various ways according to a color code. Examples include vacuum, thermal cycling, solar radiation (UV, X, gamma), charged particles (electrons, protons, ions), micrometeorites and debris and atomic oxygen.

The impact of these constraints on the proper operation of the satellite must be assessed through tests or minimized through the satellite's digital twin. For instance, electromagnetic interference from the solar wind can be detrimental to communication systems.

Figure 4.10(b) summarizes the most common forms of stress to be controlled.

As described in the second book, space environment stresses are due to the environment in which space instruments operate. The various effects are the consequence of stresses due to vibratory, thermal, microgravity, vacuum and external electromagnetic or particulate flux phenomena. The result is rapid thermal cycling, outgassing and contamination, electrostatic discharges and electrical breakdowns, as well as aging in materials. This environment needs to be well defined and understood, in order to properly identify and size any spacecraft with its payloads, which in turn requires reliability and robustness tests to qualify the instrument.

4.5.4. *Dimensions of mechanical architecture*

Setting up numerical models is important for validating satellite design. This involves using strength-of-materials and finite element methods to determine natural frequencies and modal shapes, as well as stress levels during the launch period (quasi-static load, random environment).

Mechanical loads have various origins. They are caused by transport, rocket motor ignition overpressure during launch, take-off loads, acoustic loads generated by the motors, vibratory loads generated by the motor structure, motor thrust transients, pressure oscillations of "solid" motors, wind and turbulence, aerodynamic sources, liquid in the tanks, separation of the various stages, pyrotechnic loads, maneuvers, flight operations, operation of onboard equipment, etc. The aim of the analyses is to check that the satellite complies with mechanical stresses. European standards, such as ECSS-E-HB-32-26, provide the rules for these analyses.

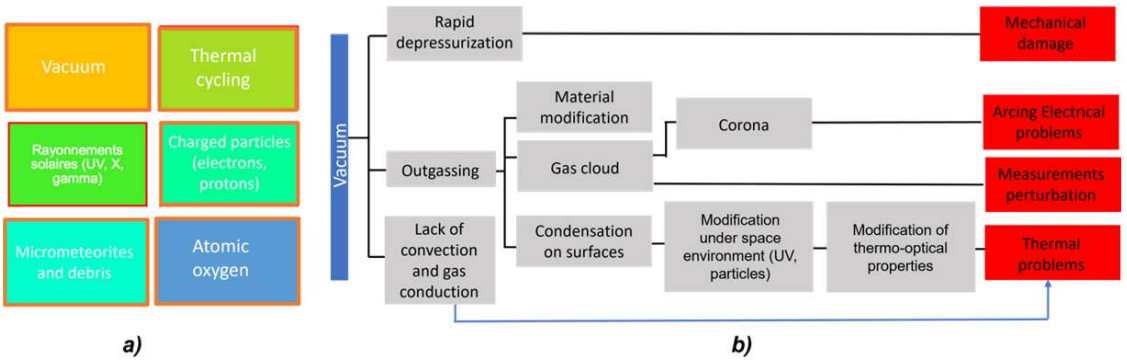

Figure 4.10. *a) Environment; b) satellite constraints*

The most common elements in satellites are beams (embedded beams subjected to a force) and plates. Mechanical problems can only be solved analytically in a limited number of cases (beams, plates, shells, etc.), and generally under considerable hypotheses.

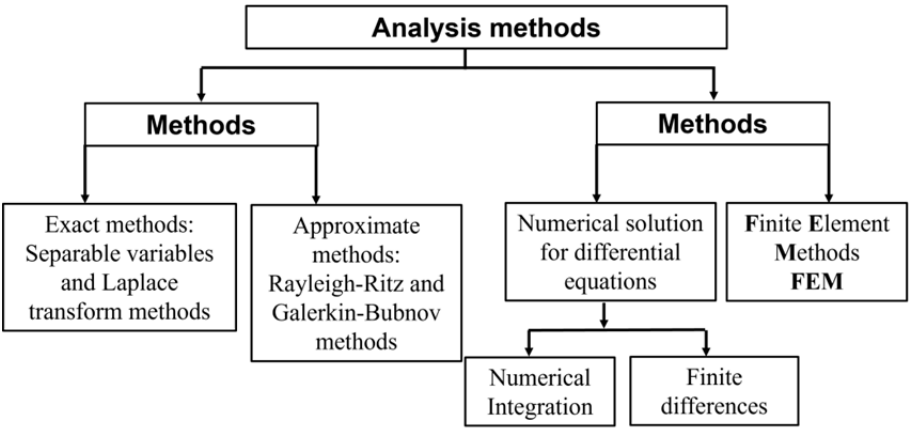

Figure 4.11. *Constraints of a satellite environment*

Figure 4.11 summarizes the various methods of solving partial differential equations (PDEs) for analyzing mechanical systems under stress.

Since a satellite structure generally behaves like a mass–spring system with a damper (link with the amplification factor during vibrations), the dynamics of this system can be studied. Figure 4.12(a) shows this model in the simple case of a system of mass m subjected to the restoring force of a spring of stiffness k, a braking force of damping coefficient b and an external force f for a displacement of u. The second-order differential equation (see Figure 4.12(b)) can be solved by applying the Laplace transform according to the algorithm in Figure 4.10(c) to determine the system displacement as a function of frequency.

Transmission, acceleration and displacement can be determined as a function of frequency, and the resonant frequency of the system can be calculated, as shown in Figure 4.13.

The equations of the mechanical problem can be simplified by discretizing it, meaning checking equations at a limited number of points. This produces a system of linear equations whose size depends on the fineness of the discretization. The solution of the discretized problem is an approximate solution of the real problem.

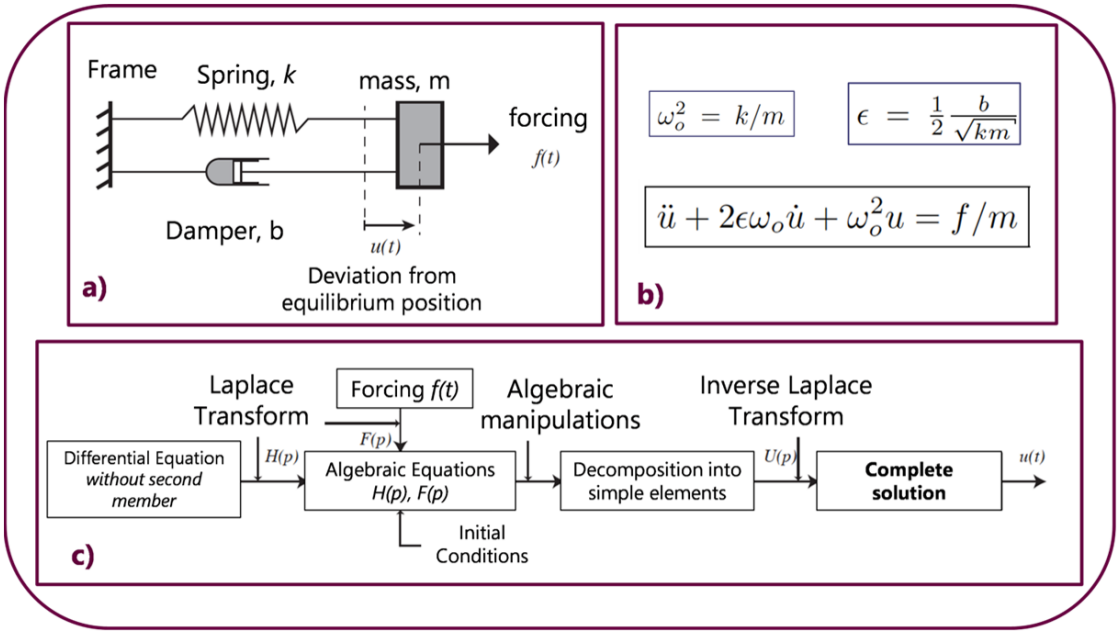

Figure 4.12. *Modeling a satellite system*

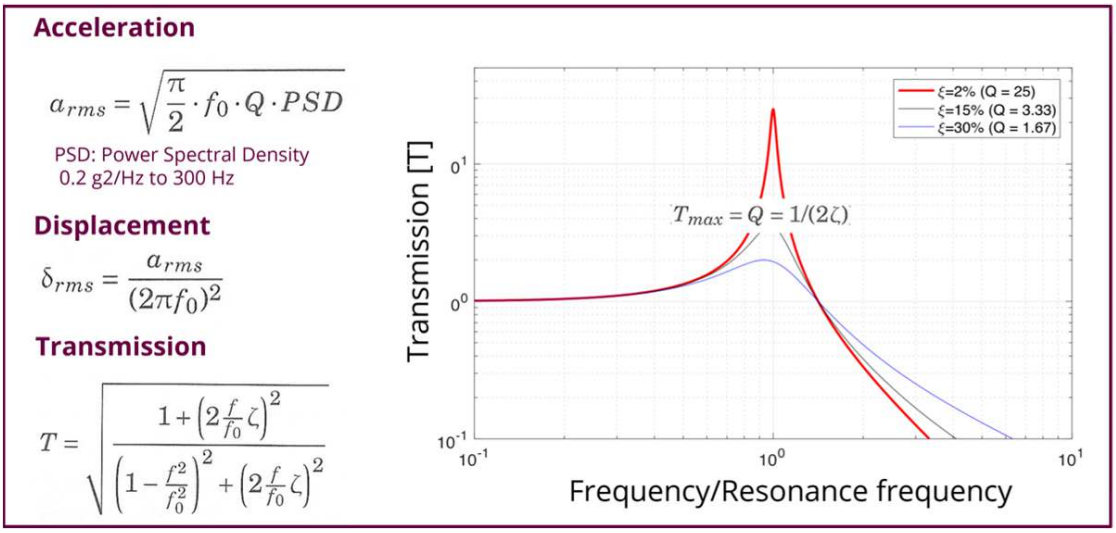

Figure 4.13. *Responses of the mass–spring system as a function of frequency*

A spacecraft is a complex system, which is why it is preferable to use numerical models to study its mechanical behavior. A compromise has to be found between finding a precise solution for an oversimplified problem, or opting for an approximate solution for a problem generally taken in its most complex form.

Generally speaking, the problem consists of determining the state of a structure subjected to loads. The structure is characterized by its geometry and one or more materials. It is subjected to stresses such as:

– volumetric or surface forces;

– imposed displacements (zero or not);

– temperatures, heat flows;

– speeds, etc.

We want to know:

– displacements at any point;

– strains, stresses, internal variables at any point;

– temperature;

– natural frequencies.

The finite element method is a discretization technique that enables us to transform a theory that deals with the continuous resulting in unsolvable mathematical problems, into a theory that deals with the discrete and leads to simple systems of equations that we can solve. This transformation is based on strong hypotheses that reduce the theory's domain of validity, and which must therefore be clearly understood.

Different types of analyses are possible with FEM: linear or nonlinear static mode, modal analysis, buckling analysis, spectral analysis, slow or fast dynamic response analysis, and multiphysics analysis (thermomechanical, electrothermal, etc.).

Various software packages can be used to perform vibration analysis based on mechanical or thermomechanical stresses, as introduced in the appendix. Examples include MSC Nastran, Ansys, COMSOL, ABACUS, ADINA, Siemens NX, RADIOSS, Dyna3D, SAP, MARC, I-deas, PAM/System, SAMCEF, etc.

Figure 4.14 shows an example of the results obtained with the UVSQ-SAT.

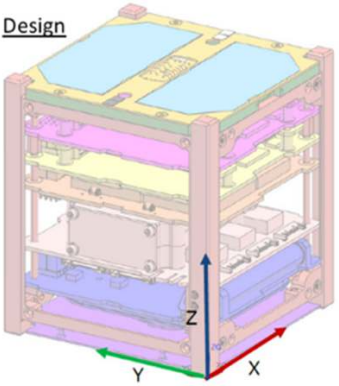

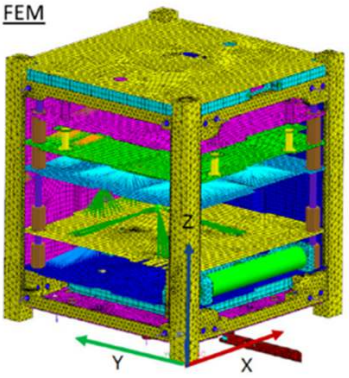

Material characteristics

Identification	E (GPa)	ν	ρ (kg/m³)	σ ULTIMATE (MPa)	σ YIELD (MPa)	Use
Aluminum 6082	69	0.3	2700	295	240	Structure (frames, ribs)
Aluminum 5754	70	0.33	2700	245	185	Solar panels
Steel 304L	210	0.3	7800	520	200	Rods
Polyimide	25*	0.18	1900	265	-	Boards

*In order to take into account the copper layers, the Young modulus taken is 30 GPa.

Stiffness requirement

- f_1 > 150 Hz

Quasi-static load cases

- Case 1: 15 g (acc / X)
- Case 2: 15 g (acc / Y)
- Case 3: 15 g (acc / Z)

Random environment

All axes	
Frequency (Hz)	Qualification level +3dB
20 – 100	0.0352 g^2/Hz
300 – 600	0.1008 g^2/Hz
740 – 850	0.28 g^2/Hz
2000	0.05152 g^2/Hz
Global level: 15.51 gRMS	

Figure 4.14. *Modeling of the UVSQ-SAT using FEM*

4.6. Conclusion

The CubeSat has made it possible to study space using small satellites. The methodology used in university projects enables small satellites to be built within a reasonable timeframe of two to three years, using teams trained in the space industry and motivated students and at affordable costs. These satellites are used for space missions designed to transmit knowledge and observe the Earth's atmosphere, with the aim of analyzing and dynamically monitoring its evolution as part of the study of global warming. In comparison, larger-scale projects that require more time – at least an order of magnitude longer – and a much larger team, as well as more interaction with different organizations or institutions, are time-consuming and require more substantial funding.

4.7. Appendix

4.7.1. *Elastic and thermal properties of a physical system*

In order to design the mechanical architecture of a CubeSat, it is necessary to carry out simulations to determine its response to an environmental constraint. This requires knowledge of its mechanical and thermomechanical properties. The content of this section can be found in detailed form in references dealing with the mechanics and strength of materials [BRI 38, BRU 55, BIO 56, NYE 61, LAN 67, ADD 87], and follows the description given in reference [DAH 21].

When modeling the effects of mechanical stress in a material in the formalism of continuum mechanics or elasticity theory, we consider volume elements to establish the constitutive relationships. These are infinitesimally small on a macroscopic scale, but very large on the scale of the material's constituents (atoms, molecules, etc.). In the case of mechanical deformation of the medium, we consider that the forces responsible for internal stresses in the infinitely small volume around each point are short-range and limited to close neighbors. In this case, the forces are exerted by one of the elements on the neighboring elements, so that in a given volume inside the material, they only act on the surface. These effects are expressed using tensors.

In a three-dimensional Euclidean space with Cartesian axes (notation $1 = x$, $2 = y$ and $3 = z$), the notion of tensor is linked to the physical quantity represented and to the way in which this quantity is transformed when coordinates are changed. Thus, the temperature T, which is a scalar, is a zeroth-order tensor (one component), the

force $\vec{F}$, which is a vector, is a first-order tensor (three components). We call this F_k. To represent the coupling between two vector quantities taken from the same system of axes, we use a second-order tensor (nine components).

To establish the constitutive equations, it is necessary to define the stress tensor acting on an elementary volume in the material. The stress tensor σ_{ik} describes the state of stress at any point of the volume considered in the material, in all directions. Its components, which correspond to a force exerted on a unit area around a point, are homogeneous to a pressure (in Pa or $N.m^{-2}$). It is a symmetrical tensor such that $\sigma_{ik} = \sigma_{ki}$. The diagonal terms of the stress tensor are given by tensile (or compressive) forces, and the nondiagonal terms by shear forces. The components have positive values in the case of tension (negative in the case of compression). In Figure 4.15, we have represented the stress tensor components by their indices on each face marked by the normal vector n_i.

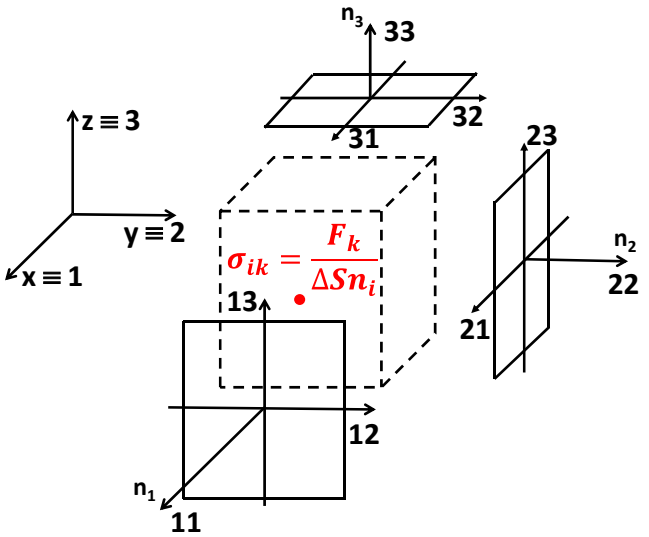

Figure 4.15. *Stress tensor σ_{ik} corresponding to the k component of the force F per unit area of the action point in the middle of a surface marked by its normal n_i*

In matrix form, the tensor σ_{ik} has the following expression:

$$\begin{pmatrix} \sigma_{xx} & \sigma_{xy} & \sigma_{xz} \\ \sigma_{yx} & \sigma_{yy} & \sigma_{yz} \\ \sigma_{zx} & \sigma_{zy} & \sigma_{zz} \end{pmatrix} = \begin{pmatrix} \sigma_{11} & \sigma_{12} & \sigma_{13} \\ \sigma_{12} & \sigma_{22} & \sigma_{23} \\ \sigma_{13} & \sigma_{23} & \sigma_{33} \end{pmatrix} \quad [4.2a]$$

As the stress tensor is symmetrical, like the strain tensor, only six of its nine terms are independent. In Voigt (or Voigt–Nye) notation, we switch from matrix representation to the following vector notation:

$$\begin{pmatrix} \sigma_{11} & \sigma_{12} & \sigma_{13} \\ \sigma_{12} & \sigma_{22} & \sigma_{23} \\ \sigma_{13} & \sigma_{23} & \sigma_{33} \end{pmatrix} \equiv \begin{pmatrix} \sigma_{11} \\ \sigma_{22} \\ \sigma_{33} \\ \sigma_{23} \\ \sigma_{13} \\ \sigma_{12} \end{pmatrix} = \begin{pmatrix} \sigma_1 \\ \sigma_2 \\ \sigma_3 \\ \sigma_4 \\ \sigma_5 \\ \sigma_6 \end{pmatrix} \quad [4.2b]$$

where (σ) is a six-row vector (6 x 1). The first three terms (σ_1, σ_2, σ_3) are tensile or compressive stresses along the perpendiculars to the surfaces, i.e. parallel to axes 1, 2 and 3 defined by the surface normal vector. The last three terms (σ_4, σ_5, σ_6) are shear stresses around axes 1, 2 and 3 or pairs in planes 2-3, 1-3 and 1-2 (see Figure 4.15).

If we consider the deformation of a material seen as a continuous medium, we assume small displacements. Deformation is then determined by a translation vector **u**(**r**) of a point in the material marked by the vector **r**, and the derivatives of this vector with respect to the coordinates. Nine derivatives are thus obtained, which are generally represented in the form of a symmetrical deformation tensor (tensor of order 2) that represents *the deformation of the point* by:

$$\varepsilon_{ik} = \frac{1}{2}\left(\frac{\partial u_i}{\partial x_k} + \frac{\partial u_k}{\partial x_i}\right) \quad [4.3a]$$

and an antisymmetrical tensor:

$$\omega_{ik} = \frac{1}{2}\left(\frac{\partial u_i}{\partial x_k} - \frac{\partial u_k}{\partial x_i}\right) \quad [4.3b]$$

representing the rotation of the material around the point.

Deformations can be defined by Hooke's law in tensorial form, such that:

$$\{\boldsymbol{\varepsilon}\} = [D]^{-1}\{\sigma\} \quad [4.3c]$$

where $\{\varepsilon\}$ is the strain vector = $[\varepsilon_{11}\ \varepsilon_{22}\ \varepsilon_{33}\ \varepsilon_{23}\ \varepsilon_{13}\ \varepsilon_{12}]^T$, $\{\sigma\}$ is the stress vector = $[\sigma_{11}\ \sigma_{22}\ \sigma_{33}\ \sigma_{23}\ \sigma_{13}\ \sigma_{12}]^T$, and $[D]^{-1}$ is the inverse matrix of elastic stiffness.

The coefficients of this matrix are such that:

$$[D]^{-1} = \begin{pmatrix} 1/E_1 & -\nu_{12}/E_1 & -\nu_{13}/E_1 & 0 & 0 & 0 \\ -\nu_{21}/E_2 & 1/E_2 & -\nu_{23}/E_2 & 0 & 0 & 0 \\ -\nu_{31}/E_3 & -\nu_{32}/E_3 & 1/E_3 & 0 & 0 & 0 \\ 0 & 0 & 0 & 1/G_{23} & 0 & 0 \\ 0 & 0 & 0 & 0 & 1/G_{13} & 0 \\ 0 & 0 & 0 & 0 & 0 & 1/G_{12} \end{pmatrix} \quad [4.4]$$

where E_i are Young's moduli, ν_{ik} are Poisson's coefficients and G_{ik} are shear moduli.

Tensor calculus is also used to model thermomechanical effects [BRI 38, BRU 55, BIO 56, NYE 61, LAN 67, ADD 87]. For example, using tensor notation, the equation for heat propagation in a body subjected to heat flux can be written as follows:

$$\frac{\Phi}{S} e_i = j_i = -\lambda_{ik} \frac{\partial T}{\partial x_k} \quad [4.5a]$$

where Φ is the heat flux (watt, W), S is the area (m^2) crossed by the flux, e_i is the basis vector of the vector space following i, j_i is the ith component of the thermal current density vector (Wm^{-2}), λ_{ik} is the thermal conductivity tensor ($Wm^{-1}.K^{-1}$) which is a second-order tensor, and $\partial T/\partial x_k$ is the k-component of the gradient of T (Km^{-1}) which is a first-order tensor. The Einstein summation convention when two indices are repeated is used to lighten the writing.

In a homogeneous body, the rise in temperature leads to its expansion. This is characterized by a coefficient of thermal expansion α, whose expression is as follows:

$$\alpha = -\frac{1}{V}\left(\frac{\partial V}{\partial T}\right)_S \quad [4.5b]$$

where V is the volume of the body and T is the temperature.

For a homogeneous variation in the material temperature of ΔT, the thermal expansion is expressed as follows:

$$\varepsilon_{ik} = \alpha_{ik} \Delta T \quad [4.5c]$$

where α_{ik} are the thermal expansion coefficients of the symmetrical tensor $[\alpha_{ik}]$, and ε_{ik} are the coefficients of the strain tensor $[\varepsilon_{ik}]$.

In matrix form, this relationship is expressed as follows:

$$\begin{pmatrix} \varepsilon_{11} & \varepsilon_{12} & \varepsilon_{13} \\ \varepsilon_{12} & \varepsilon_{22} & \varepsilon_{23} \\ \varepsilon_{13} & \varepsilon_{23} & \varepsilon_{33} \end{pmatrix} = \begin{pmatrix} \alpha_{11} & \alpha_{12} & \alpha_{13} \\ \alpha_{12} & \alpha_{22} & \alpha_{23} \\ \alpha_{13} & \alpha_{23} & \alpha_{33} \end{pmatrix} (T - T_0) \quad [4.5d]$$

Since the strain tensor is symmetrical, only six of its nine terms are independent. In this case, we can use Voigt (or Voigt–Nye) notation to switch from a matrix representation to a vector notation as follows:

$$\begin{pmatrix} \varepsilon_{11} & \varepsilon_{12} & \varepsilon_{13} \\ \varepsilon_{12} & \varepsilon_{22} & \varepsilon_{23} \\ \varepsilon_{13} & \varepsilon_{23} & \varepsilon_{33} \end{pmatrix} \equiv \begin{pmatrix} \varepsilon_{11} \\ \varepsilon_{22} \\ \varepsilon_{33} \\ \varepsilon_{23} \\ \varepsilon_{13} \\ \varepsilon_{12} \end{pmatrix} = \begin{pmatrix} \varepsilon_1 \\ \varepsilon_2 \\ \varepsilon_3 \\ \frac{\varepsilon_4}{2} \\ \frac{\varepsilon_5}{2} \\ \frac{\varepsilon_6}{2} \end{pmatrix} = \begin{pmatrix} \alpha_1 \\ \alpha_2 \\ \alpha_3 \\ \frac{\alpha_4}{2} \\ \frac{\alpha_5}{2} \\ \frac{\alpha_6}{2} \end{pmatrix} (T - T_0) \quad [4.5e]$$

where (ε) and (α) are six-row vectors (6 x 1) and $(T - T_0)$ is a scalar.

In the principal axes of the expansion tensor, we have the following equation (i = k):

$$\varepsilon_i = \alpha_i \Delta T \quad [4.5f]$$

where α_i are the principal coefficients of expansion i = 1, 2 and 3.

In this case, the following form is applicable:

$$\begin{pmatrix} \varepsilon_1 & 0 & 0 \\ 0 & \varepsilon_2 & 0 \\ 0 & 0 & \varepsilon_3 \end{pmatrix} = \begin{pmatrix} \alpha_1 & 0 & 0 \\ 0 & \alpha_2 & 0 \\ 0 & 0 & \alpha_2 \end{pmatrix} (T - T_0) \quad [4.5g]$$

or:

$$\begin{pmatrix} \varepsilon_1 \\ \varepsilon_2 \\ \varepsilon_3 \\ 0 \\ 0 \\ 0 \end{pmatrix} = \begin{pmatrix} \alpha_1 \\ \alpha_2 \\ \alpha_3 \\ 0 \\ 0 \\ 0 \end{pmatrix} (T - T_0) \quad [4.5h]$$

Using the equations of thermoelasticity [NYE 61], we can define strains and entropy density as follows:

$$\{\boldsymbol{\varepsilon}\} = [D]^{-1}\{\sigma\} + \{\alpha\}\Delta T \quad [4.6a]$$

$$\{S\} = \{\alpha\}^T\{\sigma\} + \frac{\rho C_P}{T_0}\Delta T \quad ; \Delta T = T - T_{ref} \quad [4.6b]$$

where:

– $\{\varepsilon\}$ is the total strain vector = $[\varepsilon_1\ \varepsilon_2\ \varepsilon_3\ \varepsilon_{23}\ \varepsilon_{13}\ \varepsilon_{12}]^T$;

– S is the entropy density;

– $\{\sigma\}$ is the stress vector = $[\sigma_1\ \sigma_2\ \sigma_3\ \sigma_{23}\ \sigma_{13}\ \sigma_{12}]^T$;

– T is the current temperature;

– T_0 is the absolute reference temperature = $T_{ref} + T_{off}$;

– T_{ref} is the reference temperature;

– T_{off} is the offset temperature;

– $\{\alpha\}$ is the vector of thermal expansion coefficients = $[\alpha_1\ \alpha_2\ \alpha_3\ 0\ 0\ 0]^T$;

– ρ is the bulk density;

– Cp is the specific heat at constant pressure;

– [D] is the elastic stiffness matrix.

4.7.2. *Finite element method (FEM)*

The finite element method (FEM) is used to simulate the behavior of a mechanical system under stress. FEM was first developed in the 1950s in mechanics and civil engineering. The aim was to study the behavior of structures under stress (airplane wings, bridges). It can be used to analyze bar and beam connections based on the assumptions of the strength of materials [HRE 41, HRE 42, COU 43, ARG 54, TUR 56, CLO 60, ZIE 67, WHI 76, DHA 84, DAU 85].

Note that the abstract of Hrenikoff's 1941 article reads [HRE 41]:

> Because of mathematical difficulties which make the solution of differential equations of the theory of elasticity impossible in many cases, the author has been impelled to seek some other method of approach than one of pure mathematical analysis. The method outlined in this paper is of this character and may with some qualifications be applied to problems of two-dimensional stress, bending of plates, bending of cylindrical shells, the general case of

> three-dimensional stress, and a great variety of others. Essentially, the method consists in replacing the continuous material of the elastic body being studied by a framework of bars arranged according to a definite pattern, the elements of which are endowed with elastic properties suitable to the type of problem. This framework is then analyzed, according to the procedure outlined in the paper for various types of elastic problems. Examples of the application of the principles involved are also given.

In the first book, published in 1967 by Zienkiewicz and Cheung, on FEM [ZIE 67], it is stated that:

> With the advent of digital computers, discrete problems can generally be solved easily, even if there are a very large number of elements. As the capacity of all computers is limited, continuous problems can only be solved accurately by mathematical manipulation. The mathematical techniques available for accurate solutions generally limit the possibilities to over simplistic situations.

The finite element method is one of the most widely used in industry and applied research to transform the PDEs driving the system's coupled physical phenomena into algebraic equations [DHA 84].

The behavior of the physical systems involved in complex systems is described by means of partial differential equations (PDEs equation [4.7a]), which control the dynamic evolution of these systems subject to constraints such as boundary conditions (equation [4.7b]) that cannot always be solved analytically:

$$L(u) + f = 0 \qquad [4.7a]$$

$$B(u) + g = 0 \qquad [4.7b]$$

In these equations, L and B are differential operators and u is the parameter to be determined.

Generally, equation [4.7a] is expressed as follows [4.7c]:

$$Ku = F \qquad [4.7c]$$

where K is the stiffness matrix which depends on the property of the physical system under consideration, u is the displacement vector to be determined or the system response, and F is the stress or stimulus applied by the physical system under study which may be a force, or any other form of stress, as summarized in Table 4.14.

unknown

	Property : K	Response: u	Stimulus: F
ELASTIC	Rigidity	Displacement	Force
THERMAL	Conductivity	Temperature	Heat source
FLUID	Viscosity	Speed	Pressure
ELECTROSTATIC	Permittivity Dielectric	Potential Electric	Charge

Table 4.14. *Common physical phenomena*

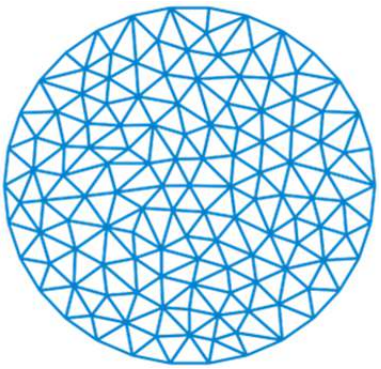

Figure 4.16. *Example of a surface and its decomposition into finite elements*

The objective is to find u using:

$$u = K^{-1}F \qquad [4.7d]$$

The FEM numerical method is used to solve PDEs which are problems with boundary conditions (equations [4.7a] and [4.7b]). To solve a given problem, FEM subdivides the domain of a large system into smaller, simpler subsystems, known as finite elements (see Figure 4.16). This is equivalent to replacing a continuous function of a continuum (given domain Ω) with an infinite number of degrees of freedom by a discrete model, approximated by a set of piecewise continuous functions with a finite degree of freedom.

4.7.2.1. *Solving a differential equation in one-dimensional space*

Consider, in one-dimensional space, the following differential equation: $u''(x) = f$ over the interval [0,1] and subject to the constraint $u(0) = u(1) = 0$, where u(x) is an unknown function of x and f is a given function. This equation can be solved directly by integrating the differential equation twice, or by applying the FEM.

To solve a problem at the limits (PL) or constraints at the domain boundary using FEM, the calculation is carried out in two steps:

– The first step is to reformulate the original PL in its weak or variational form (integral form), which is an analytical transformation.

– In the second step, the resulting weak form is discretized on a finite-dimensional space. This provides concrete formulas for a high-dimensional but finite linear problem. The solution enables the initial PL to be solved approximately. This finite-dimensional problem is then implemented on a computer in matrix form.

4.7.2.2. *Variational formulations*

The first step is to convert the differential equation into its variational equivalent. If u(x) is a solution of the differential equation, then for any regular function v(x) that satisfies the boundary conditions, i.e. v = 0 at x = 0 and at x = 1, we have:

$$\int_0^1 f(x)v(x)dx = \int_0^1 u''(x)v(x)dx \qquad [4.8a]$$

Conversely, if for a given function u(x), the above equality holds for every regular function v(x), we can show that it is the solution of the differential equation (the demonstration is nontrivial and uses Sobolev spaces).

Integrating the right-hand side of the equation by parts gives the following equation:

$$\int_0^1 f(x)v(x)dx = -\int_0^1 u'(x)v'(x)dx = -\Phi(u,v) \qquad [4.8b]$$

under the assumption that v(0) = v(1) = 0.

We can define the set $H_0^1(0,1)$ of absolutely continuous functions on (0,1), which take the value 0 at the points x = 0 and x = 1. This function is “once differentiable”, and we can show that the symmetrical bilinear form $\Phi(u, v)$ is then a scalar product that transforms $H_0^1(0,1)$ into a Hilbert space (integrable square functions). On the other hand, the left-hand side is also a scalar product, this time on the space Lp (a vector space of classes of functions whose exponent power ^{p} is integrable in the Lebesgue sense), which here is $L_2(0,1)$ (integrable square function, p = 2).

4.7.2.3. *Weak form discretization*

Essentially, the idea is to replace the infinite-dimensional linear problem, namely to find $u \in H_0^1$ such that:

$$\int_0^1 f(x)v(x)dx = -\Phi(u,v) \qquad [4.9a]$$

where $v \in H_0^1$, by a finite-dimensional version, or find $u \in V$ such that $v \in V$ where V is a finite-dimensional subspace.

There are many possible choices for V. In the case of the finite element method, it is usual to take a space of piecewise linear functions for V. For the problem at hand, let us start from the interval [0,1] and choose x_n values, such that $0 = x_0 < x_1 < \ldots < x_n < x_{n+1} = 1$, and define V by choosing functions $v(x)$ in [0,1] such that $v(x)$ is continuous and linear in the intervals $[x_k, x_{k+1}]$ for k = 0 up to n with $v(0) = v(1) = 0$ and where $x_0 = 0$ and $x_{n+1} = 1$.

Note that V functions are not differentiable according to the elementary definition. Indeed, if $v(x) \in V$, the derivative is generally not defined at points $x = x_k$, k = 1, …, n.

However, the derivative exists for any other value of x and can be used in integration-by-parts operations.

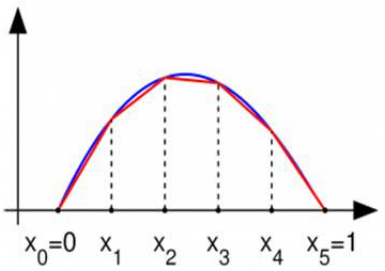

Figure 4.17. *Example of a function in H_0^1, with zero values at endpoints (blue) and piecewise linear approximation (red)*

4.7.2.4. *Base selection*

To complete the discretization, it is necessary to select a basis of V. In the one-dimensional case, for each control point x_k, it is convenient to choose a piecewise linear function $v_k \in V$, whose value is equal to 1 at x_k and 0 at x_j whenever $j \neq k$, hence:

$$v_k(x) = \begin{cases} \frac{x - x_{k-1}}{x_k - x_{k-1}} & \text{if } x \in [x_{k-1}, x_k] \\ \frac{x_{k+1} - x_k}{x_{k+1} - x_k} & \text{if } x \in [x_k, x_{k+1}] \\ 0 & \text{otherwise} \end{cases} \quad [4.9b]$$

for k = 1, …, n. This basis is a scaled and shifted triangle function.

The main advantage of this choice of bases is that the scalar products:

$$\langle v_j, v_k \rangle = \int_0^1 v_j(x) v_k(x) dx \quad [4.9c]$$

and:

$$\Phi(v_j, v_k) = \int_0^1 v_j'(x) v_k'(x) dx \quad [4.9d]$$

are zero for almost all j, k. In the one-dimensional case, the domain of v_k is the interval $[x_{k-1}, x_{k+1}]$. Consequently, the integrands of $<v_j, v_k>$ and $\Phi(v_j, v_k)$ are identically zero whenever $|j - k| > 1$.

4.7.2.5. *Matrix form of the problem*

By writing:

$$u(x) = \sum_{k=1}^{n} u_k v_k(x) \quad [4.10a]$$

and:

$$f(x) = \sum_{k=1}^{n} f_k v_k(x) \quad [4.10b]$$

equation [4.10b] can be written as:

$$\sum_{k=1}^{n} f_k \int_0^1 v_k(x) v_j(x) dx = -\sum_{k=1}^{n} u_k \Phi\left(v_k(x), v_j(x)\right) \quad [4.10c]$$

for j = 1, n, expressed in the following matrix form:

$$\sum_{k=1}^{n} f_k M_{kj} = -\sum_{k=1}^{n} u_k L_{kj} \quad [4.10d]$$

Since the matrices M and L are symmetrical, we can write the equation verified by f and u in the matrix form $-Lu = Mf$, and thus obtain u by inverting L, such that $u = -L^{-1}Mf$. Since the matrices M and L are hollow (with zeros almost everywhere and integers otherwise), matrix inversion is computationally simple.

Numerical simulation software is used to address physical problems by solving PDEs [SOM 64b] using FEM in fields such as electromagnetism, structural mechanics and thermodynamics. It can also handle multiphysical couplings by combining different physical phenomena, such as electrical and thermal (electrothermal), or thermal and mechanical (thermomechanical) [VOI 10, BRI 38, MAX 54, BRU 55, BIO 56, NYE 61, BRU 62, BRU 65, LAN 67, GER 96].

Taking into account the problem to be studied, a physical model is established for a system in 1D, 2D or 3D dimensions. This model is considered as a domain bounded by a boundary, and consists of PDEs whose solutions must verify boundary conditions and initial conditions. For instance, the equations describe the spatio-temporal variations of an unknown variable, such as deformation, and the method consists of finding an approximate solution to this deformation after discretizing the geometry of the system, broken down into meshes connected by nodes. The solution is interpolated on a basis of functions (Lagrange polynomial).

Generally, PDEs are expressed in coefficient form, which is well suited to linear PDEs. The general equation is in the following form on the domain Ω of the physical system:

$$e_a \frac{\partial^2 u}{\partial t^2} + d_a \frac{\partial u}{\partial t} + \nabla(-c\nabla u - \alpha u + \gamma) + \beta\nabla u + au = f \qquad [4.11a]$$

A domain is the topological entity denoted by Ω within a geometric model that describes the bounded parts of the model's manifolds, as well as the relationships between the different manifolds of the geometry. The different types of domains are vertex, edge, face and subdomain. A domain of dimension less than the spatial dimension is called a boundary and is denoted by $\partial\Omega$. A manifold is a mathematical function describing a surface, curve or point in a geometric model of any dimension.

Dirichlet-type boundary conditions correspond to imposed values of the function u at the $\partial\Omega$ boundaries of the domain. For equation [4.11a], it has the following expression:

$$hu = r \qquad [4.11b]$$

A Dirichlet boundary condition specifies the value of the function (dependent variable) on a boundary. In contrast, a Neumann boundary condition specifies the value of the normal flow across a boundary.

Similarly, the generalized Neumann-type boundary conditions (or mixed boundary conditions or Robin-type boundary conditions) are expressed as a linear combination of the flow of the function in the direction normal to the boundary $\partial\Omega$ of the domain

$\vec{n} \cdot (-c\nabla u - \alpha u + \gamma)$ and variables qu at the boundary $\partial\Omega$ of the domain in the following form:

$$\vec{n} \cdot (-c\nabla u - \alpha u + \gamma) + qu = g - h^T \mu \quad [4.11c]$$

In stationary mode, the e_a and d_a terms are zero. For a nonlinear model, one or more of the coefficients *c*, α, γ, β, *a* or *f* depend on the solution u or at least on one of the coefficients of equations [4.11b] and [4.11c], *q*, *g*, *h*, where *r* depends on the solution *u* or its derivatives with respect to the space variables.

Note that the term $-c\nabla u - \alpha u + \gamma$ is the flux vector sometimes noted Γ:

$$\Gamma = (-c\nabla u - \alpha u + \gamma) \quad [4.11d]$$

The software's interpolation functions are defined on each mesh element (nonzero on the element and zero elsewhere). A mesh and its interpolation functions constitute a finite element.

There are three types of PDEs: elliptic, hyperbolic and parabolic.

A second-order linear stationary elliptic PDE has the following form:

$$\nabla(-c\nabla u - \alpha u + \gamma) + \beta\nabla u + au = f \quad [4.12a]$$

where c is positive or negative. An example is the Poisson equation.

A second-order linear hyperbolic PDE has the following form:

$$e_a \frac{\partial^2 u}{\partial t^2} + \nabla(-c\nabla u - \alpha u + \gamma) + \beta\nabla u + au = f \quad [4.12b]$$

where e_a and c are positive. An example is the wave equation.

A second-order linear parabolic PDE has the following form:

$$d_a \frac{\partial u}{\partial t} + \nabla(-c\nabla u - \alpha u + \gamma) + \beta\nabla u + au = f \quad [4.12c]$$

where d_a and c are positive. An example is the heat equation.

In the software's graphical interface, there are generally three main windows: one for building the model, one for parameterizing the model and one for viewing results.

The steps involved in modeling a physical system comprise three parts: building the model, solving the PDEs and post-processing the data to extract the most significant results.

4.7.2.5.1. Building the model

– Drawing or importing geometry in 1D, 2D or 3D dimensions.

– Setting the values of the physical properties of the materials in the various domains making up the geometry, according to the physical model constructed (physical parameters such as thermal conductivity, coefficient of thermal expansion, etc., are defined).

– Determining initial and boundary conditions and source (or sink) terms.

4.7.2.5.2. Solving PDEs

– Visualization of results in graphical, tabular or animated form.

– Determining the values of unknown variables from the variables set by the boundary conditions. The software solves the equations using the finite element method, with adapted solvers to determine the values of the variables over the entire geometry by iteration until convergence (set by a convergence criterion).

4.7.2.5.3. Post-processing results

– Presentation of results in graphical, tabular or animated form.

– Data exportation.

4.7.3. *Modal analysis of structural components*

First, we determine the equations governing the vibrational behavior of a structure's components. The equations are then put into variational form and discretized by finite elements. This yields matrix systems that can be solved numerically in the frequency domain to find eigenfrequencies and modes.

4.7.3.1. *Equating the vibration problem*

The structures considered have an elastic, linear and isotropic behavior with no initial stress or deformation. In the absence of a volume source, the equation governing its vibratory behavior is given by the following equation:

$$\boldsymbol{\rho_s} \frac{\partial^2 \boldsymbol{u}}{\partial t^2} - \nabla \boldsymbol{\sigma} = \mathbf{0} \qquad [4.13a]$$

where $\boldsymbol{\rho_s}, \boldsymbol{u}$ and $\boldsymbol{\sigma}$ are the density, displacement field and stress tensor of the structure, respectively.

If we denote Γ_u the imposed displacement boundaries (Dirichlet) and Γ_f those of the imposed external force type (Neumann), the boundary conditions associated with the structure are written as follows:

$$\boldsymbol{u} \|_{\Gamma_u} = \bar{\boldsymbol{u}} \qquad [4.13b]$$

and:

$$\boldsymbol{\sigma} \cdot \boldsymbol{n} \|_{\Gamma_u} = \bar{\boldsymbol{f}} \qquad [4.13c]$$

For a linear elastic material, stresses and strains are related by Hooke's law ($\boldsymbol{\sigma} = \boldsymbol{D\varepsilon}$). We can use the symmetry of the stress and strain tensors to represent the stresses and strains as a six-component column vector.

In this case, Hooke's law can be written as follows [DAH 19, MAK 20]:

$$\begin{pmatrix} \sigma_{11} \\ \sigma_{22} \\ \sigma_{33} \\ \sigma_{23} \\ \sigma_{13} \\ \sigma_{12} \end{pmatrix} = \frac{E}{(1+\nu)(1-2\nu)} \begin{pmatrix} 1-\nu & \nu & \nu & 0 & 0 & 0 \\ \nu & 1-\nu & \nu & 0 & 0 & 0 \\ \nu & \nu & 1-\nu & 0 & 0 & 0 \\ 0 & 0 & 0 & 1-\nu/2 & 0 & 0 \\ 0 & 0 & 0 & 0 & 1-\nu/2 & 0 \\ 0 & 0 & 0 & 0 & 0 & 1-\nu/2 \end{pmatrix} \begin{pmatrix} \varepsilon_{11} \\ \varepsilon_{22} \\ \varepsilon_{33} \\ 2\varepsilon_{23} \\ 2\varepsilon_{13} \\ 2\varepsilon_{12} \end{pmatrix}$$

[4.13d]

Structural mechanics uses geometric, kinematic and stress-state approximations to simplify the three-dimensional problem, so as to reduce the number of unknowns (degrees of freedom).

This is the origin of simplified models, such as 1D bar or beam elements and 2D plate or shell elements. Table 4.15 shows the number of degrees of freedom per node for some models.

Geometry	Modeling	d.o.f. per Node	Translation	Rotation
1D	Bar	1	1	-
	Beam	2	1	1
	Axisymmetric shell	3	1	2
2D	Structure in Stress Plane State	2	2	-
	Structure in Strain Plane State	2	2	-
	Plate	3	1	2
	Shell	5	3	2

Table 4.15. *Degrees of freedom (d.o.f.) per node in 1D and 2D geometries*

4.7.3.2. *Variational formulation*

We consider $\boldsymbol{u}^*$ a virtual field that is associated with the structure. Equation [4.13a] is integrated as in [4.8b] for the 1D problem on the $\boldsymbol{\Omega_s}$ domain. After integration by parts, then application of the boundary conditions, the variational problem consists of finding u such that $\{\boldsymbol{u}|_{\Gamma_u} = \bar{\boldsymbol{u}}\}$:

$$\int_{\Omega_s} \rho_s \boldsymbol{u}^* \ddot{\boldsymbol{u}} dV + \int_{\Omega_s} \boldsymbol{\varepsilon}^* \boldsymbol{\sigma}. dV = \int_{\Omega_s} \rho_s \boldsymbol{u}^* \ddot{\boldsymbol{u}} dV + \int_{\Omega_s} \boldsymbol{\varepsilon}^* \boldsymbol{D} \boldsymbol{\varepsilon} dV = \int_{\Gamma_f} \boldsymbol{u}^* \bar{\boldsymbol{f}} dS \qquad [4.14]$$

with $\forall \boldsymbol{u}^* / \{\boldsymbol{u}^*|_{\Gamma_u} = 0\}$.

4.7.3.3. *Finite element approximation*

Initially, the domain is subdivided into several finite elements (Ω_{se}), with this meshing being carried out with reference elements [DHA 84]. At each finite element, a number of points called nodes are defined and assigned degrees of freedom (nodal displacements) according to the modeling adopted (Table 4.15). We then seek to define an approximation of the solutions for each of these elements, as in equation [4.9b] for the 1D problem.

The approximations sought can be of polynomial type and have to satisfy certain conditions: continuity, boundary conditions and completeness. This approximation is defined for the nodal displacement field, which ensures the compatibility of displacements between adjacent elements and the expression of equilibrium

conditions at the nodes. For each structural element, the nodal displacement approximation can be written as follows:

$$\{\boldsymbol{u}\} = [\boldsymbol{N}_s]\{\boldsymbol{u}\}_e \qquad [4.15a]$$

In this expression, $\{\boldsymbol{u}\}_e$ is the vector of nodal displacements of element e, and $[\boldsymbol{N}_s]$ is the matrix of interpolation functions of a structural element. Since the domain Ω_s is discretized, deformation/displacement relationships are defined in terms of node displacements as follows:

$$\{\boldsymbol{\varepsilon}\}_e = [\boldsymbol{B}]_e\{\boldsymbol{u}\}_e \qquad [4.15b]$$

The matrix $[\boldsymbol{B}]_e$ is constructed from the interpolation functions. The Galerkine method is most often used to discretize the integral function. This involves choosing the same approximation functions for the virtual displacement field as are chosen for the physical displacement field (nodal displacement). This method has the advantage of leading to symmetrical systems of equations. For each element Ω_{se}, we obtain:

$$\int_{\Omega_{\text{se}}} \rho_s \boldsymbol{u}^* \ddot{\boldsymbol{u}} dV = \int_{\Omega_{\text{se}}} \rho_s \boldsymbol{u}^* [\boldsymbol{N}_s]\{\ddot{\boldsymbol{u}}\}_e dV = \int_{\Omega_{\text{se}}} \rho_s [\boldsymbol{N}_s]^t [\boldsymbol{N}_s]\{\ddot{\boldsymbol{u}}\}_e dV \qquad [4.15c]$$

and:

$$\int_{\Omega_{\text{se}}} \boldsymbol{\varepsilon}^* \boldsymbol{D}\boldsymbol{\varepsilon} dV = \int_{\Omega_{\text{se}}} \boldsymbol{\varepsilon}^* [\boldsymbol{D}][\boldsymbol{B}]_e\{\boldsymbol{u}\}_e dV = \int_{\Omega_{\text{se}}} [\boldsymbol{B}]_e^t [\boldsymbol{D}][\boldsymbol{B}]_e\{\boldsymbol{u}\}_e dV \qquad [4.15d]$$

The terms in equations [4.15c] and [4.15d] are complicated polynomials. Their analytical integration is not straightforward. Numerical integration methods exist which allow the elementary matrices to be constructed by integration over the reference element, and the most widespread of these is the Gauss integration method [DHA 84].

After numerical integration of [4.15c] and [4.15d], we obtain the following relationships:

$$\int_{\Omega_{\text{se}}} \rho_s [\boldsymbol{N}_s]^t [\boldsymbol{N}_s]\{\ddot{\boldsymbol{u}}\}_e dV = [\boldsymbol{M}]_e\{\ddot{\boldsymbol{u}}\}_e \qquad [4.15e]$$

and:

$$\int_{\Omega_{\text{se}}} [\boldsymbol{B}]_e^t [\boldsymbol{D}][\boldsymbol{B}]_e\{\boldsymbol{u}\}_e dV = [\boldsymbol{K}]_e\{\boldsymbol{u}\}_e \qquad [4.15f]$$

where $[\boldsymbol{M}]_e$ and $[\boldsymbol{K}]_e$ are the elementary mass and stiffness matrices respectively.

The next step consists of assembling the elementary matrices (for each element) to form the global mass and stiffness matrices $[\boldsymbol{M}]$ and $[\boldsymbol{K}]$ (for the entire structure).

This ultimately leads to the following matrix equation, which represents the equation of motion of the structure:

$$[\boldsymbol{M}]\{\ddot{\boldsymbol{u}}\} + [\boldsymbol{K}]\{\boldsymbol{u}\} = \{\boldsymbol{f}\} \quad [4.16]$$

where $\{\boldsymbol{f}\}$ is the vector of forces applied to the nodes.

4.7.3.4. *Frequency domain*

Considering the case of a sinusoidal excitation of pulsation ω of the following form:

$$\{\boldsymbol{f}\} = \{\boldsymbol{f}(t)\} = \{f_0\}e^{i\omega t} \quad [4.17a]$$

the nodal displacements will also be of sinusoidal form:

$$\{\boldsymbol{u}\} = \{\boldsymbol{u}(t)\} = \{\boldsymbol{u}_0\}e^{i\omega t} \quad [4.17b]$$

In this case, the equation of motion becomes:

$$([\boldsymbol{K}] - \omega^2[\boldsymbol{M}])\{\boldsymbol{u}\} = \{\boldsymbol{f}\} \quad [4.17c]$$

4.7.3.5. *Modal analysis (eigenfrequency calculation)*

Modal analysis consists of assuming that the structure is not subject to any stimulation, and then solving the following eigenvalue/vector equation:

$$([\boldsymbol{K}] - \omega_i^2[\boldsymbol{M}])\{\boldsymbol{\varphi}_i\} = \{0\} \quad [4.18a]$$

where ω_i is the frequency of mode i and $\boldsymbol{\varphi}_i$ is the vector of nodal displacements of mode i. Note that there are as many modes as degrees of freedom.

4.7.3.6. *Calculation of the frequency response function*

Calculating the frequency response function, or FRF, of a structure following harmonic excitation involves calculating the transfer function $[\boldsymbol{H}]$ such that:

$$[\boldsymbol{H}] = ([\boldsymbol{K}] - \omega^2[\boldsymbol{M}])^{-1} \quad [4.18b]$$

4.7.4. *UVSQ-SAT production phases*

In this section, we give an example of the planning and process followed for the manufacture of UVSQ-SAT (see Figure 4.18).

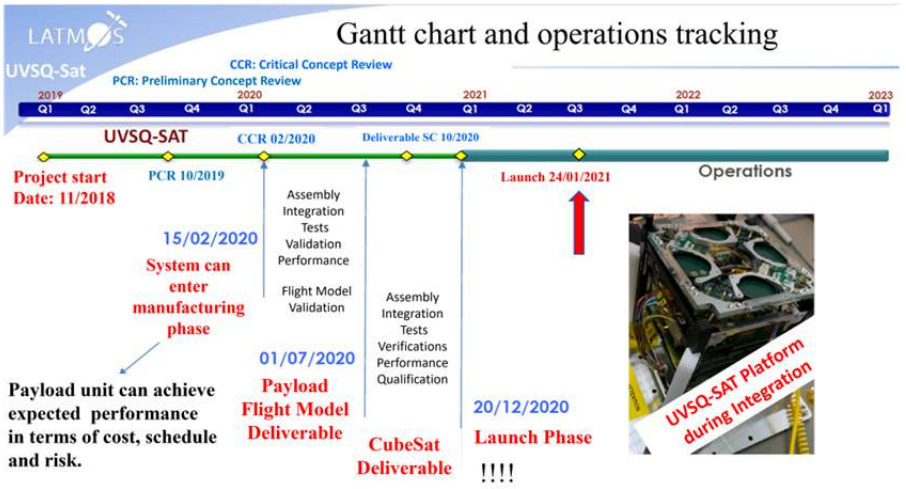

Figure 4.18. *Example of the process used to manufacture UVSQ-SAT*

The UVSQ-SAT project provides satellite observations of the Earth's radiation budget (ERB). The Earth's energy balance represents the balance between the solar energy absorbed by the planet and the energy radiated back into space in the form of infrared radiation. UVSQ-SAT data includes reflected solar radiation and radiation emitted by the Earth from the top of the atmosphere (TOA).

The aim is to study the effects on climate, which is controlled by the amount of solar flux absorbed by the Earth and the amount of infrared flux emitted to space. This balance determines the Earth's climate by influencing temperatures, precipitation, oceanic and atmospheric circulation, as well as biological processes. Any change in this balance, particularly as a result of human-made greenhouse gas emissions, leads to an energy imbalance that manifests itself as global warming. The consequences of this imbalance are numerous: rising sea levels, melting glaciers, extreme weather events, etc.

A near-infrared NIR spectrometer has been adapted for an observation CubeSat, the UVSQ-SAT NG. It was developed using the same procedure as the UVSQ-SAT, and was launched by SpaceX at 9:43 a.m. on March 15, 2025. Its mission is to observe greenhouse gases (GHGs) such as CO_2 and CH_4, measure the radiation energy balance (REB) and monitor solar spectral irradiance (SSI) at the top of the atmosphere (TOA). Figure 4.19 shows the observational configuration of the CubeSat.

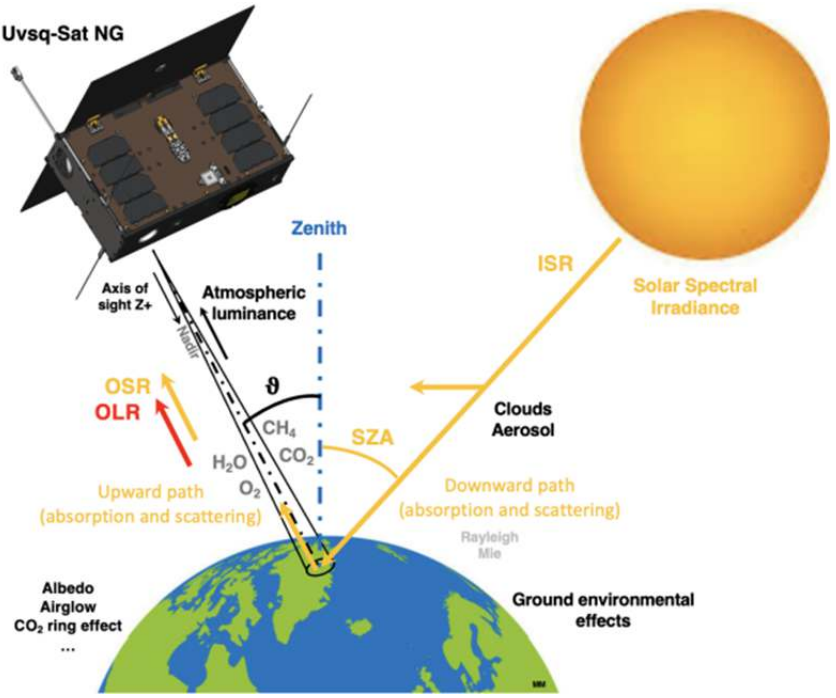

Figure 4.19. *Observation principle for the UVSQ-SAT NG CubeSat mission*

Conclusion

This book marks the first in a series of three books and discusses the space age from its origins in the mid-20th century to the NewSpace era in the 21st century. It draws on research experience gained at the Laboratoire Atmosphères et Observations Spatiales (LATMOS), for the implementation of observation instruments and data analysis, and at INSA Rouen for optimization methods in mechanics.

The chapters show the evolution of the space age from the orbiting of the first Sputniks launched by Russia in 1957 to the current NewSpace period, dominated almost unipolitically by the USA. The space age is characterized by innovations in various fields of socio-economic activity in both the tertiary and secondary sectors. These innovations include methodologies and technologies for service products and techniques. It opens the way to new prospects for industrial development, in some cases linked to the realm of dreams when it comes to the scope of possible achievements in space exploration.

CubeSats, initially developed as part of a university program by California Polytechnic State University and Stanford University in the USA, have opened up the possibility of carrying out space observation missions with reduced resources and shorter lead times than the first space missions. New design methods have been developed for these CubeSats, which come in cubes from 1U to a maximum of 24U. They take into account the shape and mass of the orbit, as well as the onboard payload for programmed observations. The debate on the orbital parameters of the CubeSats provided an opportunity to retrace the progress made in the sciences, in terms of new methodologies and concepts. This was particularly true of the work of Copernicus, Kepler, Galileo, Descartes, Newton, Einstein, Lagrange, Laplace and Hamilton, to name a few. This allowed scientists to break away from the assumptions of ancient astronomers, from the Egyptians to the Greeks, notably by consolidating the heliocentric model of planetary motion in the Solar System, within

the framework of Newton's law of gravitation or Einstein's theory of general relativity.

CubeSat implementation has been described within the framework of complex systems engineering. The organizational structure favors an agile horizontal approach, as opposed to a vertical procedure, in order to complete the space program within a reasonable timeframe right from the definition and analysis phase through to the operational phase. Once the scientific objectives of the program have been determined, and in order to build the ground segment (control center, VHF/UHF ground stations and data processing system) and the space segment (satellite platform and onboard scientific instruments), various environmental, scientific instrument calibration and verification tests are required. Right from the design stage, these tests ensure that the satellite is robust and reliable and will withstand the stresses and strains of its lifecycle: from the launch phase, through the operational phase, right up to decommissioning. They also ensure that the satellite meets mission requirements in terms of standards, safety and scientific objectives.

Nanosatellites allow us to observe the atmosphere of a planet, particularly the Earth, on a more precise scale of space and time, thanks to their size and quantity. Although it is not possible to cover all zones of the atmosphere, intelligent sampling based on priority observation zones should, like Pareto's 80-20 law, provide maximum information on key parameters such as pressure, temperature, humidity, wind speed and solar flux, enabling us to model the dynamics of the Earth's atmosphere. These satellite projects, whether for observation missions in the context of global warming or industrial activities, can be carried out within a reasonable timeframe and at affordable cost by any interested organization.

Finally, according to the European Cooperation for Space Standardization (ECSS):

> NewSpace encompasses all space initiatives that revolutionize the commercial space field through the use of highly innovative solutions and/or processes, exotic business models, simplified organizations, low-cost space, innovative risk management approaches. In the era of NewSpace, new scientific objectives are now accessible thanks to small satellites that benefit from recent technological advances in terms of miniaturization and reduced space access costs. This context makes them particularly suited to situations such as constellation operation for multi-point science (in situ or remote) in yet a high-risk, but high scientific return era.

References

[ACK 74] ACKOFF R.L., "The systems revolution", *Long Range Planning*, vol. 7, no. 6, p. 2, 1974.

[ADD 87] ADDA Y., DUPOUY J.M., PHILIBERT J. et al., *Eléments de métallurgie physique 1*, Editions INSTN CEA, Gif-sur-Yvette, 1987.

[ARG 54] ARGYRIS J.H., KELSEY S., "Energy theorems and structural analysis", *Aircraft Engineering and Aerospace Technology*, vol. 26, no. 11, pp. 383–394, 1954.

[ARN 78] ARNOLD V.I., *Mathematical Methods of Classical Mechanics*, Springer, New York, 1978.

[ASN 17] ASNER G.P., MARTIN R.E., MASCARO J., "Coral reef atoll assessment in the South China Sea using Planet Dove satellites", *Remote Sensing in Ecology and Conservation*, vol. 3, no. 2, pp. 57–65, 2017.

[AVE 97] AVENI A., *Stairways to the Stars: Skywatching in the Three Great Ancient Cultures*, John Wiley & Sons, New York, 1997.

[BAR 03] BARNEY R., TARRANT H., BURNYEAT M., *The Cambridge Companion to Plato's Timaeus*, Cambridge University Press, Cambridge, 2003.

[BER 06] BERTAUX J.L., KORABLEV O., PERRIER S. et al., "SPICAM on Mars Express: Observing modes and overview of UV spectrometer data and scientific results", *Journal of Geophysics Research*, vol. 111, no. E10, pp. 1–40, 2006.

[BER 07] BERTAUX J.L., NEVEJANS D., KORABLEV O. et al., "SPICAV on Venus Express: Three spectrometers to study the global structure and composition of the Venus atmosphere", *Planetary and Space Science*, vol. 55, no. 12, pp. 1673–1700, 2007.

[BER 08] BERTAUX J.L., VANDAELE A.C., WILQUET V. et al., "First observation of 628 CO2 isotopologue band at 3.3 μm in the atmosphere of Venus by solar occultation from Venus Express", *Icarus*, vol. 195, no. 1, pp. 28–33, 2008.

[BER 17] BERETTA F., "Les enjeux d'un procès", *Agrégation – question d'histoire moderne*, available at: https://www.lhistoire.fr/les-enjeux-dun-proc%C3%A8s, 2017.

[BIG 14] BIGGS D., CONLEY J., PEREZ A.D. et al., Small spacecraft technology state of the art, Report, SSTP, NASA, Moffett Field, 2014.

[BIO 56] BIOT M.A., "Thermoelasticity and irreversible thermodynamics", *Journal of Applied Physics*, vol. 27, no. 3, pp. 240–253, 1956.

[BLA 91] BLACKWELL R.J., *Galileo, Bellarmine, and the Bible*, University of Notre Dame Press, Notre Dame, 1991.

[BOA 08] BOARDMAN J., SAUSER B., *Systems Thinking: Coping with 21st Century Problems*, Taylor & Francis, Boca Raton, 2008.

[BON 49] BONNOT DE CONDILLAC E., *Traité des systèmes*, Fayard, Paris, 1749.

[BOR 62] BORN M., *Einstein's Theory of Relativity*, Dover Publications, New York, 1962.

[BRA 02] BRAHÉ T., *Astronomiae Instauratae Progymnasmata*, Typis Schumannianis, Prague, 1602.

[BRI 38] BRILLOUIN L., *Les tenseurs en mécanique et en élasticité*, Masson et Cie, Paris, 1938.

[BRU 55] BRUHAT G., *Mécanique*, Masson et Cie., Paris, 1955.

[BRU 62] BRUHAT G., *Thermodynamique*, Masson et Cie., Paris, 1962.

[BRU 65] BRUHAT G., *Cours de physique générale optique*, Masson et Cie, Paris, 1965.

[CAM 19] CAMPS A., "NanoSatellites and applications to commercial and scientific missions", in DEMYANOV V. and BECEDAS J. (eds), *Satellites Missions and Technologies for Geosciences*, BoD – Books on Demand, Norderstedt, doi: 10.5772/intechopen.90039, 2019.

[CAS 93] CASPAR M., *Kepler*, Dover Publications, New York, 1993.

[CHE 99] CHECKLAND P., *Systems Thinking, Systems Pratice Science*, John Wiley & Sons, New York, 1999.

[CHI 17] CHIN J., COEOLO R., FOLEY J. et al., CubeSat 101, basic concepts and processes for first-time CubeSat developers, Guide, NASA, California Polytechnic State University, San Luis Obispo, 2017.

[CHI 22] CHIU Y.C., CHANG L.C., CHAO C.K. et al., "Lessons learned from IDEASSat: Design, testing on orbit operations and anomaly analysis of a first university CubeSat intended for IonosphericScience", *Aerospace*, vol. 9, no. 2, p. 110, 2022.

[CHU 68] CHURCHMAN C.W., *The Systems Approach and its Enemies*, Dell Publishing, New York, 1968.

[CLA 95] CLAGETT M., *Ancient Egyptian Science, Calendars, Docks and Astronomy*, vol. 2, American Philosophical Society, Philadelphia, 1995.

[CLO 60] CLOUGH R.W., *The Finite Element Method in Plane Stress Analysis*, American Society Of Civil Engineers, Reston, 1960.

[COH 71] COHEN I.B., *Introduction to Newton's Principia*, Harvard University Press, Cambridge, 1971.

[COH 73] COHEN-TANNOUDJI C., DIU B., LALOË F., *Mécanique quantique*, Hermann, Paris, 1973.

[COH 87] COHEN-TANNOUDJI C., DUPONT-ROC J., GRYNBERG G., *Photons et atomes. Introduction à l'électrodynamique quantique*, CNRS Éditions, Paris, 1987.

[COP 43] COPERNICUS N., *De revolutionibus orbium coelestium*, Johannes Petreius, Nuremberg, 1543.

[COR 13] CORBARD T., SALABERT D., BOUMIER P. et al., "Helioseismology with PICARD", *Journal of Physics: Conference Series*, vol. 440, 2013.

[COU 43] COURANT R., "Variational methods for a solution of problems of equilibrium and vibrations", *Bulletin of the American Mathematical Society*, vol. 49, no. 1, pp. 1–23, 1943.

[CSI 19] CSILLIK O., KUMAR P., MASCARO J. et al., "Monotoring tropical forest carbon stocks and emissions using planet satellite data", *Scientific Reports*, vol. 9, no. 1, pp. 1–12, 2019.

[CUB 24] CUBESAT, "Origin of the new space revolution", available at: https://www.cubesat.org/, 2024.

[DAH 16] DAHOO P.R., POUGNET P., EL HAMI A., *Nanometer-scale Defect Detection Using Polarized Light*, ISTE Ltd, London and John Wiley & Sons, New York, 2016.

[DAH 19] DAHOO P.R., KHETTAB M., LINARES J. et al., "Non-destructive characterization by spectroscopic ellipsometry of interfaces in mechatronic devices", in POUGNET P. and EL HAMI A. (eds), *Embedded Mechatronic Systems 1*, 2nd edition, ISTE Ltd, London and Elsevier, Amsterdam, 2019.

[DAH 20] DAHOO P.R., "Approche système", Course, Université de Versailles St Quentin en Yvelines, ISTY, Vélizy-Villacoublay, 2020.

[DAH 21] DAHOO P.R., POUGNET P., EL HAMI A., *Applications and Metrology at Nanometer Scale 1: Smart Materials, Electromagnetic Waves and Uncertainties*, ISTE Ltd, London and John Wiley & Sons, New York, 2021.

[DAH 22] DAHOO P.R., Transformation digitale des entreprises, Course, Université de Versailles St Quentin en Yvelines, Versailles, 2022.

[DAH 23] DAHOO P.R., Les enjeux de transition numérique sur les processus d'ingénierie et son impact sur le contexte socioéconomique, Report, IUGET, Douala, 2023.

[DAN 19] DANISH M.N., "Small satellite: Military applications", *Academia*, doi: 10.1515/ARSA-2015-0013, 2019.

[DAU 85] DAUTRAY R., LIONS J-L., *Analyse mathématiques et calcul numérique pour les sciences et les techniques*, vol. 2, Masson, Paris, 1985.

[DEB 68] DE BROGLIE L., *Ondes électromagnétiques et photons*, Gauthier-Villars, Paris, 1968.

[DEJ 21] DE JONG T., "A study of Babylonian planatary theory III. The planet Mercury", *Archive for History of Exact Sciences*, vol. 75, pp. 491–522, 2021.

[DER 75] DE ROSNAY J., *Le Macroscope, vers une vision globale*, Le Seuil, Paris, 1975.

[DES 37] DESCARTES R., *Discours de la méthode : la géométrie*, Académies des Sciences, Gauthiers-Villars et fils imprimeurs de l'École polytechnique, Paris, 1637.

[DET 87] DE TYARD P., "Solitaire second", in *Les Discours philosophiques de Pontus de Tyard*, Chez Abel L'Angelier, Paris, 1587.

[DEW 11] DE WECK O.L., ROSS D., MAGEE C.L, *Engineering Systems: Meeting Human Needs in a Complex Technological World*, MIT Press, Cambridge, 2011.

[DHA 84] DHATT G., TOUZOT G., *Une présentation de la méthode des éléments finis*, Maloine S.A., Paris, 1984.

[DIC 70] DICKS D.R., *Early Greek Astronomy to Aristotle*, Cornell University Press, New York, 1970.

[DIC 06] DICK S.J., LAUNIUS R.D., *Critical Issues in the History of Spaceflight*, NASA, Washigton D.C., 2006.

[DRA 53] DRAKE S., *Discoveries and Opinions of Galileo*, Doubleday & Company Inc., New York, 1953.

[DRA 57] DRAKE S., *Galileo Studies: Personality, Tradition, and Revolution*, University of Michigan Press, Ann Arbor, 1957.

[EDM 74] EDMONDS A.R., *Angular Momentum in Quantum Mechanics*, Princeton University Press, Princeton, 1974.

[EIN 05] EINSTEIN A., "Zur Elektrodynamik bewegter Körper (On the electrodynamics of moving bodies)", *Annalen der Physik*, vol. 17, no. 10, pp. 891–921, 1905.

[EIN 15] EINSTEIN A., "Die Feldgleichungen der Gravitation (The field equations of gravitation)", *Sitzungsberichte der Königlich Preußischen Akademie der Wissenschaften*, pp. 844–847, 1915.

[EIN 16] EINSTEIN A., "Die Grundlage der allgemeinen Relativitätstheorie (The foundation of the general theory of relativity)", *Annalen der Physik*, vol. 49, no. 7, pp. 769–822, 1916.

[EIN 38] EINSTEIN A., *The Evolution of Physics: The Growth of Ideas from Early Concepts to Relativity and Quanta*, Simon and Schuster, New York, 1938.

[ENG 24] ENGLISH HERITAGE, Stonehenge, available at: https://www.english-heritage.org.uk/visit/places/stonehenge/, 2024.

[EOP 19] EOPORTAL, CubeSat concept and the provision of deployer services, available at: https://www.eoportal.org/other-space-activities/cubesat-concept#cubesat-concept-and-the-provision-of-deployer-services, 2019.

[ESA 09] ESA-ESTEC, Space project management – Project phasing and planning, Standard, ECSS-M-ST-40C, Noordwijk, 2009.

[EVA 98] EVANS J., *The History and Practice of Ancient Astronomy*, Oxford University Press, Oxford, 1998.

[EVO 18] EVONOSKY W., CHANDRAN A., BOYAJIAN S. et al., "INSPIRESat-1: An ionosphere exploring microsat", in *32nd Annual AIAA/USU Conference on Small Satellites*, Logan, 2018.

[FEY 63] FEYNMANN R.P., LEIGHTON R.B., SANDS M., *The Feynmann Lectures on Physics*, vol. 1, Addison-Wesley, Boston, 1963.

[FEY 65] FEYNMAN R.P., LEIGHTON R.B., SANDS M., *The Feynman Lectures on Physics*, vol. 2, Addison-Wesley, Boston, 1965.

[FEY 85] FEYNMAN R.P., *QED: The Strange Theory of Light and Matter*, Princeton University Press, Princeton, 1985.

[FEY 98] FEYNMAN R.P., *Quantum Electrodynamics*, Perseus Publishing, New York, 1998.

[FIN 89] FINOCCHIARO M.A., *The Galileo Affair: A Documentary History*, University of California Press, Berkeley, 1989.

[FLO 93] FLOOD R.L., CARSON E.R., *Dealing with Complexity: An Introduction to the Theory and Application of Systems Science*, Plenum Press, New York, 1993.

[FLO 99] FLOOD R.L., *Rethinking the Fifth Discipline: Learning within Unknowable*, Routledge, London, 1999.

[FOR 84] FORRESTER J.W., *Principes des systèmes*, Presses Universitaires de Lyon, Lyon, 1984.

[GAL 10] GALILEI G., *Sidereus Nuncius*, Baglioni T., Venice, 1610.

[GAL 32a] GALILEI G., *Dialogue Concerning the Two Chief World Systems*, Landini G.B., Florence, 1632.

[GAL 32b] GALILEI G., *Riposta*, Manuscript, 1632.

[GAO 16] GAO, Weapon system requirements: Detailed systems engineering prior to product development positions programs for success, Report, GAO-17-77, Washington, D.C., available at: https://www.gao.gov/products/gao-17-77, 2016.

[GER 96] GÉRADIN M., RIXEN D., *Théorie des vibrations : application à la dynamique des structures*, Masson, Paris, 1996.

[GIL 74] GILMORE R., *Lie Groups Lie Algebras and Some of their Applications*, Dover Publications, Inc., New York, 1974.

[GIN 73] GINGERICH O., *The Book Nobody Read: Chasing the Revolutions of Nicolaus Copernicus*, Walker & Company, New York, 1973.

[GLA 12] GLAESSGEN E.H., STARGEL D., "The digital twin paradigm for future NASA and US Air Force vehicles", in *AAIA 53rd Structures, Structural Dynamics, and Materials Conference*, Honolulu, 2012.

[GOL 76] GOLDSTEIN H., "Generalized coordinates in classical mechanics", *American Journal of Physics*, vol. 44, no. 12, pp. 11213–1126, 1976.

[GOL 01] GOLDSTEIN H., *Classsical Mechanics*, 3rd edition, Addison-Wesley, Boston, 2001.

[GOS 24] GOSECK CIRCLE, Sonnenobservatorium Goseck, available at: https://www.sonnenobservatorium-goseck.info/, 2024.

[GPG 07] GPG, Systems engineering, Goddard Procedures and Guidelines, GPG 7120.5, NASA, Greenbelt, 2007.

[GRI 02] GRIEVES M., Conceptual ideal for product LifeCycle management, Course, University of Michigan, Ann Arbor, 2002.

[GRI 05] GRIEVES M., "Product LifeCycle management: The new paradigm for enterprises", *International Journal Product Development*, vol. 2, no. 1, pp. 71–84, 2005.

[GRI 06] GRIEVES M., *Product LifeCycle Management: Driving the Next Generation of Lean Thinking*, McGraw-Hill, New York, 2006.

[GRI 16] GRIEVES M., Origins of the digital twin concept, Florida Institute of Technology, NASA, Melbourne, FL, doi: 10.13140/RG.2.2.26367.61609, 2016.

[HAM 34] HAMILTON W.R., "On a general method in dynamics", *Philosophical Transactions of the Royal Society of London*, vol. 124, pp. 247–308, 1834.

[HAM 44–50] HAMILTON W.R., "On quaternions or on a new system of imaginaries in algebra", *The London, Edinburgh and Dublin Philosophical Magazine and Journal of Science, Philosophical Magazines*, vols XXV–XXXVI, no. 3, 1844–1850.

[HAM 62] HAMERMESH M., DECIUS J.C., CROSS P.C., *Group Theory and its Application to Physical Problems*, Addison-Wesley, Boston, 1962.

[HEA 13] HEATH T., *Aristarchus of Samos, the Ancient Copernicus: A History of Greek Astronomy to Aristarchus Together with Aristarchus's Treatise on the Sizes and Distances of the Sun and Moon*, Cambridge University Press, Cambridge, 1913.

[HEC 05] HECHT E., *Optics*, 4th edition, Pearson Education Inc., Berlin, 2005.

[HEI 00] HEIDT H., PUIG-SUARI J., MOORE A.S. et al., "CubeSat: A new generation of picosatellite for education and industry low-cost space experimentation", in *14th Annual/USU Conference on Small Satellites*, Utah State University, Logan, 2000.

[HIT 07] HITCHINS D., *Systems Engineering: A 21st Century Systems Methodology*, John Wiley & Sons, Hoboken, 2007.

[HRE 41] HRENIKOFF A., "Solution of problems of elasticity by the framework method", *Journal of Applied Mechanics*, vol. 8, no. 4, pp. A169–A175, 1941.

[HRE 42] HRENIKOFF A., "Discussion of solution of problems of elasticity by the framework method", *ASME, Journal of Applied Mechanics*, vol. 9, no. 3, pp. A144–A145, 1942.

[HUN 01] HUNGER H., *Astronomical Diaries and Related Texts from Babylonia*, Austrian Academy of Sciences Press, Vienna, 2001.

[INC 12] INCOSE, Systems engineering handbook: A guide for system life cycle processes and activities, San Diego, 2012.

[INC 15] INCOSE, *Systems Engineering Handbook*, 4th edition, John Wiley & Sons, New York, 2015.

[JAC 98] JACKSON J.D., *Classical Electrodynamics*, 3rd edition, John Wiley & Sons, New York, 1998.

[JAL 20] JALES P., ESTERHUIZEN S., MASTERS D. et al., "The new spire GNSS-R satellite missions and products", *International Society for Optics and Photonics, Image and Signal Processing fir Remote Sensing XXVI*, vol. 11533, p. 1153316, 2020.

[JAN 11] JANSON S.W., "25 years of small satellites", in *25th Annual AIAA/USU Conference on Small Satellites*, Logan, 2011.

[JAN 21] JANSON S.W., "35 years of small satellites", in *35th Annual Small Satellite Conference*, Utah State University, Logan, available at: https://digitalcommons.usu.edu, 2021.

[JAN 23] JANSON S.W., "The concept and history of small satellites", in BRANZ F., CAPPELLETTI C., RICCO A.J., HINES J. (eds), *Next Generation CubeSats and SmallSats*, Elsevier, Amsterdam, 2023.

[JON 10] JONES A., *Ptolemy in Perspective: Use and Criticism of his Work from Antiquity to the Nineteenth Century*, Springer, Dordrecht, 2010.

[JUS 24] JUSTE D., Ptolemy's Almagest: Ptolemaeus Arabus et Latinus, available at: http://ptolemaeus.badw.de/work/19, 2024.

[KAN 18] KAN S., LUCAS J., "CeREs: The compact radiation belt explorer", in *32nd Annual AIAA/USU Conference on Small Satellites*, Utah, 2018.

[KEM 37] KEMBLE E.C., *The Fundamental Principles of Quantum Mechanics*, Dover Publications, New York, 1937.

[KEP 09] KEPLER J., *Astronomica Nova*, Hieronymus Gallerus, Heidelberg, 1609.

[KEP 10] KEPLER J., *Narratio de observatis a se quatuor Iovis satellitibus erronibus*, *Annexe à Sidereus Nuncius de Galilée*, Cosmo Giunta, Florence, 1610.

[KEP 19] KEPLER J., *Harmonices Mundi*, Johannes Planck, Linz, 1619.

[KIT 94] KITTS C., TWIGGS R.J., "The Satellite Quick Research Testbed Program (SQUIRT)", in *14th Annual/USU Conference on Small Satellites*, Logan, 1994.

[KOS 19] KOSIAK S., Small satellites in the emerging space environment: Implications for U.S. National Security – Related space plans and programs, CNAS, Washington, D.C., available at: https://www.jstor.org/stable/resrep20400, 2019.

[LAG 56] LAGRANGE J.L., "Essais sur le problème des trois corps", *Mémoires de l'Académie royale des sciences et belles-lettres de Berlin*, Chrétien Fréderic Voss, Berlin, 1756.

[LAG 67] LAGRANGE J.L., *Œuvres complètes de Lagrange*, vol. 6, Gauthier-Villars, Paris, 1767.

[LAG 72] LAGRANGE J.L., "Essais sur le problème des trois corps", in *Mémoires de l'Académie royale des sciences de Paris*, Gauthiers-Villars, Paris, 1772.

[LAG 88] LAGRANGE J-L., *Mécanique analytique*, Courcier, Paris (republished in 2009), 1788.

[LAN 66a] LANDAU L., LIFSHITZ E., *Mécanique : cours de physique théorique*, MIR, Moscow, 1966.

[LAN 66b] LANDAU L., LIFCHITZ E., *Théorie des champs*, MIR, Moscow, 1966.

[LAN 67] LANDAU L., LIFCHITZ E., *Théorie de l'élasticité*, MIR, Moscow, 1967.

[LAN 69] LANDAU L., LIFCHITZ E., *Physique théorique : electrodynamique des milieux continus*, 2nd edition, MIR, Moscow, 1969.

[LAN 75] LANDAU L., LIFCHITZ E., *Physique théorique : mécanique quantique*, 3rd edition, MIR, Moscow, 1975.

[LAN 86] LANCZOS C., *The Variational Principles of Mechanics*, 4th edition, Dover Publications, New York, 1986.

[LAN 89] LANDAU L., LIFCHITZ E., PITAEVSKI L. et al., *Electrodynamique quantique*, MIR, Moscow, 1989.

[LAP 43–46] LAPLACE P.S., *Traité de mécanique céleste*, vols I to V, Imprimerie Royale, Paris, 1843–1846.

[LAP 94] LAPLACE P.S., *Œuvres complètes de Laplace*, Académies des sciences, Gauthiers-Villars et fils imprimeurs de l'École polytechnique, Paris, 1894.

[LAS 66] LASSERRE F., *Die Fragmente des Eudoxos von Knidos*, Walter de Gruyter, Berlin, 1966.

[LAU 97] LAUNIUS R.D. (ed.), *Reconsidering SPUTNIK, 40 Years Since The Soviet Satellite*, NASA, Washington D.C., 1997.

[LAW 10] LAWSON H.A., *A Journey Through the Systems Landscape*, College Publications, Kings College, London, 2010.

[LEE 08] LEE S., Cubesat design specification, The CubeSat program, Rev.11, California Polytechnic State University, San Luis Obispo, 2008.

[LEE 14] LEE S., HUTPUTANASIN A., TOORIAN A. et al., Cubesat design specification, The CubeSat program, Rev.13, California Polytechnic State University, San Luis Obispo, 2014.

[LEM 77] LE MOIGNE J-L., *La théorie du système général : théorie de la modélisation*, PUF, Paris, 1977.

[LET 13] LE TREUT H., CHARLES L., "Climate sciences, observation and modelling: An historical perspective", in *Pollution atmosphérique*, IAEA, Vienna, 2013.

[LIN 75] LIN R.P., MCGUIRE R.E., HOWE H.C. et al., "Mapping of lunar surface remanent magnetic fields by electron scattering", *Lunar and Planetary Science Conference Proceedings*, vol. 19, pp. 2971–2973, 1975.

[LIN 04] LINTON C.M., *From Eudoxus to Einstein: A History of Mathematical Astronomy*, Cambridge University Press, Cambridge, 2004.

[LIP 65] LIPKIN H.J., *Lie Groups for Pedestrians*, North-Holland Publishing Company, Amsterdam, 1965.

[LLO 70] LLOYD G.E.R., *Early Greek Science: Thales to Aristotle*, Chatto and Windus, London, 1970.

[MAC 19] MACH E., *The Science of Mechanics: A Critical and Historical Account of its Development*, The Open Court Publishing Company, Chicago/London, 1919.

[MAC 37] MACDONALD F.C., *Plato's Cosmology: The Timaeus-Critias of Plato*, The Liberal Arts Press, New York, 1937.

[MAK 20] MAKHLOUFI A., AOUES Y., EL HAMI A., "Electro-thermo-mechanical modeling", in POUGNET P., EL HAMI A. (eds), *Embedded Mechatronic Systems 2*, 2nd edition, ISTE Press, London and Elsevier, Amsterdam, 2020.

[MAR 03] MARION J.B., THORNTON S.T., *Classical Dynamics of Particles and Systems*, 5th edition, Brooks/Cole, Pacific Grove, 2003.

[MAS 20] MASON J.P., WOODS T.N., CHAMBERLIN P.C. et al., "MinXSS-2 CubeSat mission overview: Improvements from the successful MinXSS-1 mission", *Advances in Space Research*, vol. 66, no. 1, pp. 3–9, 2020.

[MAU 44] MAUPERTIUS P.L.M., Accord de différentes lois de la nature qui avaient jusqu'ici paru incompatibles, Thesis, Académie royale des sciences de Paris, Paris, 1744.

[MAX 54] MAXWELL J.C., *A Treatise on Electricity and Magnetism*, 3rd edition, Dover Publications, New York, 1954.

[MEF 18] MEFTAH M., DAME L., BOLSEE D. et al., "SOLAR-ISS: A new reference spectrum based on SOLAR/SOLSPEC observations", *Astron. Astrophys.*, vol. 611. doi: 10.1051/0004-6361/201731316, 2018.

[MEF 20] MEFTAH M., DAME L., KECKHUT P. et al., "UVSQ-SAT, a Pathfinder CubeSat mission for observing essential climate variables", *Remote Sensing*, vol. 12, no. 92, doi: 10.3390/rs12010092, 2020.

[MEF 21] MEFTAH M., BOUTERAON T., DUFOUR C. et al., "The UVSQ-SAT/INSPIREAT-5 CubeSat mission: First in-orbit measurements of the Earth's outgoing radiation", *Remote Sensing*, vol. 13, no. 8, p. 1449, 2021.

[MEF 22a] MEFTAH M., BOUST F., KECKHUT P. et al., "INSPIRE-SAT 7, a second CubeSat to measure the Earth's energy budget and to probe the ionosphere", *Remote Sensing*, vol. 14, no. 186, doi: 10.3390/rs14010186, 2022.

[MEF 22b] MEFTAH M., Outils de simulation & conception des satellites, Master NewSpace Course, Université de Versailles St Quentin en Yvelines, Versailles, 2022.

[MEF 23] MEFTAH M., Outils de formation et de collecte de données pour l'observation de l'atmosphère, Guide, IUGET, Douala, 2023.

[MES 64] MESSIAH A., *Mécanique quantique*, vols 1 and 2, Dunod, Paris, 1964.

[MIC 87] MICHELSON A.A., MORLEY E.W., "On the relative motion of the Earth and the luminiferous ether", *American Journal of Science*, vol. 34, no. 203, pp. 333–345, 1887.

[MIL 19] MILLAN R.M., VON STEIGER R., ARIEL M. et al., "Small satellites for space science: A COSPAR scientific roadmap", *Advances in Space Research*, vol. 64, no. 8, pp. 1466–1517, 2019.

[MIS 73] MISNER C.W., THORNE K.S., WHEELER J.A., *Gravitation*, W.H. Freeman, New York, 1973.

[MIZ 72] MIZUSHIMA M., *Theoretical Physics: From Classical Mechanics to Group Theory of Microparticles*, John Wiley & Sons, New York, 1972.

[MOO 18] MOORE C.S., CASPI A., WOODS T.N. et al., "The instruments and capabilities of the miniature X-ray solar spectrometer (MinXSS) CubeSats", *Solar Physics*, vol. 293, no. 2, pp. 1–40, 2018.

[MOR 66] MOREL P., "Problems of atmospheric circulation: The EOLE experiment", in *Proceedings of the sixth International Space Science Symposium of COSPAR*, pp. 11–26, Mar Del Plata, 1966.

[MOR 02] MOREL P., "L'expérience spatiale éole et sa préparation (1962–1972)", *La Météorologie*, vol. 36, pp. 42–53, 2002.

[MPH 74] M'PHERSON P.K., "A perspective on systems science & systems philosophy", *Futures*, vol. 6, no. 3, pp. 219–239, 1974.

[MUG 71] MUGLER C., *Archimède, Œuvres. Tome II : Des spirales – De l'équilibre des figures planes – L'Arénaire – La Quadrature de la parabole*, Les Belles Lettres, Paris, 1971.

[NAS 95] NASA, *NASA Systems Engineering Handbook*, Washington, D.C., 1995.

[NAS 19] NASA, *NASA Systems Engineering Handbook*, Washington, D.C., 2019.

[NEU 55] NEUGEBAUER O., *Astronomical Cuneiform Texts*, ACT, London, 1955.

[NEU 60] NEUGEBAUER O., PARKER A., *Egyptian Astronomical, Text I, The Early Decans*, Brown University Press/Providence Rhode Island/Lund Humphries, London, 1960.

[NEU 67] NEUGEBAUER O., SACHS A.J., "Some atypical astronomical cuneiform texts", *Journal of Cuneiform Studies*, vol. 21, pp. 183–217, 1967.

[NEU 75] NEUGEBAUER O., *A History of Ancient Mathematical Astronomy*, HAMA, Berlin, 1975.

[NEW 80] NEWELL H.E., *Beyond the Atmosphere, Early Years of Space Science*, NASA, Washington D.C., 1980.

[NEW 87] NEWTON I., *Philosophiae Naturalis Principia Mathematica*, Jussu Societatis Regiae ac Typis Josephi Streater, London, 1687.

[NEW 99] NEWTON I., *The Principia: Mathematical Principles of Natural Philosophy*, COHEN I.B. and WHITMAN A. (eds). University of California Press, Berkeley, 1999 [1687].

[NEW 12] NEWTON I., *De motu corporum in gyrum*, RUSSELL J., COHN R. (eds), Book on Demand, Norderstedt, 2012 [1686].

[NOR 96] NORTH J., *Stonehenge: Neolithic Man and the Cosmos*, Harper Collins, New York, 1996.

[NOR 14] NORTON C.D., PELLEGRINO S., JOHNSON M., ARYA M., STEEVES J., KULKARNI S., MARTIN C.D., Findings of the KECK Institute for Space Studies Program on Small Satellites: A Revolution in Space Science, Final Report, Keck Institute for Space Studies, Pasadena, 2014.

[NYE 61] NYE J.F., *Propriétés physiques des cristaux, leur représentation par des tenseurs et des matrices*, Dunod, Paris, 1961.

[PAR 43] PARS L.A., "A treatise on analytical dynamics", *American Mathematical Monthly*, vol. 50, no. 7, pp. 412–420, 1943.

[PAR 50] PARKER R.A., *The Calendars of Ancient Egypt: Studies in Ancient Oriental Civilization*, The University of Chicago Press, Chicago, 1950.

[PAR 08] PARKER P., MIKE UGGLES C.L.N., "The age of Stonehenge", *Antiquity*, vol. 82, no. 316, pp. 617–639, 2008.

[PAS 79] PASSET R., *L'économique et le vivant*, Éditions Payot, Paris, 1979.

[PAS 06] PASZTOR E., ZSOLT C.S., "Astronomical orientation of European Neolithic Enclosures", *Journal for the History of Astronomy*, vol. 37, no. 3, pp. 343–359, 2006.

[PIC 13] PICARD D., MARC E., "Gregory Bateson : de l'anthropologie à la systémique", in PICARD D. (ed.), *L'École de Palo Alto*, PUF, Paris, available at: https://www.cairn.info/l-ecole-de-palo-alto--9782130606628-page-7.htm, 2013.

[PIN 97] PINGREE D., *From Astral Omens to Astrology from Babylon to BIKANER*, Gherardo Gnoli/Instituto Italiano Per l'Africa E l'Oriente, Rome, 1997.

[POP 45] POPPER K., *The Open Society and its Enemies*, Routledge, London, 1945.

[POP 59] POPPER K., *The Logic of Scientific Discovery*, Routledge, London, 1959.

[POP 63] POPPER K., *Conjectures and Refutations: The Growth of Scientific Knowledge*, Routledge, London, 1963.

[POP 72] POPPER K., *Objective Knowledge: An Evolutionary Approach*, Clarendon Press, Oxford, 1972.

[POR 98] PORTREE D.S.F., NASA's origins and the dawn of the space age, NASA History Division/Office of Policy and Plans, Washington D.C., 1998.

[POU 20] POUGNET P., DAHOO P.R., ALVAREZ J.P., "Highly accelerated testing", in POUGNET P., EL HAMI A. (eds), *Embedded Mechatronic Systems 2*, 2nd edition, ISTE Press, London and Elsevier, Amsterdam, 2020.

[RAD 11] RADNER K., ROBSON E., *The Oxford Handbook of Cuneiform Culture*, Oxford University Press, Oxford, doi: 10.1093/oxfordhb/9780199557301.001.0001, 2011.

[RAM 09] RAMAGE M., SHIPP K., *Systems Thinkers*, Springer, Dordrecht, 2009.

[ROB 09] ROBSON E., STEDALL J., *The Oxford Handbook of the History of Mathematics*, Oxford University Press, Oxford, 2009.

[ROC 80] ROCKEY K.C., EVANS H.R., GRIFFITHS D.W. et al., *The Finite Element Method*, 2nd edition, John Wiley & Sons, New York, 1980.

[ROS 67] ROSE M.E., *Elementary Theory of Angular Momentum*, John Wiley & Sons, New York, 1967.

[ROS 93] ROSEN N., *The Einstein Decade (1905–1915)*, Dover Publications, New York, 1993.

[RUG 99] RUGGLES C.L.N., *Astronomy in Prehistoric Britain and Ireland*, Yale University Press, New Haven, 1999.

[RUG 05] RUGGLES C.L.N., *Ancient Astronomy: An Encyclopedia of Cosmologies and Myth*, ABC-CLIO, Santa Barbara, 2005.

[SAK 94] SAKURAI J.J., *Modern Quantum Mechanics*, Addison Wesley, Boston, 1994.

[SAK 02] SAKODA D., HORNING J.A., "Overview of the NPS spacecraft architecture and technology demonstration satelitte, NPSat-1", in *Proceedings of the AIAA/USU Conference on Small Satellites*, Logan, 2002.

[SAK 06] SAKODA D., HORNING J.A., MOSELEY S.D., "Naval postgraduate school NPSat-1 small satellite: Small satellite systems and services", in *Proceedings of the 4S Symposium*, Chia Laguna, 2006.

[SAK 11] SAKURAI J.J., NAPOLITANO J., *Modern Quantum Mechanics*, 2nd edition, Addison-Wesley/Pearson, Boston, 2011.

[SCH 24] SCHERRER, D., Ancient observatories: Timeless knowledge, Stanford Solar Center, Stanford, available at: https://solar-center.stanford.edu/AO/Ancient-Observatories.pdf, 2024.

[SEN 93] SENGE P.M., *The Fifth Discipline*, Century Business, London, 1993.

[SHA 03] SHAW I., *The Oxford History of Ancient Egypt*, Oxford University Press, Oxford, 2003.

[SHA 10] SHAFTO M., CONROY M., DOYLE R. et al., Modeling, simulation, information technology and processing roadmap, Technical Report, NASA, Washington, D.C., 2010.

[SHE 70] SHEA W.R.., *Galileo's Intellectual Revolution: Middle Period*, Science History Publications, New York, 1970.

[SHE 03] SHEA W.R., ARTIGAS M., *Galileo in Rome: The Rise and Fall of a Troublesome Genius*, Oxford University Press, Oxford, 2003.

[SID 00] SIDDIQI A.A., Challenge to Apollo: The Soviet Union and the Space Race, 1945–1974, NASA History Division/Office of Policy and Plans, Washington, D.C., 2000.

[SOM 64a] SOMMERFELD A., *Partial Differential Equations in Physics*, Academic Press, New York, 1964.

[SOM 64b] SOMMERFELD A., *Mechanics: Lectures on Theoretical Physics*, vol. 1, Academic Press, New York, 1964.

[SON 24] SONG Y., GNYAWALI D., QIAN L., "From early curiosity to space wide web: The emergence of the small satellite innovation ecosystem", *Research Policy*, vol. 53, no. 2, p. 104932, 2024.

[SWE 98] SWERDLOW N.M., *The Babylonian Theory of the Planets*, Princeton University Press, Princeton, 1998.

[SWE 00] SWERDLOW N.M., *Ancient Astronomy and Celestial Divination*, MIT Press, Cambridge, 2000.

[TAN 21] TAN F., KHALIL N., "State of NASA science with SmallSats", in *35th Annual Small Satellite Conference*, Utah State University, Logan, 2021.

[TAY 05] TAYLOR J.R., *Classsical Mechanics*, MIT Press, Cambridge, MA, 2005.

[TIN 03] TINKHAM M., *Group Theory and Quantum Mechanics*, Dover Publications, New York, 2003.

[TOO 87] TOOMER G.J., PEDERSEN O., "Ptolemy's Almagest", *Journal for the History of Astronomy*, vol. 18, no. 1, p. 59, doi: 10.1177/002182868701800105, 1987.

[TUR 56] TURNER M.J., CLOUGH R.W., MARTIN H.C. et al., "Stiffness and deflection analysis of complex structures", *Journal of Aerosol Science*, vol. 23, pp. 805–823, 1956.

[VOI 10] VOIGT W., *Lehrbuch der Kristallphysik*, Teubner Verlag, Leipzig, 1910.

[VON 50] VON BERTALANFFY L., "An outline of general system theory", *British Journal for the Philosophy of Science*, vol. 1, no. 2, pp. 134–165, doi: 10.1093/bjps/I.2.134, 1950.

[VON 68] VON BERTALANFFY L., *General System Theory: Essays on its Foundations and Development*, George Braziller, New York, 1968.

[WAL 21] WALSH B.M., COLLIER M.R., ATZ E. et al., "The cusp plasma imaging detector (CuPID) CubeSat: Mission overview", *Journal of Geophysical Research: Space Physics*, vol. 126, no. 4, doi: 10.1029/2020JA029015, 2021.

[WEI 51] WEIBULL W., "A statistical distribution function of wide applicability", *Journal of Applies Mechanics Transaction, ASME*, vol. 18, no. 1, pp. 293–297, 1951.

[WEI 72] WEINBERG S., *Gravitation and Cosmology: Principles and Applications of the General Theory of Relativity*, John Wiley & Sons, New York, 1972.

[WEI 75] WEINBERG G.M., *An Introduction to General Systems Thinking*, John Wiley & Sons, New York, 1975.

[WES 80] WESTFALL R.S., *Never at Rest: A Biography of Isaac Newton*, Cambridge University Press, Cambridge, 1980.

[WHE 92] WHEELER J.A., TAYLOR E.F., *Spacetime Physics: Introduction to Special Relativity*, W.H. Freeman, New York, 1992.

[WHI 37] WHITTAKER E.T., *A Treatise on the Analytical Dynamics of Particles and Rigid Bodies*, Cambridge University Press, Cambridge, 1937.

[WHI 70] WHITEHEAD A.N., *Archimède, l'arénaire*, Cornell University Press, New York, 1970.

[WHI 76] WHITEMAN J.R., *The Mathematics of Finite Element and Applications II*, Academic Press, London, 1976.

[WIE 48] WIENER R., *Cybernetics: Or Control and Communication in the Animal and the Machine*, Hermann & Cie, Paris and MIT Press, Cambridge, 1948.

[XIA 22] XIAOCHEN Z., JINZHI L., KIRTSIS D., "The emergence of cognitive digital twin: Vision, challeges and opportunities", *International Journal of Production, Research*, vol. 60, no. 24, pp. 7610–7632, doi: 10.1080/00207543.2021.2014591, 2022.

[ZIE 67] ZIENKIEWICZ O.C., CHEUNG Y.K., *The Finite Element Method in Structural and Continuum Mechanics*, McGraw-Hill, New York, 1967.

Index

N, O

P, S

T, U, W

Other titles from

in

Space Science and Technology

2024

LARDIER Christian
Yuzhnoye Launchers and Satellites

2018

LARDIER Christian, BARENSKY Stefan
The Proton Launcher: History and Developments

2017

LEFEBVRE Jean-Luc
Space Strategy

WILEY END USER LICENSE AGREEMENT

Go to www.wiley.com/go/eula to access Wiley’s ebook EULA.